CORONARY SMOOTH MUSCLE CELL CYTODIFFERENTIATION AND INTRACELLULAR Ca^{2+} HANDLING IN CORONARY ARTERY DISEASE

Jill Kimberly Badin

Submitted to the faculty of the University Graduate School
in partial fulfillment of the requirements
for the degree
Doctor of Philosophy
in the Department of Cellular & Integrative Physiology,
Indiana University

August, 2019

Accepted by the Graduate Faculty, Indiana University, in partial fulfillment of the requirements for the degree of Doctor of Philosophy.

Doctoral Committee

_____
Michael S. Sturek, Ph.D., Chair

_____
Carmella Evans-Molina, M.D./Ph.D.

May 6, 2019

_____
Sharon Moe, M.D.

_____
Johnathan D. Tune, Ph.D.

DEDICATION

To my family for their unwavering love and support.

ACKNOWLEDGEMENTS

To my advisor, Dr. Mike Sturek, thank you for your patience, encouragement, and guidance. You have been a tremendous mentor for me. I would like to thank you for encouraging my research and for allowing me to grow as a research scientist. Your advice on both research as well as on my career have been invaluable. This research work was possible only because of your unconditional support. I quite simply cannot imagine a better adviser.

To my research committee, Dr. Carmella Evans-Molina, Dr. Sharon Moe, and Dr. Johnathan D. Tune, thank you for the meetings, support, guidance, and constructive criticisms that have been invaluable contributions to this research.

To my lab mates Mouhamad Alloosh, Jim Byrd, Sarah Davis, Caleb Eggenberger, Jane Hooker, Ayeeshik Kole, Mikaela McKenney-Drake, and Stacey Rodenbeck for their intellectual contribution to this dissertation. Thank you for making my graduate school experience enjoyable and fun.

To the IUSM Department of Cellular & Integrative Physiology, thank you for providing a collaborative and supportive environment.

To Dr. Keith Condon, thank you for processing the histology and allowing me to use his lab's equipment. To Dr. Robert Considine's laboratory, thank you for performing insulin assays. To the Indiana University Center for Medical Genomics (Dr. Yunlong Liu, Dr. Xiaoling Xuei, and Dr. Hongyu Gao), thank you for performing the single cell RNA sequencing and allowing me to use their equipment.

Last but not least, I would like to express my deepest gratitude to my friends and family. This dissertation would not have been possible without their warm love, continued patience, and endless support. To my friends Moriah Ellenbogen, Taylor and Darcey Hignite, and Jacob and Elizabeth Layman, thank you for your constant concern and

support during the completion of this project. To my siblings Brett Badin and Holly Burnett, thank you for your emotional support throughout my graduate school experience. To my parents Joseph and Mindy Badin, thank you for setting me off on the road to this PhD a long time ago. Your guidance and dedication to my education has been monumental.

This research was supported by the Fortune-Fry Ultrasound Research Fund, Eli Lilly & Co., National Institutes of Health P30 DK097512, HL125385, and T32 HL079995, the CorVus Diabetes Research Fund, the Purdue University Hugh W. and Edna M. Donnan Fellowship, and the Indiana University School of Medicine Center of Excellence in Cardiovascular Research.

Jill Kimberly Badin

CORONARY SMOOTH MUSCLE CELL CYTODIFFERENTIATION AND INTRACELLULAR Ca^{2+} HANDLING IN CORONARY ARTERY DISEASE

Metabolic syndrome (MetS) affects 1/3 of all Americans and is the clustering of three or more of the following cardiometabolic risk factors: obesity, hypertension, dyslipidemia, glucose intolerance, and insulin resistance. MetS drastically increases the incidence of coronary artery disease (CAD), which is the leading cause of mortality globally. A cornerstone of CAD is arterial remodeling associated with coronary smooth muscle (CSM) cytodifferentiation from a contractile phenotype to proliferative and osteogenic phenotypes. This cytodifferentiation is tightly coupled to changes in intracellular Ca^{2+} handling that regulate several key cellular functions, including contraction, transcription, proliferation, and migration. Our group has recently elucidated the time course of Ca^{2+} dysregulation during MetS-induced CAD development. Ca^{2+} transport mechanisms, including voltage-gated calcium channels, sarcoplasmic reticulum (SR) Ca^{2+} store, and sarco-endoplasmic reticulum Ca^{2+} ATPase (SERCA), are enhanced in early, mild disease and diminished in late, severe disease in the Ossabaw miniature swine. Using this well-characterized large animal model, I tested the hypothesis that this Ca^{2+} dysregulation pattern occurs in multiple etiologies of CAD, including diabetes and aging. The fluorescent intracellular Ca^{2+} ($[Ca^{2+}]_i$) indicator fura-2 was utilized to measure $[Ca^{2+}]_i$ handling in CSM from lean and diseased swine. I found that $[Ca^{2+}]_i$ handling is enhanced in mild disease with minimal CSM phenotypic switching and diminished in severe disease with greater phenotypic switching, regardless of CAD etiology. We are confident of the translatability of this research, as the Ca^{2+} influx, SR Ca^{2+} store, and SERCA functional changes in CSM of humans with CAD are similar to those found in

Ossabaw swine with MetS. Single-cell RNA sequencing revealed that CSM cells from an organ culture model of CAD exhibited many different phenotypes, indicating that phenotypic modulation is not a discreet event, but a continuum. Transcriptomic analysis revealed differential expression of many genes that are involved in the osteogenic signaling pathway and in cellular inflammatory responses across phenotypes. These genes may be another regulatory mechanism common to the different CAD etiologies. This study is the first to show that CSM Ca^{2+} dysregulation is common among different CAD etiologies in a clinically relevant animal model.

Michael S. Sturek, Ph.D., Chair

TABLE OF CONTENTS

LIST OF TABLES

LIST OF FIGURES

LIST OF ABBREVIATIONS

$[Ca^{2+}]_i$ – Intracellular Ca^{2+}
AHA – American Heart Association
ALP – Alkaline phosphatase
ALT – Alanine aminotransferase
AngII – Angiotensin II
ANOVA – One-way analysis of variance
ANXA2/5 – Annexin A2/5
AST – Aspartate aminotransferase
BUN – Blood urea nitrogen
CAC – Coronary artery calcification
CAD – Coronary artery disease
CaMKII – Ca2+/calmodulin kinase
CFX – Circumflex artery
CRAC – Ca^{2+}-release activated Ca^{2+} channel
CREB – cAMP response element binding
CSM – Coronary smooth muscle
DAB – 3, 3' diaminobenzidine
DM – Diabetes mellitus
ECM – Extracellular matrix
EEL – External elastic lamina
ER – Endoplasmic reticulum
GLUT2 – Glucose transporter 2
GSIS – Glucose-stimulated insulin secretion
HOMA-IR – Homeostasis model assessment-insulin resistance
IEL – Internal elastic lamina
IP_3R – Inositol trisphosphate receptors
IPA – Ingenuity Pathway Analysis
IVGTT – Intravenous glucose tolerance test
IVUS – Intravascular ultrasound
LAD – Left anterior descending artery
LCA – Left main coronary artery
LDL – Low density lipoprotein cholesterol
MAP – Mean arterial pressure
MetS – Metabolic syndrome
MetS/D-A – Metabolic Syndrome/Diabetic-Alloxan
MetS-A – Metabolic Syndrome-Alloxan
MGP – Matrix Gla protein
MLCK – Myosin light chain kinase
MMP2/9 – Matrix metallopeptidase 2/9
MTT – Meal tolerance test
NCX – Sodium-calcium exchangers
NFAT – Nuclear factor activated T-cells
Ox-LDL – Oxidized low-density lipoprotein
PLN – Phospholamban
PMCA – Plasma membrane Ca^{2+} ATPase
PVAT – Perivascular adipose tissue
RAGE – Receptor of advanced glycation end-products
RANKL – Receptor activator of nuclear factor kappa-B ligand
RAS – Renin-angiotensin system
RCA – Right coronary artery
ROS – Reactive oxygen species
Runx2 – Runt-related transcription factor 2
RyR – Ryanodine receptors
ScRNA-seq – Single-cell RNA sequencing
SERCA – Sarco-endoplasmic reticulum Ca^{2+}-ATPase
SMC – Smooth muscle cell
SMPDL3B – Sphingomyelin phosphodiesterase acid like 3B
SOCE – Store-operated Ca^{2+} entry
SR – Sarcoplasmic reticulum
SRF – Serum response factor
STZ – Streptozotocin
T1D – Type 1 diabetes
T2D – Type 2 diabetes
TIRF – Total internal reflection fluorescence
TNFα – Tumor necrosis factor alpha
TRP – Transient receptor potential
T-SNE – t-distributed stochastic neighbor embedding
VGCC – Voltage-gated Ca^{2+} channels
VK – Von Kossa
VSMC – Vascular smooth muscle cell
VVG – Verhoeff-Van Gieson

CHAPTER 1: INTRODUCTION

Obesity

Obesity, as defined by a BMI greater than or equal to 30.0, is a growing epidemic in the United States (Fig. 1.1). Currently, 39.8% of adults and 18.5% of children are obese in the US [1]. This is clearly a growing public health crisis that negatively affects health, quality of life, and national healthcare budgets. In the United States alone, healthcare costs of obesity and obesity-related health conditions are $275 billion/year, which is more than 20% of total healthcare spending [2].

While obesity was once considered an issue exclusively for developed nations, the presence of obesity had doubled worldwide from 1980 to 2008, and currently over 600 million people are classified as obese [3]. In children, the global obesity rate has increased from 8% in 1980 to 13% in 2013 [3]. The obesity rate in children is a growing concern, as juvenile obesity is associated with both adipocyte hyperplasia and hypertrophy [4]. Juvenile adipocyte hyperplasia increases the risk for obesity in adulthood, indicating that the obesity epidemic will only become exponentially worse in the future.

Human evolution has helped fuel the obesity epidemic. In the hunter-gatherer stage of human evolution, there were times of feast and famine that occurred cyclically with the seasons. Individuals who were better able to store calories in the form of adipose tissue were favored in times of food shortage [5]. While this “thrifty genotype” was useful tens of thousands of years ago, the current constant abundance of affordable, calorie-rich food coupled with a sedentary lifestyle, humorously referred to as our “obesogenic environment,” has only exacerbated the obesity epidemic [5-7].

Metabolic Syndrome

Obesity is one of the main risk factors associated with metabolic syndrome (MetS), which is defined by the American Heart Association (AHA) as the clustering of three or more of the following five cardiometabolic risk factors: central obesity, insulin resistance,

glucose intolerance, hypertension, and dyslipidemia [8]. More specifically, MetS is clinically defined by a blood pressure >130/85 mmHg, a fasting blood glucose >100 mg/dL, an HDL-C level <40 mg/dL for men or <50 mg/dL for women, a triglyceride level >150 mg/dL, and a BMI ≥30.0 kg/m^2 [8]. MetS affects 1 in 3 Americans and greatly increases the risk of developing comorbidities such as type 2 diabetes, non-alcoholic fatty liver disease (NAFLD), and coronary artery disease (CAD) [8]. MetS and its comorbidities significantly raise health care costs and are a burden on national economies [9].

While each individual component of MetS increases the risk for cardiovascular events, a positive MetS diagnosis triples the risk for adverse cardiovascular outcomes [10] (Fig. 1.2, adapted from [10]). Several studies have determined that patient MetS score is associated with increased Gensini score, a measurement of CAD severity [11-14]. It is readily apparent that when these metabolic abnormalities are clustered together there is a greatly enhanced risk of cardiovascular events, indicating that MetS is greater than the sum of its parts.

Coronary Artery Disease

CAD is responsible for 1 in 7 deaths in the United States and is the leading cause of mortality globally [8]. The cost of CAD in the United States was estimated at $108.9 billion and was the second most expensive hospital discharge diagnosis in 2011 [8, 15]. The incidence of CAD is expected to rise 40.6% with a doubling in the resulting medical costs by the year 2030 [8, 15].

Healthy coronary arteries have three distinct layers. The adventitia is composed mainly of connective tissue, the tunica media is the largest layer and is composed mainly of contractile coronary smooth muscle (CSM) cells, and the tunica intima is a one-cell-thick layer of endothelial cells that are in constant contact with the lumen (Fig. 1.3A-E, adapted from [16]). However, CAD is accompanied by the pathophysiological remodeling

of the coronary arteries that restricts blood flow to the myocardium, resulting in myocardial infarction and other adverse cardiovascular events.

CAD is initiated by endothelial damage or dysfunction leading to the upregulated expression of adhesion molecules that bind to circulating macrophages. Chemoattractant cytokines regulate the transmigration of these macrophages into the arterial wall, where they engulf lipid depositions including oxidized low-density lipoproteins (ox-LDL) and progress into foam cells. Contractile CSM cells that populate the media layer dedifferentiate into proliferative, synthetic cells and are recruited into the developing lesion where they secrete extracellular matrix (ECM) proteins, including collagen, which contributes to plaque stabilization and outward remodeling. As the lesion continues to form, debris from apoptotic CSM and other cells as well as lipid droplets accumulate to form a necrotic core. Further CSM dedifferentiation into an osteogenic phenotype contributes to the deposition of hydroxyapatite crystals in the ECM, resulting in vascular calcification (Fig. 1.4, adapted from [17, 18]). Detailed mechanisms of CSM phenotypic switching and vascular calcification are described later in this work. Later stages of CAD are associated with increased cardiac mortality, risk of plaque rupture, and clinical narrowing of the lumen. Although the heart has a low coronary flow reserve, a blockage of about 75-80% of the lumen is required to have any detrimental effects on myocardial health, so CAD may remain clinically silent for decades [19].

Type 2 Diabetes

Diabetes mellitus (DM) is composed of heterogeneous metabolic diseases that result in hyperglycemia due to pancreatic beta cell failure, insulin resistance in peripheral tissues, or both [20]. There are two main classifications of DM: type 1 diabetes (T1D) and type 2 diabetes (T2D). T1D is the autoimmune destruction of pancreatic beta cells, leading to a complete dependence on exogenous insulin. The onset of T1D usually occurs before age 40, with the average age of diagnosis around 14 years [21]. T2D is the progressive

loss of pancreatic beta cell function and is responsible for 90-95% of DM cases in North America [8]. T2D is a complex condition resulting from long-term glucose intolerance and insulin resistance. As such, it is a common comorbidity with MetS and is a major risk factor for cardiovascular diseases including CAD. It has been well-documented that humans with DM and MetS develop greater CAD severity and have a higher incidence of cardiovascular events than individuals with MetS alone [14, 22-26]. Like obesity, T2D is a growing epidemic. In 2014, an estimated 31 million adults in the United States have T2D, ¼ of those cases undiagnosed, costing the US $245 billion a year in medical expenses [8, 27].

T2D has a complex and dynamic etiology, as it is a progressive disease that manifests clinically as chronic hyperglycemia over the course of decades and is usually coupled with other cardiometabolic conditions. The pathophysiology of T2D follows a pathway eventually leading to beta cell failure [27]. The first stage of T2D is beta cell compensation. Peripheral insulin resistance necessitates an increase in glucose-stimulated insulin secretion (GSIS) of pancreatic beta cells, which is done both by increases in overall beta cell mass and in beta cell hypertrophy [28]. As such, this stage is accompanied by hyperinsulinemia. T2D progresses when beta cells can no longer compensate for the peripheral insulin resistance and glucose intolerance, resulting in a state of hypoinsulinemia [29]. This impaired GSIS could be due to glucotoxicity, where chronic hyperglycemia causes a depletion of insulin secretory granules from beta cells, and/or lipotoxicity, where increased fatty acid levels lead to infiltration of pancreatic islets and beta cell dysfunction [28, 29].

Studying the interplay between T2D and obesity is of utmost importance, as individuals with T2D are being diagnosed earlier and living longer, leading to an increased risk of developing cardiovascular complications [29].

The positive energy balance of obesity leads many cellular processes to become imbalanced. An excess of nutrients stimulates adipose tissue to release tumor necrosis

factor alpha (TNFα) and IL-6, leading to a pro-inflammatory state that is a common factor in obesity, MetS, and T2D [30-32]. An increased serum level of these inflammatory mediators have been found to reduce the synthesis and secretion of adiponectin, an adipocyte that normally functions as an insulin sensitizer and anti-atherosclerotic agent [33, 34]. Indeed, patients with T2D have a lower level of circulating adiponectin than their normoglycemic counterparts [35]. Adiponectin has been found to reduce NADPH oxidase activity, so a lower level of adiponectin is correlated to increased ROS generation [35, 36]. The resulting increase in ROS contributes to reduced insulin secretion in beta cells, insulin resistance in skeletal muscle and adipocytes, and endothelial dysfunction, all mechanisms of T2D and atherogenesis [37]. Finding the common disease mechanisms of these comorbidities is important, as it could lead to pharmacotherapies that can treat multiple different linked conditions.

Aging as a Risk Factor for Cardiovascular Disease

William Osler, a prolific physiologist and one of the founders of Johns Hopkins University, once said, “A man is as old as his arteries” [38]. Indeed, aging is a major unmodifiable risk factor for CAD. An advanced age is associated with increased risk of developing several cardiometabolic abnormalities, with 54.9% of the population aged 60 and over having MetS [39]. In 2010, adults 65 years and older had a T2D rate of 26.9%, well above the rate of 9.4% for the general population [8]. The incidence of CAD increases progressively with age, with more than 50% of CAD-related deaths occurring in those aged 75 and older [40, 41]. In fact, is it hypothesized by some that the rise of T2D is mainly due to the aging population, as the incidence of MetS has remained relatively constant for the past decade [42].

Even physiologically healthy aging is associated with several cardiometabolic changes that are independently associated with MetS and CAD, such as increases in plasma low density lipoprotein cholesterol (LDL) and triglyceride levels, making the aged

vasculature more susceptible to disease [43]. Age-associated increases in NADPH oxidase activity increase cellular concentrations of reactive oxygen species (ROS), which contributes to the activation of NF-κB leading to an increased inflammatory state [44-47]. This inflammatory state is associated with the upregulation of many inflammatory cytokines, chemokines, and adhesion molecules that promote atherosclerosis [44, 48-53]. High concentrations of ROS are also known to inactivate NO, which, along with the age-related decline in eNOS activity, causes impairments in vasodilation [47]. Several structural differences in aged vessels, such as increased collagen content, decreased elastin content, and changes in Ca^{2+} homeostasis, contribute to arterial stiffening and subsequent age-related hypertension [47, 54]. Elderly patients exhibit more extensive vascular calcification associated with lipid oxidation and inflammation [55, 56]. Detailed mechanisms of vascular calcification are described later in this work.

Aging is associated with cellular senescence, which is accompanied by growth arrest, DNA damage, telomere shortening, and reduced proliferation [54]. The senescence-associated secretory phenotype contributes to age-related diseases by secreting effectors such as IL-6, IL-8, and MCP-1 that alter the ECM and impair the functioning of surrounding cells [47, 57]. Atherosclerotic plaques even in young subjects showed signs of cellular senescence, indicating that atherosclerosis may be classified as premature vascular aging [54]. Indeed, arterial intima/media thickening is a process associated with aging independent from atherosclerosis [58]. Overall, the aging cellular milieu contributes substantially to the pathophysiology of coronary atherosclerosis.

Coronary Circulation

All the risk factors described so far in this work increase the risk of developing cardiovascular diseases, including CAD. As such, physiological knowledge of the coronary circulation is of utmost importance.

The heart is the only organ in the body that supplies blood to itself. The left and right main coronary arteries branch from the left and right ostium in the proximal aorta directly above the aortic semilunar valve. Unlike every other organ, blood flows into the coronary arteries mainly during diastole when the myocardium is relaxed and there is some level of retrograde flow in the proximal aorta [19]. The left main coronary artery (LCA) branches into the left anterior descending (LAD) artery, which lies in the anterior interventricular groove, and the circumflex (CFX) artery, which lies in the left atrioventricular groove. The right coronary artery (RCA) lies in the right atrioventricular groove. These large conduit arteries wrap around the heart, eventually narrowing and branching into first, second, and third order resistance arterioles. These resistance arterioles extensively branch into microvessels and infiltrate the myocardium transmurally to deliver oxygen to the myocardium (Fig. 1.5, adapted from [19]).

As the heart has a very high oxygen demand, if coronary blood flow is perturbed or reduced even to a small degree it will have negative effects on the myocardium and result in adverse health consequences.

Coronary Smooth Muscle

CSM cells reside in the media layer of coronary arteries and are responsible for relaxation and contraction that regulates coronary blood flow. CSM are spindle-shaped cells ranging from 5-10 μm in diameter and 50-600 μm in length [59]. CSM are associated with sustained, tonic contractions while smooth muscle from veins and nonvascular tissues are associated with rapid, phasic contraction [16, 60]. Unlike striated muscle, CSM lacks an organized subcellular contractile filament structure [16, 60]. Instead, CSM contains thin filaments composed of actin, tropomyosin, and binding proteins such as myosin light chain kinase (MLCK), caldesmon, and calponin, and thick filaments composed mainly of myosin [16, 61]. The thin filaments are anchored into membrane plaques at the polar ends of the cell membrane and dense bodies in the cytoplasm [16].

These structures are similar to the Z-lines in striated muscle. The intracellular filament lattice structure is highly plastic, allowing the CSM to rapidly adapt and provide contractile forces over a wide length range [62].

CSM cell contraction can be accomplished through mechanical stimuli, chemical stimuli, and electrical stimuli [16]. For this work, I will focus on the latter, also termed "excitation-contraction coupling." Depolarization of the plasma membrane leads to the influx of extracellular Ca^{2+} via voltage-gated calcium channels (VGCC) where it binds to calmodulin, activating MLCK which phosphorylates myosin light chain (MLC) [16, 60, 63]. MLC phosphorylation in the presence of ATP causes the formation of cross-bridges between myosin heads and actin filaments, resulting in contraction [16, 60]. CSM relaxation can be accomplished by the decrease of intracellular Ca^{2+} either through efflux mechanisms or by sequestration into the sarcoplasmic reticulum (SR) [60, 61]. Since intracellular Ca^{2+} concentration is largely responsible for CSM contraction, tight Ca^{2+} regulation is vital for CSM function and is reviewed in detail in the following section of this work.

Cell-cell communication between CSM cells is accomplished by gap junctions, which form a functional syncytium that enables the free flow of small molecules and ions [61]. Therefore, depolarization and repolarization can spread freely from one cell to another, resulting in a concerted action of contraction and relaxation [16, 61]. Simultaneous, controlled contraction and relaxation is vital for arterial function and regulation of blood flow.

Coronary Smooth Muscle Intracellular Ca^{2+} Regulation

Extracellular Ca^{2+} can enter the cell through VGCC after membrane depolarization or through transient receptor potential (TRP) channels, which are activated by ligands such as G proteins, phosphoinositides, and diacylglycerol and do not require membrane depolarization [16, 64]. Intracellular Ca^{2+} ($[Ca^{2+}]_i$) can exit the cell via plasma membrane

Ca^{2+} ATPases (PMCA) or sodium-calcium exchangers (NCX). $[Ca^{2+}]_i$ can also be buffered by the SR via the sarco-endoplasmic reticulum Ca^{2+}-ATPase (SERCA), where sequestered Ca^{2+} can be released by inositol trisphosphate receptors (IP_3R) and ryanodine receptors (RyR) to rapidly increase the concentration of $[Ca^{2+}]_i$ (Fig. 1.6).

As $[Ca^{2+}]_i$ must be tightly controlled, how these Ca^{2+} transporters interact with the changing concentrations of Ca^{2+} in the cellular environment is immensely important. Phospholamban (PLN) inhibits SERCA activity when cytosolic concentrations of Ca^{2+} are low, but high $[Ca^{2+}]_i$ activates Ca^{2+}/calmodulin kinase (CaMKII), which phosphorylates PLN leading to the disinhibition of SERCA [65]. In this way, $[Ca^{2+}]_i$ homeostasis can be maintained. However, when the SR Ca^{2+} store is depleted, a Ca^{2+} sensing protein located in the SR membrane called STIM1 activates Orai1 and TRPC channels on the plasma membrane, which cause an efflux of Ca^{2+} that can be re-sequestered into the SR by SERCA [63, 66, 67]. This process is referred to as store-operated Ca^{2+} entry (SOCE). Ca^{2+} can also be released from the SR via RyR when there is a rise in $[Ca^{2+}]_i$, a process called Ca^{2+}-induced Ca^{2+}-release (CICR) [16]. These localized increases in $[Ca^{2+}]_i$ can activate Ca^{2+}-dependent K^+ channels, leading to repolarization and closure of VGCC [16]. All these mechanisms work in harmony to contribute to the function and Ca^{2+} homeostasis of CSM.

Smooth Muscle Phenotypic Modulation and $[Ca^{2+}]_i$ Handling Alterations

Differentiated, contractile CSM have a low proliferation rate and are largely stationary [68]. However, CSM can dedifferentiate into a proliferative, migratory phenotype that secretes ECM proteins as a wound-healing response in times of stress [68]. As CAD is associated with a constant low level of inflammation and cellular stress, CSM continually dedifferentiate into other phenotypes, contributing to disease pathology. These dedifferentiated CSM cells can migrate to the growing plaque, secrete ECM proteins, and rapidly proliferate, contributing to disease pathology [68, 69].

Phenotypic modulation is closely coupled to changes in $[Ca^{2+}]_i$ handling, as $[Ca^{2+}]_i$ controls many cellular functions such as migration, proliferation, and transcription (Fig. 1.6). This is accomplished by Ca^{2+}-dependent transcription factors such as serum response factor (SRF), cAMP response element binding (CREB), and nuclear factor of activated T-cells (NFAT) [69]. Ca^{2+} signaling in contractile CSM depends on local $[Ca^{2+}]_i$ signaling in the form of Ca^{2+} sparks and waves on a background of low global $[Ca^{2+}]_i$. The low $[Ca^{2+}]_i$ that facilitates this kind of $[Ca^{2+}]_i$ handling is mostly attributable to the SERCA pump, which has been shown to sequester more than 70% of $[Ca^{2+}]_i$ [70, 71]. Local dramatic increases in $[Ca^{2+}]_i$ activates SRF, which binds to the serum response element in the promoter region of target genes, many of which are involved in contraction and contractile phenotypic maintenance [68, 69]. SERCA dysfunction results in an inability to sequester Ca^{2+}, leading to greater store-operated Ca^{2+} entry via transient receptor potentiation (TRP) channels, STIM-1, and Orai1 and a dramatic, sustained increase in $[Ca^{2+}]_i$ [70, 72, 73]. High global $[Ca^{2+}]_i$ activates Ca^{2+}/calmodulin-dependent protein kinase II, which phosphorylates CREB allowing for its translocation to the nucleus where it serves as a transcription factor for genes involved in survival and proliferation [73]. Similarly, high global $[Ca^{2+}]_i$ increases the activation of calcineurin, which dephosphorylates and thus activates NFAT, where it promotes transcription of genes involved in the immune response [72]. In this way, $[Ca^{2+}]_i$ handling patterns regulate gene expression and ultimately phenotype. This is referred to as excitation-transcription coupling.

Previously, my group has described paradoxical trends in CSM $[Ca^{2+}]_i$ handling alterations in swine models of MetS-induced CAD. Ca^{2+} influx after membrane depolarization and SERCA function have been found to both increase [74-76] ([77, 78] and decrease [79, 80] in disease. However, these studies used different breeds of swine that were fed an atherogenic diet for varying lengths of time with different comorbidities. My lab has recently resolved this discrepancy, elucidating the time-course of changes in

$[Ca^{2+}]_i$ handling during the progression of MetS-induced CAD. $[Ca^{2+}]_i$ handling alterations occur in a biphasic manner, with enhanced Ca^{2+} influx, SR Ca^{2+} store, and SERCA function occurring in early, mild disease that was diminished in late, severe disease [81]. While this CSM $[Ca^{2+}]_i$ handling alteration pattern has been established in MetS-induced CAD, the $[Ca^{2+}]_i$ handling alteration patterns of other etiologies of CAD have yet to be determined.

Coronary Artery Calcification

Coronary artery calcification (CAC) is the accumulation of hydroxyapatite crystals in the ECM, a process resembling endochondral bone formation [82, 83]. There are two main types of CAC: intimal calcification and medial calcification, also known as Monckeberg's sclerosis. Intimal calcification is associated with CAD and spotty calcification (microcalcification) increases plaque instability and rupture [84], while Monckeberg's sclerosis is associated with diabetes and chronic kidney disease and decreases vascular compliance [85]. These pathologies follow different mechanisms, so for this project I will focus on intimal calcification.

CAC is one of the most reliable predictors of future cardiovascular events, even in asymptomatic individuals [86, 87]. Individuals with CAC had a 4-10 times greater risk for a cardiac event [88]. The extent of CAC is usually correlated to the progression of CAD [84, 89]. In a seminal 1994 study by Fleckenstein-Grün and colleagues, it was found that vascular calcification increases in an exponential fashion throughout the progressive stages of atherosclerosis [90]. This relationship could be due to the close association of CAC with inflammation [82, 85, 86, 91-93], apoptosis [85, 86, 89, 93], oxidative stress [85, 86, 89], endoplasmic reticulum stress [89], hyperglycemia [84, 86, 94], and dyslipidemia [85, 89, 93], which are all also mechanistically linked with CAD progression. Indeed, the extent of CAC increases with the number of MetS risk factors, similar to CAD severity [10, 14, 95].

CSM cytodifferentiation is necessary for the initiation and progression of CAC [91, 96, 97]. When CSM dedifferentiate into a proliferative phenotype, the cells synthesize and secrete ECM proteins that serve as the nidus for vascular calcification [91, 96]. As stated previously, this proliferative phenotype is associated with increased basal cytosolic Ca^{2+} levels, VGCC activity, SR Ca^{2+} store, and SERCA function [75, 76, 81]. Continued stress signals such as cytokines and ROS in the cellular milieu contribute to further CSM dedifferentiation into an osteogenic phenotype [91, 93]. In this phenotype, certain osteogenic transcription factors like runt-related transcription factor 2 (Runx2), Sox9, and osterix promote the transcription of several genes that are normally expressed in bone, such as alkaline phosphatase (ALP), receptor activator of nuclear factor kappa-B ligand (RANKL), and osteocalcin [91, 98].

Osteogenic CSM contribute to CAC by the increased release of exosomes that contain calcifying cargo (Fig. 1.7) [82, 92]. Under physiological conditions, exosomes traffic cargo that includes minerals, lipids, proteins, calcification inhibitors, and miRNA between cells [99, 100]. This represents another avenue of cell-cell communication. However, in osteogenic CSM, exosome secretion is enhanced and its contents change to contribute to the vascular calcification process. Calcification inhibitors such as matrix Gla protein (MGP) and fetuin-A are downregulated, while calcification promotors such as annexins A2, A5, and A6, phosphatidylserine (PS), matrix metalloproteinase-2 (MMP-2), and hydroxyapatite crystals themselves ae upregulated [82, 92, 97, 99]. Furthermore, the miRNA content is modified to include more miRNA transcripts that promote continued expression of the osteogenic phenotype, contributing to prolonged CAC progression [100]. When exosomes from calcifying vascular smooth muscle cells from rats with chronic kidney disease were co-cultured with vascular smooth muscle cells from healthy littermates, the recipient cells experienced phenotypic switching to an osteogenic phenotype and increased calcification [96].

Enhanced exosome shuttling and pro-calcifying cargo are, at least in part, a result of altered $[Ca^{2+}]_i$ homeostasis. Calcifying exosomes have been identified in proliferative CSM, which exhibit higher basal $[Ca^{2+}]_i$ levels that may result from increased Ca^{2+} influx via VGCC, increased release from intracellular Ca^{2+} stores, or decreased Ca^{2+} efflux that is characteristic of this phenotype [75, 76, 96, 101]. A higher basal $[Ca^{2+}]_i$ level has been connected to the exosomal downregulation of calcification inhibitors and the enrichment of calcification promoters [97, 101]. This Ca^{2+} overload, especially upon switching to an osteogenic phenotype where Ca^{2+} handling alterations favor decreased Ca^{2+} buffering, leads to the increased release of calcifying exosomes. Chelation of intracellular Ca^{2+} and certain Ca^{2+} channel blockers such as verapamil and diltiazem have been found to block exosome shuttling and vascular calcification [90, 97]. Therefore, I can conclude that CSM phenotypic switching from a contractile phenotype to a proliferative and osteogenic phenotype and subsequent changes in $[Ca^{2+}]_i$ handling serve as the driver for vascular calcification via exosomes.

Ossabaw Miniature Swine

Ossabaw miniature swine were first introduced to a small island off the coast of Georgia in the 1500s by Spanish explorers [102]. Due to ecological barriers, the Ossabaw swine have been confined to the island where they have thrived for hundreds of years. A recent eradication effort has focused on this invasive species, but not before a subpopulation was transferred to a breeding colony at Indiana University to be used for biomedical research purposes [102].

Ossabaw swine exhibit a “thrifty genotype,” similar to humans, and thus have a propensity to develop all the risk factors associated with MetS when kept in captivity with a constant food supply, more so than any other swine model (Fig. 1.8, adapted from [103]; Table 1.1, adapted from [102]). Their size and cardiovascular anatomy and physiology are incredibly similar to humans, and Ossabaw have been found to develop diffuse, human-

like coronary plaques [80]. Ossabaw swine have been used as an animal model to successfully recapitulate MetS [103, 104], CAD [80, 81], CAC [105, 106], NAFLD [107-109], and other human cardiometabolic diseases [110-112].

Summary

The prevalence, severity, and cost of obesity, MetS, and CAD have plagued the United States and the world at large. Understanding how CSM $[Ca^{2+}]_i$ handling and homeostasis are altered in disease states is of utmost importance, as this divalent cation plays a role in a great number of cellular functions. This thesis work seeks to elucidate whether some major etiologies of CAD, including MetS, diabetes and aging, work through similar cellular mechanisms of $[Ca^{2+}]_i$ handling disruption to contribute to the common pathophysiology of CAD. I am particularly interested in SR Ca^{2+} store capacity, as SR Ca^{2+} store capacity and release are essential in Ca^{2+} signaling and homeostasis.

Major Hypotheses

1. SR Ca^{2+} store capacity is correlated with coronary smooth muscle cytodifferentiation and subsequent arterial remodeling in Ossabaw miniature swine models of different CAD etiologies.

2. Proliferative and osteogenic coronary smooth muscle cells will exhibit altered transcriptomic profiles and SR Ca^{2+} store capacity depending on disease progression.

3. CSM SR Ca^{2+} store capacity changes in humans with coronary artery disease (CAD) and heart failure are similar to those found in Ossabaw swine.

Figures

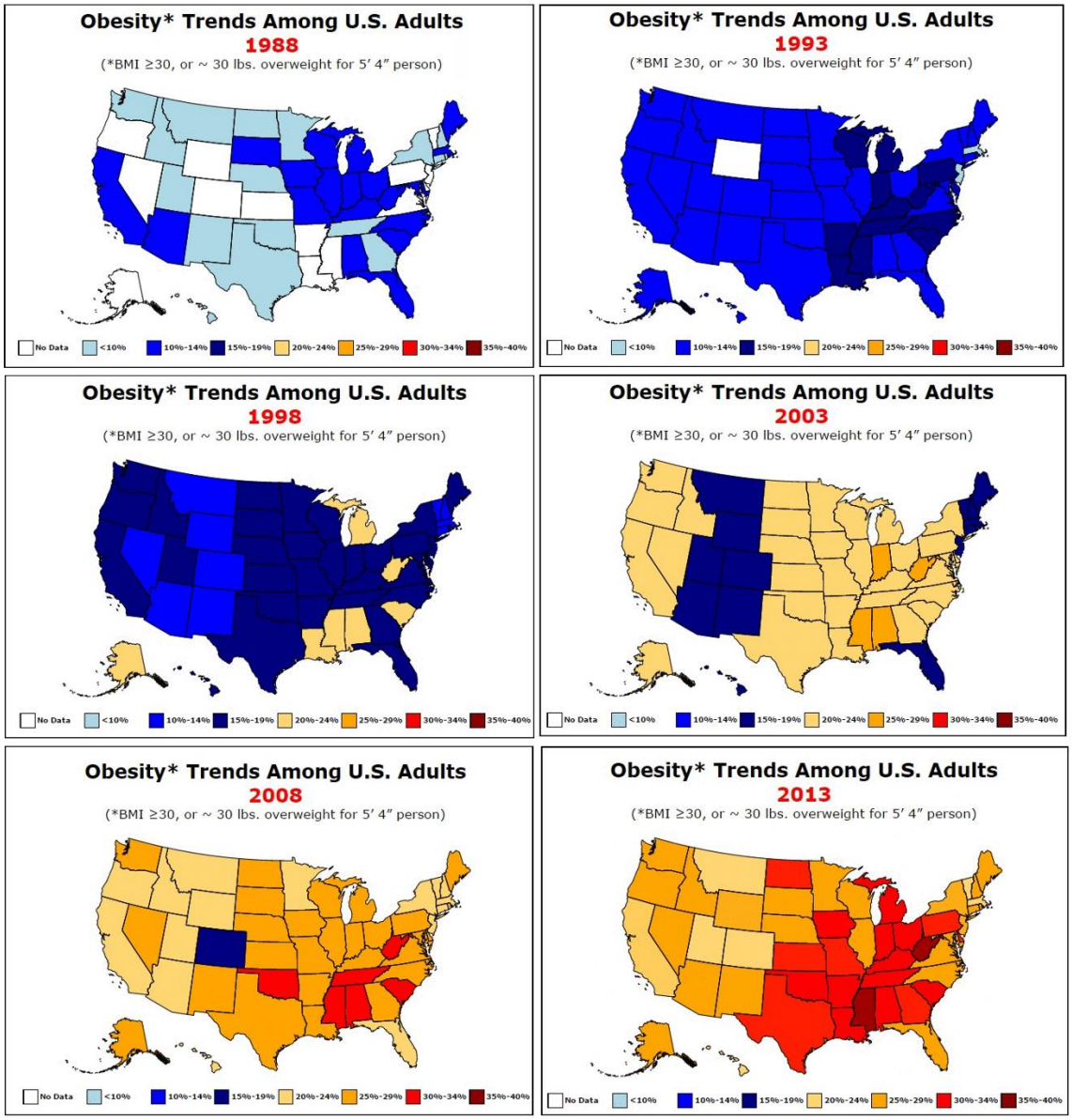

Figure 1.1: Obesity trends among U.S. adults. Over the past 25 years every state has seen a marked increase in the prevalence of obesity in the adult population. Figure adapted from [113].

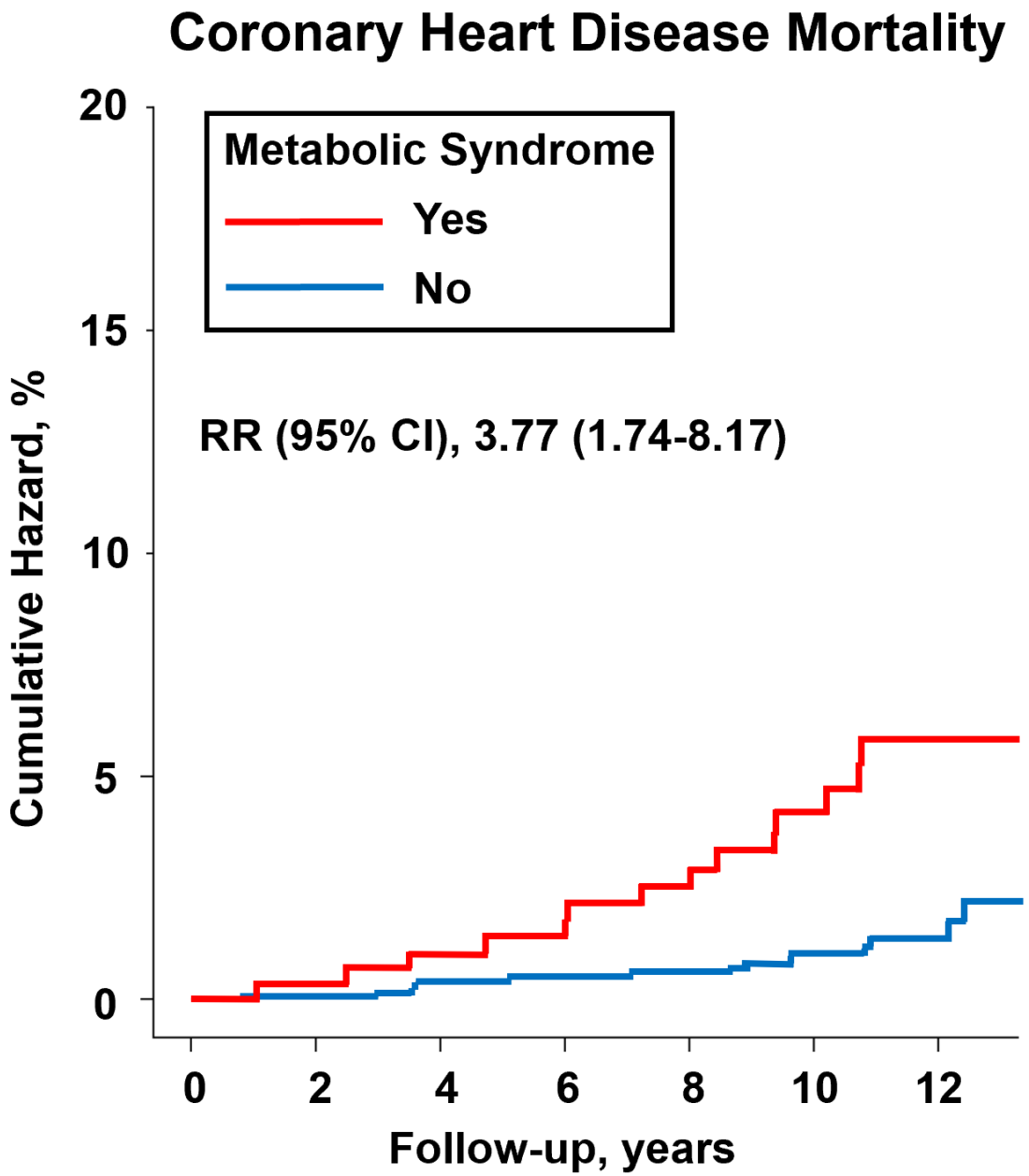

Figure 1.2: Presence of MetS increases a patient's risk of coronary heart disease mortality. A positive diagnosis of MetS has been shown to increase patient mortality due to cardiovascular events, even when adjusting for conventional cardiometabolic risk factors. Figure adapted from [10].

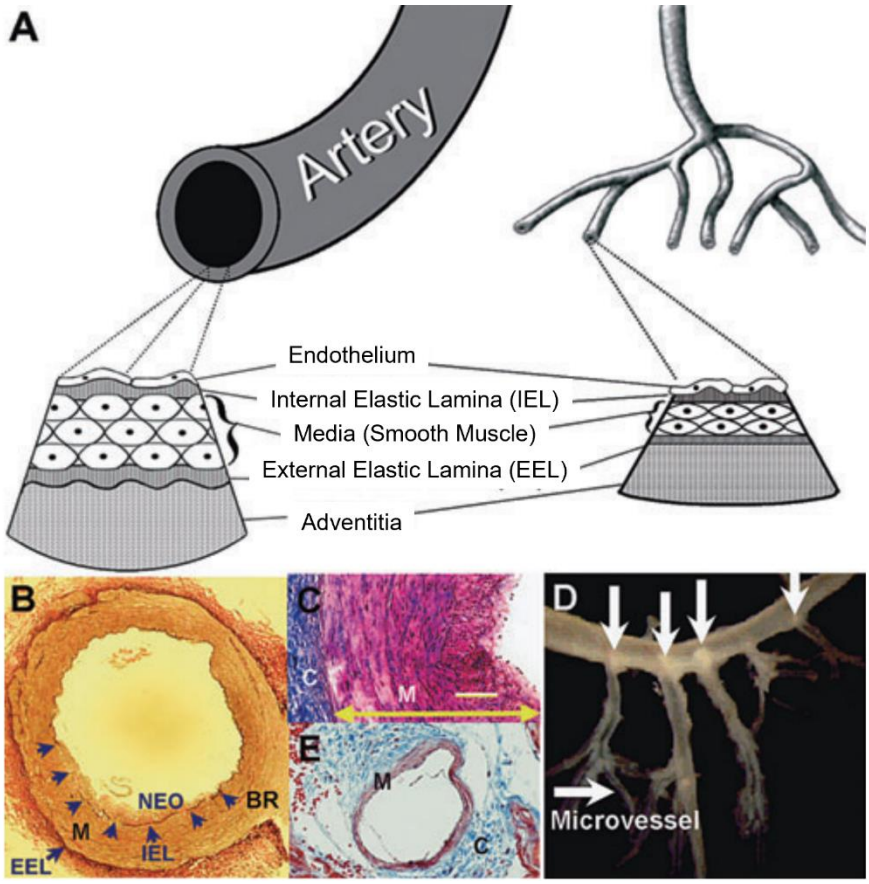

Figure 1.3: Histology of the vascular wall elucidates its structure. (A) Schematic representation shows that both conduit arteries (left) and resistance arterioles (right) have similar structure. The intima is shown as a single-cell layer of endothelial cells, the media contains smooth muscle cells, and the thickness of this layer is dependent on the size and function of the artery. The adventitia, composed of collagen and other extracellular matrix proteins, surrounds the artery. The arterial layers are separated by layers rich in elastin that give the arterial wall plasticity. The internal elastic lamina (IEL) separates the intimal and media layers, while the external elastic lamina (EEL) separates the media layer and the adventitia. (B) Verhoeff van Gieson's histological stain of a large conduit coronary artery shows the neointima (NEO), media layer (M), EEL, and IEL. A branch site (BR) can also be seen. (C) Masson's trichrome histological stain of a large conduit coronary artery shows smooth muscle (red) in the media (M, yellow double-headed arrow) and collagen

(c, blue) in the adventitia. There is also some positive collagen staining between smooth muscle cells in the media. (D) Arterial tree shows a large conduit artery branching into resistance arterioles, which then branch into microvessels. White arrows indicate sites of atheroma development, as visualized by the white “cotton ball-like” structures at the branch points. (E) Masson’s trichrome histological stain of a venule highlights the collagen (c, blue) in the adventitia and smooth muscle (red) in the media (M). Note the difference in media thickness and smooth muscle cell content between the arteries and this venule. Figure adapted from [16].

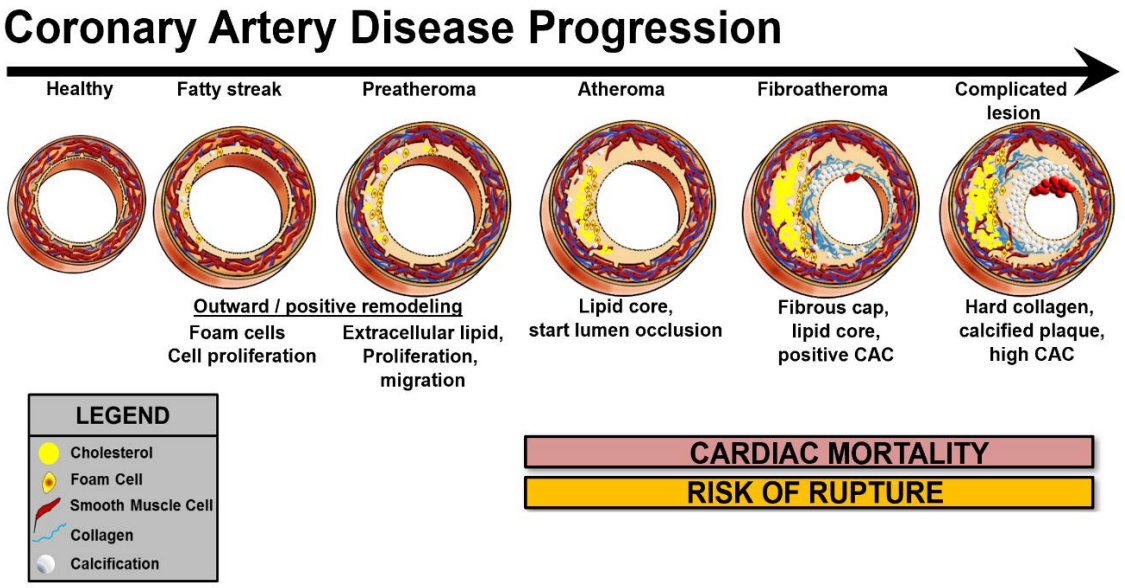

Figure 1.4: Progression of CAD. A healthy artery will have an intimal layer that is comprised of a single layer of endothelial cells. Initial endothelial dysfunction causes the overexpression of adhesion molecules that attract circulating macrophages which turn into foam cells when they engulf ox-LDL particles. This causes a fatty streak that can advance to a preatheroma, characterized by expansive smooth muscle cell proliferation and migration into a growing neointima layer along with foam cell accumulation. Atheromas accumulate cholesterol crystals and begin to occlude the artery. Smooth muscle synthesis and secretion of extracellular matrix proteins like collagen can form a fibrous cap, leading to a biomechanical stabilization of the plaque. Complicated lesions can contain a necrotic lipid core, thinning of the fibrous cap, and clinical occlusion. Vascular calcification in the form of hydroxyapatite deposition is usually readily apparent in complicated lesions, but recent evidence suggests this calcification process occurs in much earlier stages of plaque development [105]. Figure adapted from [17, 18, 114].

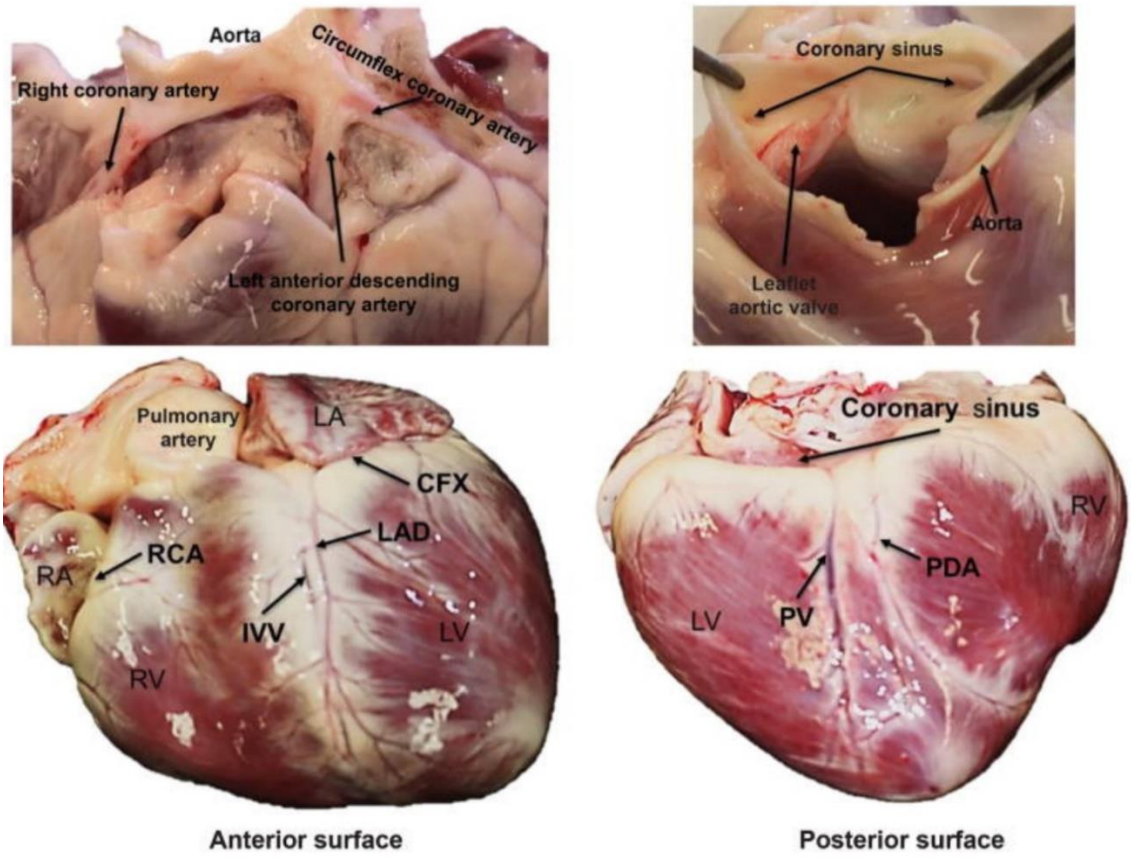

Figure 1.5: Anatomy of the coronary circulation. LA = Left atrium; CFX = Circumflex artery; LAD = Left anterior descending artery; LV = Left ventricle; IVV = Interventricular vein; RV = Right ventricle; RCA = Right coronary artery; RA = Right atrium; PV = Posterior vein; PDA = Posterior descending artery. Figure adapted from [19].

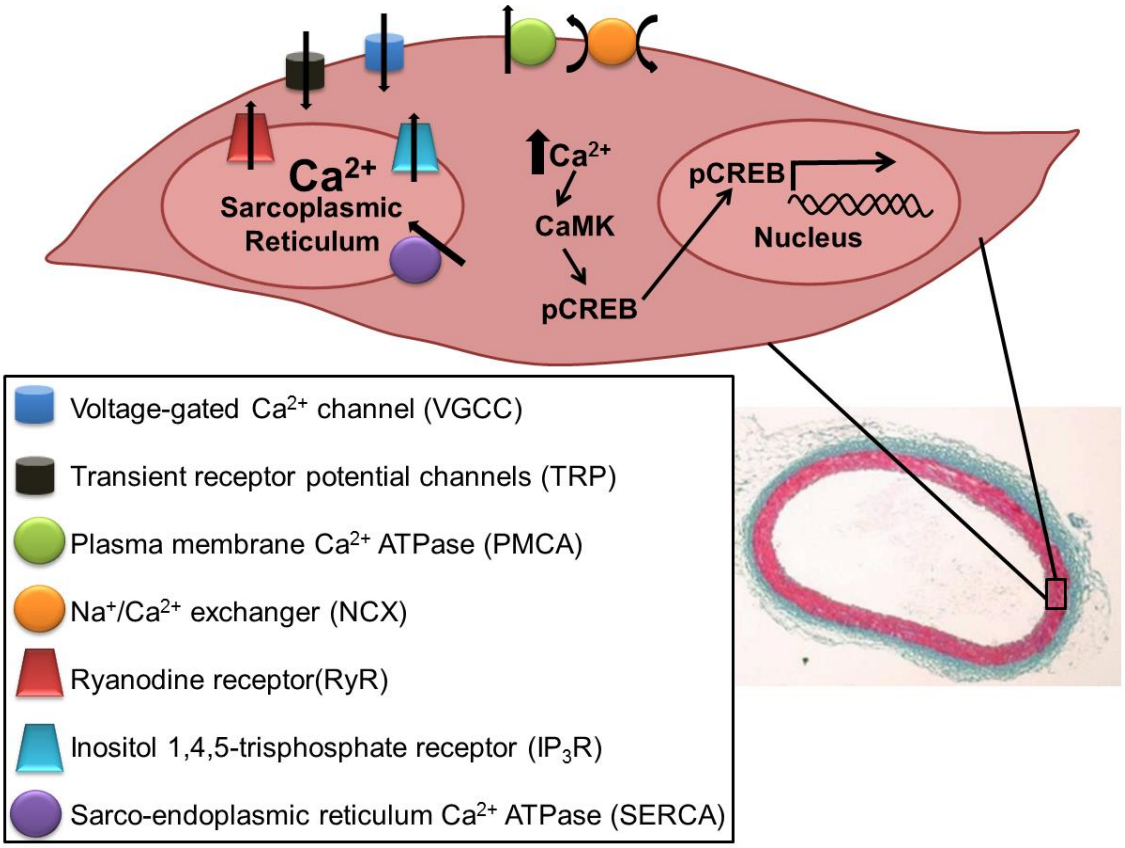

Figure 1.6: Calcium transporters in CSM. Ca^{2+} influx is accomplished with voltage-gated Ca^{2+} channels (VGCC) and transient receptor potential (TRP) channels. Intracellular Ca^{2+} can be sequestered into the sarcoplasmic reticulum (SR) via the sarco-endoplasmic reticulum Ca^{2+} ATPases (SERCA). Ca^{2+} release from the SR is accomplished through ryanodine receptors (RyR) and inositol 1,4,5-trisphosphate receptors (IP_3R). Ca^{2+} efflux is achieved through plasma membrane Ca^{2+} ATPases (PMCA) and sodium-calcium exchangers (NCX). Sustained $[Ca^{2+}]_i$ elevation can change gene expression through excitation-transcription coupling. For example, elevated $[Ca^{2+}]_i$ leads to increased Ca^{2+}/calmodulin binding, which activates Ca^{2+}/calmodulin-dependent protein kinase II (CaMK). CaMK phosphorylates the cAMP response element-binding protein (CREB), enabling its translocation to the nucleus where it serves as a transcription factor for genes involved in survival and proliferation.

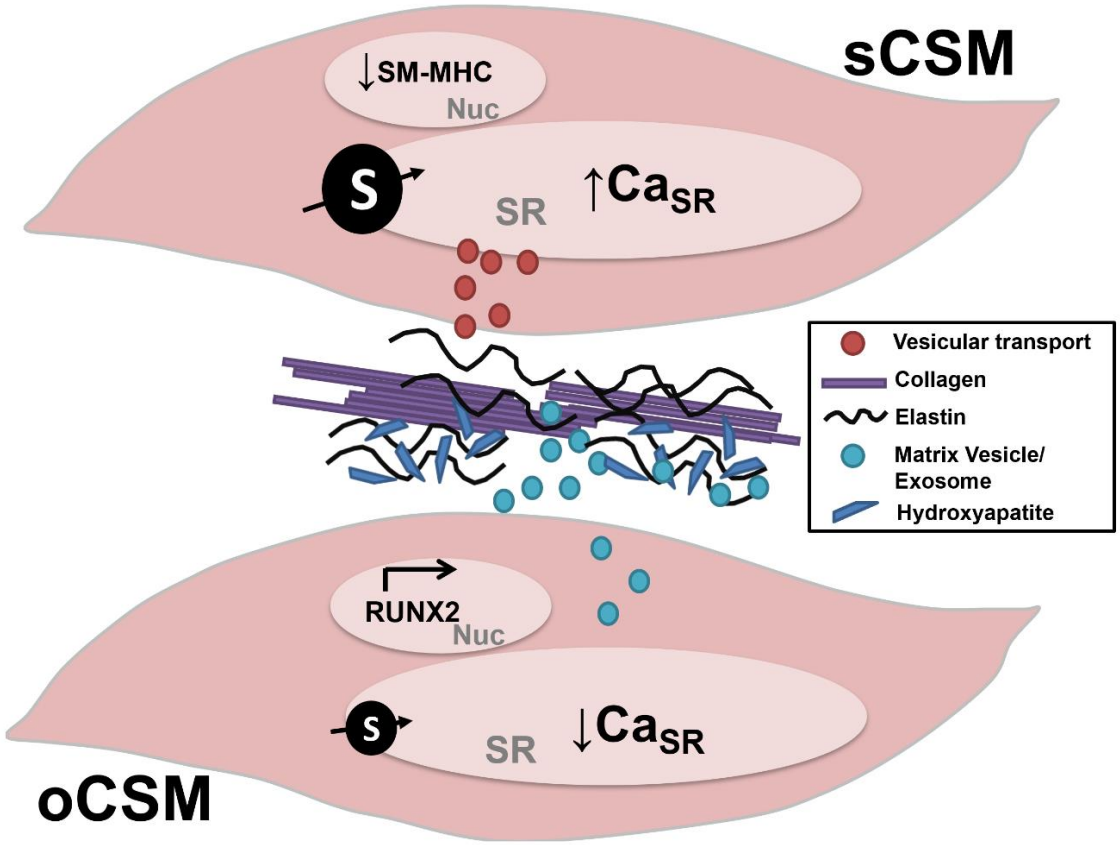

Figure 1.7: Vascular calcification requires CSM phenotypic switching. Synthetic CSM (sCSM) is associated with a decrease in contractile markers such as smooth muscle myosin heavy chain (SM-MHC), an increase in SERCA activity and SR storage capacity [81], and increased vesicle transport. sCSM also synthesize and secrete extracellular matrix proteins such as collagen and elastin that form the nidus for calcification. Osteogenic CSM (oCSM) is associated with an increased expression of osteo/chondrogenic genes such as Runx2, decreased SERCA activity and SR storage capacity [81], and an increase in calcifying exosome secretion. These calcifying exosomes deposit their cargo, which includes hydroxyapatite crystals and pro-calcifying proteins, on the newly-synthesized extracellular matrix, leading to vascular calcification.

Figure 1.8: Their "thrifty genotype" predisposes Ossabaw miniature swine to obesity. When given an atherogenic diet, Ossabaw swine reliably develop obesity and other risk factors for MetS, making these swine excellent models to study MetS-induced CAD. Figure adapted from [103].

Tables

Table 1.1: Comparison of MetS risk factors in Yucatan and Ossabaw swine†

Characteristic	Yucatan	Ossabaw	Reference
Obesity	No	Oss>Yuc	[74, 80, 103, 104, 107, 108, 110, 115-148]
Insulin resistance	No	Yes	[80, 103, 107, 110, 112, 116, 123-127, 130, 132, 133, 135, 137, 139, 141, 146, 148-153]
Glucose intolerance	No	Yes	[74, 76, 80, 103, 104, 107, 110, 112, 116, 117, 120, 121, 123-125, 127, 130, 132, 133, 135, 138, 141, 146, 147, 151-157]
Dyslipidemia (↑LDL/HDL)	Yes	Yes	[74, 76, 80, 103, 107, 112, 115, 116, 118, 121, 122, 124, 125, 132, 134-137, 145, 146, 148, 152, 155, 156, 158-161]
Dyslipidemia (↑triglycerides)	No	Yes	[77, 103, 107, 110, 112, 115, 116, 121-125, 130, 132, 135, 138, 146-148, 152, 153, 155, 157, 159, 161]
Hypertension	No	Yes	[74, 103, 104, 107, 115, 118, 121, 123-125, 127, 132, 135, 138, 146, 148, 151]

†Adapted from [102]

CHAPTER 2: ALLOXAN-INDUCED DIABETES EXACERBATES CORONARY ATHEROSCLEROSIS AND CALCIFICATION IN OSSABAW MINIATURE SWINE WITH METABOLIC SYNDROME

Background

Metabolic syndrome (MetS) affects more than one-third of all adults in the United States and is defined by the American Heart Association as the presence of three or more of the following conditions: central obesity, impaired glucose tolerance, hyperinsulinemia, dyslipidemia in the form of either elevated triglycerides or decreased HDL cholesterol, and hypertension [162]. MetS has been shown to be associated with increased risk of developing type 2 diabetes, which is rapidly increasing in incidence in the United States. Both type 2 diabetes and MetS are independently associated with increased risk of developing coronary heart disease, which continues to be the leading cause of death in the United States [162, 163].

Although studies on human subjects have consistently shown that diabetes exacerbates MetS-induced coronary artery disease (CAD) [14, 23, 25, 26, 164], studies in swine models have failed to reach a consensus regarding the effects of concurrent diabetes and MetS on CAD severity [157, 158, 165-168].

In this study, I further investigated the effects of diabetes in augmenting CAD in the Ossabaw miniature swine. The Ossabaw swine has been characterized as a clinically relevant animal model with the natural propensity to develop MetS, contributing to CAD without genetic manipulation due to their “thrifty genotype” that allows for excess fat storage [81, 102, 106-108, 114, 124, 169]. As these swine with diet-induced MetS develop diffuse, human-like plaques [80], I tested the hypothesis that CAD will be more severe in pigs with the comorbidity of diabetes as opposed to MetS alone. I also determined whether the pattern of impaired $[Ca^{2+}]_i$ handling in mild through advanced CAD/CAC is noted in MetS swine with diabetes. This will further strengthen the role of Ossabaw swine as a

clinically relevant animal model for investigating human CAD and studying the complex interplay between MetS and diabetes.

Methods

Animals and Induction of Diabetes

All experimental procedures involving animals were approved by the Institutional Animal Care and Use Committee at Indiana University School of Medicine with the recommendations outlined by the National Research Council and the American Veterinary Medical Association Panel on Euthanasia [170, 171]. Alloxan, a pancreatic beta cell toxin, was administered intravenously to Ossabaw miniature swine of mixed gender aged 4-7 months to induce diabetes. Briefly, alloxan (100-175 mg/kg; Sigma Chemical Co., St. Louis, MO) was dissolved in 14 mL of 1M NaOH and 20 mL of 0.9% NaCl, for a final volume of 34 mL and a pH of 7.4. The alloxan solution was delivered through a 0.20-μm sterile filter into the jugular vein via a central venous line. To protect against possible renal toxicity, animals were given 250 mL of 0.9% NaCl through intravenous drip prior to and after alloxan delivery (for full protocol, see Appendix A). The pigs were fed ad libitum and received 24 hours of critical care following induction of diabetes to monitor for hypoglycemic shock. Ossabaw swine responded heterogeneously to alloxan; therefore, pigs that did not incur sufficient beta cell damage with the first alloxan dose, as indicated by normoglycemia (fasting bG < 100 mg/dL), were administered a repeat dose (75-150 mg/kg) 48 hours after the initial dose. Swine were placed into two groups: non-responders that were normoglycemic (Metabolic Syndrome-Alloxan; MetS-A) and responders that were hyperglycemic, with a fasting blood glucose greater than 100 mg/dL (Metabolic Syndrome/Diabetic-Alloxan; MetS/D-A). All swine (n = 8 in each group) were fed a hypercaloric atherogenic diet for 6 months (1000-1350 g/day) consisting of 43% of total caloric intake from fat, 16% from protein, and 41% from carbohydrates. Swine in the MetS/D-A group received insulin glargine according to an algorithm previously published

in my lab [120] to maintain glycemic control below 300 mg/dL, a clinically relevant hyperglycemic level [172]. Full insulin therapy is outlined in Table 2.1. Food adjustment was included to prevent wasting syndrome, a common condition seen in diabetic animals [120, 173]. For healthy control, an additional subset of Ossabaw swine (Lean; n = 9) were fed a standard chow diet (1000 g/day) yielding 11% of the total caloric intake from fat, 18% from protein, and 71% from carbohydrates (5L80; Purina Test Diet, Richmond, IN). A fourth group of Ossabaw swine with diet-induced MetS, without alloxan exposure, was included for metabolic comparisons (MetS; n = 10). Body weight in all groups was monitored weekly.

Metabolic Phenotyping

Blood was collected pre-alloxan, post-alloxan, 3 months post-diet induction, and at time of sacrifice (6 months post-diet induction) for analysis (ANTECH Diagnostics, Fishers, IN).

Intravenous Glucose Tolerance Test

To assess pancreatic beta cell response to glucose, a 50% glucose solution (0.5 g/kg) was injected intravenously via the central venous line. To obtain fasting glucose concentration, blood samples (3 mL) were taken at –10, –5, and 0 min before glucose injection, then at 5, 10, 20, 30, 40, 50, and 60 min after glucose injection. Blood glucose values were monitored by use of an Accu-Chek Advantage glucose meter, and plasma insulin values were obtained by insulin assays done at the Indiana University School of Medicine Diabetes Research Core. A tail cuff was used to measure peripheral blood pressure throughout the procedure. MetS/D-A swine did not receive their daily insulin glargine injection on the day of testing.

Meal Tolerance Test

Pigs were given a standard meal (1000-1350 g chow) and allowed 45 minutes to eat the entire meal. Blood (3 mL) was sampled before administration of the meal (fasting)

and again at 1, 2, 5, 7, and 24 hours post-feeding. Blood glucose values were monitored by use of an Accu-Chek Advantage glucose meter. Eight lean swine and three swine in each the MetS, MetS-A, and MetS/D-A groups were used as a sampling group of the overall postprandial glucose clearance trend. MetS/D-A swine did not receive their daily insulin glargine injection on the day of testing.

Intravascular Ultrasound

After an overnight fast, swine were anesthetized via intramuscular injection of 2.2 mg/kg xylazine and 5.5 mg/kg Telazol (Fort Dodge Animal Health, Fort Dodge, IA). Swine were intubated and anesthesia was maintained with 2-4% isoflurane in 100% O_2. The isoflurane level was adjusted to maintain anesthesia with stable hemodynamics. Heart rate, aortic blood pressure, respiratory rate, and electrocardiographic data were continuously monitored throughout the procedure. Following a right femoral artery cut-down, a 7 F introducer sheath was inserted for access and heparin was administered (200 U/kg). Next, a 7 F guiding catheter (Amplatz L, Cordis, Bridgewater, NJ) was advanced to the left main coronary ostium. A 3.2 F, 45 MHz intravascular ultrasound (IVUS) catheter (Revolution, Volcano, Corp., Rancho Cordova, CA) was advanced over a percutaneous transluminal coronary angioplasty guide wire and positioned in the left anterior descending (LAD) artery. Automated IVUS pullback was performed and recorded at 0.5 mm/sec and 30 frames/second. Pigs were euthanized after the IVUS procedure via cardiectomy and coronary arteries were removed for further analysis. Still frame IVUS pullback images were obtained and analyzed offline at 1 mm intervals. Percent plaque burden and calcium index measures were obtained using ImageJ software (1.48v, National Institutes of Health, USA).

Immunohistochemistry

Sections from the tail of the pancreas were placed in 10% phosphate-buffered formalin for 24-48 hours then embedded in paraffin. Tissue sections were stained with

guinea pig anti-insulin ready-to-use polyclonal antibody (Agilent, Santa Clara, CA) as a marker for beta cells by the Department of Pathology at Indiana University School of Medicine (Indianapolis, IN). Images were captured using a Leica DM 3000 photomicroscope and analyzed with ImageJ software. Relative beta-cell mass was quantified by calculating the percentage of 3, 3' diaminobenzidine (DAB)-stained nuclear area to the total nuclear area using the ImmunoRatio ImageJ plugin.

Histology

Coronary artery segments from the proximal LAD (2-4 mm in length) were placed in 10% phosphate-buffered formalin for 24-48 hours, then transferred to 70% ethanol. Histology was performed in the Department of Anatomy and Cell Biology at Indiana University School of Medicine (Indianapolis, IN). All images were captured with a Leica DM3000 microscope connected to Leica Application Suites V4.1 software (Leica Microsystems GmbH, Wetzlar, Germany) and analyzed using (Adobe Photoshop® CS6) (for full protocols, see Appendices B, C, and D).

Intracellular Free Calcium Imaging

Whole-cell intracellular free Ca^{2+} levels were measured at room temperature (22 to 25 °C) by using the fluorescent Ca^{2+} indicator fura-2 AM (InCa++ Ca^{2+} Imaging System, Intracellular Imaging, Cincinnati, OH) as previously described [76, 80, 125, 174]. Briefly, freshly dispersed smooth muscle cells from the LAD were incubated with 3.0 μM fura-2 AM (Molecular Probes, Eugene, OR) in a shaking water bath at 37 °C for 45 min before being washed in a solution containing low Ca^{2+} concentration (for full protocol, see Appendix E). An aliquot of cells loaded with fura-2 AM was placed on a coverslip contained within a constant-flow superfusion chamber that was mounted on an inverted epifluorescent microscope (model TMS-F, Nikon, Melville, NY). Cells were superfused with various solutions at a constant rate of 1-2 mL/min, including solutions that contain 80 mM K^{+} to induce Ca^{2+} influx, 5 mM caffeine to induce sarcoplasmic reticulum store release,

and 2 mM barium to measure voltage-gated calcium channel activity (for solution recipes, see Appendix F). Fura-2 was excited by light from a 300 W xenon arc lamp that was passed through a computer-controlled filter changer containing 340 nm and 380 nm bandpass filters. The fluorescence emission at 510 nm was collected by using a monochrome charge-coupled device camera (COHU, San Diego, CA). Whole-cell fura-2 fluorescence was expressed as the 340 nm/380 nm ratio of fura-2 emission.

IVUS Analysis

The proximal 45 mm of the LAD was used for all IVUS analysis. All analysis was conducted by two blinded operators. To analyze for wall coverage, the circumference of the vessel cross-section was divided into 16 equal segments. Percent wall coverage was then calculated as: (total # of segments containing a thickened intimal layer ÷ 16) X 100. Wall coverage was quantified for the proximal 45 mm of the artery, in 1 mm intervals. To analyze for plaque burden, the external elastic lamina (EEL) area and lumen area were measured using ImageJ. Percent plaque burden was then calculated as: (EEL area - lumen area)/EEL area X 100. Plaque burden was quantified for the proximal 45 mm of the artery, in 1 mm intervals. To analyze for calcification, the entire IVUS pullback for the proximal 45 mm was viewed a minimum of two times. Calcification was defined as any strongly echogenic signal with acoustic shadowing. When identified, the frame numbers in which the deposit appeared and disappeared were noted to calculate the length. A representative frame of each deposit was used to calculate the arc angle using ImageJ, with each ray following the acoustic shadowing and the vertex at the center of the vessel lumen. If multiple deposits were identified per cross-section, the angles were added together. Calcium index for each artery was calculated as: (total length of calcification/ 45 mm) X (maximum arc angle/360^{o}) [175, 176].

Statistics

Statistical analysis was performed using GraphPad Prism 5.0 (San Diego, CA). Student's t-test, one-way analysis of variance (ANOVA) with Newman-Keuls post-hoc analysis, or two-way ANOVA with Bonferroni post-hoc analysis was performed. Data are represented as mean ± SEM. $p < 0.05$ was considered statistically significant.

Results

Ossabaw swine cardiometabolic characteristics

The swine in the MetS, MetS-A, and MetS/D-A groups were obese and had higher levels of total cholesterol compared to swine in the lean group (Table 2.2). The MetS/D-A group had greater total cholesterol and serum triglycerides than all other groups. The AST/ALT ratio was also increased in the MetS/D-A group as compared to the lean control, indicating possible liver dysfunction. However, there was no significant difference in creatinine and blood urea nitrogen (BUN) levels between the MetS/D-A and the lean groups, indicating normal kidney function (Table 2.2). Taken together, these metabolic data show that the MetS/D-A swine had more severe MetS than the other groups, despite being fed identical atherogenic diets.

Assessment of glucose clearance from a meal tolerance test

Blood glucose was monitored 7 hours after administration of a meal and revealed that blood glucose measurements were significantly higher in the MetS-A and MetS/D-A swine when compared to lean swine (Fig. 2.1A). This is further supported by area under the curve analysis, which shows that MetS-A swine exhibit postprandial hyperglycemia as compared to the MetS and lean group, and this hyperglycemia is exacerbated in the MetS/D-A swine (Fig. 2.1B).

Assessment of glucose clearance from an intravenous glucose tolerance test

Blood glucose was monitored 60 minutes after intravenous administration of a bolus of glucose and revealed that blood glucose measurements were significantly higher

in the MetS, MetS-A, and MetS/D-A groups when compared to the lean group (Fig. 2.2A). However, while area under the curve analysis revealed that the MetS, MetS-A, and MetS/D-A groups had impaired glucose clearance when compared to the lean control group (Fig. 2.2B), only the MetS/D-A swine exhibited a higher fasting blood glucose over lean (Fig. 2.2C).

Assessment of serum insulin levels during the intravenous glucose tolerance test

Serum levels of insulin were measured during IVGTT (Fig. 2.3A). All swine groups except MetS/D-A showed a robust insulin peak at 20 minutes after the glucose bolus (Fig. 2.3A). Area under the curve analysis revealed that MetS/D-A swine exhibit hypoinsulinemia compared to the lean, MetS, and MetS-A groups (Fig. 2.3B).

Assessment of pancreatic beta cell mass

Although the MetS-A swine did not exhibit postprandial or fasting hyperglycemia (Figs. 2.1B and 2.2C) or significant hypoinsulinemia (Fig. 2.3B), they show a decrease in pancreatic beta cell area compared to lean, non-alloxanized swine (Fig. 2.4). MetS/D-A swine show an even greater decrease in beta cell mass (Fig. 2.4), which is reflected in their postprandial and fasting hyperglycemia and their hypoinsulinemia (Figs. 2.1B, 2.2B-C, and 2.3B).

IVUS assessment of coronary artery disease severity

After angiography was employed to locate the LAD and circumflex (CFX) coronary arteries for catheter placement (Fig. 2.5A), cross-sectional images of the arteries were collected by automated IVUS pullback (representative IVUS still frames in Fig. 2.5B-C). MetS-A swine exhibited greater percent wall coverage compared to lean swine, while MetS/D-A swine exhibited greater percent wall coverage compared to both lean and MetS-A swine (Fig. 2.5D). Additionally, MetS/D-A swine exhibited greater percent plaque burden compared to lean and MetS-A swine (Fig. 2.5E). These data suggest that MetS/D-A swine have greater CAD severity than the lean and MetS-A groups.

IVUS assessment of coronary artery calcification (CAC)

CAC was measured both by calculating the calcium index from IVUS images (Fig. 2.6A) and from Von Kossa histological staining (Fig. 2.6B). Most calcified lesions were determined to be spotty calcification. MetS/D-A swine had a significantly greater IVUS-derived calcium index than lean and MetS-A swine (Fig. 2.6C). The IVUS-derived measures show strong positive correlation to the percent calcification values calculated from histological analysis (Fig. 2.6D). These data are strong evidence that MetS/D-A swine have more severe CAC compared to the lean and MetS-A groups.

Assessment of effects of diabetes on CSM $[Ca^{2+}]_i$ regulation

Figure 2.7A-B shows representative $[Ca^{2+}]_i$ responses from a CSM cell isolated from a lean swine. I assessed the caffeine-sensitive SR store release in the absence of extracellular Ca^{2+} to measure the sarcoplasmic reticulum (SR) storage capacity. The MetS-A swine had an elevated SR store that was diminished to control levels in the MetS/D-A swine (Fig. 2.7C). The time to half recovery to baseline was higher in the MetS/D-A swine, indicating impaired plasmalemmal $[Ca^{2+}]_i$ extrusion mechanisms (Fig. 2.7D). When voltage-gated calcium channel (VGCC) activity was assessed using a Ba^{2+} challenge, CSM cells from MetS-A swine exhibited an increased Ba^{2+} influx rate and net accumulation of Ba^{2+}, but this decreased to lean control levels in the MetS/D-A swine (Fig. 2.7E). These data suggest that CSM $[Ca^{2+}]_i$ is different in animals with the comorbidities of MetS and diabetes compared to animals with only MetS.

Discussion

There is a pressing need to establish an animal model for the common comorbidities of MetS and diabetes. This study shows for the first time that Ossabaw swine, which are a clinically relevant animal model already utilized for the study of MetS [103, 104], CAD [80, 81], CAC [106, 114], non-alcoholic steatohepatitis [107-109], and

other diseases [110, 112], can be used to study MetS/diabetes and the complications and mechanisms associated with those comorbidities.

Using metabolic analyses such as IVGTTs, MTTs, and insulin assays, as well as immunohistochemistry to determine pancreatic beta cell damage, I show that alloxan treatment induced a diabetic state, as defined as fasting hyperglycemia and hypoinsulinemia. Furthermore, using *in vivo* intravascular ultrasound imaging I show that MetS swine with alloxan-induced diabetes had increased circumferential wall coverage, plaque burden, and calcium index compared to swine with MetS alone.

While this study determined that diabetes exacerbates MetS-induced CAD in a clinically relevant porcine model, it does not delve into the mechanisms that drive this accelerated atherosclerosis. It has been reported that hyperglycemia can contribute to a dyslipidemic state by producing circulating advanced glycation end-products (AGEs) that bind lipoproteins and delay their clearance [177], generate intracellular ROS [178], and increase expression of adhesion molecules [178, 179]. Chronic high levels of glucose can also lead to mitochondrial dysfunction, resulting in increased superoxide production which, in turn, increases inflammation and ox-LDL levels [179, 180]. All these metabolic and transcriptional changes lead to the acceleration of the atherosclerotic process. Diabetes and dyslipidemia are often comorbidities due at least in part to this mechanism, and diabetic patients are at a much greater risk for developing cardiovascular diseases [179, 181].

Recently, much attention has been given to the diseased vessel's paracrine effects on surrounding tissues. For example, inflammation in the vasculature results in smaller, de-differentiated adipocytes around the plaque area [35]. In fact, the cross-talk between perivascular adipose tissue (PVAT) and the diseased vasculature is a growing field that has generated great interest [182]. My group has showed that PVAT potentiates leptin-induced endothelial dysfunction and increases vasomotor tone in coronary arteries of

Ossabaw swine [136, 138]. Ossabaw swine can be used as a clinically relevant animal model for future studies delving into the mechanisms responsible for this bidirectional communication.

While IVUS is a robust method for determining plaque morphology *in vivo*, it cannot determine plaque composition. Future studies should investigate whether plaque morphology changes in the presence of diabetes. This is of particular interest, as diabetes is associated with plaques that are more vulnerable to rupture [183]. Intravascular photoacoustic ultrasound includes morphological imaging and has chemical specificity to determine lipid content inside atherosclerotic plaque [70, 184-186]. This advancement will enable longitudinal characterization of plaque composition *in vivo* during progression of coronary atherosclerosis and calcification [70].

Ca^{2+} is an important second messenger that plays a vital role in contraction [68, 187], proliferation [68, 70], migration [184, 185], and transcription [186, 188]. Recently, my lab has clarified that CSM $[Ca^{2+}]_i$ handling dysfunction occurs in a biphasic manner during CAD progression, with SR Ca^{2+} store capacity and sarco-endoplasmic reticulum Ca^{2+} ATPase (SERCA) function being upregulated in early, mild CAD and downregulated in late, more severe CAD [81]. Additionally, it has previously been shown that plasmalemmal Ca^{2+} extrusion mechanism function, as measured by the time to half recovery, is decreased in advanced disease [76]. These Ca^{2+} handling alterations can be seen in CSM from MetS-A swine, which exhibited changes associated with mild CAD, and in CSM from MetS/D-A swine, which exhibited changes associated with more severe CAD.

Increased VGCC and SERCA function are associated with greater CSM proliferation [81]. While the MetS-A swine had increased VGCC and SERCA function, they only exhibited greater percent wall coverage compared to lean swine. MetS/D-A swine exhibited both greater percent wall coverage and percent plaque burden, even though their VGCC and SERCA activity was comparable to lean swine. This could be due to the

severity of the metabolic conditions, which is proportional to the duration of MetS. The MetS/D-A swine could have exhibited a longer period of CSM proliferation before VGCC and SERCA activity decreased back down to baseline, while the MetS-A swine were still undergoing proliferation at the time of euthanasia. Future studies should investigate the effect of the diabetic state on CSM proliferation.

High serum Ca^{2+} and phosphorous may contribute to the increased CAC seen in the MetS/D-A swine [101]. However, serum Ca^{2+} is not significantly elevated when compared to the lean swine and, while serum phosphorous is elevated in the MetS/D-A swine, it is still comparable to the MetS-A group. Therefore, the greater CAC seen in the MetS/D-A group cannot be contributed to the uremic milieu alone. It is hypothesized in several papers that impairments in $[Ca^{2+}]_i$ buffering can lead to Ca^{2+} overload and subsequent vascular calcification [101, 189]. The changes in SERCA and VGCC function and the dysfunction seen in the calcium extrusion mechanisms, which include the sodium-calcium exchanger and the plasma membrane calcium ATPase, could lead to the increased calcification seen in histology and IVUS analysis. However, even though MetS/D-A swine have impaired Ca^{2+} extrusion mechanisms, they only exhibit spotty calcification. Calcification is “spotty” if the arc of calcium is less than 90 degrees [176]. Spotty calcification has been reported to destabilize atherosclerotic plaques and increase the incidence of acute myocardial ischemia [190, 191]. Therefore, although spotty calcification is a precursor to macrocalcification, it has serious clinical implications [192]. Future studies should focus on $[Ca^{2+}]_i$ dysregulation and vascular calcification in diabetic swine fed an atherogenic diet for a longer period of time.

Overall, I found that MetS swine with alloxan-induced diabetes had greater CAD severity and calcium handling that was indicative of severe CAD while normoglycemic MetS swine showed less severe CAD and calcium handling that was indicative of mild

CAD. This mirrors the patterns seen in human studies [14, 23, 25, 26, 164] and establishes Ossabaw swine as a relevant animal model for MetS/diabetes.

There is no shortage of literature investigating the role of diabetes in exacerbating CAD in the context of MetS in swine models. However, there have been conflicting results in these studies. Gerrity *et al.* showed that diabetic/hyperlipidemic Yorkshire pigs developed more stenotic and advanced atherosclerotic lesions, compared to the nondiabetic/hyperlipidemic control group [165]. Additionally, my group has shown that the induction of diabetes in Sinclair and Yucatan miniature pigs with hyperlipidemia leads to increased CAD development [167]. In contrast, a recent study by Al-Mashhadi *et al.* showed that Yucatan minipigs with a PCSK9 gain-of-function mutation developed severe hyperlipidemia, but no augmentation of CAD with the induction of diabetes by streptozotocin (STZ) [166]. However, because of the dramatic effect increase in LDL cholesterol levels and subsequent CAD development in this transgenic model, it is unclear if a contribution of hyperglycemia to atherogenesis was present, but masked by the severity of disease. Ludvigsen *et al.* showed that diet-induced atherosclerosis in Gottingen minipigs was not augmented by STZ-induced diabetes, but the sample size in this study (n = 6) was not large enough to be conclusive [168]. Interestingly, another study from my group found that in Yucatan swine diabetes without dyslipidemia was not enough to increase early atheroma [157]. This study also showed that hyperlipidemic diabetic swine did not exhibit greater CAD severity than swine with hyperlipidemia alone [157]. This may have been because of the large effect of plasma lipids that nullified the synergistic effects of diabetes.

None of the previously mentioned studies used Ossabaw miniature swine, for which there is remarkably similarity to human MetS and CAD [80]. Ossabaw swine develop more severe CAD with diabetes on a MetS background, which is similar to results seen in human patients. Thus, this study provides support for Ossabaw swine as an

excellent model for translation to human clinical medicine. Taken together, the data in this study provide evidence supporting the use of Ossabaw swine in future studies that investigate mechanisms or outcomes of diabetes superimposed on a MetS background. By having a reliable, clinically relevant animal model that recapitulates human disease researchers can be far more certain of the translatability of their research.

Conclusion

In conclusion, swine exhibiting both MetS and alloxan-induced diabetes have more severe CAD and coronary artery calcification when compared to swine with only MetS as measured by IVUS. Additionally, coronary smooth muscle from swine with MetS alone show similar calcium handling alterations as mild CAD, and swine with both MetS and diabetes show similar calcium handling alterations as more severe CAD. Ossabaw swine, similar to humans, reliably develop more severe CAD with the comorbidities of diabetes and MetS, which supports their use as a clinically relevant animal model for future studies investigating the mechanisms of diabetes superimposed on a MetS background.

Figures

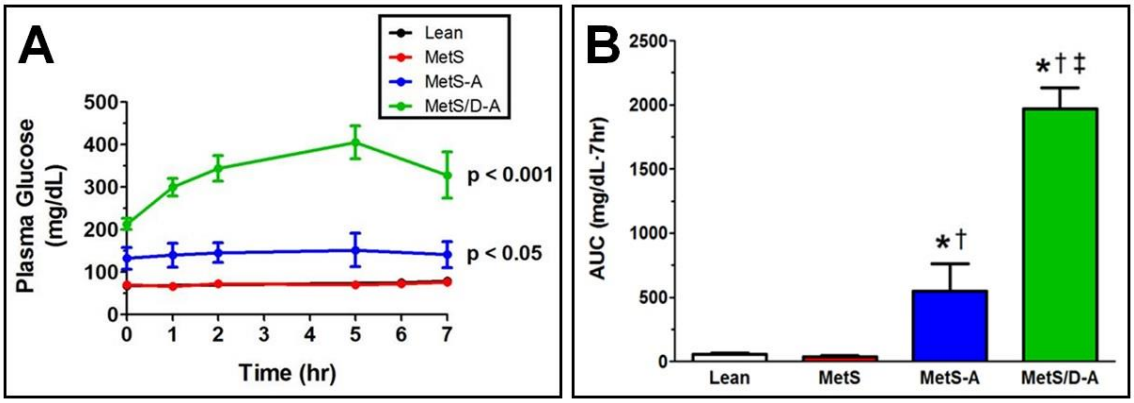

Figure 2.1: Impaired glucose clearance after a meal tolerance test in MetS/D-A swine. (A) Plasma glucose was monitored for 7 h after a meal, which revealed the lean and MetS group had comparable glucose clearance and the MetS/D-A group had impaired glucose clearance. p values are compared to lean group. (B) Area under the curve analysis shows postprandial hyperglycemia in the MetS/D-A swine as compared to all other groups. *$p < 0.05$ compared with lean swine; †$p < 0.05$ compared with MetS swine; ‡$p < 0.05$ compared with MetS-A swine. (Lean = 8; MetS = 3; MetS-A = 3; MetS/D-A = 3.)

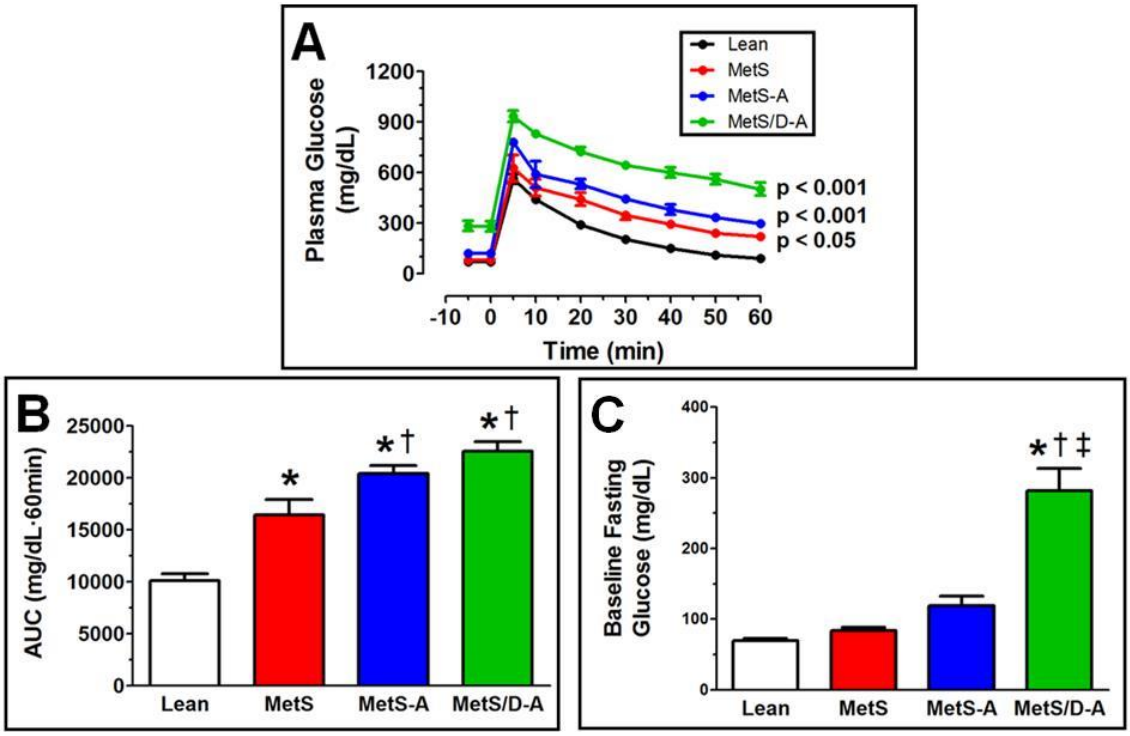

Figure 2.2: IVGTT supports the conclusion that MetS/D-A swine exhibit impaired glucose clearance. (A) Blood glucose levels were tested for 60 min after a bolus of glucose (0.5 mg/kg body weight). p values are compared to lean group. (B) Area under the curve analysis shows impaired glucose clearance in the MetS-A and MetS/D-A groups. (C) MetS/D-A swine exhibited a fourfold higher fasting blood glucose before the bolus of glucose was administered. *p < 0.05 compared with lean swine; †p < 0.05 compared with MetS swine; ‡p < 0.05 compared with MetS-A swine. (Lean = 10; MetS = 5; MetS-A = 8; MetS/D-A = 8.)

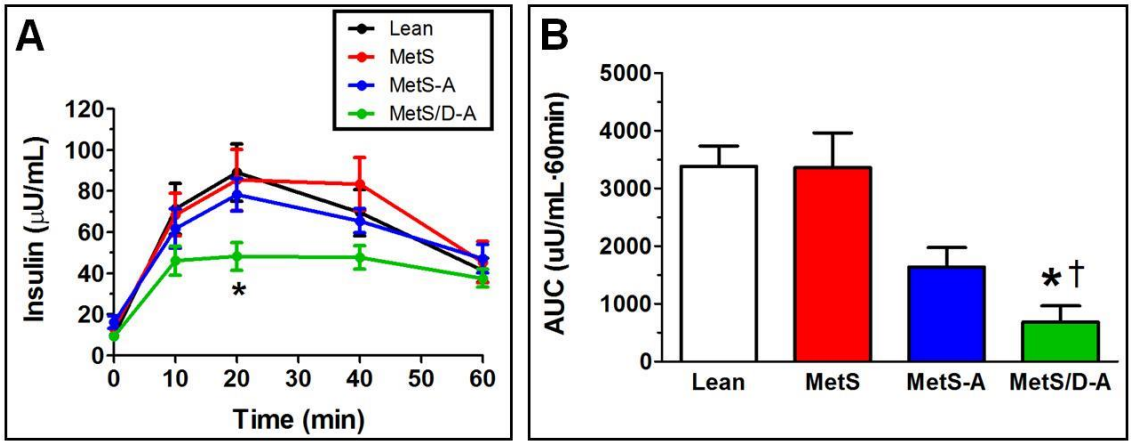

Figure 2.3: Serum insulin levels were lower in the MetS/D-A group than in the MetS-A group. (A) Insulin levels were measured at minutes 0, 10, 20, 40, and 60 during the IVGTT protocol. (B) Area under the curve analysis revealed that MetS/D-A swine exhibited hypoinsulinemia as compared to the swine in the lean and MetS groups. *$p < 0.05$ compared with lean swine; †$p < 0.05$ compared with MetS swine. (Lean = 10; MetS = 5; MetS-A = 8; MetS/D-A = 8.)

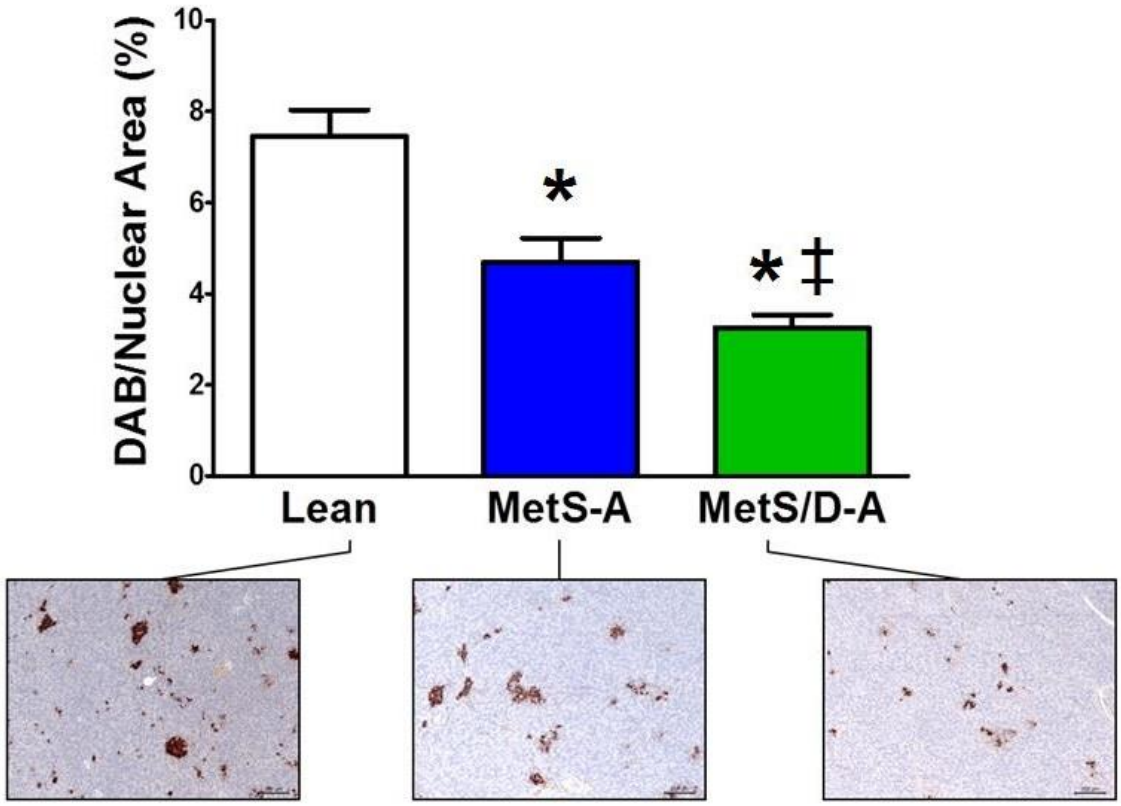

Figure 2.4: IHC shows diminished pancreatic beta cell mass in MetS-A and MetS/D-A swine. Immunohistochemical analysis using antibodies against insulin revealed that beta cell mass was decreased in MetS-A swine as compared to lean swine, and even less in MetS/D-A swine. Taken together, these data show that swine in the MetS/D-A group were indeed diabetic, due to alloxan-induced beta-cell damage. *$p < 0.05$ compared with lean swine; ‡$p < 0.05$ compared with MetS-A swine. (Lean = 7; MetS-A = 7; MetS/D-A = 8.)

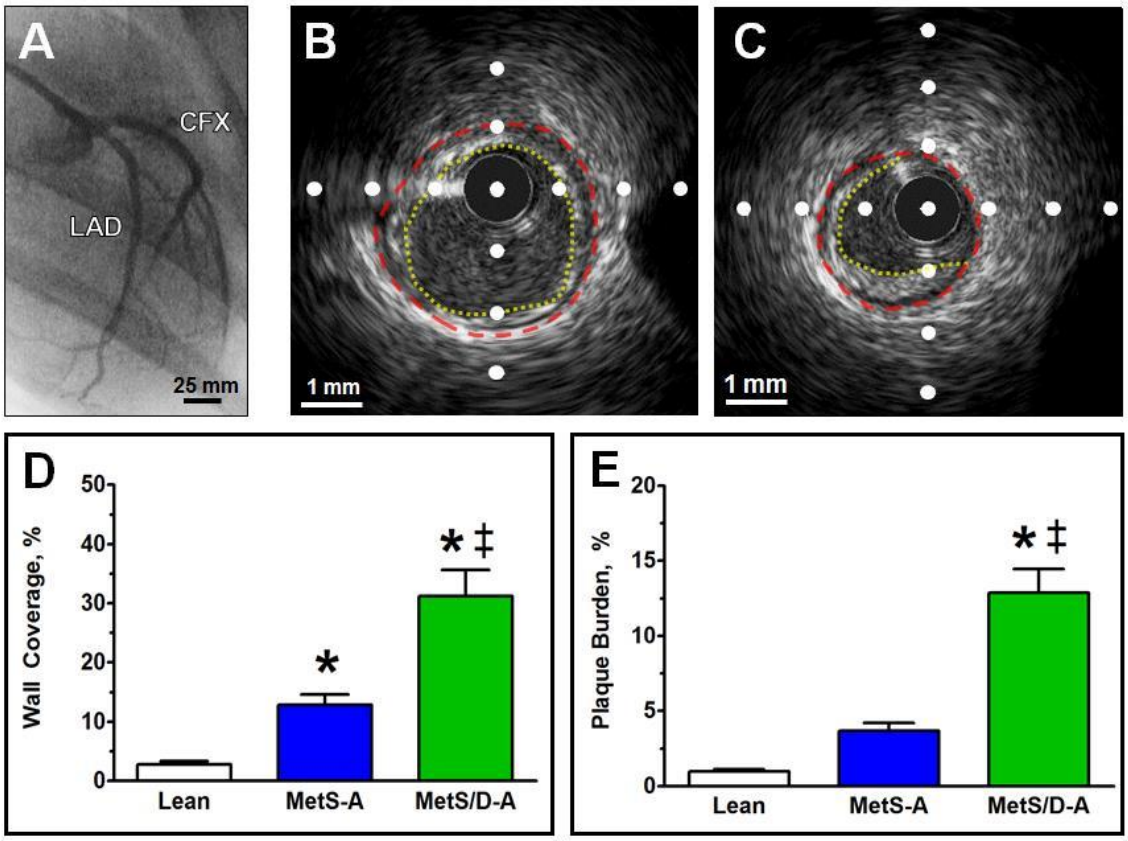

Figure 2.5: MetS/D-A swine had more advanced disease than lean and MetS-A swine. (A) Angiogram showing the LAD and CFX coronary arteries. All IVUS still frames collected for analysis were from the proximal 45 mm of the LAD. (B) Representative IVUS image of the LAD of a MetS/D-A swine showing 100% wall coverage, the percent of the circumference of the arterial wall covered by intimal thickening (original lumen highlighted in red, intimal thickening highlighted in yellow). (C) Representative IVUS image of the LAD of a MetS/D-A swine illustrating plaque burden, the percent of original lumen that is now occupied by a lesion (original lumen highlighted in red, new lumen with lesion highlighted in yellow). (D) The MetS/D-A swine had significantly greater wall coverage compared to MetS-A and lean swine. (E) The MetS/D-A swine had significantly greater plaque burden, compared to MetS-A and lean swine. *$p < 0.05$ compared with lean swine; ‡$p < 0.05$ compared with MetS-A swine. (Lean = 6; MetS-A = 7; MetS/D-A = 7.)

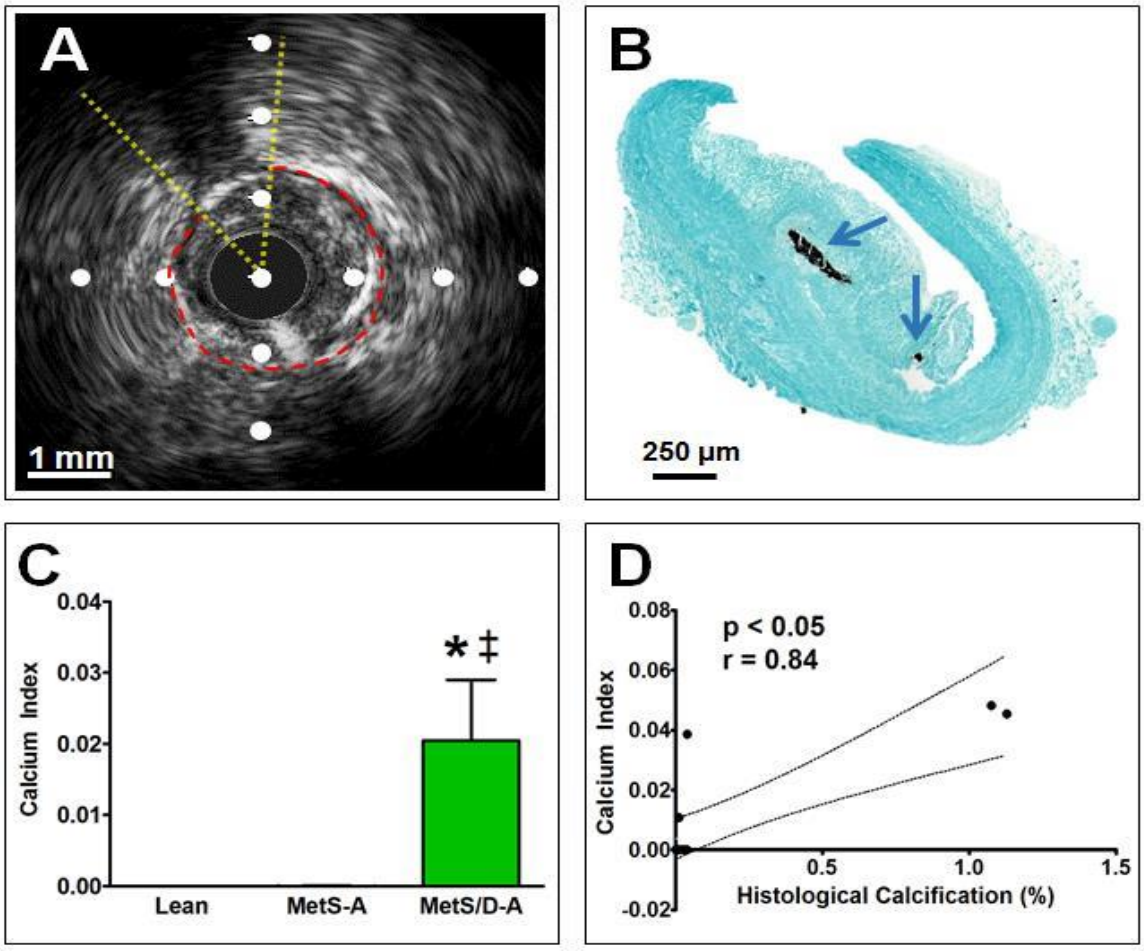

Figure 2.6: MetS/D-A swine showed greater spotty calcification compared to lean swine and MetS-A swine. (A) Representative IVUS image from the proximal LAD of a MetS/D-A swine. IVUS images were analyzed for calcification severity by using the calcium index measurement. The lumen is outlined in red, with the arc of spotty calcification and acoustic shadowing outlined in yellow. (B) Representative Von Kossa-stained histological section from the proximal LAD of a MetS/D-A swine, with noticeable spotty calcification in the neointimal layer (blue arrows). (C) Calcium index is higher in MetS/D-A swine as compared to lean and MetS-A swine. (D) Findings from analysis of IVUS data correlate to the Von Kossa histological staining analysis. *$p < 0.05$ compared with lean swine; ‡$p < 0.05$ compared with MetS-A swine. (Lean = 6; MetS-A = 7; MetS/D-A = 7.)

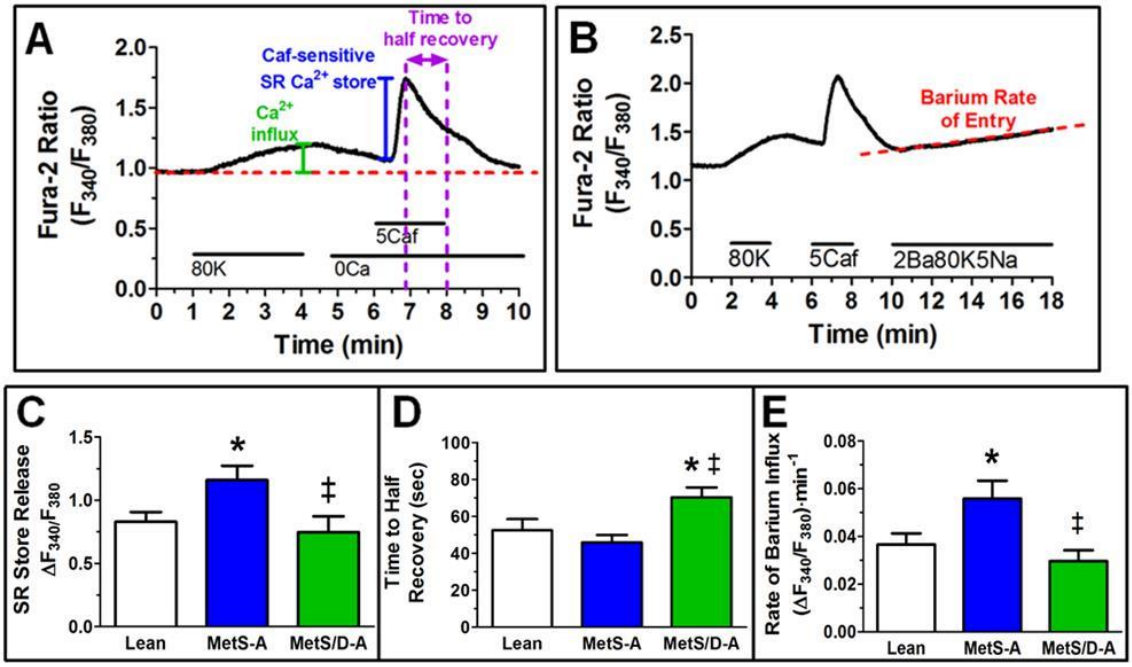

Figure 2.7: MetS-A swine showed greater SR store and VGCC function compared to lean and MetS/D-A swine. (A) After depolarization with 80 mM K^+ to induce calcium influx and maximal SR Ca^{2+} loading, the SR store was released by activating RyR with 5 mM caffeine. The time to half signal recovery was measured during caffeine wash-out and corresponds to the activity of calcium extrusion mechanisms. (B) A similar protocol was used with an additional exposure to a 2 mM barium solution, which enters the cell via VGCC and binds to fura-2 but is not transported by Ca^{2+} ATPases, providing a more selective measure of Ca entry. (C) The measured SR store release from CSM in MetS-A swine is greater than that seen in MetS/D-A and lean swine. This is consistent with previous findings which show biphasic calcium handling alterations in CSM as CAD progresses in severity. (D) Extrusion mechanism activity as measured by time to half recovery is impaired in MetS/D-A swine. (E) The activity of voltage-gated calcium channels as measured by barium influx is increased in CSM from MetS-A swine and decreases back to baseline in CSM from MetS/D-A swine. *p < 0.05 compared with lean swine; ‡p < 0.05 compared with MetS-A swine. (Lean = 6; MetS-A = 8; MetS/D-A = 8.)

Tables

Table 2.1: Insulin therapy and feed algorithms for the maintenance of blood glucose and weight gain

Measurements			**Adjustments**	
Blood glucose (mg/dL)	**Behavior**	**Body weight (kg)**	**Insulin glargine (U)**	**Food (by weight)**
> Diabetic target range of 120–200	Normal		Base + 0.1 U/kg	No change
> Diabetic target range of 120–200	Lethargic		Base + 0.2 U/kg	No change
120–200	Normal		Base (0.1–0.3 U/kg)	No change
< Diabetic target range of 120–200	Normal		Base (0.1–0.3 U/kg)	Increase 15%
< Diabetic target range of 120–200	Lethargic		Base (0.1–0.3 U/kg)	Increase 15%
		Decrease >5% in one week	Base + 1 U/kg	Increase 30%
		Less than target weight gain at weeks 4, 8, 12, 16, 20	No change	Increase 15%
		Increase >10% in 1 week	No change	Decrease 15%
		>10% over target weight gain at weeks 4, 8, 12, 16, 20	No change	Decrease 15%

Table 2.2: Metabolic characteristics of swine show hyperlipidemia and hyperglycemia in the MetS/D-A group

	Lean	MetS	MetS-A	MetS/D-A
Body weight at sacrifice (kg)	48 ± 2	87 ± 5*	73 ± 1*,†	70 ± 4*,†
Age at sacrifice (mo)	17 ± 1.4	15 ± 0.7	11 ± 0.2	14 ± 0.1
% Male	37.5	50	50	50
Creatinine (mg/dL)	0.96 ± 0.05	1.26 ± 0.13*	1.14 ± 0.07	1.06 ± 0.10
BUN (mg/dL)	14.33 ± 1.44	12.11 ± 1.65	15.00 ± 0.98	16.75 ± 0.96
AST/ALT ratio	0.95 ± 0.08	1.43 ± 0.30	1.29 ± 0.14	2.12 ± 0.49*
Serum calcium (mg/dL)	10.4 ± 0.1	10.6 ± 0.1	10.1 ± 0.1	10.3 ± 0.2
Serum phosphorous (mg/dL)	8.1 ± 0.6	7.0 ± 0.3	12.9 ± 0.7*,†	11.6 ± 0.7*,†
Total chol (mg/dL)	87 ± 3	398 ± 1*	547 ± 109*,†	1005 ± 158*,†,‡
Serum TG (mg/dL)	29 ± 3	42 ± 4	40 ± 6	236 ± 96*,†,‡

All measurements were taken 6 months after atherogenic diet (except lean swine) and 1 week before euthanasia. Data are mean ± SEM. MetS metabolic syndrome, MetS-A metabolic syndrome-alloxan, MetS/D-A metabolic syndrome with diabetes-alloxan, BUN, blood urea nitrogen, AST aspartate transaminase, ALT alanine transaminase, bG blood glucose, Chol cholesterol, TG triglycerides. *, $p < 0.05$ compared with lean swine; †, $p < 0.05$ compared with MetS swine; ‡, $p < 0.05$ compared with MetS-A swine. (Lean = 9; MetS = 10; MetS-A = 8; MetS/D-A = 8.)

CHAPTER 3: DIABETOGENIC ACTIONS OF ALLOXAN ARE DEPENDENT ON AGE IN OSSABAW MINIATURE SWINE

Background

The diabetic effect of alloxan was discovered in 1943, and since then it has been used in biomedical research to recapitulate the physiology of diabetes in various animal models [193]. Alloxan is a glucose analogue specific to glucose transporter 2 (GLUT2), which is expressed almost exclusively by hepatocytes and pancreatic beta cells [193, 194]. When GLUT2 transports alloxan into the cytosol of pancreatic beta cells it reacts with intracellular glutathione in a redox reaction, resulting in the formation of reactive oxygen species that cause beta cell death [194-196]. After administration of alloxan extensive beta cell necrosis is often observed [193]. Some studies show a long-term recovery from alloxan-induced diabetes, which is suspected to be due to either multiplication of surviving beta cells or the formation of new beta cells from the duct epithelium or the exocrine portion of the pancreas [193, 197-199].

The efficacy of alloxan can be unpredictable and is dependent on several factors, including species [196], route of administration [195, 198], speed of administration [198], and diet [193]. Although it is widely accepted that alloxan and streptozotocin, another diabetogenic agent, affect younger animals to a lesser extent compared to older animals, this is only based on a small number of studies in mice [200, 201]. The only study to cite the age-dependence of alloxan in a large animal model was published almost 70 years ago in dogs [193, 195, 198, 202]. With the variation between species and even between individuals in the same species, the possible age-dependent effects of alloxan in large animal models need to be re-examined.

In this study, I used the clinically relevant Ossabaw miniature swine (*Sus scrofa domestica*) model of metabolic syndrome (MetS), which is the clustering of risk factors that include obesity, dyslipidemia, glucose intolerance, insulin resistance, and

hypertension, to determine whether there is age-conferred protection against the diabetic effects of alloxan in swine. This will either contradict the alloxan/age dogma or serve as more evidence of the age-dependent effects of alloxan in large animal models.

Methods

Animals, Housing, and Diet

All experimental procedures involving animals were approved by the Institutional Animal Care and Use Committee at Indiana University School of Medicine with the recommendations outlined by the National Research Council and the American Veterinary Medical Association Panel on Euthanasia [170, 171]. Swine were obtained from a closed, SPF breeding colony at Purdue University. The swine herd has historically tested negative for Brucella spp, pseudorabies, vesicular stomatitis virus serovars Indiana and New Jersey, Mycoplasma hyopneumoniae, porcine reproductive and respiratory syndrome virus, porcine parvovirus, swine influenza virus serotypes H1N1 and H3N2, antibody levels to transmissible gastroenteritis virus, and Leptospira interrogans serovars (canicola, grippotyphosa, hardjo, icterohaemorrhagiae, pomona, and bratislava). All animals were housed in pairs in 24 ft^2 pens and provided a 12:12-h light:dark cycle. Temperature was maintained at 20-22°C throughout the study, and humidity was not controlled. After induction of diabetes (see below), all swine were immediately placed on a hypercaloric atherogenic diet for 6 months (1000-1350 g/day for both groups) consisting of 43% of total caloric intake from fat, 16% from protein, and 41% from carbohydrates (KT324, Purina Test Diet, Richmond, IN), similar to previous studies [203]. Swine were fed once a day in order to promote gorging behavior to ensure the daily allotment of food was completely consumed. Feed intake and blood glucose were measured daily, and body weight was monitored weekly. Water was provided ad libitum.

Central Venous Line Placement

Swine were restrained in a sling and anesthetized with 5% isoflurane in 100% O_2 administered by mask. The unconscious pig was placed in the supine position and a percutaneous needle with a syringe attached was inserted into the angle formed by the sternum and clavicle. Negative pressure was maintained in the syringe, and when it began to fill with dark red venous blood the needle was held in place and the syringe was removed. A guidewire was fed through the percutaneous needle, at which point the needle was removed. A central venous catheter was fed over the guidewire, which was then removed. The catheter was capped and secured to the animal using a non-absorbable suture. The pig was moved back to the sternal position and isoflurane was discontinued, allowing the swine to regain consciousness under observation. The central line catheter was flushed twice a week to ensure its patency.

Induction of Diabetes

Alloxan, a pancreatic beta cell toxin, was rapidly administered intravenously to Ossabaw miniature swine of mixed gender aged 4-8 months to induce diabetes. Swine were placed into two age groups at time of alloxan administration: “juvenile” (age < 6 months; n = 8) and sexually mature “adult” (age > or equal to 6 months; n = 8) [102]. Briefly, alloxan (Sigma Chemical Co., St. Louis, MO) was dissolved in 14 mL of 1M NaOH and 20 mL of 0.9% NaCl, for a final volume of 34 ml and a pH of 7.4. The alloxan solution was delivered through a 0.20-μm sterile filter into the jugular vein via a central venous line at an average dose of 140 mg/kg (range: 125-175 mg/kg). Two juvenile swine only had one dose while six juvenile swine were given two doses over the course of one week due to lack of hyperglycemic response from the first dose. The average first dose was 140 mg/kg (range: 75-175), and the average second dose was 120 mg/kg (range: 125-150 mg/kg). To protect against possible renal toxicity, pigs were given 250 mL of 0.9% NaCl through intravenous drip prior to and after alloxan dosing (for full protocol, see Appendix

A). The pigs were fed ad libitum and received 24 hours of critical care following induction of diabetes to monitor for hypoglycemic shock. Swine received daily insulin glargine (Eli Lilly and Company, Indianapolis, IN) via subcutaneous injection to the flank according to an algorithm previously published in my lab [120, 204] to maintain glycemic control below 300 mg/dL, a clinically relevant hyperglycemic level[172]. The insulin dose for all pigs was between 0.1-0.6 U/kg and was individually adjusted based on daily blood glucose measurements, weight measurements obtained weekly, and the presence or absence of lethargic behavior [204]. The diabetic disease state was allowed to stabilize for one week after alloxan administration, at which point all swine were immediately placed on a hypercaloric atherogenic diet for 6 months (see above). Non-alloxanized age-matched controls on the same hypercaloric atherogenic diet were utilized in some analyses.

Metabolic Phenotyping

Blood was collected one week pre-alloxan, one week post-alloxan, and 6 months post-alloxan for analysis (ANTECH Diagnostics, Fishers, IN). Homeostasis model assessment-insulin resistance (HOMA-IR) is a calculation that takes into account fasting glucose and insulin concentrations in order to assess insulin resistance [205]. A larger HOMA-IR value indicates greater insulin resistance [206]. HOMA-IR was calculated using the following equation: fasting insulin (µU/mL) x fasting glucose (mg/dL)/405.

Blood Pressure Measurements

From the beginning of the study, pigs were acclimated to a low-stress sling [151, 207] for conducting intravenous glucose tolerance tests (see below) and blood pressure measurements. Blood pressures were measured by using a tail cuff sphygmomanometer [151].

Intravenous Glucose Tolerance Test

Insulin treatments were suspended 2 days prior to testing to determine endogenous glucose regulation. To assess pancreatic beta cell response to glucose,

conscious swine that were fasted overnight were given a 50% glucose solution intravenously at 1 g glucose/kg body weight via the central venous line. To obtain fasting glucose concentration, pigs were placed in a low-stress restraint sling (see above) and blood samples (3 mL) were taken at –10, –5, and 0 min before glucose injection, then at 5, 10, 20, 30, 40, 50, and 60 min after glucose injection. Blood glucose values were monitored by use of an Accu-Chek Advantage glucose meter, and plasma insulin values were obtained by insulin assays done at the Indiana University School of Medicine Diabetes Research Core.

Euthanasia

After an overnight fast, swine were anesthetized via intramuscular injection of 2.2 mg/kg xylazine and 5.5 mg/kg Telazol (Fort Dodge Animal Health, Fort Dodge, IA). Swine were intubated and anesthesia was maintained with 2–4% isofurane in 100% O_2. The isofurane level was adjusted to maintain anesthesia with stable hemodynamics. Pigs were euthanized via cardiectomy.

Immunohistochemistry

Sections from the tail of the pancreas were placed in 10% phosphate-buffered formalin for 24-48 hours then embedded in paraffin. Tissue sections were stained with guinea pig anti-insulin polyclonal antibody (Agilent, Santa Clara, CA) as a marker for beta cells by the Department of Pathology at Indiana University School of Medicine (Indianapolis, IN). Images were captured using a Leica DM 3000 photomicroscope and analyzed with ImageJ software. Relative beta-cell mass was quantified by calculating the percentage of 3,3′ diaminobenzidine (DAB)-stained nuclear area to the total nuclear area using the ImmunoRatio ImageJ plugin.

Statistics

Statistical analysis was performed using GraphPad Prism 5.0 (San Diego, CA). Student’s t-test, one-way analysis of variance (ANOVA) with Tukey post-hoc analysis, or

two-way analysis of variance (2-way ANOVA) with Bonferroni post-hoc analysis was performed. Data are represented as mean ± SEM. $p < 0.05$ was considered statistically significant.

Results

Adult swine have more severe metabolic syndrome and insulin resistance

The juvenile and adult swine had comparable metabolic parameters before alloxan administration, so they were pooled into the “pre-alloxan” group. The juvenile swine were significantly younger than the adult swine, but both exhibited comparable weights and BMI measurements after 6 months on an atherogenic diet. Total cholesterol was elevated in juveniles 6 months post-alloxan compared to levels before alloxan administration and one week after. Total cholesterol and serum triglycerides were elevated in the adult swine 6 months post-alloxan compared to levels before alloxan administration and juvenile swine 6 months post-alloxan. HOMA-IR calculations show that adult swine 6 months post-alloxan were more insulin resistant than swine before alloxan administration and juveniles 6 months post-alloxan. To determine kidney function, creatinine and blood urea nitrogen (BUN) levels were measured. Creatinine levels were comparable between groups, with non-alloxanized controls exhibiting slightly elevated levels, while adult swine one-week post-alloxan exhibited elevated BUN levels that normalized by six months post-alloxan. To measure liver function, the aspartate aminotransferase (AST)/alanine aminotransferase (ALT) ratio was calculated. Both groups at six months post-alloxan had elevated AST/ALT, but this was equivalent to the non-alloxanized high-fat fed control swine. Blood pressure measurements were not statistically different between groups (Table 3.1).

Glucose clearance is more severely impaired in adult versus juvenile swine treated with alloxan

Blood glucose was monitored 60 minutes after intravenous administration of a bolus of glucose one week (Fig. 3.1A-C) and six months (Fig. 3.1D-F) after alloxan administration. One week post-alloxan, intravenous glucose tolerance test (IVGTT) analysis showed that adult swine had significantly higher blood glucose measurements at all time points when compared to both juvenile swine and all swine before alloxan administration (Fig. 3.1A). This is reflected in a higher baseline fasting glucose (Fig. 3.1B) and a greater area under the glucose curve (Fig. 3.1C). This hyperglycemia persists six months after alloxan administration, with adult swine exhibiting significantly higher glucose at most time points during glucose challenge compared to juveniles and pre-alloxan swine (Fig. 3.1D), higher baseline fasting glucose (Fig. 3.1E), and a greater area under the glucose curve (Fig. 3.1F). Juvenile swine had significantly greater area under the glucose curve compared to non-alloxanized swine six months after alloxan administration (Fig. 3.1F), demonstrating a progression of glucose intolerance in juvenile pigs.

Age is correlated to fasting blood glucose in alloxanized swine

Fasting blood glucose of swine one week after the final alloxan dose was plotted against age when each individual swine was alloxanized (Fig. 3.2). Analysis revealed that there is a strong positive correlation of blood glucose with age at the time of alloxan administration, even at comparable dosages of alloxan.

Hypoinsulinemia persists in both juvenile and adult swine

Serum insulin levels were measured during IVGTT assessments. One week after alloxan administration, both the juvenile and adult swine exhibited lower glucose levels compared to swine before alloxan administration at all time points except t=0 (Fig. 3.3A). This is reflected in the area under the insulin curve analysis (Fig. 3.3B). This hypoinsulinemia persists six months after alloxan administration, with juvenile and adult

swine exhibiting lower insulin levels at several time points when compared to non-alloxanized, age-matched swine (Fig. 3.3C). Again, juvenile and adult alloxanized swine have a lower area under the insulin curve compared to non-alloxanized swine (Fig. 3.3D). An outlier in the juvenile group that was 5x greater than the standard deviation was removed from this analysis.

Juvenile swine exhibited greater insulin response recovery

The areas under the insulin curves (Figs. 3.3B and 3.3D) were used to determine potential recovery from alloxan. Juvenile swine exhibited a ~2.5 fold increase in peripheral insulin levels from one week to six months post-alloxan (Fig. 3.3E). The peripheral insulin levels in adult swine, however, remained constant six months after alloxan administration (Fig. 3.3E).

Pancreatic beta cell area is decreased in juvenile and adult swine

Immunohistochemical analysis of sections of pancreas from juvenile (Fig. 3.4A), and adult (Fig. 3.4B) swine shows that both juvenile and adult alloxanized swine have comparable pancreatic beta cell area six months after alloxan administration (Fig. 3.4C). This is lower than non-alloxanized high-fat fed swine, whose pancreatic beta cell mass was calculated previously to be ~7.5% [204].

Discussion

In this study I showed that juvenile swine administered alloxan had a blunted response to the drug and did not have the severe diabetic effects that developed in adult swine administered alloxan. Swine that received alloxan regardless of age exhibited decreased pancreatic beta cell mass (Fig. 3.4C) and reduced peripheral plasma insulin after a bolus of glucose (Fig. 3.3C-D). However, only the juvenile swine exhibited insulin response recovery, which I define as the recovery or partial recovery of peripheral insulin levels, six months post-alloxan (Fig. 3.3E). Adult alloxanized swine developed more severe MetS, as evidenced by their elevated HOMA-IR and increased levels of total

cholesterol and serum triglycerides (Table 3.1). These swine did not exhibit hepatoxicity or renal toxicity, as indicated by their BUN, creatinine, and AST/ALT levels (Table 3.1), similar to previous studies [151, 167]. Also, fasting blood glucose was higher and significantly correlated to age of swine one week after alloxanization even though the dosages of alloxan were comparable (Fig. 3.2). Glucose clearance was more impaired in the adult swine, as well (Fig. 3.1F). Taken together these results show that fasting glucose and glucose clearance is more impaired in Ossabaw miniature swine administered alloxan as adults compared to as juveniles and that juvenile swine can at least partially recover from the alloxan treatment.

Pancreatic beta cell mass and peripheral plasma insulin were not statistically different between the juvenile and adult alloxanized swine, even though adult swine exhibited greater hyperglycemia, both fasting and after a glucose challenge, compared to juvenile swine. At its surface this seems like a paradox, but it can be explained partly by the increased peripheral resistance seen in the adult swine as calculated by the HOMA-IR [208, 209]. Under normal physiological conditions, insulin resistance is counteracted by increased insulin secretion by beta cell compensation [210]. However, the decreased beta cell mass due to alloxan treatment of adult swine was accompanied by a decreased functional compensation to increasing insulin secretion. So, comparable levels of circulating insulin would have less of an impact on glucose clearance in the insulin-resistant adult swine as compared to juvenile swine.

Hyperglycemia-induced secondary insulin resistance is a well-documented phenomenon in type 1 diabetic humans [211, 212] and in animal models, including swine [151, 213-218]. In a previous publication, my lab has determined that the drastic decrease in insulin sensitivity observed in alloxan-induced diabetic Yucatan swine is almost solely due to hyperglycemia [151]. This hyperglycemia-induced insulin resistance is at least partially due to the downregulation of glucose transfer type 4 in skeletal muscle by high

circulating glucose levels [215]. The initial hyperglycemic event after alloxan administration would cause the adult swine to become more insulin-resistant. This would also partially explain why the adult swine had glucose clearance that is more impaired than the juvenile swine six months after alloxan administration (Fig. 3.1D-F), even though peripheral insulin levels (Fig. 3.3C-D) and pancreatic beta cell mass (Fig. 3.4) were comparable between those two groups. The initial differential effects of alloxan in juvenile versus adult swine contribute to the greater hyperglycemia exhibited in adult swine.

The liver plays a vital role in glucose metabolism and may have a role in the differential effects seen in the alloxanized juvenile and adult swine. Insulin secreted from the pancreas travels via the portal vein to the liver where it binds 60% of the insulin [219]. The remaining insulin then goes into the peripheral circulation where it binds to insulin-sensitive tissues such as skeletal muscle and adipose. However, it has been found that hepatic insulin binding doubles in streptozotocin-induced diabetes [220]. As there is an inverse relationship between circulating insulin levels and hepatic insulin binding [220], this may affect insulin circulation in the alloxanized animals. It is possible that more insulin was secreted in juvenile pigs, but much of the insulin was bound by the liver, thereby resulting in greater insulin-mediated glucose uptake by the liver and lower fasting glucose compared to these parameters in adult pigs. Portal vein insulin levels or c-peptide levels would be needed to provide direct evidence for this possibility.

While juvenile swine six months post-alloxan exhibited elevated levels of total cholesterol and serum triglycerides that were on par with non-alloxanized pigs fed the same atherogenic diet, adult swine exhibited 5 times higher triglyceride levels and 2 times higher cholesterol levels compared with juvenile and non-alloxanized swine (Table 3.1). This may be attributed, at least in part, to the alloxan treatment itself. Alloxan causes chronic hyperglycemia due to ablation of pancreatic beta cells. Hyperglycemia is a main cause of insulin resistance [151], which has been shown to alter several components

involved in metabolic processes. For example, rabbits with alloxan-induced diabetes had increased intestinal HMG-CoA reductase levels, leading to increased cholesterol synthesis and thus increased transport of cholesterol from the intestine to the circulation and increased availability of cholesterol for lipoprotein formation [221, 222].

Chronic hyperglycemia also alters components of the renin-angiotensin system (RAS), which includes increasing production of angiotensin II (AngII). AngII has been shown to reduce glucose utilization and insulin sensitivity, increase insulin resistance, impair insulin signaling, and impair insulin secretion [223]. Hyperglycemia also decreases the activity of angiotensin converting enzyme, leading to increased levels of AngII and decreased production of angiotensin-(1-7) [224]. In fact, when angiotensin-(1-7) was upregulated in a rat model it enhanced glucose tolerance, insulin sensitivity, and insulin-stimulated glucose uptake [225]. Triglyceride and cholesterol levels were also lower [225]. Furthermore, inhibition of RAS has been shown to improve TG, HDL, LDL, and total cholesterol [223], and administration of exogenous insulin to hyperglycemic rats reversed some of these negative effects, including normalizing the expression levels of several compounds involved with AngII synthesis and activity [223].

Several studies have shown that creatinine increases progressively with time in alloxanized animals, signaling kidney dysfunction [226-228]. However, both groups six months post-alloxan have comparable creatinine and BUN levels as pre-alloxan and non-alloxanized controls, and the AST/ALT ratio is comparable to non-alloxanized controls, indicating little kidney damage and no additional liver damage due to the drug.

Spontaneous recovery from streptozotocin- and alloxan-induced diabetes has been well-documented [193, 198, 199, 229] and works through several potential mechanisms. A recent study in mice found evidence that islet delta cells can be converted into beta cells, an ability which is lost in adulthood [229]. Other hypotheses involve proliferation of surviving beta cells [193, 197, 198, 229], islet alpha cells reprogramming

into beta cells [229, 230], and duct epithelium conversion to beta cells [193, 197, 198]. This is the first study to show recovery from alloxan-induced diabetes in a large animal model. However, while this study determined that peripheral insulin levels recover in juvenile swine, it does not delve into the mechanisms that drive this recovery. Future studies should focus on non-beta islet cell reprogramming in swine of different ages.

Swine do not reach developmental maturity until 6 months of age [102, 231-233]. In this study, although there is only a difference of about three months between the ages of the two experimental groups, developmentally it is the difference between juvenile and adulthood [102, 232, 233]. In addition to the blunted acute (1 week) beta cell destruction by alloxan in juvenile pigs, they also showed more relative recovery of glucose tolerance and peripheral insulin responses 6 months after alloxan compared to adult pigs. This speaks to the immense sensitivity of alloxan to age and the more robust resistance of juvenile pig beta cells to alloxan.

The juvenile group contained 3 castrated males and 5 females, while the adult group contained 5 castrated males and 3 females (Table 3.1). The non-alloxanized control group contained 4 of each sex (Table 3.1). These sex differences could potentially impact metabolic parameters, but the differences were not statistically significant. The effect of sex in regard to weight gain shows different results in different studies, depending on the diet and breed of pig [234, 235]. In Large White x Landrace pigs, intact boars were larger than females while the weights of castrated males were comparable to that of females [235]. Female swine reliably exhibit elevated serum cholesterol [234, 236-238], but the effects of sex on triglyceride levels and insulin resistance are less predictable [234, 237, 238]. Of note, the blood urea nitrogen, creatinine, alanine aminotransferase, and aspartate aminotransferase levels are comparable between male and female swine [237, 238]. In this study, even though the adult swine group contained more males than females these swine exhibited greatly elevated serum triglycerides, cholesterol, and HOMA-IR (Table

3.1). If sex did impact the metabolic profile, then correcting for it would only make these results more robust.

Furthermore, the vasoprotective effects of estrogen in the circulation have been well documented [239-241], as well as the harmful effects of testosterone [241, 242]. However, the sex differences in this study might not be that simplistic, as female Yucatan swine have similar serum testosterone levels as castrated males [79] and intact female dogs have comparable estradiol as neutered males [243]. While serum estrogen levels were not measured in this study, the literature supports the hypothesis that females and castrated males from various species have a similar sex hormone profile.

This is the first study since 1949 to investigate whether the effects of alloxan are dependent on age in large animals. Since alloxan is a very mercurial drug, different species at different stages of maturity need to be tested. Alloxan is widely used to elicit diabetes in animal models, so by characterizing responses to alloxan researchers can be sure the drug will have the desired effects. Studies examining how the diabetic effects of alloxan are dependent on age in different species is of the utmost importance, as different animal species and even different breeds within a species react differently. For example, it has been found that pigs require a higher dose of alloxan to develop a similar diabetic state as rats, dogs, and rabbits [196, 244]. Clearly, alloxan has very different effects based on the physiology of the species and breed. Therefore, one study in one species is not adequate to make such a sweeping generalization about the age of an animal on a drug's effectiveness. The field of diabetic animal models needs additional studies both to verify Creutzfeldt's 1949 findings and to determine if this effect is typical among commonly used animal models of diabetes.

In the current study, I show that alloxan more efficaciously elicited acute and sustained hyperglycemia when administered to adult swine compared to juvenile swine. This supports the 70-year-old dogma that the diabetic effects of alloxan are dependent on

age, at least in the dog and the minipig [202]. Future studies will need to examine other laboratory animal species to determine the ubiquity of this age-dependence. These studies should focus on several ages to create a dose-response curve for frequently used animal models. This study provides an important step in clarifying the effects of a widely used yet relatively unpredictable drug, thereby enabling researchers to better choose which animal and stage of maturation will be best for their study design. This information can save researchers time and money and can prevent needlessly wasting research animal lives.

Figures

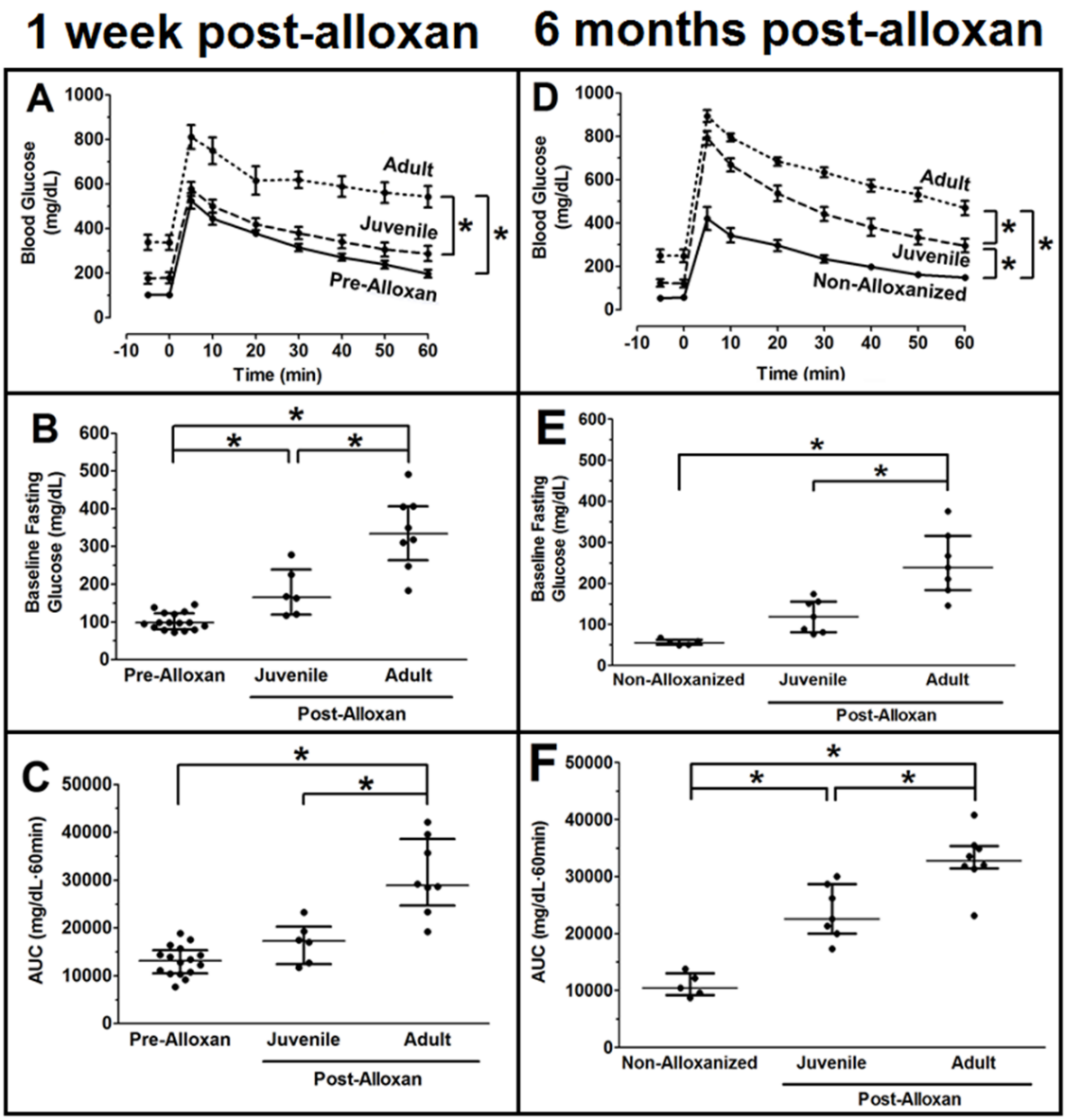

Figure 3.1: Adult swine exhibited prolonged impaired glucose clearance after an intravenous glucose tolerance test. Blood glucose levels were tested for 60 minutes after a bolus of glucose. (A) Adult swine showed a deficit in glucose clearance at all time points compared to pre-alloxanized and young swine one week after alloxan administration. (B) Baseline fasting blood glucose was elevated in juvenile animals and higher in the adult group one week after alloxan administration. (C) Area under the curve analysis shows impaired glucose clearance in adult alloxanized animals. (D) Adult swine

continued to exhibit impaired glucose clearance at most time points compared to non-alloxanized swine and juvenile swine six months after alloxanization. (E) Baseline fasting glucose was elevated in adult swine six months after alloxan administration. (F) Area under the curve analysis using the fasting blood glucose as a baseline for each group shows impaired glucose clearance in juvenile alloxanized animals compared to non-alloxan controls, and this impaired glucose clearance is exacerbated in adult alloxanized animals six months after alloxan administration. *, $p < 0.05$. (Pre-Alloxan = 16; Non-Alloxanized = 5; Juvenile = 8; Adult = 8).

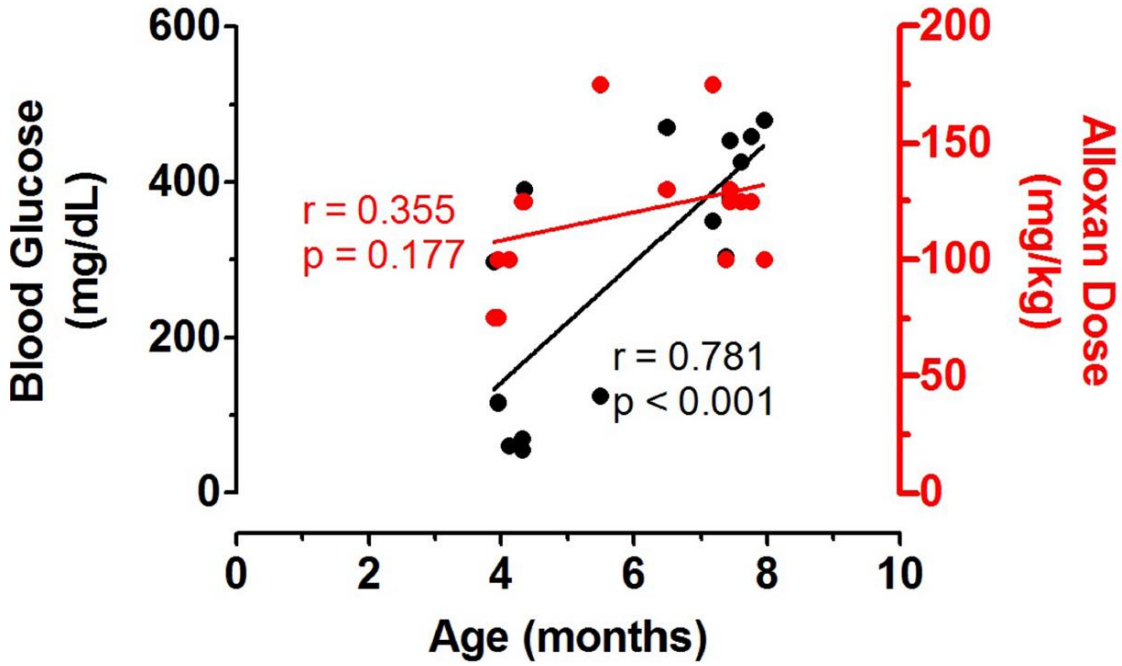

Figure 3.2: Fasting blood glucose correlates to age at alloxan administration. Fasting blood glucose taken one week after alloxan administration is significantly positively correlated to the age of swine at time of alloxan administration (black). The dose of alloxan, however, is not correlated to age (red) and is not significantly different between groups. In animals given two doses of alloxan the average of the doses was used.

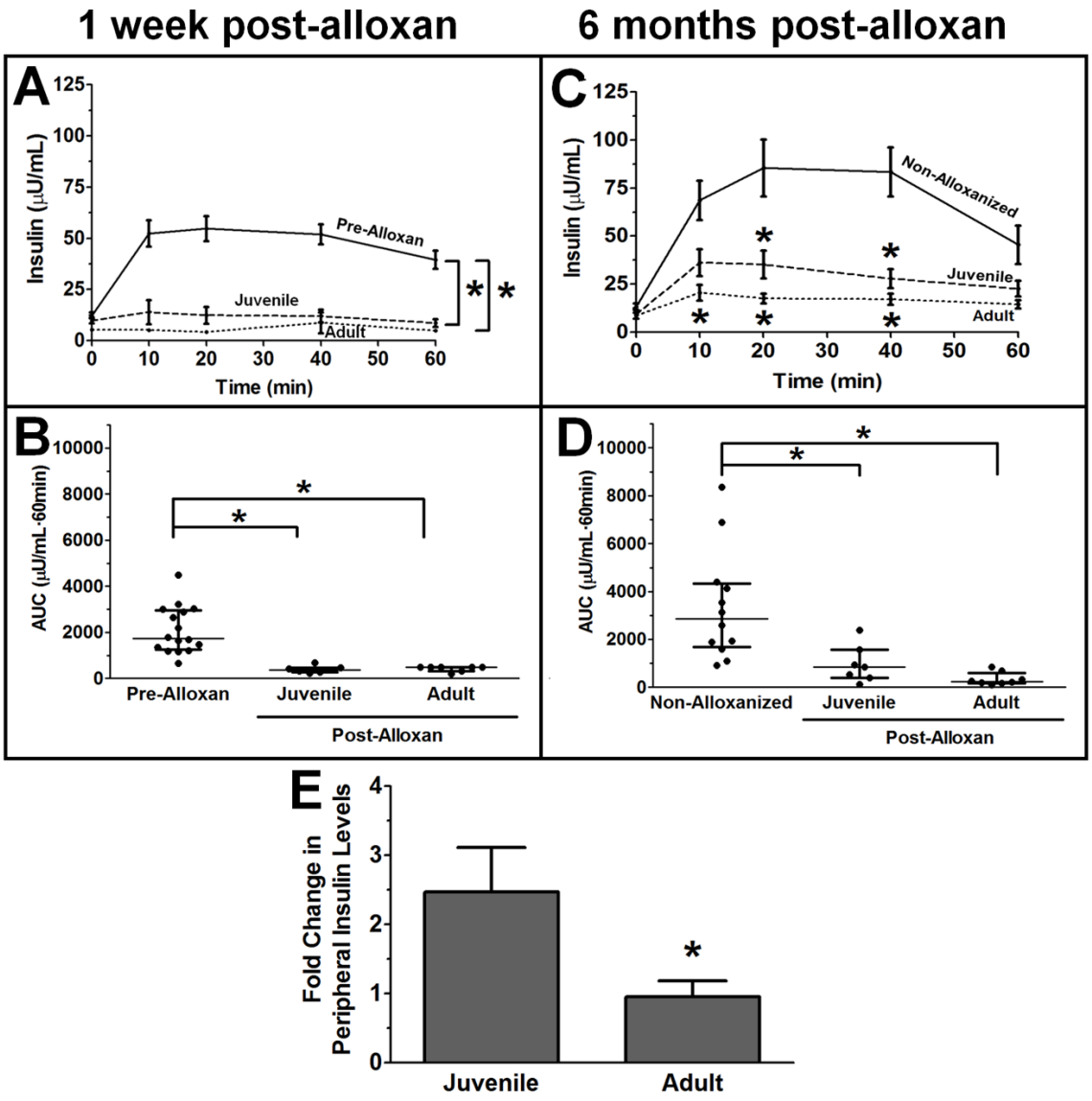

Figure 3.3: Hypoinsulinemia persists in both juvenile and adult swine six months after alloxanization. (A) Time course of peripheral insulin during intravenous glucose tolerance test was significantly lower in juvenile and adult swine compared to pre-alloxan controls one week after alloxan administration. (B) Area under the curve analysis reveals comparable hypoinsulinemia in both the juvenile and adult alloxanized swine one week after alloxan administration. (C) Juvenile and adult swine still exhibited hypoinsulinemia at several time points compared to non-alloxanized, age-matched controls six months after alloxan administration. (D) Area under the curve analysis revealed comparable

hypoinsulinemia in both juvenile and adult alloxanized swine six months after alloxan administration. (E) The fold change in peripheral insulin from one week to six months post-alloxan was greater in juvenile than adult swine. *, $p < 0.05$ vs. Pre-Alloxan or Non-Alloxanized. (Pre-Alloxan = 16; Non-alloxanized = 8; Juvenile = 7; Adult = 8).

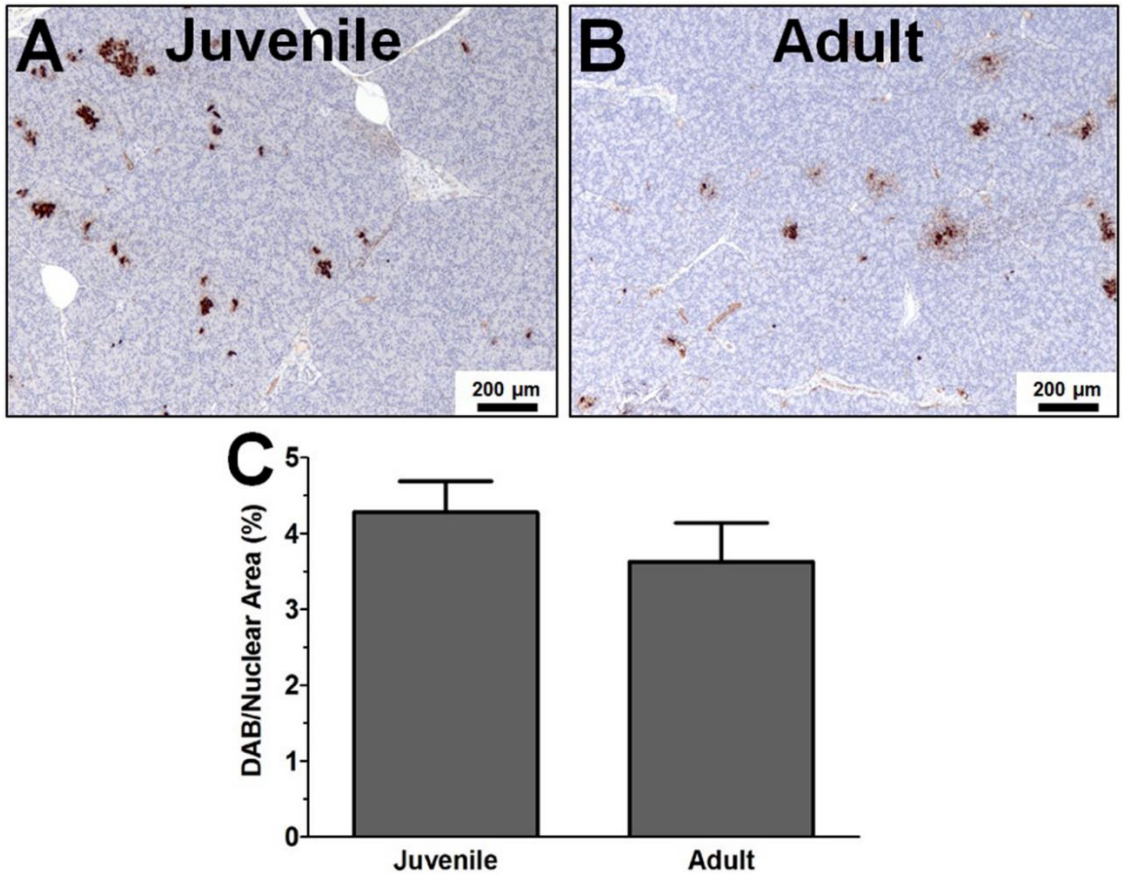

Figure 3.4: Decreased beta cell mass is evident in both young and older alloxanized swine. Immunohistochemical staining of insulin in pancreas sections from juvenile (A) and adult (B) swine revealed that 6 months post-alloxan both juvenile and adult swine had a lower beta cell mass when compared to non-alloxanized controls having insulin staining area of ~15%, but it was not statistically different between the juvenile and adult groups (C).

Tables

Table 3.1: Metabolic profiles show hyperlipidemia and insulin resistance in swine six months after consumption of an atherogenic diet

	Pre-Alloxan	1 Week Post-Alloxan		6 Months Post-Alloxan		Non-alloxanized MetS swine
		Juvenile	Adult	Juvenile	Adult	
Age (mo)	-	4.3 ± 0.2	7.4 ± 0.2†	11.0 ± 0.2†‡	14.0 ± 0.1†‡§	12.6 ± 1.1†‡
Sex (M/F)	8/8	3/5	5/3	3/5	5/3	4/4
Body Weight (kg)	24.9 ± 1.6	22.2 ± 1.0	29.7 ± 1.0	67.8 ± 2.6*†‡	73.5 ± 2.8*†‡	91.7 ± 2.6*†‡$
BMI (kg/m^2)	-	-	-	58.6 ± 2.4	59.4 ± 3.2	69.4 ± 1.3§$
Serum TG (mg/dL)	33 ± 16	66 ± 15	82 ± 16	41 ± 7	211 ± 87*§	40 ± 5$
Total Chol (mg/dL)	91 ± 16	93 ± 5	110 ± 7	500 ± 114*†‡	988 ± 138*†‡§	421 ± 59*†‡$
HOMA-IR	2.9 ± 0.4	3.3 ± 0.3	4.6 ± 0.3	2.3 ± 0.3	5.4 ± 1.0*§	2.7 ± 0.2$
Creatinine (mg/dL)	1.1 ± 0.1	0.9 ± 0.1	1.2 ± 0.1	1.1 ± 0.1	1.1 ± 0.1	1.3 ± 0.1†
BUN (mg/dL)	14.7 ± 0.8	16.5 ± 3.1	27.4 ± 3.4*†	14.9 ± 0.9‡	16.9 ± 1.0‡	11.9 ± 1.5‡
AST/ALT	0.66 ± 0.04	0.99 ± 0.06	0.74 ± 0.07	1.68 ± 0.43*	1.73 ± 0.36*	1.56 ± 0.30*
Systolic BP (mmHg)	131 ± 6	-	-	142 ± 10	158 ± 6	138 ± 9
Diastolic BP (mmHg)	74 ± 5	-	-	83 ± 6	88 ± 3	90 ± 7
MAP (mmHg)	93 ± 5	-	-	103 ± 6	112 ± 3	106 ± 7

Data are means ± SEM. M, male; F, female; TG, triglycerides; Chol, cholesterol; HOMA-IR, homeostasis model assessment-insulin resistance; BUN, blood urea nitrogen; AST, aspartate aminotransferase; ALT, alanine aminotransferase; BP, blood pressure; MAP,

mean arterial pressure. Measurements were taken either one week or six months after alloxan administration. *, $p < 0.05$ compared with pre-alloxan swine; †, $p < 0.05$ compared with juvenile swine one week post-alloxan; ‡, $p < 0.05$ compared with adult swine one week post-alloxan; §, $p < 0.05$ compared with juvenile swine six months post-alloxan; $, $p < 0.05$ compared with adult swine six months post-alloxan.

CHAPTER 4: EFFECT OF METABOLIC SYNDROME AND AGING ON Ca^{2+} DYSFUNCTION IN CORONARY SMOOTH MUSCLE AND CORONARY ARTERY DISEASE SEVERITY IN OSSABAW MINIATURE SWINE

Background

Atherosclerosis is a complex, progressive disease that develops over many years when cholesterol, fatty material, cellular waste products, fibrin, collagen, and extracellular Ca^{2+} accumulate in large and medium-sized arteries throughout the body. Coronary artery disease (CAD) is the build-up of atherosclerotic plaque in the coronary arteries leading towards occlusion and myocardial ischemia and is the leading cause of death in industrialized nations [245].

Modifiable risk factors such as physical inactivity and an unhealthy diet can potentiate metabolic changes like hypertension, dyslipidemia, obesity, insulin resistance, and glucose intolerance. Metabolic syndrome (MetS) is the clustering of 3 or more of these cardiometabolic risk factors and is associated with a 2-fold greater risk of developing CAD and a 1.6-fold increase in mortality [246, 247]. However, modifiable risk factors are only part of the story. Sir William Osler, a prolific physiologist and one of the founders of Johns Hopkins University, once wrote, “A man is as old as his arteries” [38]. Indeed, advancing age is one of the major non-modifiable risk factors for CAD. The prevalence of CAD increases progressively with age, and more than 50% of CAD-related deaths occur in individuals older than 75 [40, 41]. The population aged 65 and older in the US is projected to double to 83.7 million by the year 2050, causing a growing public health concern [248].

Ca^{2+} is vital to vascular smooth muscle function, as cytosolic Ca^{2+} levels regulate various cellular functions including contraction [68, 187], proliferation [68, 70, 249, 250], migration [184, 185], and transcription [186, 188]. Previous research (reviewed in ([69]))

has identified several functional alterations in Ca^{2+} transporters associated with metabolic disorders (MetS, diabetes, dyslipidemia) that induce CAD.

The Ossabaw miniature swine model of MetS/CAD has been well-characterized [102]. These swine exhibit a “thrifty genotype” that allows them to store excess fat for later use during times of famine in their natural habitat [102, 107]. In captivity, when the pigs are kept sedentary and fed a high-calorie atherogenic diet, they reliably develop all the risk factors associated with MetS in addition to diffuse atheroma and coronary artery calcification (CAC), making them a clinically relevant animal model of human MetS and subsequent CAD/CAC [80, 81, 103, 105, 106, 108, 124].

Age-related alterations in Ca^{2+} transporter activity depend heavily on the tissue, animal, and co-existing disease states [251]. These heterogeneous patterns of Ca^{2+} dysregulation are similar to the heterogeneity of metabolic dysfunction [69]. It is astounding that there are no reports on age-related alterations in Ca^{2+} transporter activity in coronary smooth muscle (CSM), especially since CSM Ca^{2+} dysregulation would precede extracellular CAC, which has been extensively documented in aging [41]. The pathophysiology of MetS- and aging-induced atherosclerotic disease may be different; however, MetS-induced and aging-induced atherosclerotic CAD and the associated alterations in CSM intracellular Ca^{2+} transporter activities have yet to be compared directly.

Methods

Animals

All experimental procedures involving animals were approved by the Institutional Animal Care and Use Committee at Indiana University School of Medicine with the recommendations outlined in the Guide for the Care and Use of Laboratory Animals and the American Veterinary Medical Association Panel on Euthanasia [170, 171]. Ossabaw miniature swine were separated into four groups based on age and diet: lean young, MetS young, lean old, and MetS old swine (Table 1). Both lean groups were fed 725 g/day of

regular chow (5L80, Purina Test Diet, Richmond, IN) that contained 18% kcal from protein, 71% kcal from complex carbohydrates, and 11% kcal from fat. To induce MetS, swine in both MetS groups were fed 1000 g/day of an excess-calorie, atherogenic diet for 11 months (KT324, Purina Test Diet, Richmond, IN) that provided 16.3% kcal from protein, 40.8% kcal from complex carbohydrates, 19% kcal from fructose, and 42.9% kcal from fat. Fat calories were derived from a mixture of lard, hydrogenated soybean oil, and hydrogenated coconut oil and was supplemented with 2.0% cholesterol and 0.7% sodium cholate by weight. All animals had free access to drinking water.

Intravenous glucose tolerance testing

Prior to intravenous glucose tolerance testing (IVGTT), conscious swine were acclimatized to low-stress restraint in a sling. The pigs fasted overnight before an IVGTT and fasting baseline blood samples were obtained. Glucose (1 g/kg body weight, IV) was administered and timed blood samples were collected as previously described by my laboratory [80, 102, 124] for blood glucose measurements (YSI 2300 STAT Plus Glucose analyzer, YSI Life Sciences, Yellow Springs, OH).

Metabolic phenotyping

Blood samples were obtained before euthanasia and triglycerides, total cholesterol, and blood chemistry profiles were assessed (Antech Diagnostics, West Lafayette, IN). Blood pressures were measured while swine were under anesthesia with isoflurane.

Intravascular ultrasound

Swine were anesthetized and intravascular ultrasound was performed as previously described [80, 135]. Still frame IVUS pullback images were obtained offline at 1 mm intervals. Percent wall coverage and percent plaque burden were obtained using Image J software (1.48v, National Institutes of Health, USA). Pigs were euthanized after

the IVUS procedure via cardiectomy and coronary arteries were removed for further analysis.

Assessment of $[Ca^{2+}]_i$ regulation

CSM cells from the freshly-dissected left anterior descending (LAD) coronary artery were enzymatically isolated and loaded with the ratiometric fluorescent Ca^{2+} indicator, fura-2 AM (3.0 mmol/L Molecular Probes, Life Technologies, Eugene, OR) as previously described [252, 253] (for full protocol, see Appendix E). Measurements of whole CSM cell $[Ca^{2+}]_i$ levels were obtained using the InCa++ Calcium Imaging System (Intracellular Imaging, Cincinnati, OH) as previously described [76, 80, 174, 252].

Histology

Coronary artery segments were collected at euthanasia and fixed in 10% phosphate buffered formalin for 24 hours before being switched to 70% ethanol solution. Samples were paraffin embedded, sectioned (5 μm thick), mounted on a slide and stained by the Indiana University Histology Core (Indiana University School of Medicine, Indianapolis, IN). Verhoeff-Van Gieson (VVG) elastin staining was performed to determine the location of the external elastic lamina (EEL) and the internal elastic lamina (IEL) to assess wall thickness, medial area, and the intima/media ratio as measures of atherosclerosis progression [80, 81]. Wall thickening (percent media plus percent neointima) was measured by the following equation:

$$\left[\left(\frac{Area\ within\ EEL - Area\ within\ IEL}{Area\ within\ EEL}\right) + \left(\frac{Area\ within\ IEL - Area\ of\ Lumen}{Area\ within\ EEL}\right)\right] \times 100\%$$

The media area was calculated as the area within the EEL minus the area within the IEL. The intima area was calculated as the area within the IEL minus the area of the lumen. All images were captured with a Leica DM3000 microscope connected to Leica Application Suites V4.1 software (Leica Microsystems GmbH, Wetzlar, Germany) and analyzed using (Adobe Photoshop® CS6) (for full protocol, see Appendix C).

Statistics

Statistical analysis was performed using GraphPad Prism 5.0 (San Diego, CA). One-way analysis of variance (ANOVA) with Tukey post hoc analysis was performed. Data are represented as mean ± SEM and $p < 0.05$ was considered statistically significant.

Results

Ossabaw Swine Cardiometabolic Characteristics

The experimental groups' cardiometabolic characteristics are presented in Table 4.1. The Ossabaw swine were separated by age and disease state. Lean old swine were shown to be healthy as indicated by their normal body weight, blood pressure, cholesterol triglyceride, and fasting glucose levels, and peak glucose and area under the curve analysis derived from the IVGTT assessment. My laboratory and others have extensively characterized cardiometabolic profiles in Ossabaw swine fed regular chow diets and hypercaloric, atherogenic diets to induce MetS [69, 80, 81, 107, 110, 135, 149, 203]. MetS was confirmed in the MetS young and MetS old swine groups, both of which developed obesity, hypercholesterolemia, and elevated peak glucose and area under the curve during IVGTTs [80, 135]. However, only the MetS old swine exhibited hypertension, with elevated systolic blood pressure and mean arterial pressure (MAP). Blood pressures were measured while swine were anaesthetized. The lean old swine had significantly lower serum triglycerides and fasting blood glucose, which is characteristic of older swine [238, 254].

Histological Assessment of Vascular Health

Atherosclerosis progression was assessed by VVG staining in the proximal right coronary arteries (Fig. 4.1A-D) that enabled measurement of wall thickness (%media + %neointima), media thickness, and intima:media ratio (Fig. 4.1E-G). MetS young and lean old swine had similarly elevated wall thickening over the lean young swine group, and MetS old swine had significantly greater wall thickening than the other three groups (Fig.

4.1E). MetS young and lean old swine had similarly elevated media thickness over the lean young swine group, and MetS old swine had comparable media thickness to lean young swine (Fig. 4.1F). To determine whether this change was due mainly to media thickening, which is characteristic of aging [255, 256], or intimal thickening, which is characteristic of CAD [255], the intima:media area ratio was assessed (Fig. 4.1G). The MetS young swine trended towards a higher intima:media ratio and the MetS old swine had a significantly higher intima:media ratio, indicating that a bulk of the wall thickening in both MetS groups was due to neointimal thickening while the wall thickening in the lean old swine was due to medial thickening.

IVUS Assessment of Coronary Plaque Severity

After angiography was employed to locate the LAD and circumflex (CFX) arteries for catheter placement (Fig. 4.2A), cross-sectional images of the arteries were taken using an IVUS catheter (representative IVUS still frames in Fig. 4.2B-C). Unfortunately, 2 out of the 3 MetS old swine died on the operating table before IVUS could be recorded, so this group was not included in the IVUS analyses. Percent wall coverage increased in MetS young swine (Fig. 4.2D) and percent plaque burden increased in both MetS young and lean old swine (Fig. 4.2E). These data suggest that MetS young swine and lean old swine have similar disease severities.

Correlation of percent wall coverage and percent plaque burden with age

Percent wall coverage (Fig. 4.2F) and percent plaque burden (Fig. 4.2G) of the lean young and lean old swine were plotted against age of the individual pig. Analysis revealed that both percent wall coverage and plaque burden are positively correlated with age. This supports the notion that CAD severity increases with age and that older individuals are more at risk for atherosclerotic vessel occlusion.

Assessment of the Effects of MetS and Advancing Age on CSM cell $[Ca^{2+}]_i$

Figure 4.3A-B shows a representative CSM $[Ca^{2+}]_i$ response from a cell isolated from a lean young swine. When I assessed the caffeine-sensitive sarcoplasmic reticulum (SR) store release in the absence of extracellular Ca^{2+} to measure the SR storage capacity, I observed that the MetS young swine had an elevated SR store that was even higher in the lean old swine compared with the lean young group (Fig. 4.3C). The MetS old swine had a comparable SR store release when compared to lean young and MetS young swine but not lean old swine (Fig. 4.3C). When I measured the undershoot after SR store release in the absence of extracellular Ca^{2+} to get an index of sarco-endoplasmic reticulum Ca^{2+} ATPase (SERCA) activity, I observed that the lean old swine had an attenuated undershoot compared with the lean young and MetS young swine (Fig. 4.3D). The SERCA activity of the MetS old swine seemed to mirror that of the MetS young swine, but neither of these were significantly different from the lean young swine. When voltage-gated calcium channel (VGCC) activity was assessed using a Ba^{2+} challenge, CSM cells from MetS young and MetS old swine trended towards an increased Ba^{2+} influx rate and net accumulation of Ba^{2+}, but only the lean old swine had a significantly higher Ba^{2+} influx rate and net accumulation of Ba^{2+} compared with the lean young swine group (Fig. 4.3E).

Discussion

Cytosolic Ca^{2+} is a primary regulator of contraction and phenotypic modulation of CSM, which plays an integral role in atherosclerosis pathology and has been reviewed elsewhere [68, 69]. MetS- and aging-induced changes of the structure of the vascular have been well documented, but CSM Ca^{2+} dysregulation in MetS- and age-induced CAD have never before been directly compared.

This study characterized aging-related CSM Ca^{2+} dysregulation and provides insight into the disease characteristics of two common etiologies of atherosclerosis. I show for the first time that, although MetS-induced CAD and aging occlude the arteries to a

similar degree in the swine model, the Ca^{2+} handling mechanisms present in lean old swine are exaggerated compared with MetS-induced CAD. This indicates that MetS young swine have CSM Ca^{2+} dysregulation that mirrors severe disease and lean old swine have CSM Ca^{2+} dysregulation that mirrors mild disease [81]. The MetS old swine had similar Ca^{2+} dysregulation as the MetS young swine, but a much greater wall thickness and neointima formation.

My laboratory has explored changes in Ca^{2+} handling in CSM throughout the time-course of CAD progression in Ossabaw swine from healthy, lean pigs to obese, MetS pigs with advanced calcified CAD lesions. “Early stages” of CAD were characterized by pigs on the same atherogenic diet used in the present study for 6-9 months, while “later stages” of CAD were defined by pigs on an atherogenic diet for ~12 months [81]. In vivo assessment of atherosclerosis confirmed greater CAD burden in those pigs fed an atherogenic diet for a longer duration [81]. Interestingly, Ca^{2+} influx after membrane depolarization with 80 mM K^+ and caffeine-sensitive SR store-release was elevated in early CAD, which began to decline in later stages of CAD [81].

Specific Ca^{2+} handling dysfunction is associated with certain structural changes in the arterial wall. For example, increased SR Ca^{2+} store has been implicated with CSM proliferation and wall thickening [69, 257, 258]. In the present study, I show that lean young swine and MetS old swine have similar medial thickness (Fig. 4.2B), which is reflected in their comparable SR Ca^{2+} store release capacities (Fig. 4.3C). This could be due to the decreased proliferative ability of CSM cells or an increase in apoptotic CSM cells in MetS old swine [259, 260]. MetS young swine have elevated media thickness that is related to their elevated SR Ca^{2+} store release and lean old swine had even more elevated media thickness and associated SR Ca^{2+} store release. Thus, functional alterations in Ca^{2+} handling mechanisms affect the structural changes that are typical of the different age and disease states.

Aging-induced changes in Ca^{2+} handling in smooth muscle vary depending on tissue bed and species [251]. Although cardiac events are the leading cause of death in aged individuals [245], there is a paucity of literature about the effects of age on CSM Ca^{2+} handling despite its structural and functional importance. I fill that gap of knowledge by demonstrating that swine with MetS exhibit Ca^{2+} dysfunction that is characteristic of severe CAD regardless of the age of the animal, and lean old swine exhibit Ca^{2+} dysfunction that is characteristic of mild CAD. The lean old swine have increased SR Ca^{2+} store, increased VGCC activity, and decreased SERCA function in CSM (Fig. 4.3C-E).

While the short maturation time and lifespan of rodents and rabbits makes them tempting to use in aging studies, their size and cardiovascular anatomy brings their clinical relevance into question [261]. However, because of their anatomy and physiology, the Ossabaw swine are a far more superior model than rodents or rabbits. Due to cost, space, and time limitations, Ossabaw swine have not previously been used in an aging study. This truly unique study compared CSM Ca^{2+} dysfunction in lean young, MetS young, lean old, and MetS old swine, a feat never before published due to the long lifespan of swine.

The concept that MetS accelerates vascular aging is supported in this study. Even though plaque severity was comparable between the MetS young and lean old group (Fig. 4.2E), the MetS young swine exhibited Ca^{2+} dysfunction that was on par with more severe CAD (Fig. 4.3C-E) [81]. In fact, the Ca^{2+} dysfunction exhibited by the MetS young swine more closely resembled that of MetS old swine as opposed to the lean young swine, indicating that MetS causes Ca^{2+} dysregulation that is typical of severe CAD regardless of the actual age of the individual animal. Lean old swine exhibited Ca^{2+} dysfunction that is characteristic of mild disease, where Ca^{2+} transporter function is enhanced (Fig. 4.3C-E) [81].

The similarities in Ca^{2+} dysfunction, but differences in plaque severity, between the MetS young and MetS old swine brings forth the possibility that the aging milieu

predisposes individuals to exhibit accelerated plaque growth. Indeed, age has been associated with dyslipidemia [262], oxidative stress [263], insulin resistance [264], hypertension [263], and inflammation [265]. These, along with increased cellular senescence, which has been shown to play a part in atherosclerotic progression at all stages of the disease and is associated with advanced atherosclerotic plaques [266], comprise a perfect storm for plaque progression, and could cause plaques to develop more rapidly after Ca^{2+} dysfunction develops.

Dyslipidemia, particularly elevated levels of LDL-cholesterol (LDL-C) is a strong individual risk factor predicting coronary artery disease progression [267]. Cumulative LDL exposure over a lifetime will be higher in older individuals and results in a greater risk of CAD development and progression [267]. This could explain why the lean old swine have similar wall thickness and plaque burden compared to MetS young swine even though the lean old swine had significantly lower cholesterol levels at time of sampling (Table 4.1). This cumulative LDL exposure could be considered a part of the aging milieu that contributes to accelerated CAD progression.

One limitation of this study is the sex differences between groups. While the two MetS groups only contained female swine, the two lean groups contained both female and castrated male swine (Table 4.1). Estrogen has been shown to be vasoprotective in the coronary circulation in several studies [239, 240, 268], while testosterone has been shown to be harmful in the context of the coronary circulation [242, 268]. However, castrated male and intact female Yucatan swine have similar serum testosterone levels [79]. Furthermore, intact female dogs have similar estradiol levels as neutered males [243]. While the current study did not include serum estrogen levels of all the swine, the literature supports the hypothesis that castrated males and intact females have a similar sex hormone profile.

I report here that MetS young and lean old swine have similar elevated plaque burden and wall thickening due to media remodeling while MetS old swine have even greater wall thickening due to neointima formation. However, the Ca^{2+} dysfunction seen in MetS young and MetS old are comparable and follow the same pattern as that seen in severe CAD. Lean old swine have Ca^{2+} dysfunction that is indicative of mild disease. Therefore, I can conclude that, although Ca^{2+} handling is similar in a younger animal with less overt disease, the aging milieu causes more advanced coronary plaques to develop in the context of MetS.

Figures

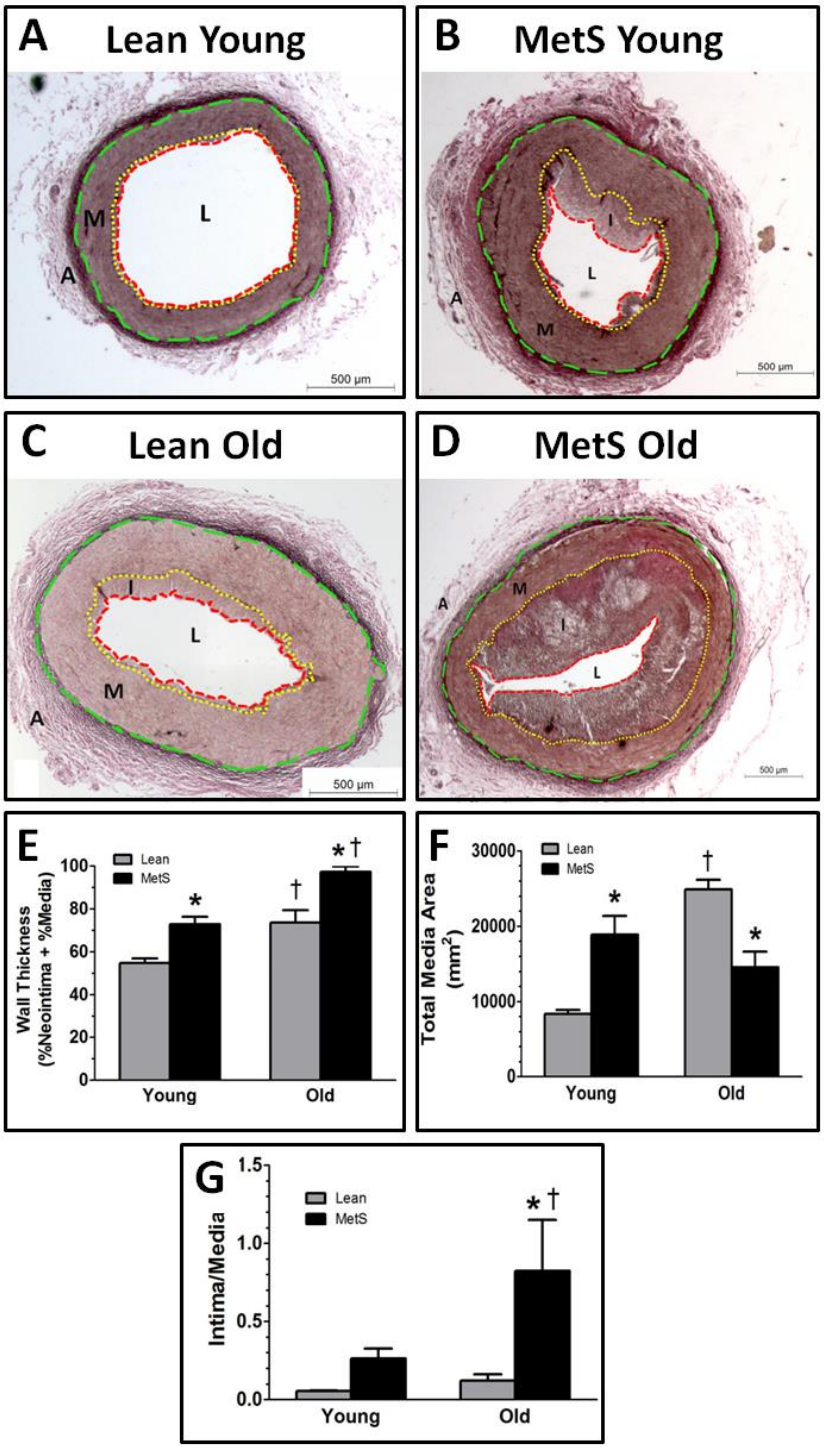

Figure 4.1: Histological staining reveals structural changes in MetS and old swine. Representative VVG histological stain of right coronary arteries reveals lean young swine (A) have almost no neointima formation. MetS young swine (B) and lean old swine (C)

have similar media thickness. MetS old swine (D) had the most advanced neointimal thickening. (E) MetS young and lean old swine both have significantly greater wall thickness compared to lean young swine, and MetS old swine exhibited the most severe wall thickness. (F) MetS young and lean old swine both exhibit media thickening that is significantly greater compared to lean young swine. (G) MetS young swine trend towards a greater intima:media area ratio compared to lean young, and MetS old swine have a greater intima:media ratio than the other groups, indicating a greater contribution of neointimal growth to disease pathology. External elastic lamina = green dashed line; internal elastic lamina = yellow dotted line; lumen = red dashed line. A, adventitia; M, media (wall); I, intima (plaque); L, lumen. *, $p < 0.05$ compared with lean swine; †, $p < 0.05$ compared with young swine. (Lean young = 6; MetS young = 9; Lean old = 4; MetS old = 3.)

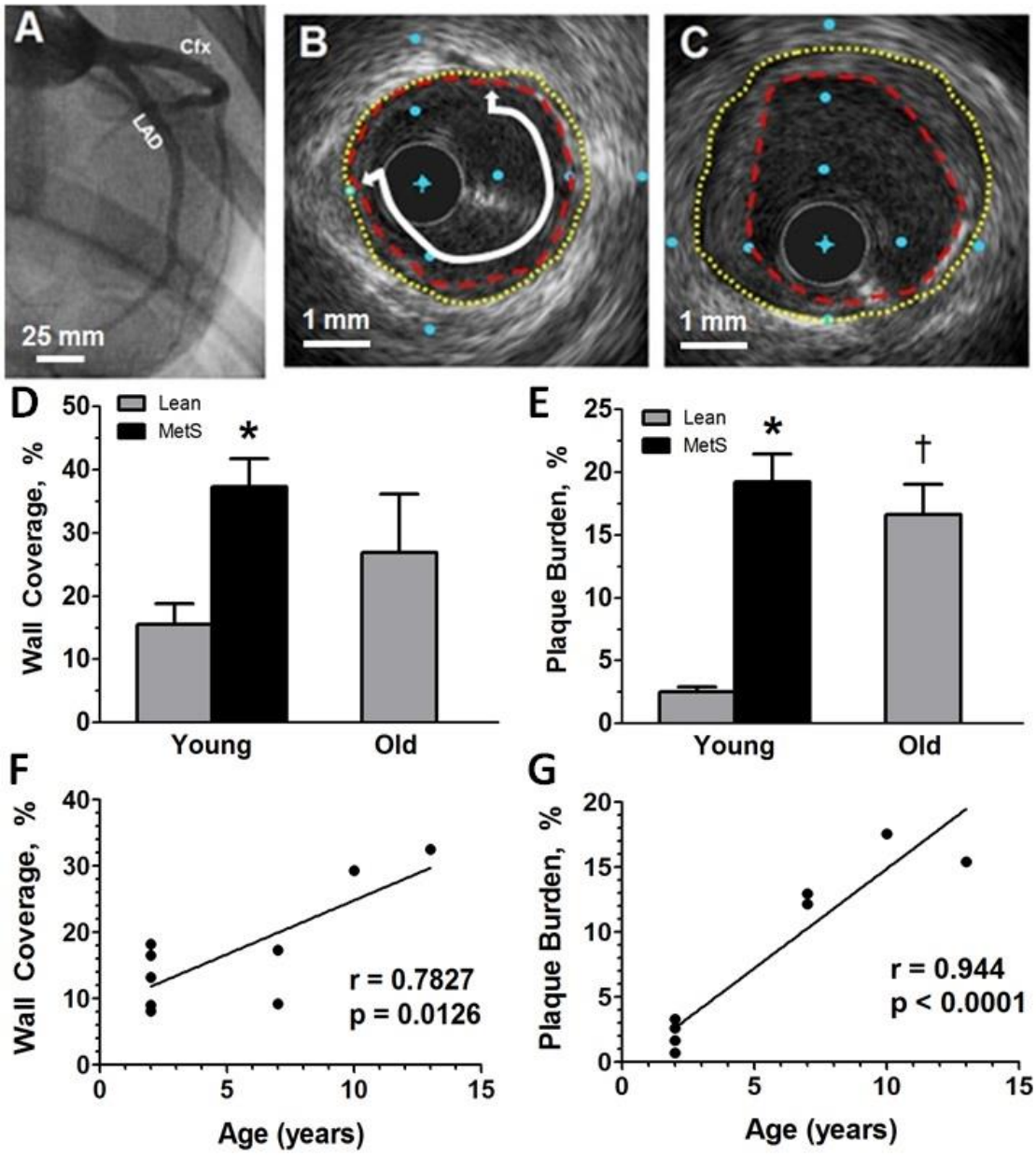

Figure 4.2: MetS young swine and lean old swine have comparable CAD severity as measured by intravascular ultrasound. (A) Angiogram showing the LAD and Cfx coronary arteries from a lean young swine. (B) Cross sectional view of a lean old swine with mild disease. (C) Cross sectional view of a MetS young swine with more severe disease. (D) MetS young swine have higher percent wall coverage than lean young swine in the proximal 15 mm of the LAD. (E) MetS young and lean old swine have greater percent plaque burden compared to lean young swine. Both percent wall coverage (F) and percent

plaque burden (G) are positively correlated to age in lean swine. Original lumen = yellow dotted line; plaque encroachment = red dashed line; wall coverage = white line with arrows. The distance between blue dots in B and C is 1 mm. *, $p < 0.05$ compared with lean swine; †, $p < 0.05$ compared with young swine.

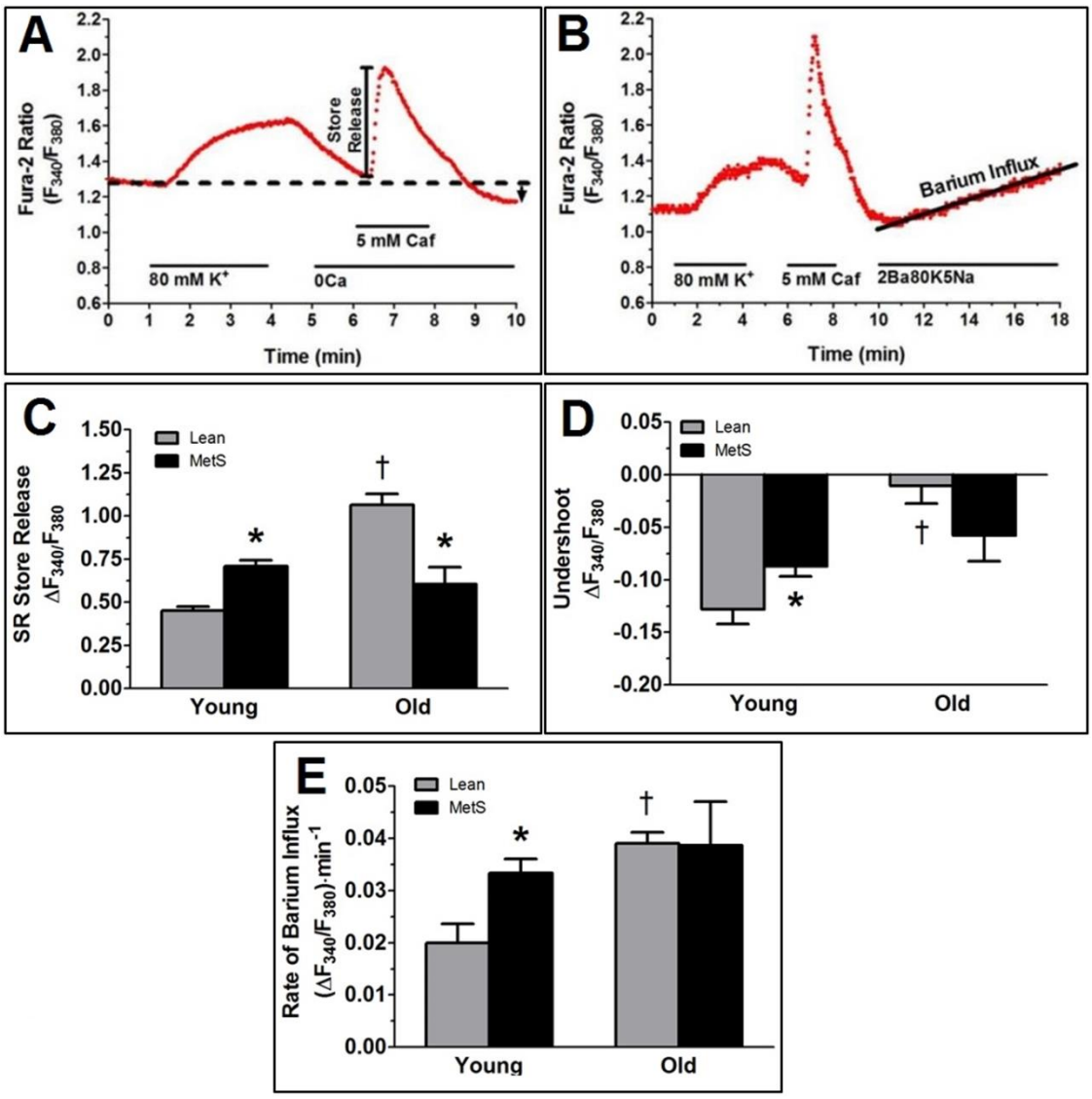

Figure 4.3: Ca^{2+} handling changes observed in MetS young and MetS old swine are exacerbated in old lean swine. (A) Representative tracing showing the change in the F_{340}/F_{380} excitation fluorescence emission ratio of a CSM cell isolated from a lean young swine. Treatments and duration are indicated by solid lines. Ca^{2+} influx was initiated by depolarization of the cell with an 80 mM K^+ solution, which maximally loaded the SR store. The 5 mM caffeine activated ryanodine receptors, causing total SR store release. After caffeine wash-out, the undershoot (black arrow), which is indicative of SERCA activity, was measured. (B) Representative tracing of a CSM cell isolated from a lean young swine

and treated with a solution containing 2 mM Ba^{2+}, 80 mM K^{+}, and 5 mM Na^{+} (2Ba80K5Na). Rate of barium entry is indicative of VGCC activity. Caf, caffeine. (C) Caffeine-induced SR store release was elevated in MetS young and lean old swine. (D) The undershoot, which is a direct measurement of SERCA function, was attenuated in MetS young and lean old swine (E) Increased Ba^{2+} influx was observed in the MetS young and lean old swine. *, $p < 0.05$ compared with young lean swine; †, $p < 0.05$ compared with young MetS swine; ‡ $p < 0.05$ compared with old lean swine. (Lean young = 6; MetS young = 10; Lean old = 4; MetS old = 3.)

Tables

Table 4.1: Ossabaw swine cardiometabolic characteristics

	Lean Young	MetS Young	Lean Old	MetS Old
Age (years)	2.0 ± 0.0	2.5 ± 0.2	9.2 ± 1.1* †	8.8 ± 1.2* †
Body Weight (kg)	74 ± 4	108 ± 2*	87 ± 5†	113 ± 7* ‡
Sex (Male/Female)	2/4	0/10	3/2	0/3
Total Cholesterol (mg/dL)	77 ± 6	474 ± 79*	60 ± 4†	411 ± 66‡
Triglycerides (mg/dL)	65 ± 18	56 ± 5	17 ± 4* †	20 ± 6
Fasting Glucose (mg/dL)	70 ± 2	81 ± 2	52 ± 12†	78 ± 7
Peak Glucose (mg/dL)	563 ± 27	755 ± 22*	688 ± 20	733 ± 44*
Blood Glucose AUC	10120 ± 667	18124 ± 919*	12237 ± 464†	15297 ± 1556*

Data are means ± SEM. MetS, metabolic syndrome; MAP, mean arterial pressure; AUC, area under curve. Fasting glucose was taken during intravenous glucose tolerance tests or during routine blood glucose monitoring for the lean old group. *, $p < 0.05$ compared with young lean swine; †, $p < 0.05$ compared with young MetS swine; ‡, $p < 0.05$ compared with old lean swine. (Lean young = 6; MetS young = 10; Lean old = 5; MetS old = 3.)

CHAPTER 5: SINGLE CELL RNA SEQUENCING ANALYSIS OF ORGAN-CULTURED PORCINE CORONARY ARTERIES REVEALS TRANSCRIPTOMIC DIVERSITY BETWEEN CORONARY SMOOTH MUSCLE CELL PHENOTYPES, BUT NO DIFFERENCE IN THE EXPRESSION OF INTRACELLULAR Ca^{2+} HANDLING GENES

Background

Under certain environmental stimuli such as growth factors, inflammation, and vascular injury, quiescent, contractile coronary smooth muscle (CSM) cells that normally populate the tunica media and are responsible for vascular tone undergo phenotypic modulation [70, 269]. This phenotypic transition is characterized by a downregulation of genes involved in contraction and an upregulation of genes involved with various other cellular functions, such as proliferation, migration, inflammation, and calcification [270]. Phenotypic plasticity is a hallmark of CSM and is necessary for adaptations to a dynamic, changing microenvironment [72, 269].

CSM phenotypic modulation plays a major role in the development and progression of several diseases such as diabetes, hypertension, and coronary artery disease (CAD) [72]. In fact, the phenotypic modulation from a contractile phenotype to a synthetic phenotype is arguably required for cardiovascular diseases [269]. In atherogenesis, endothelial dysfunction leads to the upregulation of cell adhesion molecules, which bind circulating macrophages and immune cells and facilitate their infiltration into the vessel wall [271]. This early stage inflammation and vascular injury sparks CSM dedifferentiation into a synthetic phenotype that migrates to the neointima, proliferates, and secretes extracellular matrix (ECM) proteins. As such, synthetic CSM are associated with outward remodeling, neointimal formation and growth, and collagen deposition. Further dedifferentiation into an osteogenic phenotype is associated with the initiation of vascular calcification and the progression of calcified lesions. Coronary artery calcification (CAC) is a major independent predictor of acute myocardial infarction and

mortality in patients with CAD and there are currently no known therapies to treat CAC [8, 272].

Ca^{2+} is an important secondary messenger in many signaling pathways that regulate a diverse range of basic cellular functions, including contraction [68, 187], transcription [186, 188], proliferation [68, 70], and migration [184, 185]. Different CSM phenotypes differ in their intracellular Ca^{2+} ($[Ca^{2+}]_i$) signaling, due at least in part to the differential expression and functionality of resident Ca^{2+} transport proteins [72, 273]. The contractile phenotype is associated with high voltage-gated Ca^{2+} channel (VGCC) activity and a functional sarco-endoplasmic reticulum Ca2+ ATPase (SERCA) that maintains low basal $[Ca^{2+}]_i$ [72, 274]. The synthetic phenotype is associated with greater sarcoplasmic reticulum (SR) Ca^{2+} storage capacity, greater SERCA function, and increased basal $[Ca^{2+}]_i$ due to greater VGCC activity [69, 70, 72, 73, 81, 274]. The osteogenic phenotype is associated with diminished $[Ca^{2+}]_i$ handling, including a decreased SR Ca^{2+} store and decreased SERCA activity [80, 81]. This pattern of augmented Ca^{2+} handling in the synthetic phenotype and diminished Ca^{2+} handling in the osteogenic phenotype is consistent with the biphasic nature of $[Ca^{2+}]_i$ dysregulation seen in CAD [81]. Clearly, the $[Ca^{2+}]_i$ handling modifications seen in these disparate phenotypes have important clinical ramifications for cardiovascular diseases [69, 81, 125, 155, 158].

The contractile and synthetic phenotypes have classically been defined as two ends of a phenotypic spectrum [269, 270, 275, 276], but increasing evidence for the heterogeneity of VSMC suggests much more complexity. As stated previously, several phenotypes have been identified, including inflammatory, osteogenic, chondrogenic, fibroblastic, and adipogenic [277]. These CSM phenotypes have diverse functions, indicating that they have highly differential gene expression [269, 278]. However, while contractile CSM cells have well-defined characteristics, phenotypically-modulated, non-contractile CSM represent a broad range of cells with different characteristics and

functions that have no formal definition or guidelines for identification [72, 273, 275]. Indeed, after vascular injury it was found that, although global expression levels of contractile phenotypic markers decreased, the response among CSM in the vessel wall was highly heterogeneous, indicating many intermediate phenotypes [278-281].

To further complicate this situation, many studies delving into CSM cell phenotypic heterogeneity have been conducted in mice. Using this animal model may have led to the underestimation of the true diversity of CSM phenotypic modulation [276]. Ossabaw miniature swine superbly mimic human metabolic syndrome (MetS) and CAC, indicating that the phenotypic diversity observed in CSM from Ossabaw miniature swine may better reflect the heterogeneity seen in the human population [69, 80].

Although CSM cell phenotypes have been extensively studied, no large-scale transcriptome-wide comparison of CSM has been accomplished yet. Individual cell transcriptomics is important for understanding complex biological tissues, but the heterogeneity of transcriptomes in a CSM cell population has not yet been fully elucidated. Therefore, the aims of the present study were to utilize organ-cultured coronary arteries from lean Ossabaw miniature swine and single-cell RNA sequencing (scRNA-seq) to 1) characterize the heterogeneity of a CSM cell population from a singular tissue source, 2) determine the extent to which osteogenic media modulates the CSM transcriptome, and 3) examine whether differential expression of $[Ca^{2+}]_i$ transporter genes is associated with dysregulated $[Ca^{2+}]_i$ handling in different CSM cell subpopulations.

Methods

Animals

All experimental procedures involving animals were approved by the Institutional Animal Care and Use Committee at Indiana University School of Medicine with the recommendations outlined by the National Research Council and the American Veterinary Medical Association Panel on Euthanasia [170, 171]. Ossabaw miniature swine (n = 7)

provided by CorVus Biomedical, LLC were fed 725 g/day of standard chow (5L80, Purina Test Diet, Richmond, IN) that contained 18% kcal from protein, 71% kcal from complex carbohydrates, and 11% kcal from fat. Swine were euthanized via cardiectomy. Coronary arteries were excised and stored for no longer than 24 hours in a physiological salt solution containing (in mM): 2 CaCl 2 , 138 NaCl, 1 MgCl 2 , 5 KCl, 10 HEPES, 10 glucose; pH 7.4.

Ex vivo coronary artery organ culture

Conduit coronary arteries were cut into 2-4 mm long segments and organ cultured for 3 days in osteogenic media (DMEM supplemented with 10% FBS, 1% Penicillin-Streptomycin, 180 mg/dL glucose, 3.8 mM inorganic phosphate, and 7.5 U/ml alkaline phosphatase (ProMega, Madison, WI)) at 37°C in a 95% O_2, 5% CO_2 incubator. The osteogenic media was changed on day 2 (for full protocol, see Appendix G).

CSM cell dispersion

CSM in the arterial segments were enzymatically dispersed with serial dispersions in 300 U/mL collagenase (Worthington Biochemical, Lakewood, NJ) and suspended in a 0.2% bovine serum albumin solution in 0.9% NaCl on ice. Greater than 95% of cells acutely isolated from coronary arteries are elongated, thus highly indicative of CSM phenotype [282]. To facilitate separation of cells for single-cell RNA-sequencing, cells were exposed to 0.25% trypsin to yield spherical cells and then passed through a 40 μm cell strainer to remove cells too large for single-cell RNA-sequencing (for full protocol, see Appendix H).

Single-cell RNA-sequencing

Single-cell RNA-sequencing was performed in the Center for Medical Genomics at Indiana University School of Medicine (Indianapolis, IN). The Chromium Single Cell 3' Library & Gel Bead Kit v2 (10X Genomics) was used, and all the steps outlined in the 10X protocol were followed (http://resources.qiagenbioinformatics.com/manuals/

clcgenomicsworkbench/752/User_Manual.pdf). Briefly, all samples and reagents were prepared and loaded into the chip. Then, the Chromium Controller generated droplets where reverse transcription was conducted. cDNA was recovered through demulsification and bead purification. Pre-amplified cDNA was further subjected to library preparation. Libraries were sequenced on an Illumina Hiseq 4000 and aligned to the publicly available *Sus scrofa* genome.

Intracellular free Ca^{2+} imaging

Whole-cell intracellular free Ca^{2+} levels were measured at room temperature (22–25 °C) by using the fluorescent Ca^{2+} indicator fura-2 AM (InCa++ Ca2+ Imaging System, Intracellular Imaging, Cincinnati, OH) as previously described [80, 81, 204, 283]. Briefly, freshly dispersed smooth muscle cells from the left anterior descending (LAD) artery were incubated with 3.0 μM fura2 AM (Molecular Probes, Eugene, OR) in a shaking water bath at 37 °C for 45 min before being washed in a solution containing low Ca^{2+} concentration. An aliquot of cells loaded with fura-2 AM was placed on a coverslip contained within a constant-flow superfusion chamber that was mounted on an inverted epifluorescent microscope (model TMS-F, Nikon, Melville, NY), with flow maintained at a constant rate of 1–2 mL/min. Basal Ca^{2+} levels were measured in physiologic salt solution composed of the following (in mM): 2 $CaCl_2$, 138 NaCl, 1 $MgCl_2$, 5 KCl, 10 HEPES, 10 glucose; pH 7.4. Calcium influx and maximal sarcoplasmic reticulum (SR) Ca^{2+} loading was accomplished by depolarization with high (80 mM) K^+ solution (2 $CaCl_2$, 63 NaCl, 1 $MgCl_2$, 80 KCl, 10 HEPES, 10 glucose; pH 7.4) (Neeb et al., 2010). SR Ca^{2+} stores were released with 5 mM caffeine in Ca^{2+}-free solution (138 NaCl, 1 $MgCl_2$, 5 KCl, 10 HEPES, 10^{-5} M K^+-EGTA, 10 glucose; pH 7.4) (for solution recipes, see Appendix F). The undershoot below baseline after caffeine wash-out was used to measure SERCA function. Fura-2 in CSM was excited by light from a 300 W xenon arc lamp that was passed through a computer-controlled filter changer containing 340 nm and 380 nm bandpass filters every 0.30 and 0.05 s,

respectively. The fluorescence emission at 510 nm was collected by using a monochrome charge-coupled device camera (COHU, San Diego, CA) (for full protocol, see Appendix E). Whole-cell fura-2 fluorescence was expressed as the 340 nm/380 nm ratio of fura-2 emission. A graph demonstrating the experimental protocol is shown in Fig. 6A.

Histology

Coronary artery segments (2–4 mm in length) were placed in 10% phosphate-buffered formalin for 24–48 hours, then transferred to 70% ethanol. Histology was performed in the Department of Anatomy and Cell Biology at Indiana University School of Medicine (Indianapolis, IN). Verhoeff van Gieson (VVG) staining was used to assess the percent media (for full protocol, see Appendix B), Masson's trichrome staining was used to assess the percent collagen (for full protocol, see Appendix C), and Von Kossa (VK) staining was used to assess the percent vascular calcification (for full protocol, see Appendix D). Images were captured using a LEICA DM 300 inverted microscope and analyzed with Adobe Photoshop CS6 (Adobe Systems, Inc. San Jose, CA).

Immunohistochemistry

Coronary artery segments (2–4 mm in length) were placed in 10% phosphate-buffered formalin for 24–48 hours, then embedded in paraffin. Tissue sections were stained with anti-mouse CD9 monoclonal antibody (BD Pharmingen, San Diego, CA) as a marker for VSMC-derived exosomes by the Department of Pathology at Indiana University School of Medicine (Indianapolis, IN). Images were captured using a LEICA DM 300 inverted microscope and analyzed with Adobe Photoshop CS6 (Adobe Systems, Inc. San Jose, CA).

Statistics

I used the Seruat software package (https://satijalab.org/seurat/) for tSNE analysis [284, 285] and Ingenuity Pathway Analysis (IPA) for analysis of canonical pathways (QIAGEN, Inc., https://www.qiagenbioinformatics.com/products/ingenuity-pathway-

analysis). Statistical analysis was performed using GraphPad Prism 5.0 (San Diego, CA). Student's t test was performed when appropriate. $P < 0.05$ was considered statistically significant.

Results

Organ-cultured arterial rings exhibited pathological remodeling

After three days cultured in osteogenic media, coronary rings exhibited greater medial thickening (Fig. 5.1A, D, G), greater collagen formation (Fig. 5.1B, E, H), and a greater vascular calcification (Fig. 5.1C, F, I) compared to non-cultured rings.

Organ culture conditions induce greater expression of exosomes

CD9 expression, a marker of vascular smooth muscle cell-derived exosomes that form the nidus for calcification [276, 286], was increased after 3 days in culture (Fig. 5.2A-C).

CSM from organ-cultured arterial rings exhibited lower overall expression of contractile markers

Global RNA analysis revealed a decrease in contractile markers in CSM harvested from cultured arterial rings compared to CSM from non-cultured rings (Fig. 5.3A-C). Cells from cultured arteries also showed greater expression of proliferative markers (Fig. 5.3D-E) and osteogenic markers (Fig. 5.3F).

Counting Map Reads

Control, non-cultured rings yielded data from 3,296 cells. On average, there were 71,715 reads per cell and 92% of the reads were confidently mapped to the genome. An average of 14,786 genes were detected, with 787 genes per cell. Cultured rings yielded data from 5,322 cells. On average, there were 62,735 reads per cell and 93 of the reads were confidently mapped to the genome. An average of 15,230 genes were detected, with 1,666 genes per cell. The t-distributed stochastic neighbor embedding (t-SNE) method of unsupervised learning was used to visualize the various cell types present in the sample,

as represented by differently colored clusters (Fig. 5.4A-B). There were 11 unique cell types identified in the cells isolated from control arterial rings (Fig. 5.4A) and 12 unique cell types identified in the cells isolated from cultured arterial rings (Fig. 5.4B). Cell clusters were identified as CSM if they had positive expression of at least three genes associated with either the contractile or synthetic CSM phenotype (Table 5.1). 46% of the total cells from 5 unique clusters in the control condition and 39% of the total cells from 6 unique clusters in the organ-culture condition were identified as smooth muscle. Various other cell types were identified in the sample, such as fibroblasts, macrophages, endothelial cells, and adipocytes (data not shown). In the control condition, 32% of total smooth muscle cells were identified as contractile, while 69% were identified as synthetic. In the organ-culture condition, only 17% of total smooth muscle cells were identified as contractile, 78% were identified as synthetic, and 5% were identified as an intermediate phenotype expressing three or more markers for both the contractile and synthetic phenotype.

Coronary smooth muscle exhibited remarkable diversity

Two cell clusters from the control condition were identified as contractile and three were identified as synthetic. Different clusters of CSM exhibited augmented expression of genes involved in different cellular processes, as illustrated by the top ten highly expressed genes for each cluster (Fig. 5.5A-B). For example, one cluster of contractile CSM cells exhibited increased expression of genes involved in transcription and cell cycle activation (“Contractile #1”) while the other contractile CSM cell group (“Contractile #2”) had a lower expression of these genes but even higher expression of genes involved in contraction (Fig. 5.5A). Synthetic CSM cells were enriched in genes involved in extracellular matrix remodeling and inflammation (Fig. 5.5A). The organ-cultured condition contained one contractile CSM cell cluster, four synthetic CSM cell clusters, and one CSM cell cluster that was an “intermediate” phenotype between contractile and synthetic (Fig.

5.5B). Similar genes were upregulated in the cultured clusters compared to the non-cultured clusters, but genes involved in vascular calcification, including matrix metallopeptidase 9 (MMP9), osteopontin (SPP1), and sphingomyelin phosphodiesterase acid like 3B (SMPDL3B), were also upregulated in some cell clusters from organ-cultured arteries (Fig. 5.5B).

Coronary smooth muscle cells show extensive intra-phenotype variation in gene expression

Both contractile and synthetic CSM cells from cultured arterial rings exhibited extensive variation in gene expression when compared to their phenotypic counterparts in cells from non-cultured rings. Culture conditions induced greater pro-inflammatory, pro-calcific gene expression in both contractile and synthetic CSM cells (Table 5.2). Furthermore, even the contractile markers themselves were lower in contractile CSM cells from cultured arteries compared to contractile CSM cells from non-cultured arteries (Table 5.2).

Intracellular calcium handling is dysregulated in coronary smooth muscle cells from cultured arterial rings

Fig. 5.6A shows a representative CSM $[Ca^{2+}]_i$ response from a freshly isolated control CSM cell. Treatments and durations are marked by the solid lines. The basal $[Ca^{2+}]_i$ levels during superfusion with a physiological salt solution were lower in cells from arteries cultured for 3 days (Fig. 5.6B). Depolarization-induced Ca^{2+} influx and the SR Ca^{2+} storage capacity, as measured by the caffeine-sensitive SR Ca^{2+} store release, both drastically decreased in CSM cells from cultured arteries (Fig. 5.6C-D). SERCA function as measured by the undershoot below baseline was comparable between groups (data not shown).

Coronary smooth muscle from cultured rings did not exhibit any direct changes in Ca^{2+} transporter gene expression

None of the CSM cell clusters from either condition exhibited differential expression of transcripts for Ca^{2+} transporters, including VGCC, transient receptor potentiation (TRP) channels, SERCA, sodium-calcium exchangers (NCX), plasma membrane Ca^{2+}-ATPases (PMCA), IP_3 receptors (IP_3R), and ryanodine receptors (RyR). The phosphate transporters PiT-1 and PiT-2 also did not exhibit any changes in gene expression (data not shown).

CSM exhibited extensive canonical pathway diversity

The canonical pathways feature from IPA was used to determine the cell clusters' relative activation or repression of signaling pathways implicated in SMC differentiation, phenotypic switching, disease severity, and cellular stress responses (Fig. 5.7). Every cell cluster from both conditions exhibited an upregulation of at least one canonical signaling pathway associated with contractile phenotype maintenance and synthetic phenotypic modulation. Even though baseline $[Ca^{2+}]_i$, Ca^{2+} influx, and SR store release were diminished in cells from organ cultured arteries (Fig. 5.5B-D), specific clusters such as the "Contractile #2" and "Synthetic #1" groups from the control condition and the "Contractile" group from the organ-cultured condition exhibited upregulated Ca^{2+} signaling. All of these groups displayed upregulation of the NFAT pathway, a Ca^{2+}-dependent transcription factor [273]. However, many other cell clusters that did not show augmented Ca^{2+} signaling still exhibited the upregulation of the Ca^{2+}-dependent transcription factors NFAT and CREB. The Wnt/β-catenin canonical pathway, which is involved in osteogenic dedifferentiation and vascular calcification [287-291], was downregulated in both contractile groups from the control, non-cultured condition and in the "Synthetic #2" and "Synthetic #3" groups from the organ cultured condition. However, the synthetic groups also exhibited upregulation of the osteoarthritis canonical pathway, which has also been

implicated in CSM osteogenic dedifferentiation and vascular calcification [292]. Clearly, the regulation of these signaling pathways and their downstream effects in the cell are highly complex.

Several genes involved in vascular calcification are upregulated in synthetic CSM

Many genes involved in the canonical osteoarthritis pathway are involved in the active vascular calcification process [292]. Synthetic CSM cell clusters exhibited enhanced expression of several genes involved in vascular calcification, including osteopontin (SPP1), annexins A2 and A5 (ANXA2/5), matrix metallopeptidase 9 (MMP9), and sphingomyelin phosphodiesterase acid like 3B (SMPDL3B). Both contractile groups from the control condition exhibited the lowest expression of genes involved in this pathway (Fig. 5.8).

Discussion

This study validates the concept of extensive CSM phenotypic heterogeneity in both control and pathological conditions by utilizing single-cell RNA-sequencing and tissue from a clinically relevant large animal model (Fig. 5.3). Organ-cultured arteries exhibited greater media area, collagen content, and vascular calcification (Fig. 5.1), with a dramatic overexpression of CD9, a marker for vascular smooth muscle cell-derived exosomes (Fig. 5.2). CSM cell subpopulations that were identified as synthetic were present in both the control and organ-cultured conditions (Fig. 5.4). However, different genes were upregulated in the synthetic phenotype groups from the different conditions; synthetic cells from organ-cultured conditions exhibited the upregulation of several genes involved in inflammation and vascular calcification (Table 5.2). All cell clusters expressed an upregulation of at least one canonical pathway associated with the contractile and synthetic phenotypes (Fig. 5.6). All cell groups exhibited upregulation of at least four genes that are involved in the osteoarthritis pathway, and both contractile cell groups from the control condition exhibited the lowest expression levels of genes involved in this pathway

(Fig. 5.7). While basal $[Ca^{2+}]_i$ levels and $[Ca^{2+}]_i$ handling was dysregulated after 3 days in organ culture (Fig. 5.5), there was no difference in Ca^{2+} transporter gene expression in any of the CSM groups. Therefore, the differences seen in $[Ca^{2+}]_i$ handling may be due to protein expression and/or post-translational modifications that change the functionality of the Ca^{2+} transporters.

CSM phenotypic modulation is associated with altered $[Ca^{2+}]_i$ handling and Ca^{2+} transporter gene expression. In the current study the organ culture conditions induced a global decrease in basal $[Ca^{2+}]_i$, Ca^{2+} influx, and SR Ca^{2+} store release, all indicative of the osteogenic phenotype present in severe CAD [80, 105]. Despite this profound Ca^{2+} dysregulation, none of the Ca^{2+} transporters exhibited differential expression in any of the cell subpopulations. Therefore, the difference seen in $[Ca^{2+}]_i$ handling might be exclusively due to functional changes. Many cell populations in this study exhibited evidence of oxidative stress through the pathways that were upregulated, such as the NRF2-mediated oxidative stress response. When SERCA is irreversibly oxidized on cysteine residues its activity is greatly reduced [293, 294]. This reduces the sequestration of $[Ca^{2+}]_i$, leading to increased basal $[Ca^{2+}]_i$ levels and decreased SR Ca^{2+} storage capacity [294]. This could diminish Ca^{2+} transporter function without affecting expression of that transporter. Although in this study no change in SERCA function was detected, oxidative stress has also been associated with modified activity of many other Ca^{2+} transporters, including VGCC, RyR, IP_3R, and PMCA [295-297]. These translate into functional changes *in vivo* such as decreased contractility [295]. Future studies will be needed to delineate the contributions of specific Ca^{2+} transporter functional changes to dysregulated $[Ca^{2+}]_i$ handling. Further, the possibility should be investigated that decreased SR Ca^{2+} storage capacity could trigger endoplasmic reticulum stress response genes that have been implicated in vascular calcification [89].

Even though overall $[Ca^{2+}]_i$ handling was diminished in CSM cells from cultured arteries, the IPA canonical pathways analysis predicted that some cell clusters would exhibit increased Ca^{2+} signaling. These clusters were the “Contractile #2” group and the “Synthetic #1” group from the control condition and the “Contractile” group from the organ-cultured condition. This finding is expected, as localized Ca^{2+} signaling events such as Ca^{2+} sparks and waves are necessary for CSM contraction [69]. Subsequently, these clusters also predicted greater activation of the Ca^{2+}-dependent transcription factor NFAT, which was consistent with the NFAT gene expression. The $[Ca^{2+}]_i$ handling patterns in CSM cells from a single tissue source exhibit vast diversity. Therefore, future experiments using VSMCs should not treat them as a monolith.

In the current study, I show that CSM phenotypic modulation is not a discreet event or a continuum, but rather is a network of interconnected phenotypes. Indeed, CSM cells have the capacity to exhibit characteristics and markers of several different phenotypes. This is in agreement with the literature, with several studies identifying the upregulation of genes associated with both the contractile and synthetic phenotypes in the neointima after vascular injury [269, 298, 299]. Some studies even point to a range of contractile phenotypes in certain vascular beds [276].

The complex heterogeneity of phenotypic modulation is exemplified by differing identity markers present in vascular smooth muscle cells (VSMC). More than 80% of VSMC-derived cells lacked any measurable expression of VSMC markers and 30% expressed traditional markers for macrophages *in vivo* in $ApoE^{-/-}$ mice [300-302]. This is in contrast to *in vitro* experiments showing that a vast majority of proliferating VSMC continue to express contractile markers for several days in culture [303, 304]. To further complicate the situation, a study using human coronary artery sections discovered that 40% of foam cells express VSMC markers [301, 302]. While the macrophage-like, inflammatory SMC phenotype is common in human atherosclerotic lesions, these studies

indicate that even cells expressing VSMC markers may not be of VSMC origin [302, 305]. Future studies should use caution when identifying VSMC by phenotype, as traditional markers may not be adequate.

The great range of VSMC phenotypes points to complex transcriptional regulatory pathways that are involved in phenotypic modulation [276]. Different canonical pathways are associated with VSMC switching to various phenotypes. For example, the PI3K/AKT pathway is associated with maintenance of the contractile phenotype [306-308], the PDGF, ERK, and VEGF pathways are associated with the synthetic phenotype [307-312], and the STAT3 and Wnt/β-catenin pathways are associated with the osteogenic phenotype [276, 287-291]. However, some pathways such as TGF-β, PKA, and NF-κB are involved in the expression of multiple VSMC phenotypes [273, 276, 311-316]. The balance of these pathways has an important role in phenotypic modulation. In fact, one study found that VSMC phenotype is determined primarily by the balance between the PI3K/AKT pathway and the ERK and p38 MAPK pathways [307]. This balancing act of various different canonical pathways adds to the complexity and heterogeneity of CSM cells.

In this study, coronary arteries were cultured in osteogenic media supplemented with high amounts of inorganic phosphorous. Hyperphosphatemia is associated with VSMC transition to an osteogenic phenotype and vascular calcification [276, 317]. High calcium and phosphate levels have been implicated in the differential expression of genes involved with ion transport, such as PiT-1 and PiT-2 [318]. PiT-1 and PiT-2 may have had augmented functionality, as none of the CSM cell groups exhibited differential expression of these transporters. Genes involved in the calcification process such as annexins A2 and A5, osteopontin, and aggrecanases were upregulated even before differential expression of Ca^{2+} transporters. This supports the notion that events leading to vascular calcification occur early in the atherosclerotic process [105].

The osteogenic media did induce phenotypic switching, as evidenced by the changes in the transcriptome and the higher level of vascular calcification. Elevated extracellular Ca2+ has been found to induce calcification through an exosome-dependent pathway through upregulation of sphingomyelin phosphodiesterase acid like 3B (SMPDL3B) [286]. The current study showed the upregulation of the SMPDL3B gene in several CSM cell subpopulations in the cultured arteries, along with higher expression of the vascular SMC-derived exosome marker CD9 (Fig. 5.2). This points to the osteogenic shift in transcriptomes of cells from the cultured condition.

A major conclusion is that the markedly impaired $[Ca^{2+}]_I$ handling in the absence of decrease in the Ca^{2+} transporter gene expression indicate a crucial role for Ca^{2+} signaling in excitation-transcription coupling [63, 188] in regulation of vascular calcification [286]. Wamhoff and coworkers elegantly showed that upregulation of Ca^{2+} influx through voltage-gated Ca^{2+} channels increased activation of vascular smooth muscle differentiation marker gene expression [286]. The functional increase in Ca^{2+} influx occurred with no change in Ca^{2+} channel gene expression. The proatherogenic stimuli act on Ca^{2+} transporters to cause Ca^{2+} dysregulation. The “proatherogenic stimuli” in the current organ culture study are the calcification media and organ culture itself. I also showed the phenomenal increase in CD9 expression (Fig. 5.2), providing the exosome nidus for vascular calcification and the expression of sphingomyelin phosphodiesterase acid like 3B (SMPDL3B) that drives exosome trafficking to the plasma membrane [286]. The functional studies of $[Ca^{2+}]_I$ handling and single-cell RNA sequencing of the vascular transcriptome enabled the elucidation of these links to vascular calcification.

Figures

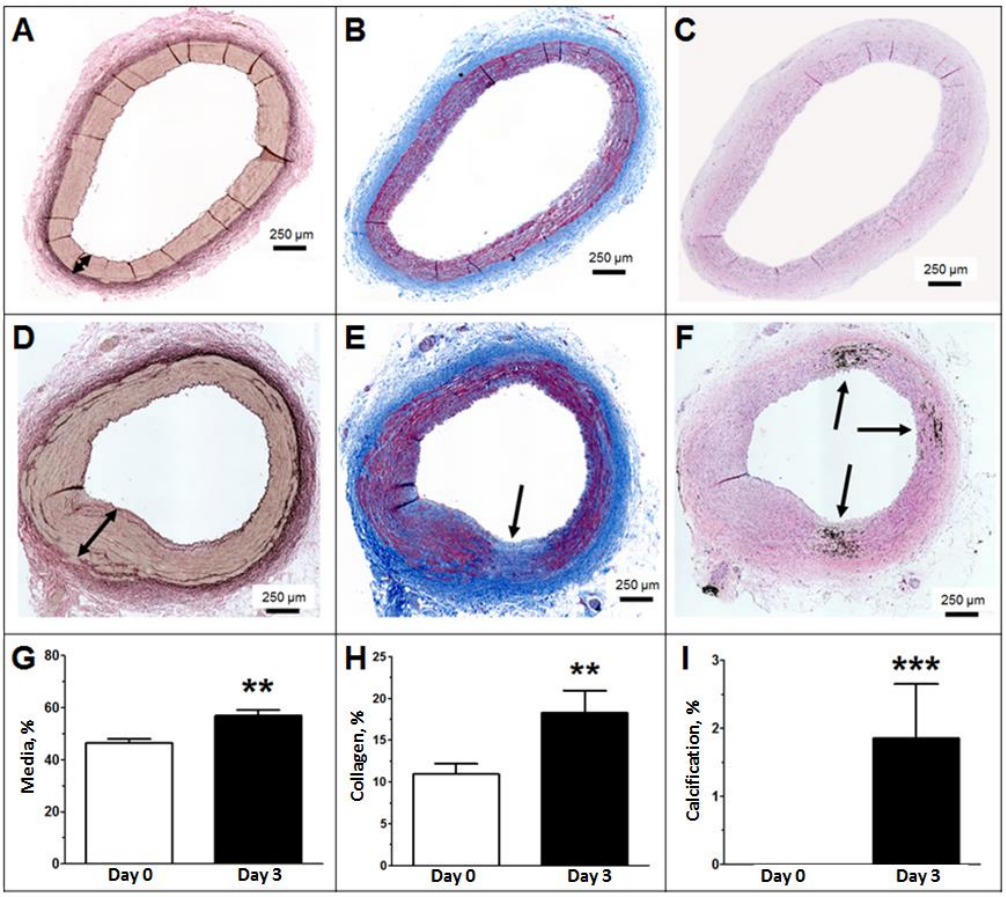

Figure 5.1: Organ culture induced pathological arterial remodeling. Representative Verhoeff van-Gieson histological staining from a control, non-cultured artery (A) and an artery cultured for 3 days in osteogenic media (D) exemplifies significant medial thickening in the organ culture condition (G). Representative Masson's trichrome histological staining from a control artery (B) and an artery cultured for 3 days in osteogenic media (E) exemplifies significant collagen accumulation (H). Representative Von Kossa histological staining from a control artery (C) and an artery cultured for 3 days in osteogenic media (F) shows overt vascular calcification in the culture conditions (I). Black arrows point to the thickened media (A, D), an area of collagen accumulation (E), and areas of calcification (F). (n = 16 arterial rings for control; n = 12 arterial rings for day 3.)

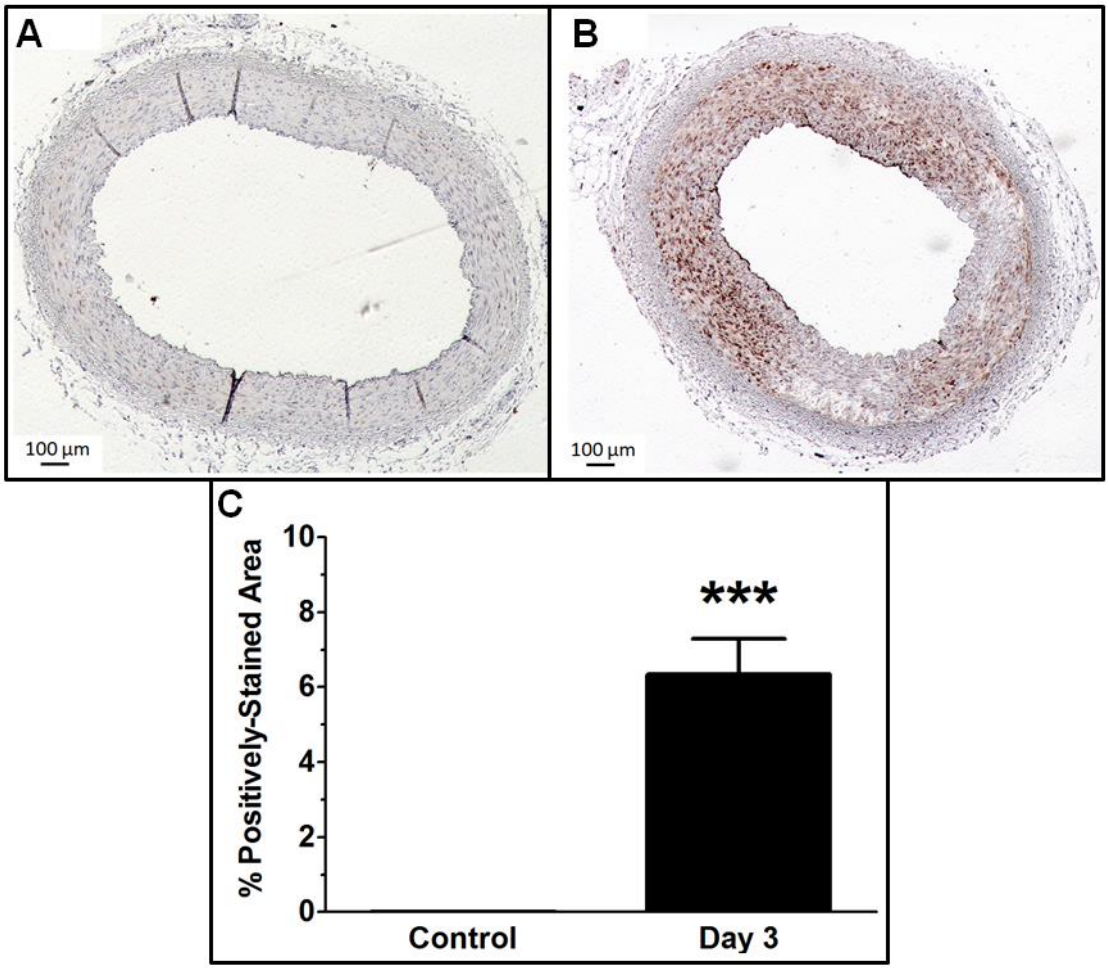

Figure 5.2: Exosome expression is increased in cultured arterial rings. Immunohistochemical analysis using an antibody against CD9, a marker of VSMC-derived exosomes, revealed minimal to no expression in non-cultured arteries (A) and extensive expression (brown staining) in cultured arteries (B). The expression of CD9 is significantly upregulated in cultured arteries (C). (n = 18 arterial rings for control; n = 12 arterial rings for day 3.)

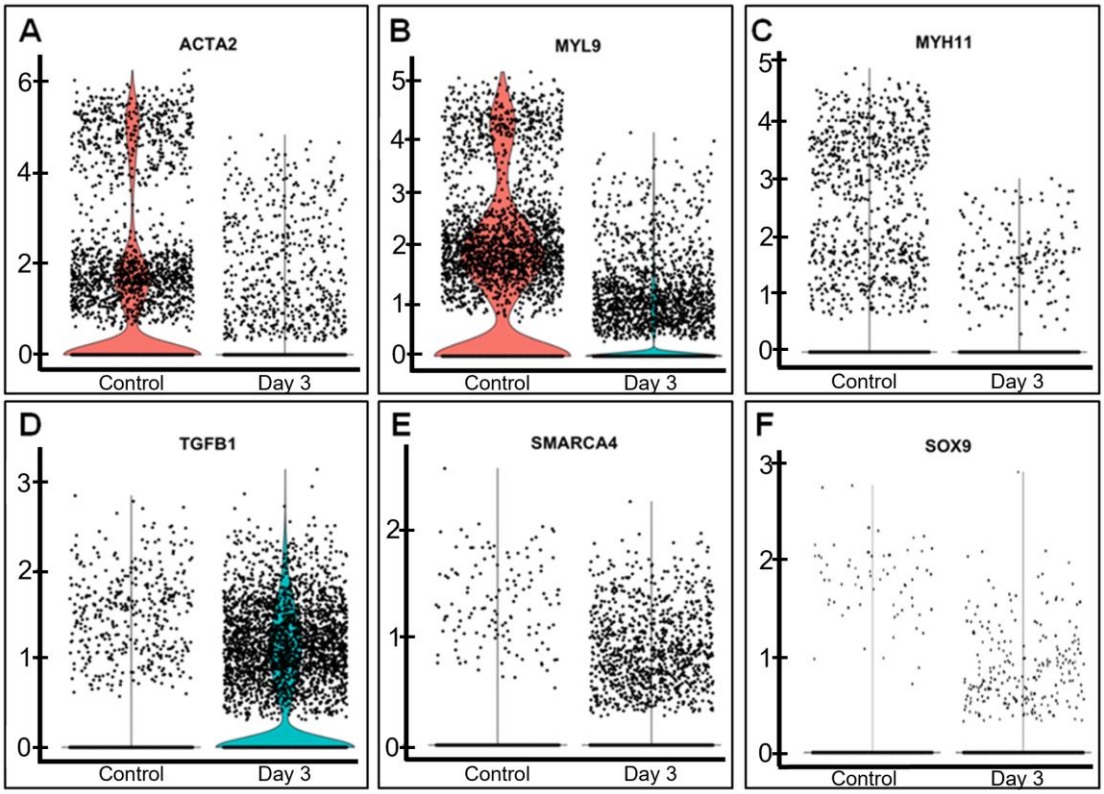

Figure 5.3: Culture conditions induce a global decrease of contractile smooth muscle cell markers. Violin plots show the expression level and density of expression for the ACTA2 (A), MYL9 (B), and MYH11 (C) genes, which are decreased after 3 days in organ culture. TGFB1 (D) and SMARCA4 (E), makers of the synthetic smooth muscle cell phenotype, exhibited higher expression after 3 days in organ culture. Sox9 (F), a marker for the osteo/chondrogenic phenotype, was also upregulated after 3 days in organ culture. Each black dot is one cell.

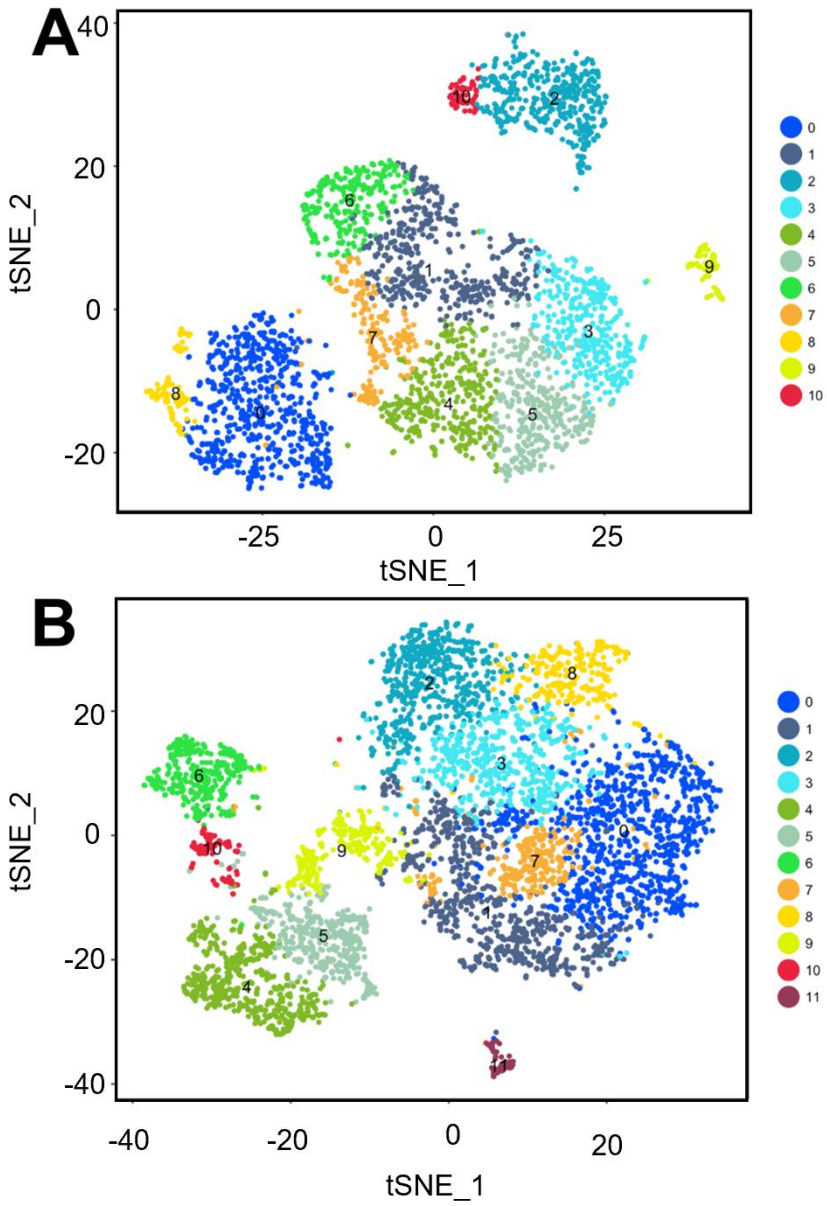

Figure 5.4: t-SNE analysis shows the heterogeneity of cells that compose the coronary vasculature. (A) Unsupervised clustering for cells dispersed from control arterial rings. There were 11 distinct cell clusters, of which 5 (clusters 0, 2, 6, 8, 10) were identified as CSM. (B) Unsupervised clustering for cells dispersed from arterial rings cultured in osteogenic media for 3 days. There were 12 distinct cell clusters, of which 6 (clusters 2, 4, 5, 6, 10, 11) were identified as CSM. Unsupervised clustering provides a means to identify cells of interest that share a common phenotype.

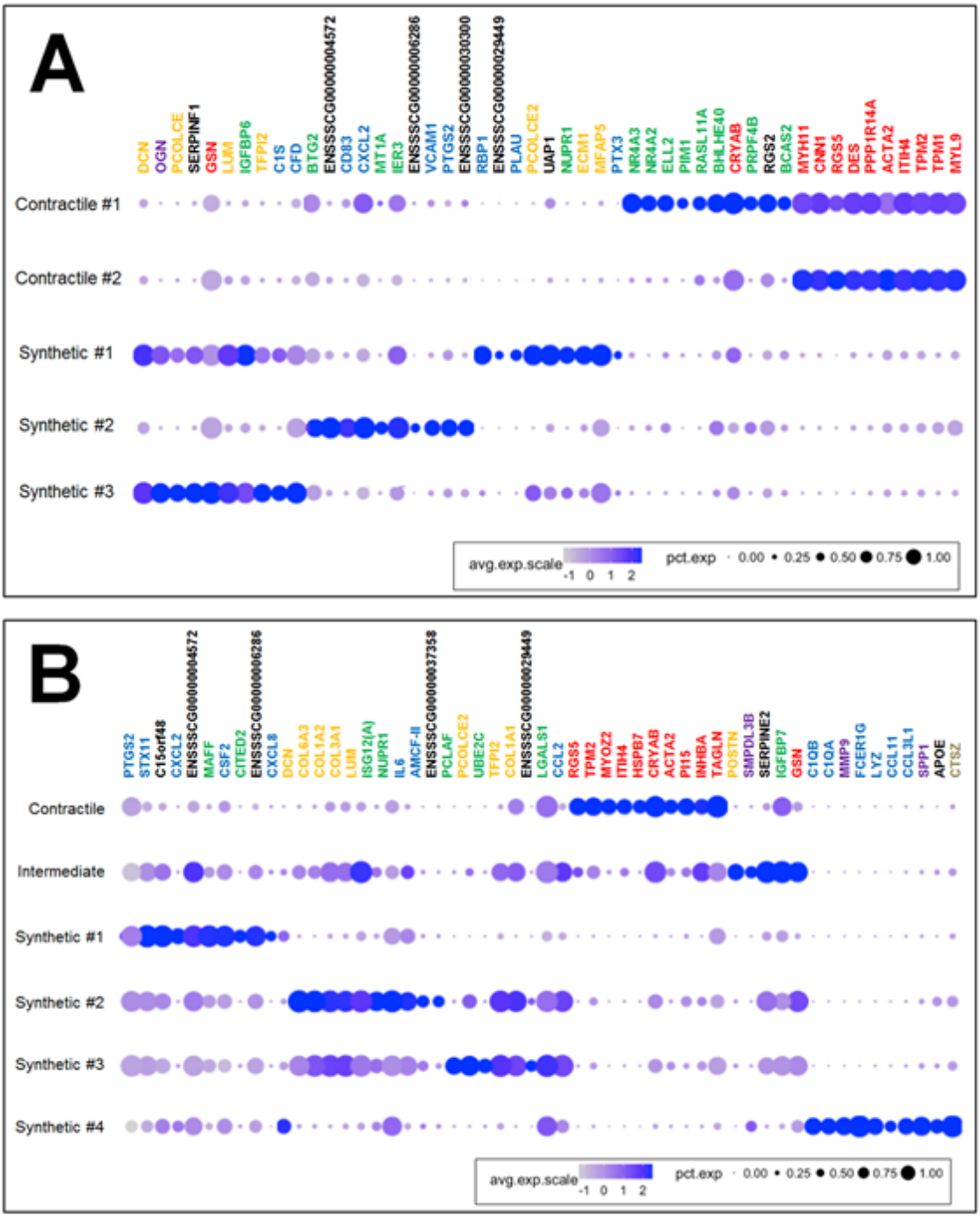

Figure 5.5: The top ten differentially expressed genes per CSM cluster show that CSM from cultured arterial rings have greater phenotypic diversity. (A) CSM dispersed from non-cultured arteries showed actively proliferating contractile cells ("Contractile #1) and non-proliferating contractile cells ("Contractile #2). Cells with the

synthetic phenotype were characterized by the upregulation of genes involved in extracellular matrix remodeling (“Synthetic #1 and #2”) and genes involved in the immune response (“Synthetic #3”). (B) CSM dispersed from cultured arteries exhibited the contractile phenotype and a phenotype that was between contractile and synthetic (“Intermediate”). Cells with the synthetic phenotype were characterized by the upregulation of genes involved in inflammation (“Synthetic #1), extracellular matrix remodeling (“Synthetic #2 and #3), and vascular calcification (“Synthetic 4”). Genes are color-coded based on function: orange, extracellular matrix remodeling; blue, immune response; green, proliferation; red, contraction and cytoskeleton organization; purple, vascular calcification; brown, apoptosis.

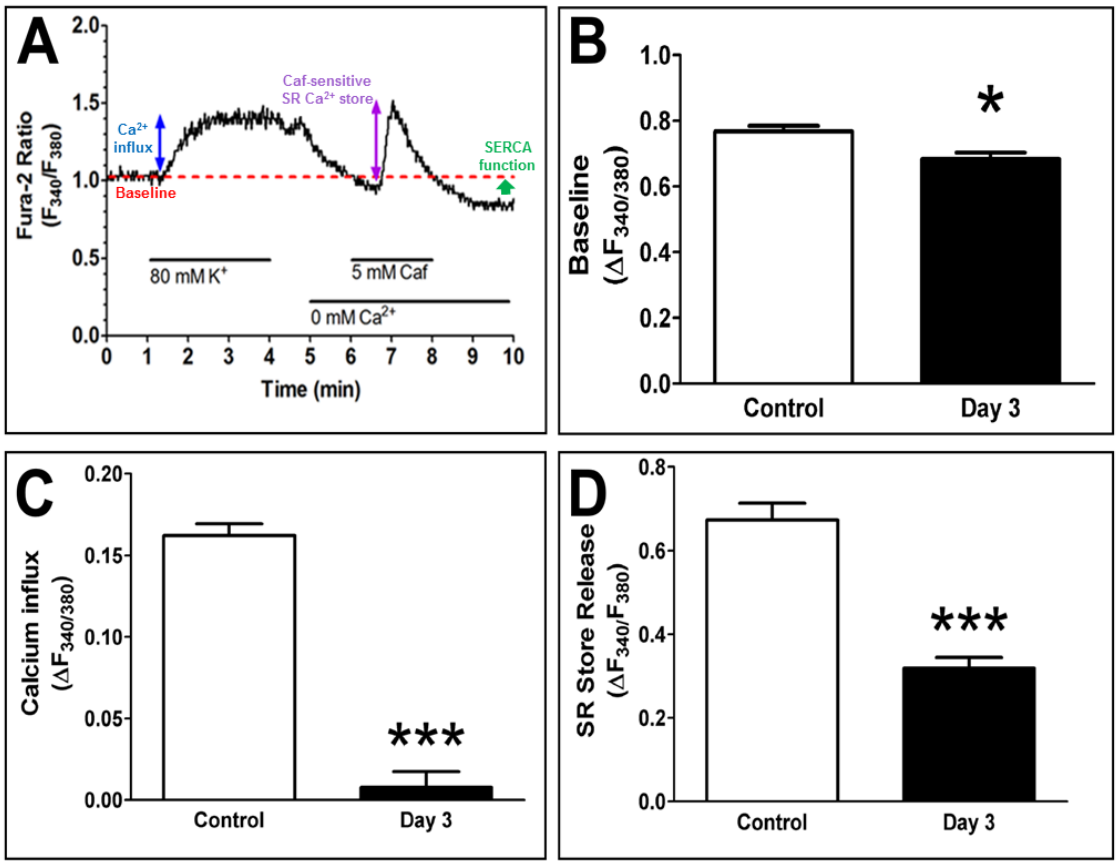

Figure 5.6: CSM from rings cultured for 3 days in osteogenic media exhibited blunted $[Ca^{2+}]_i$ handling. (A) After measuring baseline $[Ca^{2+}]_i$ levels (red dashed line), the cell was depolarized with an 80 mM K^+ solution to induce Ca^{2+} influx via voltage-gated Ca^{2+} channels (blue double-headed arrow) and to maximally load the sarcoplasmic reticulum (SR) store. The SR Ca^{2+} store (purple double-headed arrow) was then released by activating ryanodine receptors with 5 mM caffeine. SERCA function (small green arrow) was measured as the undershoot below baseline after a caffeine wash-out phase. (B) Baseline $[Ca^{2+}]_i$ levels were lower 3 days after organ culture. (C) The measured Ca^{2+} influx upon membrane depolarization was drastically reduced in CSM from cultured arteries. (D) The measured SR store release from CSM from cultured arteries was also greatly reduced. (n = 169 cells for control; n = 31 cells for day 3.)

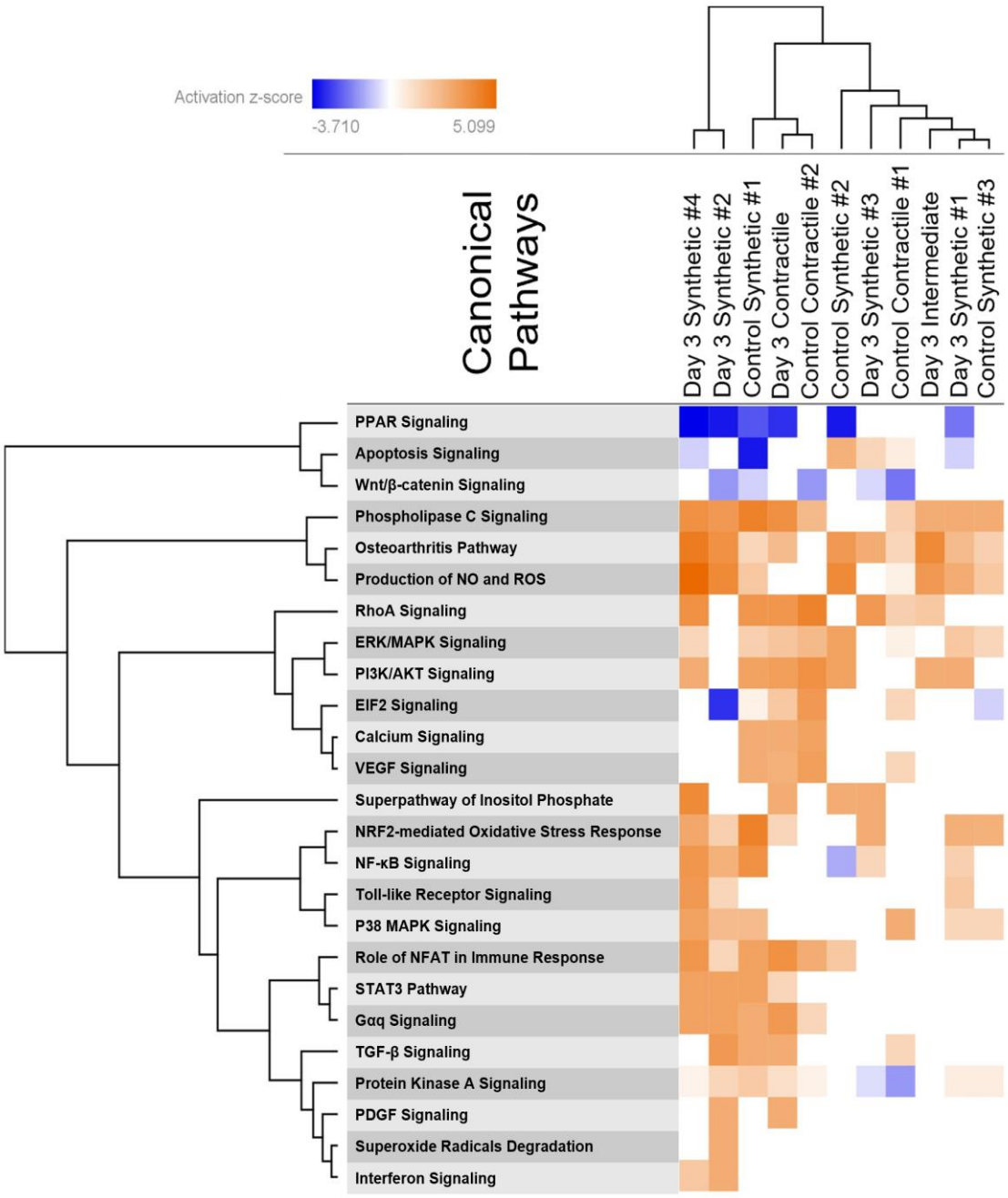

Figure 5.7: Heat map of canonical pathways differentially expressed in CSM clusters. While clusters differed in their relative expression of canonical pathways, every cell cluster exhibited upregulation of at least one pathway involved in contractile phenotype maintenance and in phenotypic switching to a synthetic phenotype.

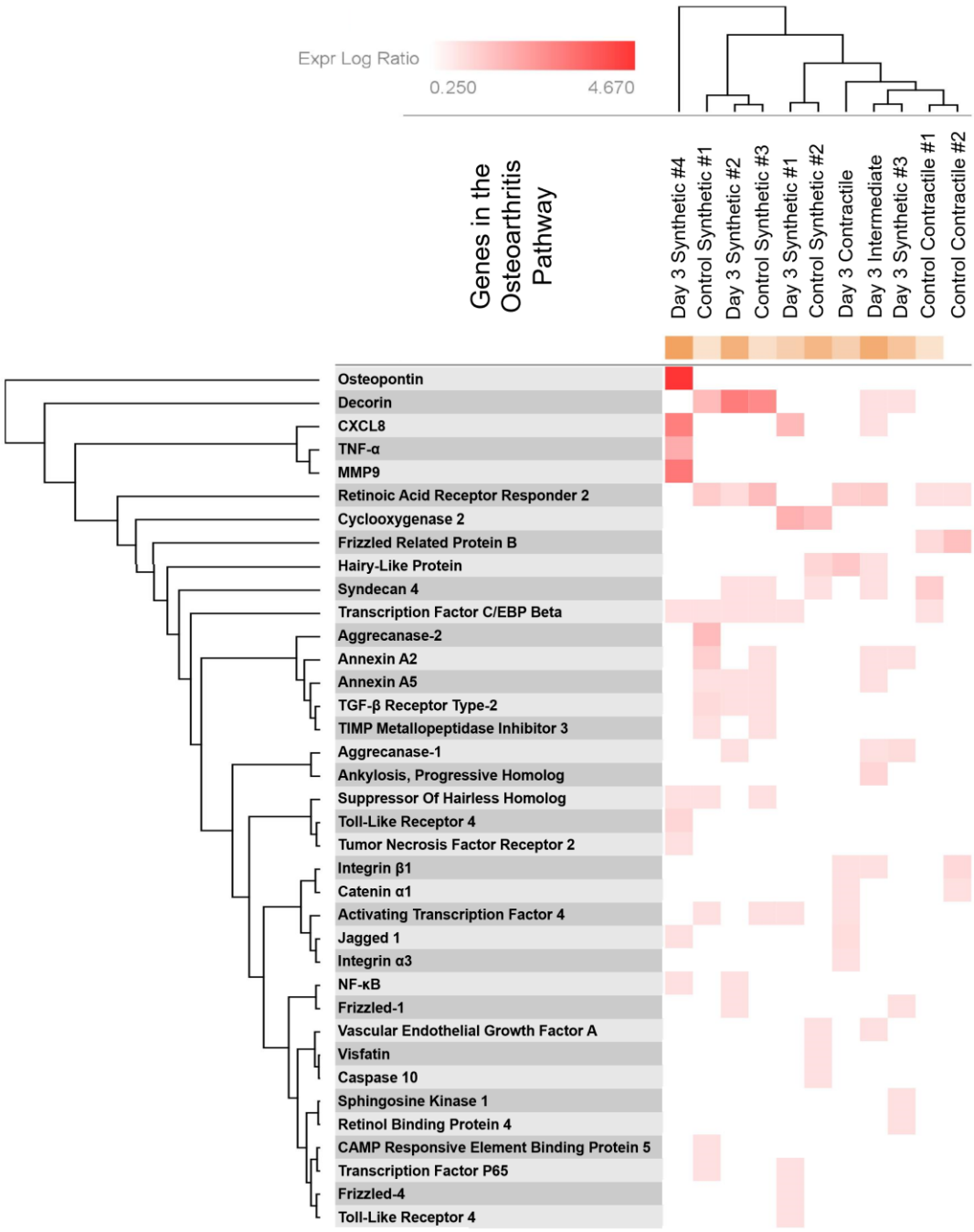

Figure 5.8: Genes involved in the canonical osteoarthritis pathway. Pathways and cell clusters are grouped based on hierarchical clustering. The “Day 3 Synthetic #4” cluster had greatly augmented expression of several genes involved in the vascular calcification process. The contractile clusters from the non-cultured control arteries exhibited the lowest expression of genes involved in this pathway.

Tables

Table 5.1: Markers used for identifying SMC phenotypes

	Symbol	Gene Name	References
Contractile Phenotypic Markers	ACTA2	Smooth muscle alpha-2 actin	[319-323]
	CALD1	Caldesmon 1	[324-327]
	CNN1	Calponin 1	[324, 328-330]
	MYH11	Myosin heavy chain 11	[319, 331-333]
	MYL9	Myosin light chain 9	[334-336]
	MYLK	Myosin light chain kinase	[337-340]
	MYOCD	Myocardin	[341-344]
	SMTN	Smoothelin	[324, 333, 339]
	TAGLN	Smooth muscle 22-alpha	[323, 324, 345]
	TPM2	Tropomyosin 2	[325, 346, 347]
Synthetic Phenotypic Markers	COL1A1/2	Collagen type 1A1/2	[342, 348-351]
	COL3A1	Collagen type 3A1	[333, 350, 352]
	GJA1	Gap junction alpha-1; connexin 43	[278, 320, 331, 353]
	ICAM1	Intercellular adhesion molecule 1	[321, 354-356]
	MMP2/9	Matrix metallopeptidase 2/9	[332, 333, 357]
	MSN	Moesin	[278, 358-360]
	NFAT	Nuclear factor of activated T-cells	[72, 273, 305, 342, 361]
	SDC4	Syndecan 4	[278, 322, 323, 345]
	SMARCA4	SWI/SNF related matrix associated actin dependent regulator of chromatin A4	[362-364]
	TGFB1	Transforming growth factor beta-1	[365, 366]
	TPM4	Tropomyosin 4	[324, 341, 367, 368]
	VCAM1	Vascular cell adhesion molecule 1	[342, 354, 369]
	VIM	Vimentin	[319, 324, 328, 370]

For a cluster to be identified as either contractile or synthetic smooth muscle, it had to exhibit expression of at least three of these markers.

Table 5.2: CSM cells from cultured arterial rings follow similar expression pattern changes when compared to the same cellular phenotype in fresh, non-cultured arteries

		Select Specific Genes Involved	
Cellular Function	**Change from Control**	**Contractile Phenotype**	**Synthetic Phenotype**
Contractile SMC marker	Decrease	TPM1/2, ACTA2, MYL9, CNN1, SMTN, MYH11	N/A
Pro-inflammatory	Increase	LGALS3, MIF	SERPINB2, CCL20,CCL2, IL-6, CXCL14, CXCL8
Anti-proliferative	Decrease	DUSP1, FZP36, WIF1, BTG2, IER5, RASSF3	DUSP1, FZP36, BTG2, SERPINF1, RASD1
Pro-calcification	Increase	ANXA1	MMP14, CTSB, SMPDL3B
Anti-calcification	Decrease	MGP, ASPN	MGP, TIMP3, ASPN
Pro-Apoptosis	Increase	BNIP3, CAP6, RASSF1	TNFRSF12A, ACSL4
Anti-protein aggregation	Decrease	CLU, ITM2B, HSPH1, DNAJB1	DNAJA1, CRYAB, HSPH1, DNAJB1, SELENBP1
Endoplasmic Reticulum/ Ox stress response modulator	Increase	SOD2, NUPR1, GPX1	SOD2, NUPR1, SRXN1

CHAPTER 6: INTRACELLULAR Ca^{2+} DYSREGULATION IN CORONARY SMOOTH MUSCLE IS SIMILAR IN CORONARY DISEASE OF HUMANS AND OSSABAW MINIATURE SWINE

Background

Metabolic syndrome (MetS) is characterized by a clustering of three or more of the following five conditions: central obesity, hypertension, dyslipidemia, insulin resistance, and glucose intolerance [8]. MetS affects one-third of all adults in the United States and increases the risk of developing coronary artery disease (CAD), which continues to be the primary cause of mortality worldwide and accounts for 1 in 7 deaths in the United States [8]. CAD-induced ischemic cardiomyopathy is the leading cause of heart failure, followed by dilated non-ischemic cardiomyopathy, hypertension, and valvular heart disease [371].

CAD is a progressive disease where initial endothelial damage leads to lipid and inflammatory cell infiltration of the arterial wall, causing medial thickening and neointima formation [372, 373]. This arterial restructuring is exacerbated by the proliferation and recruitment of coronary smooth muscle (CSM) cells to the plaque, which is accomplished by the phenotypic switching of CSM from a differentiated, contractile phenotype to a proliferative, migratory phenotype [68]. These migratory CSM cells secrete and deposit extracellular matrix like collagen, elastin, and fibrin into the thickening artery wall. While the presence of CSM inside the plaque contributes to plaque stability, over time the accumulation of lipid and cellular debris results in a necrotic core and plaque destabilization often leading to plaque rupture and myocardial infarction. In one study, patients hospitalized for ST elevation myocardial infarction who had multivessel CAD had an 8-year mortality from heart failure rate of 11%, as opposed to only a 1% mortality rate for individuals similarly hospitalized without multivessel CAD [374]. Further, CSM dedifferentiation into an osteogenic phenotype is associated with vascular calcification,

which is directly related to increased mortality and cardiac events [162], plaque instability, and rupture [163].

Ca^{2+} is a vital secondary messenger involved in the regulation of several key smooth muscle cell functions such as transcription [186, 188], migration [184, 185], proliferation [68, 70, 249, 250], and contraction [68, 187]. Previous research (reviewed in [69]) has shown that CAD is accompanied by alterations in many CSM Ca^{2+} transporters, including voltage-gated Ca^{2+} channels [74, 76], transient receptor potential channels [125], sarco-endoplasmic reticulum Ca^{2+} ATPases [76, 77, 80], plasma membrane Ca^{2+} ATPases [76], and Na^{+}/Ca^{2+} exchangers [76]. My lab recently showed that intracellular Ca^{2+} ($[Ca^{2+}]_i$) handling alterations that accompany CAD occur in a biphasic manner in Ossabaw miniature swine, with enhanced Ca^{2+} handling in early, mild disease and decreased Ca^{2+} handling in late, severe disease [81]. Furthermore, when the plaque was separated from the arterial wall in diseased coronary arteries, CSM isolated exclusively from the plaque region exhibited diminished SR Ca^{2+} store and SR Ca^{2+} pump activity, while CSM isolated from the arterial wall exhibited increased SR Ca^{2+} store SR Ca^{2+} pump activity [81].

There is difficulty in finding an animal model for human CAD, as there are many risk factors and uncontrollable variables in the human population. My lab has thoroughly characterized the Ossabaw miniature swine model of MetS and CAD. Due to their “thrifty genotype,” Ossabaw swine have a propensity to develop all the characteristics of MetS when fed an atherogenic, hypercaloric diet without any further chemical or genetic interventions [204, 283]. While Ossabaw swine develop diffuse, human-like coronary plaques [80], CSM $[Ca^{2+}]_i$ handling patterns have never been compared to freshly isolated CSM from human patients. Therefore, the aims of the current study are: 1) to determine how disease severity, arterial restructuring, and cardiometabolic risk factors are associated with $[Ca^{2+}]_i$ dysfunction in fresh, non-cultured human CSM and 2) to determine

whether the Ossabaw miniature swine is a clinically relevant large animal model of MetS and CAD with regards to $[Ca^{2+}]_i$ handling. These results will aid in characterizing the association between pathological arterial remodeling and dysfunctional $[Ca^{2+}]_i$ handling in human heart failure patients and will strengthen the Ossabaw miniature swine as a model for CAD and CAD-related heart failure at the cellular level.

Methods

Collection of human tissue

The current study implemented the collection of explanted human hearts from 24 patients (15 male, 9 female; aged 51.0 ± 2.5 years) undergoing heart transplantation surgery at the Methodist Hospital in Indianapolis, IN between September 2015 and March 2018. Explanted human hearts were collected at time of removal and stored for no longer than 24 hours in a physiological salt solution containing (in mM): 2 $CaCl_2$, 138 NaCl, 1 $MgCl_2$, 5 KCl, 10 HEPES, 10 glucose; pH 7.4. Epicardial coronary arteries were excised and used for further analyses.

Animals

All experimental procedures involving animals were approved by the Institutional Animal Care and Use Committee at Indiana University School of Medicine with the recommendations outlined by the National Research Council and the American Veterinary Medical Association Panel on Euthanasia [170, 171]. Ossabaw miniature swine were fed either 1000 g/day of standard chow diet yielding 11% of total caloric intake from fat, 18% from protein, and 71% from carbohydrates for 11 months (5L80; Purina Test Diet, Richmond, IN) or 1000 g/day of a hypercaloric, atherogenic diet yielding 43% of total caloric intake from fat, 16% from protein, and 41% from carbohydrates, supplemented with cholesterol (2.0%), hydrogenated coconut oil (4.70%), hydrogenated soybean oil (8.40%), cholate (0.70%), and high fructose corn syrup (5.0%) by weight (n = 7 for both groups).

Pigs were euthanized via cardiectomy and coronary arteries were removed for further analysis.

Swine metabolic phenotyping

Blood from Ossabaw swine was collected at time of euthanasia and used for analysis (ANTECH Diagnostics, Fishers, IN).

Histology

Coronary artery segments from proximal epicardial arteries (2–4 mm in length) were placed in 10% phosphate-buffered formalin for 24–48 h, then transferred to 70% ethanol. Histology was performed in the Department of Anatomy and Cell Biology at Indiana University School of Medicine (Indianapolis, IN). Arterial cross-sections were stained using Verhoeff-Van Gieson (VVG), Von Kossa (VK), and Masson's Trichrome staining techniques. The VVG elastin stain was used to determine media area and plaque burden, which I define as the percentage of the original lumen that is occupied by atherosclerotic plaque. The VK staining technique stains calcified areas black to determine the overall percent vascular calcification. The Masson's Trichrome staining technique was used in order to visualize the collagen (blue) and cellular composition (red) in the coronary artery sections. All images were captured with a Leica DM3000 microscope connected to Leica Application Suites V4.1 software (Leica Microsystems GmbH, Wetzlar, Germany) and analyzed using Adobe Photoshop® CS6) (for full protocols, see Appendices B, C, and D).

Assessment of $[Ca^{2+}]_i$ regulation

Whole-cell intracellular free Ca^{2+} levels were measured at room temperature (22 to 25°C) by using the fluorescent Ca^{2+} indicator fura-2 AM (InCa++ Ca2+ Imaging System, Intracellular Imaging, Cincinnati, OH) as previously described [80, 125, 204, 283]. Briefly, freshly dispersed smooth muscle cells from the left anterior descending (LAD) artery were incubated with 3.0 μM fura-2 AM (Molecular Probes, Eugene, OR) in a shaking water bath

at 37 °C for 45 min before being washed in a solution containing a low Ca^{2+} concentration. An aliquot of cells loaded with fura-2 AM was placed on a coverslip contained within a constant-flow superfusion chamber that was mounted on an inverted epifluorescent microscope (model TMS-F, Nikon, Melville, NY), with flow maintained at a constant rate of 1-2 mL/min. Basal Ca^{2+} levels were measured in physiologic salt solution composed of the following (in mM): 2 $CaCl_2$, 138 NaCl, 1 $MgCl_2$, 5 KCl, 10 HEPES, 10 glucose; pH 7.4. Calcium influx and maximal sarcoplasmic reticulum (SR) Ca^{2+} loading was accomplished by depolarization with high (80 mM) K^+ solution (2 $CaCl_2$, 63 NaCl, 1 MgCl, 80 KCl, 10 HEPES, 10 glucose; pH 7.4) to activate voltage-gated Ca^{2+} channels (VGCCs). SR Ca^{2+} stores were released with 5 mM caffeine in Ca^{2+}-free solution (138 NaCl, 1 $MgCl_2$, 5 KCl, 10 HEPES, 10^{-5} M K^+-EGTA, 10 glucose; pH 7.4) to activate ryanodine receptors (RyRs) (for solution recipes, see Appendix F). A caffeine wash-out phase was used to determine sarco-endoplasmic reticulum Ca2+ ATPase (SERCA) function via the undershoot below baseline during this recovery period [105, 203, 375]. The increased $[Ca^{2+}]_i$ after caffeine exposure stimulates Ca^{2+} extrusion, allowing $[Ca^{2+}]_i$ to equilibrate to baseline levels [376]. However, SERCA is also stimulated by high $[Ca^{2+}]_i$ and low concentrations of Ca^{2+} inside the SR after caffeine exposure [376, 377]. As the SR initially accumulates Ca^{2+} quicker than Ca^{2+} can enter the cell, the signal drops below baseline (the “undershoot”) [376]. Furthermore, application of the SERCA inhibitor cyclopiazonic acid abolishes this undershoot [376]. Therefore, SERCA function is directly responsible for this undershoot below baseline [376-378]. Fura-2 in CSM was excited by light from a 300 W xenon arc lamp that was passed through a computer-controlled filter changer containing 340 nm and 380 nm bandpass filters every 0.30 and 0.05 seconds, respectively. The fluorescence emission at 510 nm was collected by using a monochrome charge-coupled device camera (COHU, San Diego, CA) (for full protocol, see Appendix E). Whole-cell fura-2 fluorescence

was expressed as the 340 nm/380 nm ratio of fura-2 emission. A graph demonstrating the experimental protocol is shown in Fig. 6.2.

Statistics

Statistical analysis was performed using GraphPad Prism 5.0 (San Diego, CA). Unpaired student's t test was performed for comparisons in swine and one-way analysis of variance (ANOVA) with Newman–Keuls post hoc analysis for comparison of the human groups was performed. Data are presented as mean ± standard error. Correlations were determined using Pearson's product-moment coefficient of correlation. Simple regression analyses were performed to determine statistical significance of the correlations. $p<0.05$ was considered statistically significant.

Results

Structure of human and swine coronary arteries

Representative histological stains for humans (Fig. 6.1A-F) and swine (Fig. 6.1G-L) are shown. Human arteries show great diversity in disease state and structure and have been grouped based on percent plaque burden (Fig. 6.1M). While calcification was similar between human groups due to high within-group variability (Fig. 6.1N), fibrosis as measured by percent collagen was increased in the >75% plaque burden group compared to the <50% plaque burden group (Fig. 6.1O). Similar to the human groups, swine with MetS-induced CAD exhibited a significantly higher percent plaque burden (Fig. 6.1M), similar vascular calcification (Fig. 6.1N), and significantly greater collagen content (Fig. 6.1O) as compared to their lean counterparts. The double bar on the x-axes of the graphs separates the human and swine data and signifies that statistics were done only between experimental groups of the same species.

Clinical characteristics are similar in humans with different CAD severities

Clinical characteristics of patients and swine are outlined in Table 6.1. All human groups exhibit similar clinical and metabolic characteristics. Measured heart function

parameters were also similar between the groups, including ejection fraction, left ventricular end diastolic pressure, and coronary output as qualitatively recorded in patient records (data not shown). Overall, while these groups differ in terms of CAD severity, they exhibit comparable metabolic and functional disease parameters, i.e. similar increased cardiometabolic risk above healthy subjects. Swine on an atherogenic diet, however, developed significantly higher weight, systolic blood pressure, fasting blood glucose, total cholesterol, and triglyceride levels compared to lean controls. This is unsurprising, as these elevated parameters are indicative of MetS / cardiometabolic risk.

Disease severity, arterial structure, and certain metabolic parameters are correlated to changes in $[Ca^{2+}]_i$ handling

Figure 6.2 shows a sample Ca^{2+} tracing from a representative human CSM cell. Linear regression analyses were performed to evaluate the relationship between structural changes or individual cardiometabolic risk factors and alterations in CSM $[Ca^{2+}]_i$ handling (Table 6.2). Greater CAD severity, as measured by the intima/media ratio and percent collagen [81], was significantly correlated to a decreased Ca^{2+} influx (as measured by the height of the depolarization-induced Ca^{2+} influx peak and by the area under the curve of that peak) and a decreased SR Ca^{2+} store release. In contrast to those inverse correlations, an increased media area was positively correlated to enhanced Ca^{2+} influx and SR Ca^{2+} store release. Increased vascular calcification was correlated to a decreased Ca^{2+} influx. BMI and the number of MetS risk factors present in the patient were correlated to a decreased Ca^{2+} influx. Dyslipidemia, including increased LDL and total cholesterol levels, was correlated not only to decreased Ca^{2+} influx, but also to SERCA dysfunction. Age was significantly correlated to an increased SR Ca^{2+} store release. Correlation graphs are presented in Supplemental Figs. 6.1 and 6.2. Some of these correlations can also be seen in recent papers utilizing the Ossabaw miniature swine model of MetS/CAD [81, 204, 283].

$[Ca^{2+}]_i$ handling in Ossabaw swine recapitulates $[Ca^{2+}]_i$ handling in human CSM in both health and disease

A representative single cell tracing from a lean swine and a MetS swine are graphed with a representative single cell tracing from a human with mild CAD, as defined by a plaque burden below 50%, and a human with severe CAD, as defined by a plaque burden of over 75% (Fig. 6.3A). The CSM cell tracing from the human with mild CAD closely resembles the tracing from the lean swine, while the CSM cell tracing from the human with severe CAD closely resembles the tracing from the MetS swine. Humans with less than 50% plaque burden and 50-75% plaque burden did not exhibit any differences in $[Ca^{2+}]_i$ handling, while humans with greater than 75% plaque burden had a significantly lower Ca^{2+} influx (Fig. 6.3B), SR Ca^{2+} store release (Fig. 6.3C), and undershoot (Fig 6.3D). Swine with MetS-induced CAD showed remarkably similar directional changes, with a lower Ca^{2+} influx (Fig. 6.3B), SR Ca^{2+} store release (Fig. 6.3C), and undershoot (Fig 6.3D) in the MetS group compared to the lean group. This clearly illustrates that similar $[Ca^{2+}]_i$ handling alterations are present in CAD in humans and Ossabaw miniature swine.

Discussion

This study provides insight into $[Ca^{2+}]_i$ handling in freshly isolated CSM from human cardiomyopathy patients with undergoing heart transplantation. I found that a thickened media layer, which is associated with mild CAD, and aging were correlated to enhanced $[Ca^{2+}]_i$ signaling. Advanced CAD progression, as measured by plaque burden and percent collagen, and the number of MetS / cardiometabolic risk factors, BMI, and LDL and total cholesterol levels, are correlated to decreased $[Ca^{2+}]_i$ signaling. Increased vascular calcification was accompanied by a decrease in Ca^{2+} influx. A more severe dyslipidemic state, as measured by higher LDL and total cholesterol levels, was also correlated to greater SERCA dysfunction. These trends exemplify that $[Ca^{2+}]_i$ regulation is compromised in patients with severe, more occlusive disease and in patients with certain

MetS risk factors. By measuring $[Ca^{2+}]_i$ from freshly dispersed, non-cultured CSM from human patients undergoing heart transplantation, I provide novel insight into the intricacies of $[Ca^{2+}]_i$ dysregulation in diseased human CSM *ex vivo* and how CAD severity and certain metabolic risk factors are correlated with this dysregulation. The $[Ca^{2+}]_i$ dysregulation patterns seen in Ossabaw miniature swine with MetS, CAD, and advanced age are consistent with the human data [81, 204, 283], supporting the strong clinical relevance of this large animal model, both on the whole-animal level and on the cellular level.

Recently, my lab has clarified that CSM Ca^{2+} handling dysfunction occurs in a biphasic manner during CAD progression, with upregulated $[Ca^{2+}]_i$ handling in early CAD and downregulated $[Ca^{2+}]_i$ handling in late CAD [81]. Dysregulation of Ca^{2+} signaling pathways are associated with CSM dedifferentiation into a synthetic or osteogenic phenotype, which is followed by proliferation, migration to the growing neo-intima, and deposition of hydroxyapatite crystals in the extracellular matrix leading to vascular calcification [379]. Often, this change in phenotype occurs due to CSM adaptations to changes in the extracellular environment, such as increased reactive oxygen species (ROS) and dyslipidemia [310, 380, 381].

The oxidation of LDL cholesterol (ox-LDL) is a key step in atherogenesis. It has been found that exposure to ox-LDL decreases SERCA activity in cultured New Zealand white rabbit aortic smooth muscle cells and in cultured bovine aortic endothelial cells due to the irreversible oxidation of the SERCA protein [382-384]. This study supports this notion, as humans with greater dyslipidemia, including a higher level of LDL cholesterol, exhibited more dysfunctional SERCA activity.

Heart failure is a complex, heterogeneous disease with many different etiologies, risk factors, and pathophysiologies. CAD is the leading cause of heart failure, and it's been found that progression of CAD is related to progression of left ventricular dysfunction, a common characteristic of heart failure [385]. While the clinical diagnosis of ischemic

cardiomyopathy is an important predictor of 5-year mortality, the extent of CAD is a much better predictor of survival in heart failure patients [386]. In the current study I used histology obtained from the proximal segment of a conduit epicardial coronary artery from patients with cardiomyopathy in order to classify their coronary disease state. Histology can be considered a “snapshot” of one specific cross-section of the vessel, not necessarily indicative of total vessel health. However, as both humans and Ossabaw swine develop diffuse coronary plaque throughout the proximal, middle, and distal sections of the artery [80], the histology could be considered a *representative* snapshot of overall coronary health and plaque development.

I determined that patients with different cardiac and coronary disease severities have similar clinical characteristics and biochemistry. It is especially important to note, however, that the patients have similarly increased cardiometabolic risk above healthy subjects. There is enough variability within all the groups that enabled excellent regression analysis. This allowed us to test for associations between cardiometabolic risk factors and $[Ca^{2+}]_i$ regulation. Additionally, I show that the number of MetS risk factors, as opposed to the diagnosis of MetS itself, affects $[Ca^{2+}]_i$ regulation. This is in agreement with several different studies [14, 387, 388]. A Japanese study found that patients with either dilated non-ischemic cardiomyopathy or ischemic cardiomyopathy have an incidence of MetS twice as frequently as the general population and have comparable metabolic components, indicating that the risk factors associated with MetS influence the etiology of both ischemic and nonischemic cardiomyopathy [389].

Although humans and swine cannot and should not be directly compared, it is apparent that, while humans in general have a greater plaque burden than swine (Fig. 6.1M), swine exhibit more highly altered $[Ca^{2+}]_i$ handling in all the measured parameters (Fig. 6.3B-D). This may be due to the duration of the disease and severity of the risk factors. Atherosclerosis is a chronic disease occurring over several decades in the human

population. Conversely, the Ossabaw swine with MetS-induced CAD are on a diet specifically designed to expedite plaque development over a time span of only 11 months. This could lead to more rapid changes in the cellular milieu, potentially causing more extreme adaptations in CSM leading to enhanced $[Ca^{2+}]_i$ dysfunction as compared to the slower, more chronic condition as is seen in humans. This also supports the concept that $[Ca^{2+}]_i$ handling changes occur before and potentiate structural changes in the artery.

Hearts from healthy humans without heart failure were not included due to a dearth of tissue. Therefore, this study indirectly compares arteries from pathological human hearts to physiologically healthy, lean swine. While there is no perfect animal model to recapitulate human disease, this presents a weakness of this study. However, as I am concerned with relationships in $[Ca^{2+}]_i$ handling as a function of cardiometabolic risk and are not comparing these two species directly, I can still extrapolate from the data that the directional changes in $[Ca^{2+}]_i$ dysregulation patterns from a state of mild or no disease to a state of greater disease is maintained in both species. Another weakness of this study is the relatively small human sample set, so future studies should expand on these findings.

An adequate animal model for coronary artery disease and subsequent heart failure is of utmost importance, as a better understanding of the pathophysiology of cardiomyopathies could lead to the development of more effective heart failure therapeutics. This report is the first characterization of $[Ca^{2+}]_i$ dysregulation in freshly harvested CSM from explanted human hearts. The data strongly support the clinical relevance of the Ossabaw miniature swine model of MetS and CAD. A reliable, clinically relevant animal model that recapitulates human disease on a cellular level provides far more confidence of the translatability of the data.

Figures

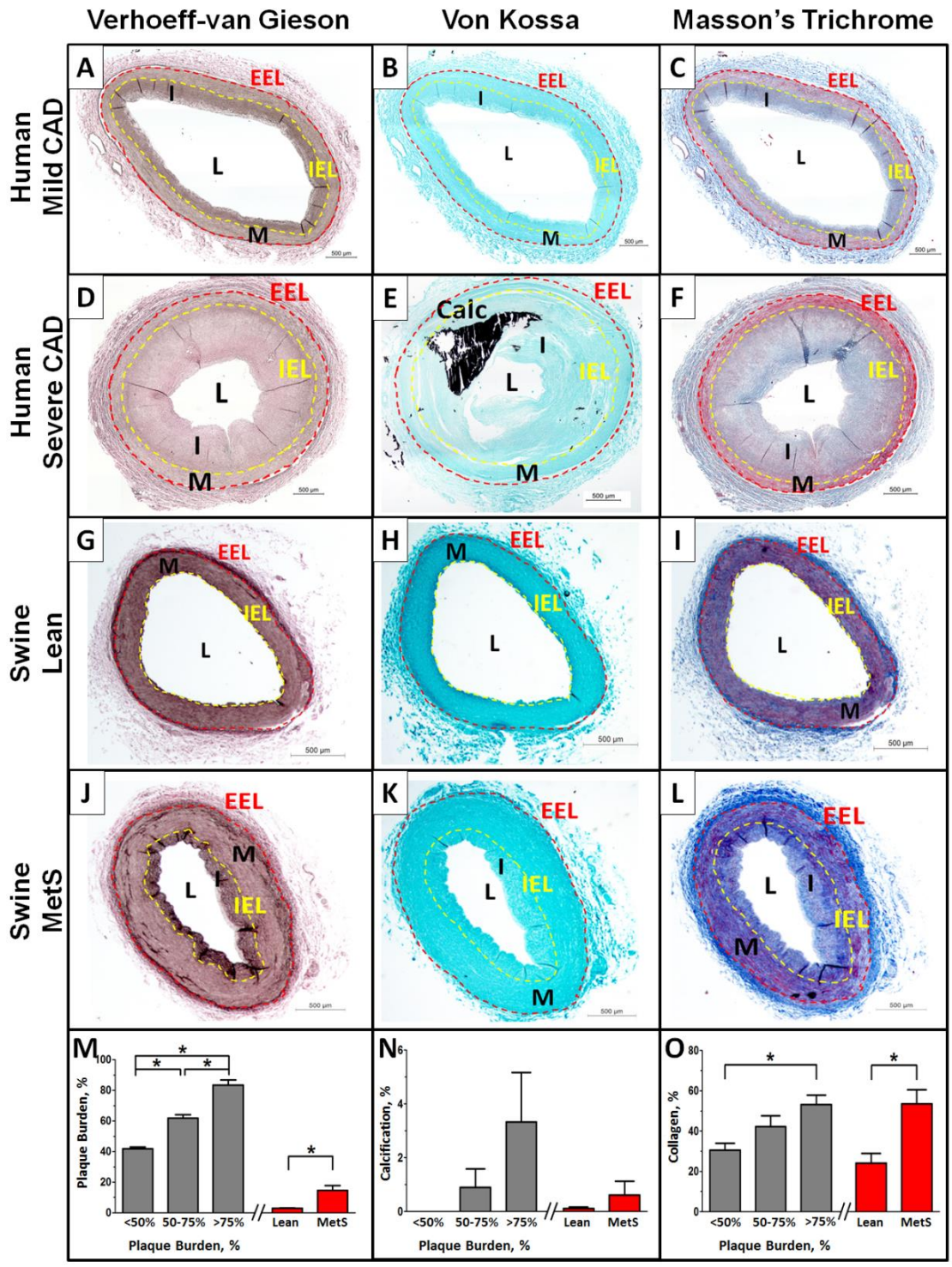

Figure 6.1: Histological staining reveals pathological remodeling in both humans and swine. Coronary artery histological sections from a human with <50% plaque burden

(A-C), a human with >75% plaque burden (D-F), a lean swine (G-I), and a MetS swine (J-L). VVG elastin staining was used to determine plaque burden and the areas of the tunica media and tunica intima using the highly visible external elastic lamina (EEL, red dashed line) and internal elastic lamina (IEL, yellow dashed line) (A, D, G, J). VK staining was used to determine percent of vascular calcification (black) (B, E, H, K). Masson's Trichrome staining was used to determine the percent collagen (blue) (C, F, I, L). Humans (grey bars) were binned based on percent plaque burden and swine (red bars) showed significantly increased plaque burden in the MetS group compared to the lean group (M). Percent vascular calcification was not significantly different between human or swine groups (N). The percent collagen increased with disease in both the human and swine groups (O). EEL, external elastic lamina; IEL, internal elastic lamina; M, tunica media; I, tunica intima; L, lumen. Double bars (M-O) separate human and swine graphs.

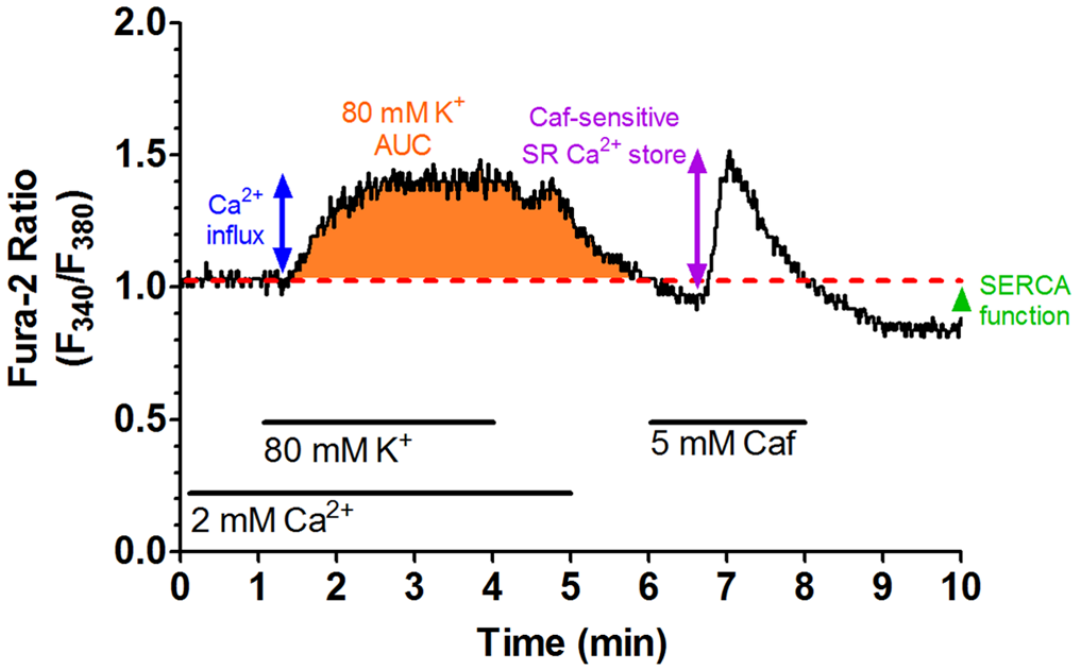

Figure 6.2: Sample Ca^{2+} tracing showing the change in the F_{340}/F_{380} excitation fluorescence emission ratio from a human CSM cell. Treatments and duration are indicated by solid lines. Baseline Ca^{2+} values were established during the first minute in a physiological salt solution (red dashed line). Cell depolarization was accomplished with an 80 mM K^+ solution, which initiated Ca^{2+} influx via VGCCs and maximally loaded the SR Ca^{2+} store. The height of the Ca^{2+} influx peak (blue arrow) and the area under the curve (orange area) were calculated to quantify Ca^{2+} influx activity. SR Ca^{2+} store was released by activating ryanodine receptors with 5 mM caffeine and can be measured by the height of the caffeine-induced peak (purple arrow). The undershoot below baseline was used to measure SERCA activity (green caret).

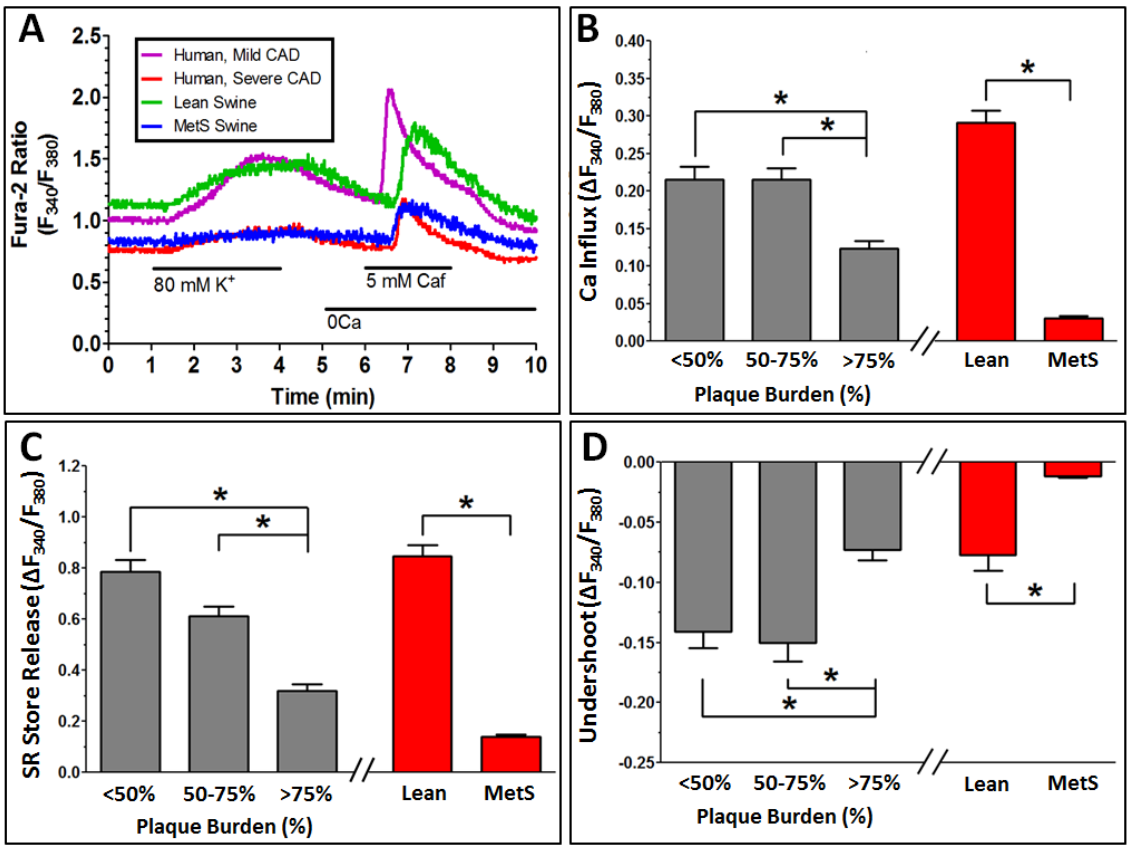

Figure 6.3: Sample Ca^{2+} tracing showing the change in the F_{340}/F_{380} excitation fluorescence emission ratio from a human and swine CSM cells. (A) Typical Ca^{2+} tracings show similarities between humans with mild CAD and lean swine and between humans with severe CAD and MetS swine (A). Mild CAD was defined by a plaque burden below 50%, while severe CAD was defined by a plaque burden of over 75%. In disease, both humans and swine exhibit decreased Ca^{2+} influx (B), SR Ca^{2+} store capacity (C), and SERCA function (D).

Tables

Table 6.1: Clinical characteristics of human subjects and swine

Humans	<50% PB	50-75% PB	>75% PB	p
N	7	11	6	-
Anthropometric Data				
Height (cm)	170 ± 4	176 ± 3	176 ± 4	N.S.
Weight (kg)	81 ± 6	86 ± 5	86 ± 10	N.S.
BMI (kg/m^2)	28 ± 2	27 ± 1	27 ± 2	N.S.
Clinical Data				
Age (years)	52 ± 5	51 ± 4	49 ± 5	N.S.
Male/Female	3/4	7/4	5/1	N.S.
SBP (mmHg)	107 ± 5	110 ± 5	104 ± 4	N.S.
DBP (mmHg)	67 ± 5	70 ± 5	69 ± 4	N.S.
Ex-smoker	2 (29%)	3 (27%)	4 (67%)	N.S.
LVAD	3 (43%)	7 (64%)	4 (67%)	N.S.
Presence of MetS	3 (43%)	4 (36%)	3 (50%)	N.S.
No. MetS risk factors	1.9 ± 0.7	2.1 ± 0.4	2.5 ± 0.6	N.S.
Biochemistry Data				
Fasting bG (mg/dL)	128 ± 18	106 ± 15	106 ± 10	N.S.
HbA1c (%)	5.6 ± 0.2	5.5 ± 0.1	5.0 ± 0.3	N.S.
Total cholesterol (mg/dL)	139 ± 7	161 ± 20	136 ± 18	N.S.
LDL (mg/dL)	75 ± 7	97 ± 17	81 ± 18	N.S.
HDL (mg/dL)	40 ± 4	38 ± 4	34 ± 2	N.S.
LDL/HDL Ratio	2.0 ± 0.2	2.7 ± 0.4	2.3 ± 0.5	N.S.
Triglycerides (mg/dL)	117 ± 19	128 ± 14	108 ± 13	N.S.
Comorbidities				
Atrial Fibrillation	2 (29%)	5 (45%)	3 (50%)	N.S.
Diabetes mellitus	2 (29%)	2 (18%)	0 (0%)	N.S.
Kidney Disease	3 (43%)	3 (27%)	1 (17%)	N.S.
Cancer	1 (14%)	1 (9%)	0 (0%)	N.S.
Clinical Depression	3 (43%)	3 (27%)	4 (67%)	N.S.
Treatments				
Aspirin	4 (57%)	10 (91%)	3 (50%)	N.S.
ACEI/ARB	2 (29%)	4 (36%)	2 (33%)	N.S.
β-blocker	3 (43%)	8 (73%)	2 (33%)	N.S.
Ca-blocker	1 (14%)	1 (9%)	0 (0%)	N.S.
Diuretics	4 (57%)	9 (82%)	4 (67%)	N.S.
Lipid-lowering drugs	2 (29%)	4 (36%)	2 (33%)	N.S.
Anti-diabetic drugs	2 (29%)	2 (18%)	0 (0%)	N.S.
Anti-arrhythmic drugs	4 (57%)	8 (73%)	4 (67%)	N.S.
Antidepressants	3 (43%)	3 (27%)	4 (67%)	N.S.

Swine	Lean	MetS	p
N	7	7	-
Weight (kg)	77 ± 4	110 ± 3	<0.05
Age (years)	2.6 ± 0.1	2.8 ± 0.2	N.S.
Male/Female	4/3	1/6	N.S.
SBP (mmHg)	82 ± 3	90 ± 5	<0.05
DBP (mmHg)	59 ± 3	60 ± 5	N.S.
Fasting bG (mg/dL)	69 ± 3	80 ± 3	<0.05
Total cholesterol (mg/dL)	80 ± 6	391 ± 108	<0.05
Triglycerides (mg/dL)	52 ± 6	67 ± 4	<0.05

Data are presented as number (%) or mean ± SEM. PB, plaque burden; BMI, body mass index; SBP, systolic blood pressure; DBP, diastolic blood pressure (humans conscious; swine under anesthesia); LVAD, left ventricular assistance device; MetS, metabolic syndrome; bG, blood glucose; HbA1c, glycated hemoglobin; LDL, low-density lipoprotein; HDL, high-density lipoprotein; ACEI, angiotensin converting enzyme inhibitors; ARB, angiotensin II receptor blockers; Ca, calcium. MetS was defined by a blood pressure above 130/85 mmHg, a fasting blood glucose above 110 mg/dL, an HDL-C level below 40 mg/dL for men or below 50 mg/dL for women, a triglyceride level above 150 mg/dL, and a BMI above 30.0 kg/m^2. N.S. = not significant.

Table 6.2: Linear regression analyses for CSM $[Ca^{2+}]_i$ handling measures versus histology measurements and patient parameters

	p	R
Structural (Histology) Parameters		
Percent Media vs.		
Ca^{2+} Influx	0.01	0.51
80K AUC	0.03	0.44
SR Store Release	0.08	0.38
Intima/Media Ratio vs.		
Ca^{2+} Influx	0.02	-0.50
80K AUC	0.03	-0.43
Percent Total Collagen vs.		
Ca^{2+} Influx	0.01	-0.51
80K AUC	<0.01	-0.60
SR Store Release	0.02	-0.49
Percent Calcification vs.		
Ca^{2+} Influx	0.02	-0.48
Patient Biochemistry Parameters		
BMI vs.		
Ca^{2+} Influx	0.03	-0.42
80K AUC	0.01	-0.52
Age vs.		
SR Store Release	0.02	0.47
Number of MetS Risk Factors vs.		
80K AUC	0.01	-0.51
LDL vs.		
Ca^{2+} Influx	0.01	-0.48
Undershoot	0.03	-0.45
Cholesterol vs.		
Ca^{2+} Influx	0.04	-0.41
Undershoot	0.03	-0.45

CHAPTER 7: CONCLUSION

Summary of Findings

Metabolic syndrome (MetS) is a growing public health concern in the United States that currently affects 1 in 3 Americans. MetS is positively associated with age and greatly increases the risk of developing comorbidities such as type 2 diabetes. MetS, age, and T2D are all independent risk factors for coronary artery disease (CAD), which continues to be the leading cause of death in the US and globally [8]. With the growing aging population, determining the mechanisms of disease progression is of utmost importance to provide molecular targets for therapies for this expanding demographic.

Pathological arterial remodeling necessitates coronary smooth muscle (CSM) phenotypic switching from a contractile phenotype to non-contractile phenotypes with differing functional capabilities, such as proliferation and extracellular matrix synthesis, inflammation, and mineralization [269]. Recently, the biological complexity of CSM phenotypic modulation is beginning to be elucidated with cutting-edge techniques such as single-cell RNA sequencing.

Calcium is a vital secondary messenger that controls numerous cellular functions, such as contraction, migration, proliferation, transcription, and apoptosis [270]. As such, intracellular Ca^{2+} ($[Ca^{2+}]_i$) handling is closely coupled to changes in phenotype. Altered $[Ca^{2+}]_i$ handling modes in different CSM phenotypes throughout CAD progression are shown in Fig. 7.1. A great number of Ca^{2+} transporters, including voltage-gated Ca^{2+} channels (VGCC), sarco-endoplasmic reticulum Ca^{2+}-ATPase (SERCA), extrusion mechanisms like the sodium-calcium exchanger (NCX) and the plasma membrane Ca^{2+}-ATPase (PMCA), as well as SR Ca^{2+} storage itself, exhibit altered activity and/or expression in CAD. This results in different global and localized $[Ca^{2+}]_i$ levels and Ca^{2+} dynamics, which are important for transcriptional events (“excitation-transcription” coupling) and lead to CSM phenotypic modulation [63, 68, 72, 273, 379, 390, 391]. In

particular, sarcoplasmic / endoplasmic reticulum (SR / ER) Ca^{2+} store capacity in vascular smooth muscle has received attention due to its association with proliferation [70, 392-396], activation (or repression) of store-operated Ca^{2+} entry (SOCE) [397-401], localized SR Ca^{2+} release ("Ca^{2+} sparks") activation of plasmalemmal ion channels [70, 402-404], and ER stress [89, 405].

Therefore, the primary aim of this dissertation work was to investigate Ca^{2+} dysregulation patterns, primarily with regard to SR Ca^{2+} store capacity, in several etiologies of MetS and how that corresponds to modulation of the coronary smooth muscle transcriptome and phenotype. This was done through several independent research projects that investigated these specific aims:

Investigative Aim 1: SR Ca^{2+} store capacity is correlated with coronary smooth muscle cytodifferentiation and subsequent arterial remodeling in Ossabaw miniature swine models of different CAD etiologies. The results of these studies show that ($[Ca^{2+}]_i$) handling throughout CAD progression is uniform in several etiologies of the disease, including T2D and aging. Diabetes on a MetS background exacerbated CAD and elicited $[Ca^{2+}]_i$ handling typical of severe disease. However, even though MetS old swine had similar Ca^{2+} dysregulation as the MetS young swine, they showed a much greater wall thickness and neointima formation. This indicates that the aging milieu may be responsible for more advanced coronary plaques in the context of MetS. Overall, these findings support the notion of common $[Ca^{2+}]_i$ handling dysregulation among different etiologies.

Investigative Aim 2: Proliferative and osteogenic coronary smooth muscle cells will exhibit altered transcriptomic profiles and SR Ca^{2+} store capacity depending on disease progression. In this novel study utilizing single-cell RNA sequencing with a singular tissue source, I determined that CSM from an organ-cultured model of CAD exhibit different transcriptomic profiles, with a decrease in global expression of contractility markers and an upregulation of genes involved in proliferation, migration, coronary artery

calcification (CAC), and inflammation. However, every CSM subgroup contained markers for many different phenotypes and an upregulation of genes associated with various cellular functions. This supports the notion that phenotypic switching is not a discreet event or a singular continuum as described previously in the literature (Fig. 7.2), but a complex network of overlapping genes and functions (Fig. 7.3).

Investigative Aim 3: CSM SR Ca^{2+} store capacity changes in humans with coronary artery disease (CAD) and heart failure are similar to those found in Ossabaw swine. Results from animal studies are only as clinically relevant as the animal model used. In this study I compared $[Ca^{2+}]_i$ dysregulation seen in Ossabaw miniature swine with MetS to humans with ischemic and non-ischemic heart failure undergoing heart transplantation. Results show similar $[Ca^{2+}]_i$ handling dysregulation in humans with heart failure and Ossabaw swine with MetS, including similar trends in reduced depolarization-induced Ca^{2+} influx, SR store release, and SERCA function. Furthermore, data in humans supports the $[Ca^{2+}]_i$ handling trends seen in aged swine, further validating the clinical relevance of this animal model.

Future Directions

There is ample evidence for CSM $[Ca^{2+}]_i$ dysregulation in CAD. In this work, I have established that $[Ca^{2+}]_i$ dysregulation patterns are common among different etiologies of CAD and that the phenotypic switching events associated with this $[Ca^{2+}]_i$ dysregulation are highly complex and deserving of further investigation.

It has been known for about three decades [406] that stimuli such as cytokines and growth factors can initiate phenotypic modulation of quiescent, contractile CSM cells to a proliferative, synthetic phenotype. This phenotypic plasticity is necessary for vascular remodeling, and as such it is associated with many various cardiovascular diseases, including CAD. The transcriptome of this complex process is just now being elucidated. While the literature repeatedly describes this phenotypic switch as a “spectrum” (Fig. 7.2),

I determined that it more closely follows a complicated upregulation of genes involved in multiple functions, including extracellular matrix synthesis, cellular proliferation, inflammation, and mineralization (Fig. 7.3). CSM cells in the vascular wall are composed of various different phenotypes that may express differential expression of genes involved in one or more of these processes. While many studies focus on either a shift in canonical phenotypic markers or simply a loss of contractile markers [278], this may not be an ideal technique of phenotype identification [407]. Several studies have shown that actively proliferating cultured cells express genes associated with both the contractile and synthetic phenotypes [269, 298, 299]. This is even more confounded by the time course of expression of certain contractile markers, with some markers like SM α-actin and transgelin expressed early in development and other markers like smooth muscle myosin heavy chain and calponin are only expressed in mature, late differentiation [408]. It has been shown that there can be multiple phenotypes of contractile cells themselves. Vascular injury induces even greater phenotypic heterogeneity, illustrating the diversity of CSM cell subpopulations in coronary plaques [276].

This complicates experiments that aim to elucidate mechanisms of phenotypic transition or characteristics of a particular phenotype, as CSM cell subpopulations do not fit into neat and orderly groups. In fact, previous studies have shown that a majority of CSM cells within atherosclerotic plaques lose expression of contractile markers, and other cells populating the plaque such as macrophages and foam cells can highly express CSM contractile markers [300-302, 409]. Therefore, the origin of cells in the vascular wall needs to be established to adequately identify CSM-derived cells. Some studies have already set out to track cell lineages to ensure the cells being studied are indeed of CSM origin as opposed to macrophage, myeloid, or adventitial origin [408]. Experiments utilizing smooth muscle cell (SMC)-specific conditional lineage tracing mouse models [408, 410] have shown that more than 80% of SMC-derived cells within advanced atherosclerotic plaques

do not have detectable levels of contractile marker expression and about 20% of cells expressing macrophage markers were of SMC origin [408]. Therefore, typical methods of CSM phenotype identification such as immunostaining may not reflect the number of CSM-derived cells and may also misidentify cell types [408].

Without adequate lineage experiments, we run the risk of mischaracterizing the origins of different cell types, possibly confounding the results. This is illustrated in a study by Tang et al., which found that mature SMCs are terminally differentiated and that the primary source of neointimal cells after vascular injury is derived from what they claimed was a novel previously uncharacterized medial stem cell population [411]. However, the conclusions made in this paper were quickly refuted by experts in the field, who also pointed to major design flaws in the Tang et al. study [303, 408]. Various other controversies surround phenotypic modulation, such as whether CSM-like cells within lesions are of myeloid origin [408, 412-414]. One study even showed that a proportion of myeloid cells can express early but not late contractile markers [408, 415]. CSM phenotypic switching is a complicated biological process involved in pathological vascular remodeling that deserves further investigating.

Phenotypic switching is accompanied by changes in $[Ca^{2+}]_i$ handling, $[Ca^{2+}]_i$ dynamics, and Ca^{2+} transporter activity and expression. Briefly, in contractile CSM that populate the tunica media, Ca^{2+} influx is primarily achieved via VGCCs. These Ca^{2+} "sparklets" increase the rate of SR Ca^{2+} loading and can induce Ca^{2+}-induced Ca^{2+} release (CICR) via ryanodine receptors (RyR) and IP_3 receptors (IP_3R) on the sarcoplasmic reticulum (SR) membrane [390, 416]. CICR results in local increases in $[Ca^{2+}]_i$ that can propagate throughout the length of the cell by activation of adjacent RyRs and IP_3Rs. This forms Ca^{2+} waves from these discreet SR Ca^{2+} release events and serves as the basis for excitation-contraction (E-C) coupling [390, 417]. RyR are known to couple with large-conductance Ca^{2+}-activated K^+ channels (BK_{Ca}), so Ca^{2+} sparks resulting from opening of

RyR can activate BK_{Ca} channels and cause membrane hyperpolarization and relaxation [70, 417]. $[Ca^{2+}]_i$ levels return to baseline by efflux mechanisms on the plasma membrane including the sodium-calcium exchanger (NCX) and the plasma membrane Ca^{2+} ATPase (PMCA), but the sarco-endoplasmic reticulum Ca^{2+} ATPase (SERCA) pump sequesters about 70% of cytosolic Ca^{2+} into the SR and is principally responsible for keeping basal $[Ca^{2+}]_i$ levels low [71, 72]. These localized and dynamic $[Ca^{2+}]_i$ changes control contraction and have been shown to promote the contractile phenotype by VGCC-dependent expression of serum response factor (SRF), a transcription factor that, along with the coactivator myocardin, stimulates the expression of CSM contractile markers [188, 418].

Phenotypic switching from a contractile state to a non-contractile state is characterized by a higher basal $[Ca^{2+}]_i$ and a greater contribution of store-operated Ca^{2+} entry (SOCE). Briefly, depletion of the SR Ca^{2+} store causes STIM1 translocation from the SR to the plasma membrane where it forms a channel with the Orai1 protein known as the Ca^{2+}-release activated Ca^{2+} channel (CRAC; I_{CRAC}). The Ca^{2+} content of the SR store dictates the activity of CRAC, and increased I_{CRAC} is associated with higher global basal $[Ca^{2+}]_i$ levels, [390, 419]. High basal $[Ca^{2+}]_i$ levels activate the Ca^{2+}-dependent transcription factors CREB and NFAT, which translocate to the nucleus and promote expression of genes involved in proliferation, migration, and inflammation [63, 72, 420, 421]. The relationship between SR Ca^{2+} store and the regulation of CSM phenotype can be considered a “dose-response” relationship. The optimal SR Ca^{2+} store promotes the contractile phenotype, an increase in SR Ca^{2+} store is associated with proliferation, and a decrease in SR Ca^{2+} store is associated with ER stress, apoptosis, and severe vascular calcification [81, 89]. Future research should focus on the relationship between SR Ca^{2+} store and MetS duration. The SR Ca^{2+} store could be experimentally altered using SERCA activators such as CDN1163 or inhibitors such as cyclopiazonic acid, then running scRNA-

seq at the same time point in order to elucidate a more definitive role of the SR Ca^{2+} store size on the CSM transcriptome.

However, cells undergoing phenotypic transition in the context of CAD display a biphasic pattern of $[Ca^{2+}]_i$ dysregulation, with increased Ca^{2+} influx via VGCC, SR Ca^{2+} store release, and SERCA function in early, mild disease and decreased Ca^{2+} influx via VGCC, SR Ca^{2+} store release, and SERCA function in late, severe disease [81]. Perhaps initial elevated Ca^{2+} transporter activity and SR Ca^{2+} store, which has been documented in phenotypic switching in some studies [419], results in greater release of Ca^{2+} via RyR and IP_3R, leading to increased basal $[Ca^{2+}]_i$ levels. Stressors in the disease milieu including reactive oxygen species (ROS), oxLDL, inflammation, and ER stress. Overproduction of ROS can lead to release of SR Ca^{2+} store via the IP_3R and inhibition of SERCA and PMCA [422]. Increased oxLDL infiltration in the vessel wall leads to increased ER stress and decreased VGCC activity [89, 423]. Inflammation is associated with decreased SERCA expression [424]. All of these listed stressors also induce CAC by upregulating genes associated with the osteogenic phenotype [425-428]. What is the specific time course of the changes in Ca^{2+} transporter activity during phenotypic switching? What triggers the biphasic Ca^{2+} handling pattern? Can any therapeutic interventions stop this aberrant $[Ca^{2+}]_i$ handling and thus prevent pathological CSM phenotypic switching? Clearly, the precise molecular switch(es) controlling the transition from increased Ca^{2+} handling in mild disease to decreased Ca^{2+} handling in late disease and the accompanying phenotypic transitions needs further investigating.

In this dissertation work, I used the intracellular Ca^{2+} indicator fura-2 on a wide-field microscope. This enabled the measurement of global $[Ca^{2+}]_i$ in individual cells. However, as discussed earlier in this section, Ca^{2+} dynamics and localized Ca^{2+} signaling events are of utmost importance for E-C coupling, E-T coupling, and phenotypic transitions. Other microscopy techniques such as laser scanning confocal microscopy and

total internal reflection fluorescence (TIRF) can measure highly localized Ca^{2+} signaling events on a micro- and nano-domain level [429]. Future studies should utilize these microscopy techniques to visualize more localized $[Ca^{2+}]_i$ handling, which may paint a more complete picture of cellular Ca^{2+} handling dysregulation in diseased cells (e.g. [394, 430]).

In this work, I investigated the CSM Ca^{2+} handling patterns and arterial structure of Ossabaw swine with alloxan-induced diabetes and advanced age. More than 65% of patients with diabetes will die from cardiovascular disease [431]. Chronic hyperglycemia has been shown to modulate CSM phenotype by the activation of NF-κB via the activation of receptor of advanced glycation end-products (RAGE) [432]. The ligand for RAGEs, advanced glycation end-products (AGEs) are also known to promote CAC by osteogenic de-differentiation [433]. Reduced production of NO also activates NF-κB to promote inflammation and is associated with a lower expression of RyR, less Ca^{2+} sparks, less BK_{Ca} activation, and less relaxation in general [431]. Changes in SR store capacity is associated with disease and aging, and $[Ca^{2+}]_i$ has been shown to increase in both diabetes and aging [402, 431]. This is consistent with the higher proliferation rate seen in CSM from older animals. The increased proliferation rate is tied to cellular senescence, which is known to increase CAC through osteogenic transition [434]. Aging is also associated with increased response to vasoconstrictors, formation of ROS, and collagen synthesis [256]. Studies in New Zealand white rabbits determined that older rabbits on a hypercholesterolemic diet developed more severe atherosclerotic lesions compared to younger counterparts despite the fact that both groups were on the same diet for the same amount of time and had similar blood lipid profiles [55, 435]. The aging milieu primes the vasculature for atherosclerotic development, and many view atherosclerosis as a form of accelerated aging [55].

Both diabetes and aging are associated with phenotypic modulation from a contractile phenotype to a synthetic and osteogenic phenotype, but through different mechanisms and in different microenvironments. Single-cell RNA sequencing analysis should be done in arterial tissue from diabetic animals and aged animals in order to characterize their unique cellular heterogeneities. This can be coupled with localized Ca^{2+} visualization with TIRF microscopy to gain a complete picture of the gene expression and Ca^{2+} signaling functionality of cell populations in these disparate etiologies.

As stated previously, CSM phenotypes differ significantly in their intracellular Ca^{2+} signaling, which is a consequence of differential expression of Ca^{2+} transport proteins [72]. However, in my study I did not observe changes in any of the Ca^{2+} transporter genes. Therefore, the dramatic differences seen in global $[Ca^{2+}]_i$ handling are most likely due to functional changes. This would be consistent with the literature, as vascular SMCs have been shown to exhibit altered Ca^{2+} transporter activity before the development of atherosclerotic lesions, indicating that functional changes precede structural changes brought about by proliferative and synthetic SMCs [436]. Organ culture conditions should be extended to 7 or 10 days in order to determine whether differential Ca^{2+} transporter expression does indeed follow functional changes. If Ca^{2+} transporter functional changes precede or even cause transcriptomic changes, one would expect to observe $[Ca^{2+}]_i$ handling changes without transcriptomic changes in arterial rings cultured for a shorter timeframe.

Future studies should continue to utilize the Ossabaw miniature swine large animal model, as the $[Ca^{2+}]_i$ handling alterations seen in Ossabaw with MetS follow a similar pattern as humans with CAD. Therefore, one can state with certainty that this breed is clinically relevant for cardiovascular studies.

Closing Remarks

This dissertation supports the previous finding that $[Ca^{2+}]_i$ handling alterations occur in a biphasic manner during atherosclerotic progression [81]. Aging and diabetes, both major risk factors for cardiovascular events and common comorbidities with MetS, exhibited $[Ca^{2+}]_i$ handling alterations that were indicative of the biphasic pattern. This indicates that $[Ca^{2+}]^i$ handling alteration patterns are common among different etiologies of CAD.

CSM phenotypic switching has previously been described either in terms of a discreet event or in terms of a spectrum with the contractile phenotype at one end and the synthetic phenotype at the other [269, 270, 275, 276]. Cutting-edge methods like single cell RNA sequencing have made possible transcriptomic analyses for individual cells, enabling the identification of many different CSM phenotypes [284, 285]. Researchers are only now starting to elucidate the true extent of phenotypic heterogeneity in cells that line the vessel walls.

There is an immense complexity of CSM phenotypic modulation, and future studies should investigate CSM phenotype diversity in different etiologies of CAD. Perhaps the different microenvironments associated with different CAD etiologies contribute to CSM diversity in different ways. While both diabetes and aging are associated with phenotypic switching to synthetic and osteogenic phenotypes, they could exhibit unique cell subpopulations. This could be a possibility, as some CAD etiologies are associated with medial calcification while others are associated with intimal calcification [437-439]. Single cell RNA sequencing could help elucidate the mechanisms and Ca^{2+} signaling events that lead to this structural difference in calcification. Understanding the diversity of CSM cell populations in CAD will allow more personalized patient treatment and care.

Figures

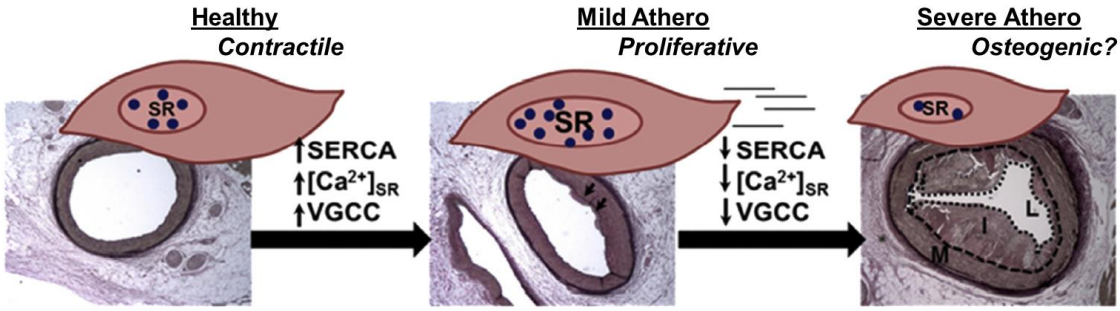

Figure 7.1: $[Ca^{2+}]_i$ handling alterations during atherosclerotic progression occurs in a biphasic manner. Mild atherosclerosis is associated with proliferation and increased VGCC activity, SERCA function, and SR Ca^{2+} store. Severe atherosclerosis is associated with vascular calcification and decreased VGCC activity, SERCA function, and SR Ca^{2+} store. SERCA, sarco-endoplasmic reticulum Ca^{2+} ATPase; $[Ca^{2+}]_{SR}$, sarcoplasmic reticulum Ca^{2+} storage capacity; VGCC, voltage-gated Ca^{2+} channel. Figure adapted from [81].

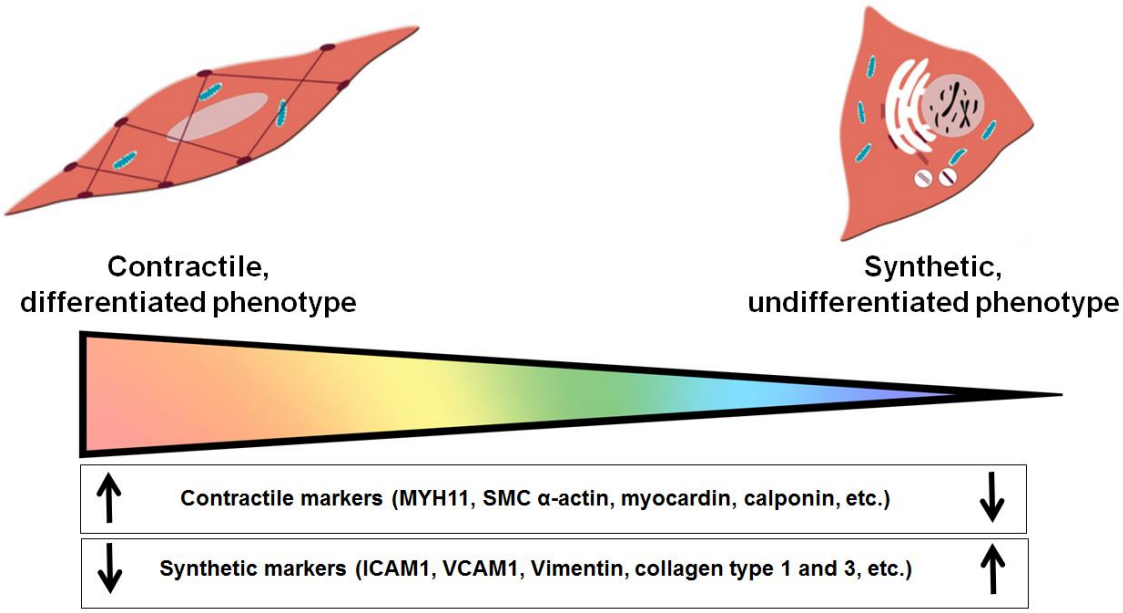

Figure 7.2: CSM phenotypic switching has traditionally been described as two ends of a phenotypic spectrum. Figure adapted from [324, 440].

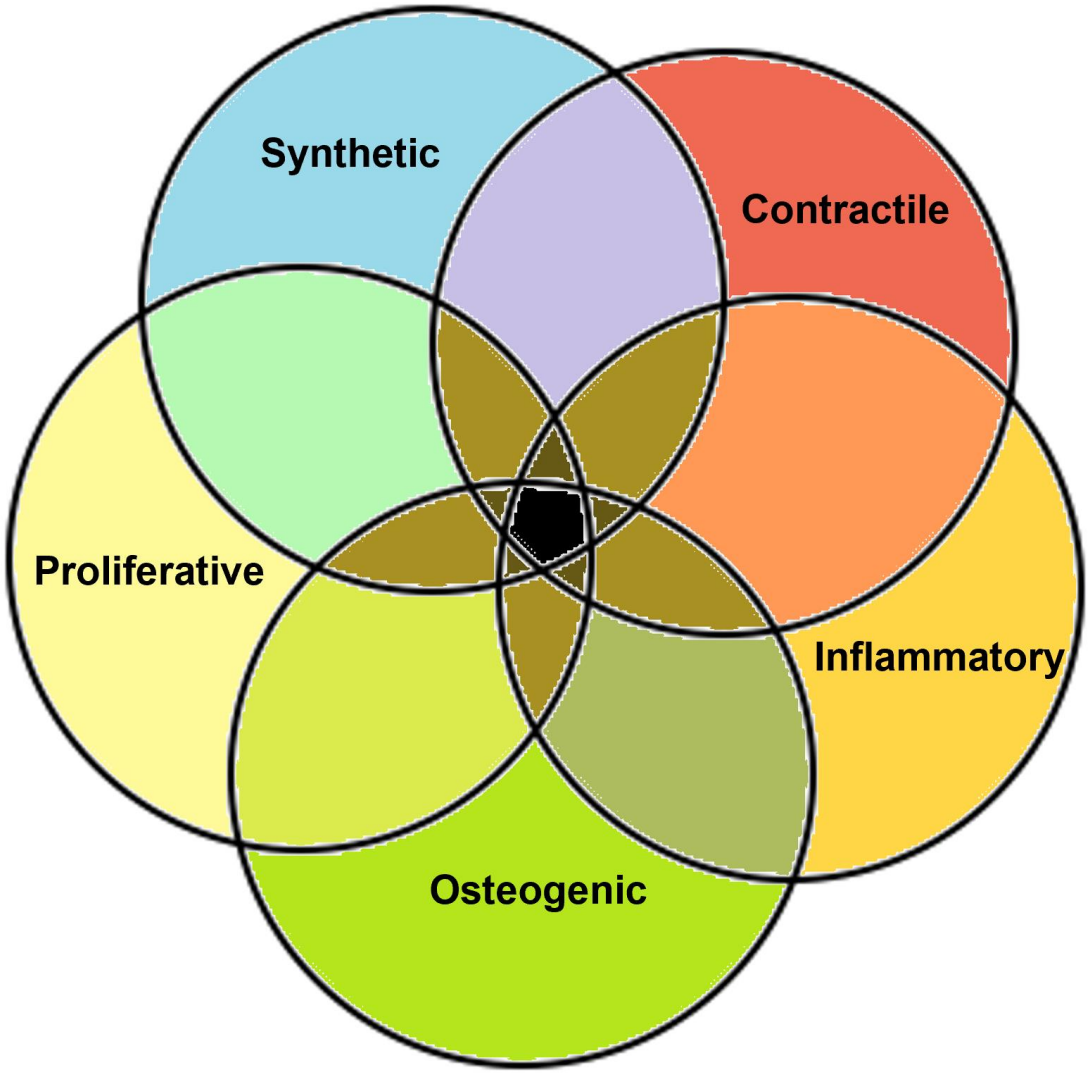

Figure 7.3: CSM phenotypic switching can more accurately be described as a network. CSM phenotypic switching involves genes associated with different cellular functions. CSM can exhibit any combination of genes, highlighting the diversity of CSM phenotypes.

LIST OF APPENDICES

APPENDIX A

PROTOCOL FOR ALLOXANIZATION OF SWINE

1. Fast the swine for at least 12 hours before alloxanization
2. Prepare alloxan dose (average: 140 mg/kg body weight) in a 50 mL centrifuge tube
3. In a separate 50 mL centrifuge tube, prepare 4 mL of NaOH (1 M) and 8 mL of NaCl for a final volume of 12 mL at a pH of 7.3.
4. Place the fasted pig in a sling so the central venous line (CVL) can be accessed. Begin administering 500 mL of 0.9% NaCl.
5. After 250 mL of 0.9% NaCl has been administered, the alloxan is mixed with the prepared NaCl-NaOH solution and shaken until a pinkish color (Note time shaken and color). Aspirate the solution into a 20 mL or 30 mL syringe and inject through a 0.20 µm sterile filter into the CVL (note time of injection).
6. Administer the remaining 250 mL of 0.9% NaCl to the pig to prevent possible renal damage
7. Closely monitor the pig for 48-72 hours following the injection of alloxan to watch for signs of hypoglycemia that can occur due to massive release of insulin into the blood. Other possible side effects include vomiting, renal damage, and lethargy.

NOTE:

Alloxan is toxic to humans. It can induce pancreatitis and a subsequent permanent state of insulin-dependent diabetes mellitus. Other organs can be damaged. Wear protective equipment including facemask, nitrile gloves, eyewear, and a laboratory coat. Mix in and administer to pigs in a well-ventilated area.

APPENDIX B

QUANTIFICATION OF MEDIAL AND INTIMAL AREA IN VERHOEFF VAN-GIESON STAINED CORONARY ARTERIES IN ADOBE PHOTOSHOP CS6

1. Open image of Verhoeff Van-Gieson stained artery (taken with 10X microscope objective) in Adobe Photoshop CS6.
2. Ensure that the measurement log is open: Window > Measurement Log.
3. To set scale: Image > Analysis > Set Measurement Scale > Custom
    a. The ruler tool is automatically selected for this activity. To set pixel length, trace the length of the scale bar.
    b. Type in scale bar length in micrometers (ie: 500) for logical length.
    c. Click OK.
4. Select magnetic lasso tool. Click once at any point along external elastic lamina (EEL) to begin tracing. Release, and drag around the external elastic laminar border. Click to close circle.
5. Click “Record Measurements” in measurement log.
6. Record “Area” value in Excel Spreadsheet as EEL Area.
7. Repeat steps 4-6, tracing along the internal elastic lamina (IEL).
8. Select the magic wand tool
9. Click inside the lumen and click “Record Measurements” in measurement log
10. Medial area = EEL Area – IEL Area
11. Intimal area = IEL Area – Lumen Area
12. To normalize medial area to artery size, calculate % Medial Area = (Medial Area/EEL Area)*100

APPENDIX C

QUANTIFICATION OF COLLAGEN CONTENT IN MASSON'S TRICHROME STAINED CORONARY ARTERY SEGMENTS IN ADOBE PHOTOSHOP CS6

1. Open image of Masson's Trichrome stained artery (taken with 10X microscope objective) in Adobe Photoshop CS6.
2. Ensure that the measurement log is open: Window > Measurement Log.
3. To set scale: Image > Analysis > Set Measurement Scale > Custom
    a. The ruler tool is automatically selected for this activity. To set pixel length, trace the length of the scale bar.
    b. Type in scale bar length in micrometers (ie: 500) for logical length.
    c. Click OK.
4. Make a "Background copy" as a new layer by right-clicking on "Background" and selecting "Duplicate Layer." Name this layer "Adventitia".
5. Working from the "Adventitia" layer, select the magnetic lasso tool, and trace along inner border of the blue adventitia, then Ctrl-X (cut) and Ctrl-V (paste) to create a new layer containing the medial layer.
6. Change name of new layer to "Media."
7. In the "Media" Layer, use the magnetic lasso to trace the inner border of the media, and click "Delete," leaving only the media in view.
8. Select both "Adventitia" and "Media" layers concurrently. Using the Magic wand tool, set "tolerance" to 20, and select "Sample All Layers." Click in Adventitia to select blue in both layers. You may add to the selected area by holding down "Shift" as you click.

9. Once you are satisfied that you've selected all of the collagen in both layers, click "Record Measurements" in the measurement log. Record the area measure under "Total Collagen Area" in an Excel file.
10. Deselect the "Media" layer.
11. Working with the "Adventitia" layer only, use the Magic Wand tool to select the adventitial collagen again. Be especially careful to ensure that you select the same amount of the adventitia as you did in step 9.
12. Click "Record Measurements."
13. Record area measure under "Adventitial Collagen Area" in Excel File.
14. Medial Collagen Area = Total Collagen Area – Adventitial Collagen Area.
15. Deselect "Adventitia" layer.
16. Select "Media" layer.
17. Determine medial area by using magic wand tool to click outside of the media. Everything that is not media will be selected. Type Ctrl-shift-I to select the inverse.
18. Click "Record Measurement."
19. Record Area measure as "Medial Area" in Excel file.
20. To express collagen content as a percentage of medial area, % Medial Collagen = (Medial Collagen Area/Medial Area)*100.

APPENDIX D

QUANTIFICATION OF VASCULAR CALCIFICATION IN VON KOSSA STAINED CORONARY ARTERIES IN ADOBE PHOTOSHOP CS6

1. Open image of Von Kossa stained artery (taken with 10X microscope objective) in Adobe Photoshop CS6.
2. Ensure that the measurement log is open: Window > Measurement Log.
3. To set scale: Image > Analysis > Set Measurement Scale > Custom
    a. The ruler tool is automatically selected for this activity. To set pixel length, trace the length of the scale bar.
    b. Type in scale bar length in micrometers (ie: 500) for logical length.
    c. Click OK.
4. Select magnetic lasso tool. Click once at any point along external elastic lamina (EEL) to begin tracing. Release, and drag around the external elastic laminar border. Click to close circle.
5. Click “Record Measurements” in measurement log.
6. Record “Area” value in Excel Spreadsheet as EEL Area.
7. Click inside the lumen and click “Record Measurements” in measurement log
8. Using the Magic wand tool, set “tolerance” to 20. Click a calcified region (black area). You may add to the selected area by holding down “Shift” as you click.
9. Once you are satisfied that you’ve selected all of the calcified areas, click “Record Measurements” in the measurement log. Record the area measure under “Total Calcification Area” in an Excel file.
10. To express calcification as a percentage of artery area, % Calcification = (Calcification Area/(EEL Area – Lumen Area))*100.

APPENDIX E

PROTOCOL FOR DISPERSION OF VASCULAR SMOOTH MUSCLE CELLS FOR INTRACELLULAR CALCIUM HANDLING QUANTIFICATION

Current Date ___-___-___ Initials_____

1. Conduit coronary arteries of swine are typically used. The artery is classified as proximal, middle, and distal thirds. At euthanasia/tissue collection, grossly dissect vessels by first locating vessel and then making a transverse cut through myocardium near ostium. Remove entire length of conduit artery with minimal adjacent cardiac muscle, fat, etc. attached. Place the tissue into wide-mouth bottle containing »50-75 ml ice-cold 2CaNa. Place immediately into cooler filled with ice. (NOTE: in the case of overnight transport, store tissue in EH storage media on ice.)

[Animal: Pig# _____, Age _____, Time dead _____, Misc. _____]

[**Portion of artery**: Proximal ___, Middle ___, Distal

Artery: LAD___ RCA ___ CFX ___ Other?_____]

[**Date** ____-____-____, Time of storage _____]

2. Clean artery of adherent connective tissue, fat, cardiac muscle, etc. in cell culture hood in 100 x 20 mm culture dish in »30 ml Low Ca. Treat artery gently (do not stretch excessively, if possible).

****At this point, the artery can be stored in the refrigerator in storage media for 2-5 days, if necessary.**

[Storage media = EH + PS]

[In refrigerator: Date ____-____-____ Time _____]

3. Cut open artery longitudinally to reveal lumen. Pin down the artery with the lumen facing up in a 30 ml Sylgard jar with 2 mL Collagenase solution. (Approximately a 1 cm^2 area of vessel is enough to yield several million SMC.) Pin the artery segment on all corners and at the middle to increase surface area.
4. Place jar in 37° C shaking water bath (100 strokes/min; 5.5 on dial) for 60 min. The jar should be placed so that the long axis of the vessel segment is parallel with the direction of the shaking.

[Collagenase batch: Date made: ____-____-____, Made by: _____]

[**Dispersion 1**: Date ____-____-____,

Time started _____, Time ended _____]

5. Aspirate supernatant and pipette over artery several times to loosen isolated CSM. Place drop of supernatant in 35 mm petri dish on microscope and observe. (At this point expect mostly connective tissue, endothelial cells (EC), etc., but few CSM. EC are round and clump together in bunches.) Note appropriately and either: 1) discard_____, 2) save in 15 ml tube for immediate fura-2 or patch-clamp studies_____. If #2, transfer supernatant to 15 mL conical tube and clearly label with pig number and cell fraction. Centrifuge at 900 rpm (**Not RCF**) for 4 min, remove supernatant (**Be careful not to aspirate the pellet!),** then resuspend pellet in 1 mL of freshly prepared 0.02%BSA in 2CaNa (20 mg BSA/10 mL 2CaNa). Add 2.5µL fura-2 AM and triturate several times. Place in 37° C water bath for ~30-45 mins.

Cell fraction: _____ (Ignore this section if discarded)

[Dye: Fura-2____, Other_____ Dye concentration _____]

[Loading: Date ____-____-____,

Time started _____, Time ended _____]

6. Add another 2 mL Collagenase solution to Sylgard jar and repeat steps 4 and 5 until isolation is complete.

Step 4:

[**Dispersion 2**: Time started _____, Time ended _____]

Step 5:

Cell fraction: _____

[Dye: Fura-2____, Other_____ Dye concentration _____]

[Loading: Date ____-____-____,

Time started _____, Time ended _____]

Step 4:

[**Dispersion 3**: Time started _____, Time ended _____]

Step 5:

Cell fraction: _____

[Dye: Fura-2____, Other_____ Dye concentration _____]

[Loading: Date ____-____-____,

Time started _____, Time ended _____]

7. Centrifuge cells at 900 rpm for 5 min, resuspend in EH solution and put in 37° C water bath for ~20 min.

   [Time started _____, Time ended _____]

8. Centrifuge cells at 900 rpm for 5 min, resuspend in 0.02%BSA in 2CaNa and chill on ice. Wrap tubes in foil to protect from light exposure.

NOTES:

1. All steps following fura-2 loading, CSM are light-sensitive. When possible, minimize exposure to light.
2. "Overnight dispersion" - It is also possible to disperse by exposing cells to 2 mL collagenase in bottle at room temp. for »8-10 hours.

APPENDIX F

EXPERIMENTAL SOLUTIONS

Collagenase (in Low Ca)

Component	Concentration	20 mL total	10 mL total	Stock Solution
Collagenase, CLS II	300 U/mL	20 mg	10 mg	300 U/mg (date, company)
BSA (Fraction V)	0.2% (wt/vol)	40 mg	20 mg	(Date, Company)
Soybean Tryspin Inhibitor Type I-S	0.1%	20 mg	10 mg	2.17 mg trypsin/mg (Date, Company)

[Batch: Date made: ____-____-____, Made by: _____]

Notes:

1. Ensure the pH is exactly 7.40 and if not, adjust
2. Make in 10-20 ml quantities. Each isolation requires at least 4-6 ml collagenase. Remaining collagenase solution may be frozen at -20° C for up to 10 days.

2 CaNa

Components	Concentration (mM)	1000 ml total
$CaCl_2$	2	20 ml of 0.1 M
NaCl	138	138 ml of 1.0 M
$MgCl_2$	1	10 ml of 0.1 M
KCl	5	5 ml of 1.0 M
HEPES	10	10 ml of 1.0 M
Glucose	10	1.8 g
pH (with NaOH)	7.4	3-4 ml of 1.0 M

NOTES:

1. Sterile solutions all contain PS and are sterilized by filtration through Millex-GS 0.2 µm filter or Millipore Stericup apparatus.
2. Penicillin Streptomycin (PS) 100 mg/ml (100 U/ml) is added in a 1:100 (vol:vol) ratio to yield a 1% PS solution.

EH (aka Storage media)

Components	Concentration (mM)	1000 ml total
$CaCl_2$	2.0	20 ml of 0.1 M
NaCl	135	135 ml of 1.0 M
$MgCl_2$	1	10 ml of 0.1 M
KCl	5	50 ml of 0.1 M
KH_2PO_4	0.44	4.4 ml of 0.1 M
Na_2HPO_4	0.34	3.4 ml of 0.1 M
$NaHCO_3$	2.6	26 ml of 0.1 M
Amino Acids	1X	20 ml of 50X
Vitamins	1X	10 ml of 100X
Phenol Red	0.001%	2 ml of 0.5%
HEPES	20	20 ml of 1.0 M
Glucose	10	1.8 g
pH	7.4	with NaOH
PS	1%	10 ml
Horse Serum	2%	20 ml

NOTES:

1. EH media is a type of Eagle's Minimal Essential Medium (EMEM), but also has HEPES as a pH buffer, so that bubbling the solution with O_2 is not necessary for maintenance of pH.
2. Sterile-filter under laminar flow hood with Millipore Stericup system.

Low Ca

Components	Concentration (mM)	1000 ml total
$CaCl_2$	0.5	5.0 ml of 0.1 M
NaCl	135	135 ml of 1.0 M
$MgCl_2$	1	10 ml of 0.1 M
KCl	5	50 ml of 0.1 M
KH_2PO_4	0.44	4.4 ml of 0.1 M
Na_2HPO_4	0.34	3.4 ml of 0.1 M
$NaHCO_3$	2.6	26 ml of 0.1 M
Amino Acids	1X	20 ml of 50X
Vitamins	1X	10 ml of 100X
Phenol Red	0.001%	2 ml of 0.5%
HEPES	20	20 ml of 1.0 M
Glucose	10	1.8 g
pH	7.4	with NaOH
PS	1%	10 ml

NOTES:

1. Low Ca is exactly like EH, except that the Ca concentration is only 0.5 mM, and no horse serum is used.
2. Low Ca with horse serum may be used to facilitate acquisition of a seal when doing patch-clamp studies.

2Ca80K

Components	Conc. (mM)	1000 ml total
$CaCl_2$	2	20 ml of 0.1 M
NaCl	63	63 ml of 1.0 M
$MgCl_2$	1	10 ml of 0.1 M
KCl	80	80 ml of 1.0 M
HEPES	10	10 ml of 1.0 M
Glucose	10	1.8 g
pH (with NaOH)	7.4	3-4 ml of 1.0 M

0CaNa

Components	Conc. (mM)	1000 ml total
$CaCl_2$	----	----
NaCl	138	138 ml of 1.0 M
$MgCl_2$	1	10 ml of 0.1 M
KCl	5	5 ml of 1.0 M
HEPES	10	10 ml of 1.0 M
KEGTA	10^{-5} M	1 ml of 0.01 M
Glucose	10	1.8 g
pH (with NaOH)	7.4	5-7 ml of 1.0 M

NOTES:

1. Rationale for low [Ca^{2+}] – Determination of the importance of extracellular Ca^{2+} (presumably Ca^{2+} influx) for a measured increase in intracellular Ca^{2+}.
2. $CaCl_2$ removal does not include equimolar addition of $MgCl_2$ or other ions. We have only used 1 and 5 mM EGTA on cells when achieving a fura-2 RATIO minimum. The cells probably become very leaky to Na^+ and other ions, thus addition of Mg^{2+} would "stabilize" the membrane.
3. Total ml of NaOH added gives number of mM extra Na added; e.g. total [Na^+] for 0CaNa is ~ 143 mM. Note that NaCl increases to 127 mM with –CaNa, 5 EGTA solution to keep [Na^+; at 143 mM as ~16 mM Na^+ used for pH.

2Ba80K5Na

Components	Conc. (mM)	1000 ml total
$BaCl_2$	2	20 ml of 0.1 M
LiCl	63	63 ml of 1.0 M
$MgCl_2$	1	10 ml of 0.1 M
KCl	80	80 ml of 1.0 M
HEPES	10	10 ml of 1.0 M
Glucose	10	1.8 g
pH (with NaOH)	7.4	3-4 ml of 1.0 M

APPENDIX G

PROTOCOL FOR ORGAN CULTURE OF SWINE CORONARY ARTERY RINGS IN OSTEOGENIC MEDIA

1. Euthanasia per standard protocol. With sterile gloves and tools, remove heart with pericardial sac intact.
2. Lay heart on inside of paper from sterile glove pack and remove pericardial sac with sterile tools.
3. Thoroughly rinse the heart with ice cold sterile-filtered 2CaNa + 2% penicillin/streptomycin (P/S).
4. Grossly dissect the coronary arteries and place in individual appropriately pre-labeled tubes of 2CaNa + 2% P/S. Keep tubes on ice.
5. Transfer collected specimens to lab on ice for dissection under the sterile laminar flow hood.
6. Open the flow hood and turn off U.V. light. Clean surface with 70% ethanol.
7. Thaw a frozen aliquot of 50 mL sterile-filtered Low Ca solution for fine dissection.
8. In flow hood, remove grossly dissected artery and place in Low Ca solution in a sterile culture dish on ice. Finely dissect coronary artery from myocardium and adventitia carefully and gently.
9. Allow clean artery to rest in ice cold Low Ca solution while preparing a 6-well plate with 4-5 mL of sterile phosphate-buffered saline (PBS) in each well.
10. Section cleaned artery into rings of 2-4 mm in length, and place in top left well of prepared 6-well plate.
11. Allow rings to sit in PBS for ~30 seconds, and then transfer clockwise to the next well. Transfer each ring separately and allow excess solution to drip off of the ring

into the previous well before transfer. Continue to transfer rings in a clockwise fashion until all rings have undergone complete 6-well serial “sterilization.”

12. Prepare a 12-well plate for culture by filling each well with 2 mL of culture media (Dulbecco’s Modified Eagle’s Medium (DMEM) + 180 mg/dL glucose + 1% P/S + 10% fetal bovine serum + 3.8 mM inorganic phosphate + 7.5 U/mL alkaline phosphatase).
13. Set aside arterial segments for cold stored controls.
14. Transfer a single coronary segment into a single well of the prepared 12-well plate.
15. Cover each plate and label appropriately with pig number, date, and culture conditions.
16. Transfer plates to the 37°C incubator. Check that the CO_2 is set to 4.6% and that the tray at the bottom of the incubator is full of distilled water.
17. Change culture media every two days.
18. Culture rings for 3 days to achieve vascular calcification.

APPENDIX H

PROTOCOL FOR DISPERSION OF VASCULAR SMOOTH MUSCLE CELLS FOR SINGLE-CELL RNA-SEQUENCING

Current Date ___-___-___ Initials_____

1. Conduit coronary arteries of swine are typically used. The artery is classified as proximal, middle, and distal thirds. At euthanasia/tissue collection, grossly dissect vessels by first locating vessel and then making a transverse cut through myocardium near ostium. Remove entire length of conduit artery with minimal adjacent cardiac muscle, fat, etc. attached. Place the tissue into wide-mouth bottle containing »50-75 ml ice-cold 2CaNa. Place immediately into cooler filled with ice. (NOTE: in the case of overnight transport, store tissue in EH storage media on ice.)

[Animal: Pig# _____, Age _____, Time dead _____, Misc. _____]

[**Portion of artery**: Proximal ___, Middle ___, Distal

Artery: LAD___ RCA ___ CFX ___ Other?_____]

[**Date** ____-____-____, Time of storage _____]

2. Very thoroughly clean artery of adherent connective tissue, fat, cardiac muscle, etc. in »30 ml Low Ca. Treat artery gently (do not stretch excessively, if possible).

****At this point, the artery can be stored in the refrigerator in storage media for 2-5 days, if necessary.**

[Storage media = EH + PS]

[In refrigerator: Date ____-____-____ Time _____]

3. Cut open artery longitudinally to reveal lumen. Pin down the artery with the lumen facing up in a 30 ml Sylgard jar with 2 mL of 150 U/mL collagenase in 0.9% NaCl. (Approximately a 1 cm^2 area of vessel is enough to yield several million SMC.) Pin the artery segment on all corners and at the middle to increase surface area.
4. Place jar in 37° C shaking water bath (100 strokes/min; 5.5 on dial) for 60 min. The jar should be placed so that the long axis of the vessel segment is parallel with the direction of the shaking.

[Collagenase batch: Date made: ____-____-____, Made by: _____]

[**Dispersion 1**: Date ____-____-____,

Time started _____, Time ended _____]

5. Aspirate supernatant and pipette over artery several times to loosen isolated CSM. Place drop of supernatant in 35 mm petri dish on microscope and observe. (At this point expect mostly connective tissue, endothelial cells (EC), etc., but few CSM. EC are round and clump together in bunches.) Note appropriately and either: 1) discard_____, 2) save in 15 ml tube for immediate scRNA-seq studies_____. If #2, transfer supernatant to 15 mL conical tube and clearly label with pig number and cell fraction. Centrifuge at 900 rpm (**Not RCF**) for 4 min, remove supernatant (**Be careful not to aspirate the pellet!),** then resuspend pellet in 1 mL of freshly prepared 0.02% BSA in 0.9% NaCl.

Cell fraction: _____ (Ignore this section if discarded)

[Dye: Fura-2____, Other_____ Dye concentration _____]

[Loading: Date ____-____-____,

Time started _____, Time ended _____]

6. Add another 2 mL Collagenase solution to Sylgard jar and repeat steps 4 and 5 until isolation is complete.

Step 4:

[**Dispersion 2**: Time started _____, Time ended _____]

Step 5:

Cell fraction: _____

[Dye: Fura-2____, Other_____ Dye concentration _____]

[Loading: Date ____-____-____,

Time started _____, Time ended _____]

Step 4:

[**Dispersion 3**: Time started _____, Time ended _____]

Step 5:

Cell fraction: _____

[Dye: Fura-2____, Other_____ Dye concentration _____]

[Loading: Date ____-____-____,

Time started _____, Time ended _____]

9. Centrifuge cells at 900 rpm for 5 min, resuspend in 1 mL 0.25% trypsin for 5 minutes
10. Centrifuge cells at 900 rpm for 5 min, resuspend in 2 mL 0.9% saline. Repeat this wash step for a total of 3 times

11. After final wash, resuspend pellet in 0.02 BSA in 0.9% NaCl
12. Filter through a 40 µm cell strainer into a 1.5 mL centrifuge tube
13. Place on ice
14. Contact the Center for Medical Genomics to schedule a time to submit sample(s)

APPENDIX I

SUPPLEMENTAL FIGURES

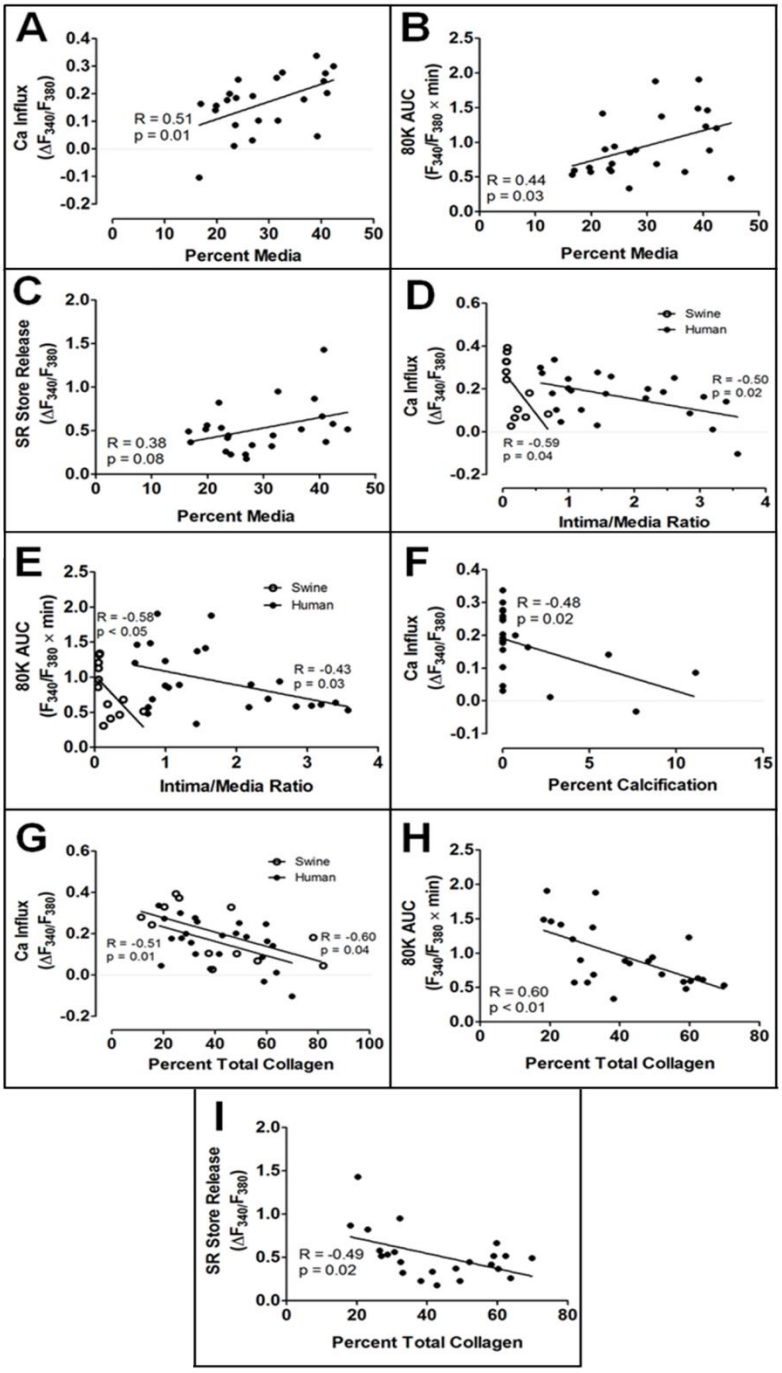

Supplemental Figure 6.1: Significant correlation of human coronary smooth muscle Ca^{2+} signaling to histological measures. The percent media (A-C), intima/media ratio

(D-E), percent calcification (F), and percent collagen (G-I) were significantly correlated to Ca^{2+} influx (A, D, F, G), area under the 80 mM K^{+} curve (B, E, H), and SR store release (C and I).

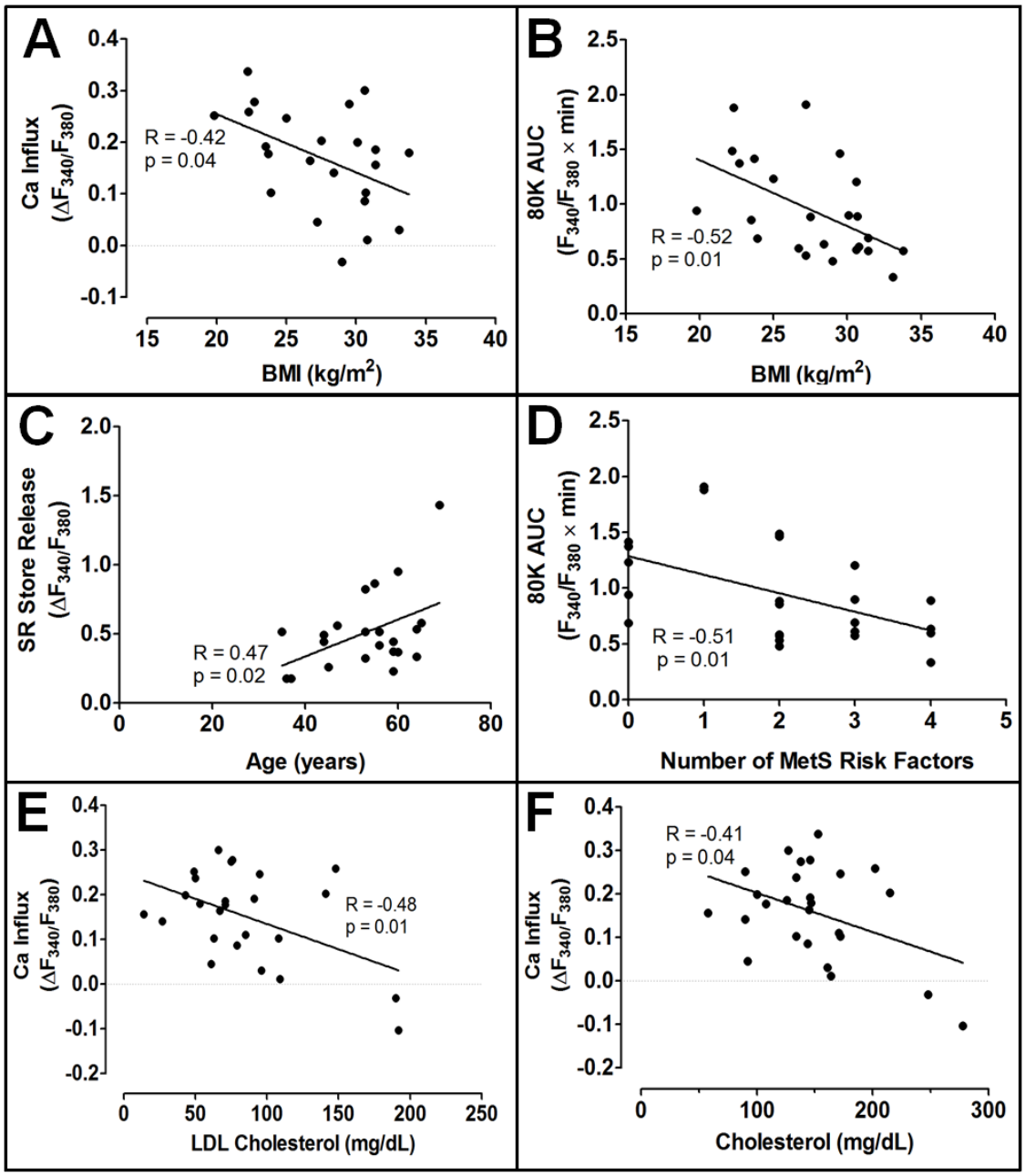

Supplemental Figure 6.2: Significant correlation of human coronary smooth muscle Ca^{2+} signaling to cardiometabolic patient data. Patient BMI (A and B), age (C), the number of MetS risk factors (D), and dyslipidemia (E-I) were correlated to Ca^{2+} influx (A, E, G), area under the 80 mM K^+ curve (B and D), SR store release (C), and undershoot (F and H).

REFERENCES

1. Hales CM, Carroll MD, Fryar CD, Ogden CL: **Prevalence of Obesity Among Adults and Youth: United States, 2015-2016.** *NCHS Data Brief* 2017**:**1-8.
2. Spieker EA, Pyzocha N: **Economic Impact of Obesity.** *Prim Care* 2016, **43:**83-95, viii-ix.
3. Seidell JC, Halberstadt J: **The global burden of obesity and the challenges of prevention.** *Ann Nutr Metab* 2015, **66 Suppl 2:**7-12.
4. Landgraf K, Rockstroh D, Wagner IV, Weise S, Tauscher R, Schwartze JT, Loffler D, Buhligen U, Wojan M, Till H, et al: **Evidence of early alterations in adipose tissue biology and function and its association with obesity-related inflammation and insulin resistance in children.** *Diabetes* 2015, **64:**1249-1261.
5. Neel JV: **Diabetes mellitus: a "thrifty" genotype rendered detrimental by "progress"?** *Am J Hum Genet* 1962, **14:**353-362.
6. O'Rourke R W: **Metabolic thrift and the genetic basis of human obesity.** *Ann Surg* 2014, **259:**642-648.
7. Levine JA: **Lethal sitting: homo sedentarius seeks answers.** *Physiology (Bethesda)* 2014, **29:**300-301.
8. Benjamin EJ, Virani SS, Callaway CW, Chamberlain AM, Chang AR, Cheng S, Chiuve SE, Cushman M, Delling FN, Deo R, et al: **Heart Disease and Stroke Statistics-2018 Update: A Report From the American Heart Association.** *Circulation* 2018, **137:**e67-e492.
9. Marangos PJ, Okamoto LJ, Caro JJ: **Economic Burden of the Components of the Metabolic Syndrome.** In *Handbook of Disease Burdens and Quality of Life Measures.* Edited by Preedy VR, Watson RR. New York, NY: Springer New York; 2010: 1135-1149
10. Lakka HM, Laaksonen DE, Lakka TA, Niskanen LK, Kumpusalo E, Tuomilehto J, Salonen JT: **The metabolic syndrome and total and cardiovascular disease mortality in middle-aged men.** *JAMA* 2002, **288:**2709-2716.
11. Grundy SM: **Hypertriglyceridemia, atherogenic dyslipidemia, and the metabolic syndrome.** *Am J Cardiol* 1998, **81:**18B-25B.
12. **Executive Summary of The Third Report of The National Cholesterol Education Program (NCEP) Expert Panel on Detection, Evaluation, And Treatment of High Blood Cholesterol In Adults (Adult Treatment Panel III).** *JAMA* 2001, **285:**2486-2497.
13. Grundy SM, Becker D, Clark LT, Cooperman RS, Denke MA, Howard WJ, Hunninghake DB, Illingworth DR, Luepker RV, McBride P, et al: **Third Report of the National Cholesterol Education Program (NCEP) Expert Panel: Final Report.** *Circulation* 2002, **106:**3143-3421.
14. Kim JY, Mun HS, Lee BK, Yoon SB, Choi EY, Min PK, Yoon YW, Hong BK, Rim SJ, Kwon HM: **Impact of metabolic syndrome and its individual components on the presence and severity of angiographic coronary artery disease.** *Yonsei Med J* 2010, **51:**676-682.
15. Heidenreich PA, Trogdon JG, Khavjou OA, Butler J, Dracup K, Ezekowitz MD, Finkelstein EA, Hong Y, Johnston SC, Khera A, et al: **Forecasting the future of cardiovascular disease in the United States: a policy statement from the American Heart Association.** *Circulation* 2011, **123:**933-944.
16. Sturek M, Mokelke EA, Sindermann JR, Adam LP, March KL: **Molecular and cellular physiology of differentiated vascular smooth muscle.** In *Cardiovascular Medicine.* Third Edition edition. Edited by Willerson JT, Cohn JN, Wellens HJJ, Holmes DR. London: Springer-Verlag; 2006: 1511-1523

17. Cocker MS, Mc Ardle B, Spence JD, Lum C, Hammond RR, Ongaro DC, McDonald MA, Dekemp RA, Tardif JC, Beanlands RS: **Imaging atherosclerosis with hybrid [18F]fluorodeoxyglucose positron emission tomography/computed tomography imaging: what Leonardo da Vinci could not see.** *J Nucl Cardiol* 2012, **19:**1211-1225.
18. McEvoy JW, Blaha MJ, Defilippis AP, Budoff MJ, Nasir K, Blumenthal RS, Jones SR: **Coronary artery calcium progression: an important clinical measurement? A review of published reports.** *J Am Coll Cardiol* 2010, **56:**1613-1622.
19. Goodwill AG, Dick GM, Kiel AM, Tune JD: **Regulation of Coronary Blood Flow.** *Compr Physiol* 2017, **7:**321-382.
20. American Diabetes A: **2. Classification and Diagnosis of Diabetes: Standards of Medical Care in Diabetes-2019.** *Diabetes Care* 2019, **42:**S13-S28.
21. Svensson M, Nystrom L, Schon S, Dahlquist G: **Age at onset of childhood-onset type 1 diabetes and the development of end-stage renal disease: a nationwide population-based study.** *Diabetes Care* 2006, **29:**538-542.
22. Innocenti F, Bartalucci F, Boni V, Vicidomini S, Mannucci E, Monami M, Pini R: **Coronary artery disease screening in type II diabetic patients: prognostic value of rest and stress echocardiography.** *Diabetes Metab Syndr* 2014, **8:**18-23.
23. Carr MC, Brunzell JD: **Abdominal obesity and dyslipidemia in the metabolic syndrome: importance of type 2 diabetes and familial combined hyperlipidemia in coronary artery disease risk.** *J Clin Endocrinol Metab* 2004, **89:**2601-2607.
24. Alexander CM, Landsman PB, Teutsch SM, Haffner SM, Third National H, Nutrition Examination S, National Cholesterol Education P: **NCEP-defined metabolic syndrome, diabetes, and prevalence of coronary heart disease among NHANES III participants age 50 years and older.** *Diabetes* 2003, **52:**1210-1214.
25. Bayturan O, Tuzcu EM, Lavoie A, Hu T, Wolski K, Schoenhagen P, Kapadia S, Nissen SE, Nicholls SJ: **The Metabolic Syndrome, Its Component Risk Factors, and Progression of Coronary Atherosclerosis.** *Arch Intern Med* 2010, **170:**478-484.
26. Nicholls SJ, Tuzcu EM, Kalidindi S, Wolski K, Moon KW, Sipahi I, Schoenhagen P, Nissen SE: **Effect of Diabetes on Progression of Coronary Atherosclerosis and Arterial Remodeling: A Pooled Analysis of 5 Intravascular Ultrasound Trials.** *J Am Coll Cardiol* 2008, **52:**255-262.
27. **Report of the Expert Committee on the Diagnosis and Classification of Diabetes Mellitus.** *Diabetes Care* 1997, **20:**1183-1197.
28. Weir GC, Bonner-Weir S: **Five stages of evolving beta-cell dysfunction during progression to diabetes.** *Diabetes* 2004, **53 Suppl 3:**S16-21.
29. Fonseca VA: **Defining and characterizing the progression of type 2 diabetes.** *Diabetes Care* 2009, **32 Suppl 2:**S151-156.
30. Klop B, Elte JW, Cabezas MC: **Dyslipidemia in obesity: mechanisms and potential targets.** *Nutrients* 2013, **5:**1218-1240.
31. Ellulu MS, Patimah I, Khaza'ai H, Rahmat A, Abed Y: **Obesity and inflammation: the linking mechanism and the complications.** *Arch Med Sci* 2017, **13:**851-863.
32. Van Gaal LF, Mertens IL, De Block CE: **Mechanisms linking obesity with cardiovascular disease.** *Nature* 2006, **444:**875-880.
33. Matsuzawa Y: **The metabolic syndrome and adipocytokines.** *FEBS Lett* 2006, **580:**2917-2921.

34. Baldasseroni S, Antenore A, Di Serio C, Orso F, Lonetto G, Bartoli N, Foschini A, Marella A, Pratesi A, Scarantino S, et al: **Adiponectin, diabetes and ischemic heart failure: a challenging relationship.** *Cardiovasc Diabetol* 2012, **11:**151.
35. Antonopoulos AS, Margaritis M, Coutinho P, Shirodaria C, Psarros C, Herdman L, Sanna F, De Silva R, Petrou M, Sayeed R, et al: **Adiponectin as a link between type 2 diabetes and vascular NADPH oxidase activity in the human arterial wall: the regulatory role of perivascular adipose tissue.** *Diabetes* 2015, **64:**2207-2219.
36. Padilla J, Vieira-Potter VJ, Jia G, Sowers JR: **Role of perivascular adipose tissue on vascular reactive oxygen species in type 2 diabetes: a give-and-take relationship.** *Diabetes* 2015, **64:**1904-1906.
37. Ceriello A, Motz E: **Is oxidative stress the pathogenic mechanism underlying insulin resistance, diabetes, and cardiovascular disease? The common soil hypothesis revisited.** *Arterioscler Thromb Vasc Biol* 2004, **24:**816-823.
38. Osler W: *The principles and practice of medicine : designed for the use of practitioners and students of medicine.* New York: D. Appleton and Company; 1892.
39. Shin D, Kongpakpaisarn K, Bohra C: **Trends in the prevalence of metabolic syndrome and its components in the United States 2007-2014.** *Int J Cardiol* 2018, **259:**216-219.
40. Rich MW, Chyun DA, Skolnick AH, Alexander KP, Forman DE, Kitzman DW, Maurer MS, McClurken JB, Resnick BM, Shen WK, et al: **Knowledge Gaps in Cardiovascular Care of the Older Adult Population: A Scientific Statement From the American Heart Association, American College of Cardiology, and American Geriatrics Society.** *J Am Coll Cardiol* 2016, **67:**2419-2440.
41. Shah M, Sikkel MB: **Coronary artery disease and age: beyond atherosclerosis.** *J Physiol* 2013, **591:**5807-5808.
42. Palmer MK, Toth PP: **Trends in Lipids, Obesity, Metabolic Syndrome, and Diabetes Mellitus in the United States: An NHANES Analysis (2003-2004 to 2013-2014).** *Obesity (Silver Spring)* 2019, **27:**309-314.
43. Liu HH, Li JJ: **Aging and dyslipidemia: a review of potential mechanisms.** *Ageing Res Rev* 2015, **19:**43-52.
44. Ungvari Z, Orosz Z, Labinskyy N, Rivera A, Xiangmin Z, Smith K, Csiszar A: **Increased mitochondrial H2O2 production promotes endothelial NF-kappaB activation in aged rat arteries.** *Am J Physiol Heart Circ Physiol* 2007, **293:**H37-47.
45. Ungvari Z, Buffenstein R, Austad SN, Podlutsky A, Kaley G, Csiszar A: **Oxidative stress in vascular senescence: lessons from successfully aging species.** *Front Biosci* 2008, **13:**5056-5070.
46. Csiszar A, Wang M, Lakatta EG, Ungvari Z: **Inflammation and endothelial dysfunction during aging: role of NF-kappaB.** *J Appl Physiol (1985)* 2008, **105:**1333-1341.
47. Ungvari Z, Kaley G, de Cabo R, Sonntag WE, Csiszar A: **Mechanisms of vascular aging: new perspectives.** *J Gerontol A Biol Sci Med Sci* 2010, **65:**1028-1041.
48. Cernadas MR, De Miguel LS, García-Durán M, González-Fernández F, Millás I, Montón M, Rodrigo J, Rico L, Fernández P, De Frutos T, et al: **Expression of constitutive and inducible nitric oxide synthases in the vascular wall of young and aging rats.** *Circ Res* 1998, **83:**279-286.

49. Csiszar A, Ungvari Z, Edwards JG, Kaminski P, Wolin MS, Koller A, Kaley G: **Aging-induced phenotypic changes and oxidative stress impair coronary arteriolar function.** *Circ Res* 2002, **90:**1159-1166.
50. Csiszar A, Ungvari Z, Koller A, Edwards JG, Kaley G: **Proinflammatory phenotype of coronary arteries promotes endothelial apoptosis in aging.** *Physiol Genomics* 2004, **17:**21-30.
51. Pearson KJ, Baur JA, Lewis KN, Peshkin L, Price NL, Labinskyy N, Swindell WR, Kamara D, Minor RK, Perez E, et al: **Resveratrol delays age-related deterioration and mimics transcriptional aspects of dietary restriction without extending life span.** *Cell Metab* 2008, **8:**157-168.
52. Csiszar A, Ungvari Z, Koller A, Edwards JG, Kaley G: **Aging-induced proinflammatory shift in cytokine expression profile in coronary arteries.** *FASEB J* 2003, **17:**1183-1185.
53. Wang M, Zhang J, Jiang LQ, Spinetti G, Pintus G, Monticone R, Kolodgie FD, Virmani R, Lakatta EG: **Proinflammatory profile within the grossly normal aged human aortic wall.** *Hypertension* 2007, **50:**219-227.
54. Wang JC, Bennett M: **Aging and atherosclerosis: mechanisms, functional consequences, and potential therapeutics for cellular senescence.** *Circ Res* 2012, **111:**245-259.
55. Tesauro M, Mauriello A, Rovella V, Annicchiarico-Petruzzelli M, Cardillo C, Melino G, Di Daniele N: **Arterial ageing: from endothelial dysfunction to vascular calcification.** *J Intern Med* 2017, **281:**471-482.
56. Virmani R, Joner M, Sakakura K: **Recent highlights of ATVB: calcification.** *Arterioscler Thromb Vasc Biol* 2014, **34:**1329-1332.
57. Coppe JP, Patil CK, Rodier F, Sun Y, Munoz DP, Goldstein J, Nelson PS, Desprez PY, Campisi J: **Senescence-associated secretory phenotypes reveal cell-nonautonomous functions of oncogenic RAS and the p53 tumor suppressor.** *PLoS Biol* 2008, **6:**2853-2868.
58. Lakatta EG: **Arterial and cardiac aging: major shareholders in cardiovascular disease enterprises: Part III: cellular and molecular clues to heart and arterial aging.** *Circulation* 2003, **107:**490-497.
59. Garfield RE, Somlyo AP: **Structure of Smooth Muscle.** In *Calcium and Contractility: Smooth Muscle.* Edited by Grover AK, Daniel EE. Totowa, NJ: Humana Press; 1985: 1-36
60. Klabunde RE: **Cellular Structure and Function.** In *Cardiovascular Physiology Concepts.* 2nd edition: Lippincott Williams & Wilkins; 2005: 41-58
61. Gabella G: **Cells of visceral smooth muscles.** *J Smooth Muscle Res* 2012, **48:**65-95.
62. Seow CY: **Myosin filament assembly in an ever-changing myofilament lattice of smooth muscle.** *Am J Physiol Cell Physiol* 2005, **289:**C1363-1368.
63. Wamhoff BR, Bowles DK, Owens GK: **Excitation-Transcription Coupling in Arterial Smooth Muscle.** *Circ Res* 2006, **98:**868-878.
64. Nishida M, Kuwahara K, Kozai D, Sakaguchi R, Mori Y: **TRP Channels: Their Function and Potentiality as Drug Targets.** In*; Tokyo*. Springer Japan; 2015: 195-218.
65. Stammers AN, Susser SE, Hamm NC, Hlynsky MW, Kimber DE, Kehler DS, Duhamel TA: **The regulation of sarco(endo)plasmic reticulum calcium-ATPases (SERCA).** *Can J Physiol Pharmacol* 2015, **93:**843-854.
66. Spinelli AM, Trebak M: **Orai channel-mediated Ca2+ signals in vascular and airway smooth muscle.** *Am J Physiol Cell Physiol* 2016, **310:**C402-413.

67. Ong HL, de Souza LB, Ambudkar IS: **Role of TRPC Channels in Store-Operated Calcium Entry.** In *Calcium Entry Pathways in Non-excitable Cells.* Edited by Rosado JA. Cham: Springer International Publishing; 2016: 87-109
68. Owens GK, Kumar MS, Wamhoff BR: **Molecular regulation of vascular smooth muscle cell differentiation in development and disease.** *Physiol Rev* 2004, **84:**767-801.
69. Sturek M: **Ca^{2+} regulatory mechanisms of exercise protection against coronary artery disease in metabolic syndrome and diabetes.** *J Appl Physiol* 2011, **111:**573-586.
70. House SJ, Potier M, Bisaillon J, Singer HA, Trebak M: **The non-excitable smooth muscle: calcium signaling and phenotypic switching during vascular disease.** *Pflugers Arch* 2008, **456:**769-785.
71. MacLennan DH, Asahi M, Tupling AR: **The regulation of SERCA-type pumps by phospholamban and sarcolipin.** *Ann N Y Acad Sci* 2003, **986:**472-480.
72. Matchkov VV, Kudryavtseva O, Aalkjaer C: **Intracellular Ca(2)(+) signalling and phenotype of vascular smooth muscle cells.** *Basic Clin Pharmacol Toxicol* 2012, **110:**42-48.
73. Berra-Romani R, Mazzocco-Spezzia A, Pulina MV, Golovina VA: **Ca2+ handling is altered when arterial myocytes progress from a contractile to a proliferative phenotype in culture.** *Am J Physiol Cell Physiol* 2008, **295:**C779-C790.
74. Berwick Z, Dick G, O'Leary H, Bender S, Goodwill A, Moberly S, Owen M, Miller S, Obukhov A, Tune J: **Contribution of electromechanical coupling between KV and CaV1.2 channels to coronary dysfunction in obesity.** *Basic Res Cardiol* 2013, **108:**370.
75. Borbouse L, Dick GM, Asano S, Bender SB, Dincer UD, Payne GA, Neeb ZP, Bratz IN, Sturek M, Tune JD: **Impaired function of coronary BK_{Ca} channels in metabolic syndrome.** *Am J Physiol Heart Circ Physiol* 2009, **297:**H1629-H1637.
76. Witczak CA, Wamhoff BR, Sturek M: **Exercise training prevents Ca^{2+} dysregulation in coronary smooth muscle from diabetic dyslipidemic Yucatan swine.** *J Appl Physiol* 2006, **101:**752-762.
77. Hill BJF, Price EM, Dixon JL, Sturek M: **Increased calcium buffering in coronary smooth muscle cells from diabetic dyslipidemic pigs.** *Atherosclerosis* 2003, **167:**15-23.
78. Hill BJF, Dixon JL, Sturek M: **Effect of atorvastatin on intracellular calcium uptake in coronary smooth muscle cells from diabetic pigs fed an atherogenic diet.** *Atherosclerosis* 2001, **159:**117-124.
79. Bowles DK, Heaps CL, Turk JR, Maddali KK, Price EM: **Hypercholesterolemia inhibits L-type calcium current in coronary macro-, not microcirculation.** *J Appl Physiol* 2004, **96:**2240-2248.
80. Neeb ZP, Edwards JM, Alloosh M, Long X, Mokelke EA, Sturek M: **Metabolic syndrome and coronary artery disease in Ossabaw compared with Yucatan swine.** *Comp Med* 2010, **60:**300-315.
81. McKenney-Drake ML, Rodenbeck SD, Owen MK, Schultz KA, Alloosh M, Tune JD, Sturek M: **Biphasic alterations in coronary smooth muscle Ca2+ regulation in a repeat cross-sectional study of coronary artery disease severity in metabolic syndrome.** *Atherosclerosis* 2016, **249:**1-9.
82. Nakahara T, Dweck MR, Narula N, Pisapia D, Narula J, Strauss HW: **Coronary Artery Calcification: From Mechanism to Molecular Imaging.** *JACC Cardiovasc Imaging* 2017, **10:**582-593.

83. Irkle A, Vesey AT, Lewis DY, Skepper JN, Bird JL, Dweck MR, Joshi FR, Gallagher FA, Warburton EA, Bennett MR, et al: **Identifying active vascular microcalcification by (18)F-sodium fluoride positron emission tomography.** *Nat Commun* 2015, **6:**7495.
84. Mori H, Torii S, Kutyna M, Sakamoto A, Finn AV, Virmani R: **Coronary Artery Calcification and its Progression: What Does it Really Mean?** *JACC Cardiovasc Imaging* 2018, **11:**127-142.
85. Vattikuti R, Towler DA: **Osteogenic regulation of vascular calcification: an early perspective.** *Am J Physiol Endocrinol Metab* 2004, **286:**E686-696.
86. Rennenberg RJ, Schurgers LJ, Kroon AA, Stehouwer CD: **Arterial calcifications.** *J Cell Mol Med* 2010, **14:**2203-2210.
87. Shaw LJ, Narula J, Chandrashekhar Y: **The Never-Ending Story on Coronary Calcium: Is it Predictive, Punitive, or Protective?** *J Am Coll Cardiol* 2015, **65:**1283-1285.
88. Detrano R, Guerci AD, Carr JJ, Bild DE, Burke G, Folsom AR, Liu K, Shea S, Szklo M, Bluemke DA, et al: **Coronary calcium as a predictor of coronary events in four racial or ethnic groups.** *N Engl J Med* 2008, **358:**1336-1345.
89. Furmanik M, Shanahan CM: **Endoplasmic Reticulum Stress in Arterial Smooth Muscle Cells: A Novel Regulator of Vascular Disease.** *Curr Cardiol Rev* 2017, **13:**94-105.
90. Fleckenstein-Grun G, Thimm F, Czirfuzs A, Matyas S, Frey M: **Experimental vasoprotection by calcium antagonists against calcium-mediated arteriosclerotic alterations.** *J Cardiovasc Pharmacol* 1994, **24 Suppl 2:**S75-S84.
91. Shanahan CM: **Inflammation Ushers in Calcification: A Cycle of Damage and Protection?** *Circulation* 2007, **116:**2782-2785.
92. Kapustin AN, Shanahan CM: **Emerging roles for vascular smooth muscle cell exosomes in calcification and coagulation.** *J Physiol* 2016, **(In Press)**.
93. Aikawa E, Nahrendorf M, Figueiredo JL, Swirski FK, Shtatland T, Kohler RH, Jaffer FA, Aikawa M, Weissleder R: **Osteogenesis Associates With Inflammation in Early-Stage Atherosclerosis Evaluated by Molecular Imaging In Vivo.** *Circulation* 2007, **116:**2841-2850.
94. Liu F, Zhong H, Liang JY, Fu P, Luo ZJ, Zhou L, Gou R, Huang J: **Effect of high glucose levels on the calcification of vascular smooth muscle cells by inducing osteoblastic differentiation and intracellular calcium deposition via BMP-2/Cbfalpha-1 pathway.** *J Zhejiang Univ Sci B* 2010, **11:**905-911.
95. Wong ND, Sciammarella MG, Polk D, Gallagher A, Miranda-Peats L, Whitcomb B, Hachamovitch R, Friedman JD, Hayes S, Berman DS: **The metabolic syndrome, diabetes, and subclinical atherosclerosis assessed by coronary calcium.** *J Am Coll Cardiol* 2003, **41:**1547-1553.
96. Chen NX, O'Neill KD, Moe SM: **Matrix vesicles induce calcification of recipient vascular smooth muscle cells through multiple signaling pathways.** *Kidney Int* 2017.
97. Kapustin AN, Davies JD, Reynolds JL, McNair R, Jones GT, Sidibe A, Schurgers LJ, Skepper JN, Proudfoot D, Mayr M, Shanahan CM: **Calcium regulates key components of vascular smooth muscle cell-derived matrix vesicles to enhance mineralization.** *Circ Res* 2011, **109:**e1-e12.
98. Sun Y, Byon CH, Yuan K, Chen J, Mao X, Heath JM, Javed A, Zhang K, Anderson PG, Chen Y: **Smooth muscle cell-specific runx2 deficiency inhibits vascular calcification.** *Circ Res* 2012, **111:**543-552.

99. Sun HJ, Zhu XX, Cai WW, Qiu LY: **Functional roles of exosomes in cardiovascular disorders: a systematic review.** *Eur Rev Med Pharmacol Sci* 2017, **21:**5197-5206.
100. Zhang C, Zhang K, Huang F, Feng W, Chen J, Zhang H, Wang J, Luo P, Huang H: **Exosomes, the message transporters in vascular calcification.** *J Cell Mol Med* 2018, **22:**4024-4033.
101. Shanahan CM, Crouthamel MH, Kapustin A, Giachelli CM: **Arterial Calcification in Chronic Kidney Disease: Key Roles for Calcium and Phosphate.** *Circ Res* 2011, **109:**697-711.
102. Sturek M, Tune JD, Alloosh M: **Ossabaw Island miniature swine: metabolic syndrome and cardiovascular assessment.** In *Swine in the Laboratory: Surgery, Anesthesia, Imaging, and Experimental Techniques.* 3rd Edition edition. Edited by Swindle MM. Boca Raton: CRC Press; 2015: 451-465
103. Kreutz RP, Alloosh M, Mansour K, Neeb Z, Kreutz Y, Flockhart DA, Sturek M: **Morbid obesity and metabolic syndrome in Ossabaw miniature swine are associated with increased platelet reactivity.** *Diabetes Metab Syndr Obes* 2011, **4:**99-105.
104. Elmadhun NY, Sabe AA, Lassaletta AD, Chu LM, Kondra K, Sturek M, Sellke FW: **Metabolic syndrome impairs notch signaling and promotes apoptosis in chronically ischemic myocardium.** *J Thorac Cardiovasc Surg* 2014, **148:**1048-1055.
105. McKenney-Drake ML, Territo PR, Salavati A, Houshmand S, Persohn S, Liang Y, Alloosh M, Moe SM, Weaver CM, Alavi A, Sturek M: **^{18}F-NaF PET imaging of early coronary artery calcification.** *JACC Cardiovasc Imaging* 2016, **9:**627-628.
106. Phillips-Eakley AK, McKenney-Drake ML, Bahls M, Newcomer SC, Radcliffe JS, Wastney ME, Van Alstine WG, Jackson G, Alloosh M, Martin BR, et al: **Effect of high-calcium diet on coronary artery disease in Ossabaw miniature swine with metabolic syndrome.** *JAHA* 2015, **4**.
107. Lee L, Alloosh M, Saxena R, Van Alstine W, Watkins BA, Klaunig JE, Sturek M, Chalasani N: **Nutritional model of steatohepatitis and metabolic syndrome in the Ossabaw miniature swine.** *Hepatology* 2009, **50:**56-67.
108. Wastney M, Lee W, Jackson GS, Alloosh M, Sturek M, Lachcik P, Peacock M, Martin B, Weaver CM: **Soft tissue calcification in the Ossabaw miniature pig: experimental and kinetic modeling studies.** *Osteoporos Int* 2013, **24:**2123-2126.
109. Liang T, Alloosh M, Bell LN, Fullenkamp AM, Saxena R, Van Alstine W, Bybee P, Werling K, Sturek M, Chalasani N, Masuoka HC: **Liver injury and fibrosis induced by dietary challenge in the Ossabaw miniature swine.** *PLoS One* 2015, **10**.
110. Newell-Fugate AE, Taibl JN, Clark SG, Alloosh M, Sturek M, Krisher RL: **Effects of diet-induced obesity on metabolic parameters and reproductive function in female Ossabaw minipigs.** *Comp Med* 2014, **64:**44-49.
111. Newell-Fugate AE, Taibl JN, Alloosh M, Sturek M, Bahr JM, Nowak RA, Krisher RL: **Effects of obesity and metabolic syndrome on steroidogenesis and folliculogenesis in the female Ossabaw mini-pig.** *PLoS One* 2015, **10:**e0128749.
112. Fullenkamp AM, Bell LN, Robbins RD, Lee L, Saxena R, Alloosh M, Klaunig JE, Mirmira RG, Sturek M, Chalasani N: **Effect of different obesogenic diets on pancreatic histology in Ossabaw miniature swine.** *Pancreas* 2011, **40:**438-443.
113. Prevention CfDCa: **Adult Obesity Prevalence Maps.** 2019.

114. McKenney-Drake ML, Moghbel MC, Paydary K, Alloosh M, Houshmand S, Moe SM, Salavati A, Sturek JM, Territo PR, Weaver CM, et al: **18F-NaF and 18F-FDG as molecular probes in the evaluation of atherosclerosis.** *Eur J Nucl Med Mol Imaging* 2018**:**1-11.
115. Moberly S, Mather K, Berwick Z, Owen M, Goodwill A, Casalini E, Hutchins G, Green M, Ng Y, Considine R, et al: **Impaired cardiometabolic responses to glucagon-like peptide 1 in obesity and type 2 diabetes mellitus.** *Basic Res Cardiol* 2013, **108:**365.
116. Bell LN, Lee L, Saxena R, Bemis KG, Wang M, Theodorakis JL, Vuppalanchi R, Alloosh M, Sturek M, Chalasani N: **Serum proteomic analysis of diet-induced steatohepatitis and metabolic syndrome in the Ossabaw miniature swine.** *Am J Physiol Gastrointest Liver Physiol* 2010, **298:**G746-G754.
117. Bender SB, Tune JD, Borbouse L, Long X, Sturek M, Laughlin MH: **Altered mechanism of adenosine-induced coronary arteriolar dilation in early-stage metabolic syndrome.** *Exp Biol Med (Maywood)* 2009, **234:**683-692.
118. Berwick ZC, Dick GM, Moberly SP, Kohr MC, Sturek M, Tune JD: **Contribution of voltage-dependent K^+ channels to metabolic control of coronary blood flow.** *J Mol Cell Cardiol* 2012, **52:**912-919.
119. Bonin EA, Mariani A, Swain J, Bingener J, Sumiyama K, Knipschield M, Sebo TJ, Gostout CJ: **Laparoscopic ultrasound-assisted liposuction for lymph node dissection: a pilot study.** *Surg Endosc* 2012, **26:**1963-1970.
120. Boullion RD, Mokelke EA, Wamhoff BR, Otis CR, Wenzel J, Dixon JL, Sturek M: **Porcine model of diabetic dyslipidemia: Insulin and feed algorithms for mimicking diabetes in humans.** *Comp Med* 2003, **53:**42-52.
121. Bratz IN, Dick GM, Tune JD, Edwards JM, Neeb ZP, Dincer UD, Sturek M: **Impaired capsaicin-induced relaxation of coronary arteries in a porcine model of the metabolic syndrome.** *Am J Physiol Heart Circ Physiol* 2008, **294:**H2489-H2496.
122. Clark BA, Alloosh M, Wenzel JW, Sturek M, Kostrominova TY: **Effect of diet-induced obesity and metabolic syndrome on skeletal muscles of Ossabaw miniature swine.** *Am J Physiol Endocrinol Metab* 2011, **300:**E848-E857.
123. Dincer UD: **Cardiac beta-adrenoceptor expression is markedly depressed in Ossabaw swine model of cardiometabolic risk.** *Int J Gen Med* 2011, **4:**493-499.
124. Dyson MC, Alloosh M, Vuchetich JP, Mokelke EA, Sturek M: **Components of metabolic syndrome and coronary artery disease in female Ossabaw swine fed excess atherogenic diet.** *Comp Med* 2006, **56:**35-45.
125. Edwards JM, Neeb ZP, Alloosh MA, Long X, Bratz IN, Peller CR, Byrd JP, Kumar S, Obukhov AG, Sturek M: **Exercise training decreases store-operated Ca^{2+} entry associated with metabolic syndrome and coronary atherosclerosis.** *Cardiovasc Res* 2010, **85:**631-640.
126. Elmadhun NY, Lassaletta AD, Chu LM, Sellke FW: **Metformin alters the insulin signaling pathway in ischemic cardiac tissue in a swine model of metabolic syndrome.** *J Thorac Cardiovasc Surg* 2013, **145:**258-266.
127. Faris RJ, Boddicker RL, Walker-Daniels J, Li J, Jones DE, Spurlock ME: **Inflammation in response to n3 fatty acids in a porcine obesity model.** *Comp Med* 2012, **62:**495-503.
128. Flum DR, Devlin A, Wright AS, Figueredo E, Alyea E, Hanley PW, Lucas MK, Cummings DE: **Development of a porcine Roux-en-Y gastric bypass survival model for the study of post-surgical physiology.** *Obes Surg* 2007, **17:**1332-1339.

129. Hamamdzic D, Wilensky RL: **Porcine models of accelerated coronary atherosclerosis: role of diabetes mellitus and hypercholesterolemia.** *J Diabetes Res* 2013, **2013:**761415.
130. Handa RK, Evan AP, Connors BA, Johnson CD, Liu Z, Alloosh M, Sturek M, Evans-Molina C, Mandeville JA, Gnessin E, Lingeman JE: **Shock wave lithotripsy targeting of the kidney and pancreas does not increase the severity of metabolic syndrome in a porcine model.** *J Urol* 2014, **192:**1257-1265.
131. Handa RK, Johnson CD, Connors BA, Evan AP, Phillips CL, Liu Z: **Shock wave lithotripsy does not impair renal function in a swine model of metabolic syndrome.** *J Endourol* 2015, **29:**468-473.
132. Lassaletta AD, Chu LM, Robich MP, Elmadhun NY, Feng J, Burgess TA, Laham RJ, Sturek M, Sellke FW: **Overfed Ossabaw swine with early stage metabolic syndrome have normal coronary collateral development in response to chronic ischemia.** *Basic Res Cardiol* 2012, **107:**243.
133. Li ZL, Woollard JR, Ebrahimi B, Crane JA, Jordan KL, Lerman A, Wang SM, Lerman LO: **Transition From Obesity to Metabolic Syndrome Is Associated With Altered Myocardial Autophagy and Apoptosis.** *Arterioscler Thromb and Vasc Biol* 2012, **32:**1132-1141.
134. Li ZL, Woollard JR, Wang SM, Korsmo MJ, Ebrahimi B, Grande JP, Textor SC, Lerman A, Lerman LO: **Increased glomerular filtration rate in early metabolic syndrome is associated with renal adiposity and microvascular proliferation.** *Am J Physiol Renal Physiol* 2011, **301:**F1078-F1087.
135. McKenney ML, Schultz KA, Boyd JH, Byrd JP, Alloosh M, Teague SD, Arce-Esquivel AA, Fain JN, Laughlin MH, Sacks HS, Sturek M: **Epicardial adipose excision slows the progression of porcine coronary atherosclerosis.** *J Cardiothorac Surg* 2014, **9:**2-12.
136. Owen MK, Witzmann FA, McKenney ML, Lai X, Berwick ZC, Moberly SP, Alloosh M, Sturek M, Tune JD: **Perivascular adipose tissue potentiates contraction of coronary vascular smooth muscle: influence of obesity.** *Circulation* 2013, **128:**9-18.
137. Padilla J, Jenkins NT, Lee S, Zhang H, Cui J, Zuidema MY, Zhang C, Hill MA, Perfield JW, 2nd, Ibdah JA, et al: **Vascular transcriptional alterations produced by juvenile obesity in Ossabaw swine.** *Physiol Genomics* 2013, **45:**434-446.
138. Payne GA, Borbouse L, Kumar S, Neeb Z, Alloosh M, Sturek M, Tune JD: **Epicardial Perivascular Adipose-Derived Leptin Exacerbates Coronary Endothelial Dysfunction in Metabolic Syndrome via a Protein Kinase C-beta Pathway.** *Arterioscler Thromb Vasc Biol* 2010, **30:**1711-1717.
139. Pedersen R, Ingerslev H-C, Salicio SC, Sturek M, Alloosh M, Christoffersen BO, Moesgaard SG, Larsen N, Boye M: **Characterization of gut microbiota in Ossabaw and Göttingen minipigs as models of obesity and metabolic syndrome.** *PLoS One* 2012, **8:**e56612.
140. Rodgaard T, Stagsted J, Christoffersen BO, Cirera S, Moesgaard SG, Sturek M, Alloosh M, Heegaard PM: **Orosomucoid expression profiles in liver, adipose tissues and serum of lean and obese domestic pigs, Gottingen minipigs and Ossabaw minipigs.** *Vet Immunol Immunopathol* 2013, **151:**325-330.
141. Sham JG, Simianu VV, Wright AS, Stewart SD, Alloosh M, Sturek M, Cummings DE, Flum DR: **Evaluating the mechanisms of improved glucose homeostasis after bariatric surgery in Ossabaw miniature swine.** *J Diabetes Res* 2014, **2014:**526972.

142. Sturek M, Alloosh M, Wenzel J, Byrd JP, Edwards JM, Lloyd PG, Tune JD, March KL, Miller MA, Mokelke EA, Brisbin IL, Jr.: **Ossabaw Island miniature swine: cardiometabolic syndrome assessment.** In *Swine in the Laboratory: Surgery, Anesthesia, Imaging, and Experimental Techniques.* 2nd Edition edition. Edited by Swindle MM. Boca Raton: CRC Press; 2007: 397-402
143. Talbott CW, See MT, Kaminsky P, Bixby D, Sturek M, Brisbin IL, Kadzere C: **Enhancing pork flavor and fat quality with swine raised in sylvan systems Potential niche-market application for the Ossabaw hog.** *Renewable Agriculture and Food Systems* 2006, **21:**183-191.
144. Toedebusch RG, Roberts MD, Wells KD, Company JM, Kanosky KM, Padilla J, Jenkins NT, Perfield JW, 2nd, Ibdah JA, Booth FW, Rector RS: **Unique transcriptomic signature of omental adipose tissue in Ossabaw swine: a model of childhood obesity.** *Physiol Genomics* 2014, **46:**362-375.
145. Trasino SE, Dawson HD, Urban JF, Jr., Wang TT, Solano-Aguilar G: **Feeding probiotic Lactobacillus paracasei to Ossabaw pigs on a high-fat diet prevents cholesteryl-ester accumulation and LPS modulation of the Liver X receptor and inflammatory axis in alveolar macrophages.** *J Nutr Biochem* 2013, **24:**1931-1939.
146. Trask AJ, Katz PS, Kelly AP, Galantowicz ML, Cismowski MJ, West TA, Neeb ZP, Berwick ZC, Goodwill AG, Alloosh M, et al: **Dynamic micro- and macrovascular remodeling in coronary circulation of obese Ossabaw pigs with metabolic syndrome.** *J Appl Physiol (1985)* 2012, **113:**1128-1140.
147. Witczak CA, Mokelke EA, Boullion RD, Wenzel J, Keisler DH, Sturek M: **Noninvasive measures of body fat percentage in male Yucatan swine.** *Comp Med* 2005, **55:**445-451.
148. Zhang X, Li ZL, Woollard JR, Eirin A, Ebrahimi B, Crane JA, Zhu XY, Pawar AS, Krier JD, Jordan KL, et al: **Obesity-metabolic derangement preserves hemodynamics but promotes intrarenal adiposity and macrophage infiltration in swine renovascular disease.** *Am J Physiol Renal Physiol* 2013, **305:**F265-F276.
149. Handa RK, Liu Z, Connors BA, Alloosh M, Basile DP, Tune JD, Sturek M, Evan AP, Lingeman JE: **Effect of renal shock wave lithotripsy on the development of metabolic syndrome in a juvenile swine model: a pilot study.** *J Urol* 2015, **193:**1409-1416.
150. Habegger KM, Penque BA, Sealls W, Tackett L, Bell LN, Blue EK, Gallagher PJ, Sturek M, Alloosh MA, Steinberg HO, et al: **Fat-induced membrane cholesterol accrual provokes cortical filamentous actin destabilization and glucose transport dysfunction in skeletal muscle.** *Diabetologia* 2012, **55:**457-467.
151. Otis CR, Wamhoff BR, Sturek M: **Hyperglycemia-induced insulin resistance in diabetic dyslipidemic Yucatan swine.** *Comp Med* 2003, **53:**53-64.
152. Potu RB, Lu H, Adeola O, Ajuwon KM: **Metabolic markers in Ossabaw pigs fed high fat diets enriched in regular or low alpha-linolenic acid soy oil.** *Nutr Metab (Lond)* 2013, **10:**27.
153. Witczak CA, Sturek M: **Exercise prevents diabetes-induced impairment in superficial buffer barrier in porcine coronary smooth muscle.** *J Appl Physiol* 2004, **96:**1069-1079.
154. Sabe AA, Elmadhun NY, Sadek AA, Chu LM, Bianchi C, Sellke FW: **Differential effects of atorvastatin on autophagy in ischemic and nonischemic myocardium in Ossabaw swine with metabolic syndrome.** *J Thorac Cardiovasc Surg* 2014, **148:**3172-3178.

155. Dixon JL, Shen S, Vuchetich JP, Wysocka E, Sun GY, Sturek M: **Increased atherosclerosis in diabetic dyslipidemic swine: protection by atorvastatin involves decreased VLDL triglycerides but minimal effects on the lipoprotein profile.** *J Lipid Res* 2002, **43:**1618-1629.
156. Hanhineva K, Barri T, Kolehmainen M, Pekkinen J, Pihlajamaki J, Vesterbacka A, Solano-Aguilar G, Mykkanen H, Dragsted LO, Urban JF, Jr., Poutanen K: **Comparative nontargeted profiling of metabolic changes in tissues and biofluids in high-fat diet-fed Ossabaw pig.** *J Proteome Res* 2013, **12:**3980-3992.
157. Mokelke EA, Hu Q, Song M, Toro L, Reddy HK, Sturek M: **Altered functional coupling of coronary K^+ channels in diabetic dyslipidemic pigs is prevented by exercise.** *J Appl Physiol* 2003, **95:**1179-1193.
158. Lee DL, Wamhoff BR, Katwa LC, Reddy HK, Voelker DJ, Dixon JL, Sturek M: **Increased endothelin-induced Ca^{2+} signaling, tyrosine phosphorylation, and coronary artery disease in diabetic dyslipidemic swine are prevented by atorvastatin.** *J Pharmacol Exp Ther* 2003, **306:**132-140.
159. Long X, Bratz IN, Alloosh M, Edwards JM, Sturek M: **Short-term exercise training prevents micro- and macrovascular disease following coronary stenting.** *J Appl Physiol (1985)* 2010, **108:**1766-1774.
160. Long X, Mokelke EA, Neeb ZP, Alloosh M, Edwards JM, Sturek M: **Adenosine receptor regulation of coronary blood flow in Ossabaw miniature swine.** *J Pharmacol Exp Ther* 2010, **335:**781-787.
161. Rector RS, Thomas TR, Liu Y, Henderson KK, Holiman DA, Sun GY, Sturek M: **Effect of exercise on postprandial lipemia following a higher calorie meal in Yucatan miniature swine.** *Metabolism* 2004, **53:**1021-1026.
162. Mozaffarian D, Benjamin EJ, Go AS, Arnett DK, Blaha MJ, Cushman M, Das SR, de Ferranti S, Despres JP, Fullerton HJ, et al: **Heart Disease and Stroke Statistics-2016 Update: A Report From the American Heart Association.** *Circulation* 2016, **133:**e38-60.
163. Karwowski W, Naumnik B, Szczepanski M, Mysliwiec M: **The mechanism of vascular calcification - a systematic review.** *Med Sci Monit* 2012, **18:**RA1-11.
164. Alexander CM, Landsman PB, Teutsch SM, Haffner SM: **NCEP-Defined Metabolic Syndrome, Diabetes, and Prevalence of Coronary Heart Disease Among NHANES III Participants Age 50 Years and Older.** *Diabetes* 2003, **52:**1210-1214.
165. Gerrity RG, Natarajan R, Nadler JL, Kimsey T: **Diabetes-induced accelerated atherosclerosis in swine.** *Diabetes* 2001, **50:**1654-1665.
166. Al-Mashhadi RH, Bjorklund MM, Mortensen MB, Christoffersen C, Larsen T, Falk E, Bentzon JF: **Diabetes with poor glycaemic control does not promote atherosclerosis in genetically modified hypercholesterolaemic minipigs.** *Diabetologia* 2015, **58:**1926-1936.
167. Dixon JL, Stoops JD, Parker JL, Laughlin MH, Weisman GA, Sturek M: **Dyslipidemia and vascular dysfunction in diabetic pigs fed an atherogenic diet.** *Arterioscler Thromb Vasc Biol* 1999, **19:**2981-2992.
168. Ludvigsen TP, Kirk RK, Christoffersen BO, Pedersen HD, Martinussen T, Kildegaard J, Heegaard PM, Lykkesfeldt J, Olsen LH: **Gottingen minipig model of diet-induced atherosclerosis: influence of mild streptozotocin-induced diabetes on lesion severity and markers of inflammation evaluated in obese, obese and diabetic, and lean control animals.** *J Transl Med* 2015, **13:**312.
169. Kreutz RP, Alloosh M, Neeb ZP, Kreutz Y, Flockhart DA, Sturek M: **Metabolic syndrome in Ossabaw miniature swine is associated with increased**

sensitivity of platelet aggregation to adenosine diphosphate (abstract). *ATVB* 2009, **29:**e122.
170. AVMA Panel on Euthanasia.American Veterinary Medical Association: **2000 Report of the AVMA panel on euthanasia.** *JAVMA* 2001, **218:**669-696.
171. Institute for Laboratory Animal Research: *Guide for the care and use of laboratory animals.* 8th edn. Washington, D.C.: National Academy Press; 2010.
172. Nathan DM, Kuenen J, Borg R, Zheng H, Schoenfeld D, Heine RJ, Group Ac-DAGS: **Translating the A1C assay into estimated average glucose values.** *Diabetes Care* 2008, **31:**1473-1478.
173. Sturek M: **Tuning in to the "right" calcium channel regulation in experimental models of diabetes.** *Br J Pharmacol* 2010, **161:**1455-1457.
174. Heaps CL, Sturek M, Price EM, Laughlin MH, Parker JL: **Sarcoplasmic reticulum Ca(2+) uptake is impaired in coronary smooth muscle distal to coronary occlusion.** *Am J Physiol Heart Circ Physiol* 2001, **281:**H223-H231.
175. Ehara S, Kobayashi Y, Yoshiyama M, Ueda M, Yoshikawa J: **Coronary artery calcification revisited.** *J Atheroscler Thromb* 2006, **13:**31-37.
176. Tamaru H, Fujii K, Fukunaga M, Imanaka T, Miki K, Horimatsu T, Nishimura M, Saita T, Sumiyoshi A, Shibuya M, et al: **Impact of spotty calcification on long-term prediction of future revascularization: a prospective three-vessel intravascular ultrasound study.** *Heart Vessels* 2016, **31:**881-889.
177. Veiraiah A: **Hyperglycemia, lipoprotein glycation, and vascular disease.** *Angiology* 2005, **56:**431-438.
178. Yamagishi S, Imaizumi T: **Diabetic vascular complications: pathophysiology, biochemical basis and potential therapeutic strategy.** *Curr Pharm Des* 2005, **11:**2279-2299.
179. Southerland JH, Taylor GW, Moss K, Beck JD, Offenbacher S: **Commonality in chronic inflammatory diseases: periodontitis, diabetes, and coronary artery disease.** *Periodontol 2000* 2006, **40:**130-143.
180. Stolar M: **Glycemic control and complications in type 2 diabetes mellitus.** *Am J Med* 2010, **123:**S3-11.
181. Howard BV: **Lipoprotein metabolism in diabetes mellitus.** *J Lipid Res* 1987, **28:**613-628.
182. Antonopoulos AS, Sanna F, Sabharwal N, Thomas S, Oikonomou EK, Herdman L, Margaritis M, Shirodaria C, Kampoli AM, Akoumianakis I, et al: **Detecting human coronary inflammation by imaging perivascular fat.** *Sci Transl Med* 2017, **9**.
183. Khazai B, Luo Y, Rosenberg S, Wingrove J, Budoff MJ: **Coronary Atherosclerotic Plaque Detected by Computed Tomographic Angiography in Subjects with Diabetes Compared to Those without Diabetes.** *PLoS One* 2015, **10:**e0143187.
184. Pauly RR, Bilato C, Sollott SJ, Monticone R, Kelly PT, Lakatta EG, Crow MT: **Role of calcium/calmodulin-dependent protein kinase II in the regulation of vascular smooth muscle cell migration.** *Circulation* 1995, **91:**1107-1115.
185. Lundberg MS, Curto KA, Bilato C, Monticone RE, Crow MT: **Regulation of vascular smooth muscle migration by mitogen-activated protein kinase and calcium/calmodulin-dependent protein kinase II signaling pathways.** *J Mol Cell Cardiol* 1998, **30:**2377-2389.
186. Hill-Eubanks DC, Werner ME, Heppner TJ, Nelson MT: **Calcium signaling in smooth muscle.** *Cold Spring Harb Perspect Biol* 2011, **3:**a004549.
187. Jiang H, Stephens NL: **Calcium and smooth muscle contraction.** *Mol Cell Biochem* 1994, **135:**1-9.

188. Wamhoff BR, Bowles DK, McDonald OG, Sinha S, Somlyo AP, Somlyo AV, Owens GK: **L-type voltage-gated Ca2+ channels modulate expression of smooth muscle differentiation marker genes via a rho kinase/myocardin/SRF-dependent mechanism.** *Circ Res* 2004, **95:**406-414.
189. Chen NX, Kircelli F, O'Neill KD, Chen X, Moe SM: **Verapamil inhibits calcification and matrix vesicle activity of bovine vascular smooth muscle cells.** *Kidney Int* 2010, **77:**436-442.
190. Kataoka Y, Wolski K, Uno K, Puri R, Tuzcu EM, Nissen SE, Nicholls SJ: **Spotty calcification as a marker of accelerated progression of coronary atherosclerosis: insights from serial intravascular ultrasound.** *J Am Coll Cardiol* 2012, **59:**1592-1597.
191. Ehara S, Kobayashi Y, Yoshiyama M, Shimada K, Shimada Y, Fukuda D, Nakamura Y, Yamashita H, Yamagishi H, Takeuchi K, et al: **Spotty Calcification Typifies the Culprit Plaque in Patients With Acute Myocardial Infarction.** *Circulation* 2004, **110:**3424-3429.
192. Amano H, Ikeda T, Toda M, Okubo R, Yabe T, Koike M, Saito D, Yamazaki J: **Assessment of angiographic coronary calcification and plaque composition in virtual histology intravascular ultrasound.** *J Interv Cardiol* 2015, **28:**205-214.
193. Rerup CC: **Drugs producing diabetes through damage of the insulin secreting cells.** *Pharmacol Rev* 1970, **22:**485-517.
194. Lenzen S: **The mechanisms of alloxan-and streptozotocin-induced diabetes.** *Diabetologia* 2008, **51:**216-226.
195. Etuk E: **Animals models for studying diabetes mellitus.** *Agric Biol JN Am* 2010, **1:**130-134.
196. King AJ: **The use of animal models in diabetes research.** *Br J Pharmacol* 2012, **166:**877-894.
197. Bunnag SC, Warner NE, Bunnag S: **Effect of alloxan on the mouse pancreas during and after recovery from diabetes.** *Diabetes* 1967, **16:**83-89.
198. Jain DK, Arya RK: **Anomalies in alloxan-induced diabetic model: It is better to standardize it first.** *Indian J Pharmacol* 2011, **43:**91.
199. O'Hea EK, Allee GL, Leveille GA, Baker DH: **Observations on the alloxan-diabetic pig.** *Int J Biochem* 1971, **2:**177-181.
200. Riley WJ, McConnell TJ, Maclaren NK, McLaughlin JV, Taylor G: **The diabetogenic effects of streptozotocin in mice are prolonged and inversely related to age.** *Diabetes* 1981, **30:**718-723.
201. Hammarstrom L, Hellman B, Ullberg S: **On the accumulation of alloxan in the pancreatic beta-cells.** *Diabetologia* 1967, **3:**340-344.
202. Creutzfeldt W: **Zur Histophysiologie des Inselapparates.** *Z Zellforsch Mikrosk Anat* 1949, **34:**280-336.
203. Dineen SL, McKenney ML, Bell LN, Fullenkamp AM, Schultz KA, Alloosh M, Chalasani N, Sturek M: **Metabolic Syndrome Abolishes Glucagon-Like Peptide 1 Receptor Agonist Stimulation of SERCA in Coronary Smooth Muscle.** *Diabetes* 2015, **64:**3321-3327.
204. Badin JK, Kole A, Stivers B, Progar V, Pareddy A, Alloosh M, Sturek M: **Diabetes exacerbates coronary atherosclerosis and calcification in Ossabaw miniature swine with metabolic syndrome.** *J Transl Med* 2018, **16**.
205. Wallace TM, Levy JC, Matthews DR: **Use and abuse of HOMA modeling.** *Diabetes Care* 2004, **27:**1487-1495.
206. Gayoso-Diz P, Otero-Gonzalez A, Rodriguez-Alvarez MX, Gude F, Garcia F, De Francisco A, Quintela AG: **Insulin resistance (HOMA-IR) cut-off values and the**

metabolic syndrome in a general adult population: effect of gender and age: EPIRCE cross-sectional study. *BMC Endocr Disord* 2013, **13:**47.
207. Panepinto LM, Phillips RW, Westmoreland NW, Cleek JL: **Influence of genetics and diet on the development of diabetes in Yucatan miniature swine.** *J Nutr* 1982, **112:**2307-2313.
208. Gutch M, Kumar S, Razi SM, Gupta KK, Gupta A: **Assessment of insulin sensitivity/resistance.** *Indian J Endocrinol Metab* 2015, **19:**160-164.
209. Matthews DR, Hosker JP, Rudenski AS, Naylor BA, Treacher DF, Turner RC: **Homeostasis model assessment: insulin resistance and beta-cell function from fasting plasma glucose and insulin concentrations in man.** *Diabetologia* 1985, **28:**412-419.
210. Ahren B, Pacini G: **Islet adaptation to insulin resistance: mechanisms and implications for intervention.** *Diabetes Obes Metab* 2005, **7:**2-8.
211. Maggs DG, Jacob R, Rife F, Caprio S, Tamborlane WV, Sherwin RS: **Counterregulation in peripheral tissues. Effect of systemic hypoglycemia on levels of substrates and catecholamines in human skeletal muscle and adipose tissue.** *Diabetes* 1997, **46:**70-76.
212. Yki-Jarvinen H, Koivisto VA: **Natural course of insulin resistance in type 1 diabetes.** *N Engl J Med* 1986, **315:**224-230.
213. Dimitrakoudis D, Ramlal T, Rastogi S, Vranic M, Klip A: **Glycaemia regulates the glucose transporter number in the plasma membrane of rat skeletal muscle.** *Biochem J* 1992, **284:**341-348.
214. Hansen BF, Hansen SA, Ploug T, Bak JF, Richter EA: **Effects of glucose and insulin on development of impaired insulin action in muscle.** *Am J Physiol* 1992, **262:**E440-E446.
215. Mathoo JMR, Shi ZQ, Klip A, Vranic M: **Opposite effects of acute hypoglycemia and acute hyperglycemia on glucose transport and glucose transporters in perfused rat skeletal muscle.** *Diabetes* 1999, **48:**1281-1288.
216. Reaven GM, Sageman WS, Swenson RS: **Development of insulin resistance in normal dogs following alloxan-induced insulin deficiency.** *Diabetologia* 1977, **133:**459-462.
217. Richardson JM, Balon TW, Treadway JL, Pessin JE: **Differential regulation of glucose transporter activity and expression in red and white skeletal muscle.** *J Biol Chem* 1991, **266:**12690-12694.
218. Richter EA, Hansen BF, Hansen SA: **Glucose-induced insulin resistance of skeletal-muscle glucose transport and uptake.** *Biochem J* 1988, **252:**733-737.
219. Wilcox G: **Insulin and insulin resistance.** *Clin Biochem Rev* 2005, **26:**19-39.
220. Davidson MB, Kaplan SA: **Increased insulin binding by hepatic plasma membranes from diabetic rats: normalization by insulin therapy.** *J Clin Invest* 1977, **59:**22-30.
221. O'Meara NM, Devery RA, Owens D, Collins PB, Johnson AH, Tomkin GH: **Cholesterol metabolism in alloxan-induced diabetic rabbits.** *Diabetes* 1990, **39:**626-633.
222. Phillips C, Bennett A, Anderton K, Owens D, Collins P, White D, Tomkin GH: **Intestinal rather than hepatic microsomal triglyceride transfer protein as a cause of postprandial dyslipidemia in diabetes.** *Metabolism* 2002, **51:**847-852.
223. Putnam K, Shoemaker R, Yiannikouris F, Cassis LA: **The renin-angiotensin system: a target of and contributor to dyslipidemias, altered glucose homeostasis, and hypertension of the metabolic syndrome.** *Am J Physiol Heart Circ Physiol* 2012, **302:**H1219-1230.

224. Ho SC, Michelakis AM: **Multiple defects in the renin-angiotensin system in alloxan-diabetic kidney.** *Proc Soc Exp Biol Med* 1985, **178:**297-303.
225. Santos SH, Braga JF, Mario EG, Porto LC, Rodrigues-Machado Mda G, Murari A, Botion LM, Alenina N, Bader M, Santos RA: **Improved lipid and glucose metabolism in transgenic rats with increased circulating angiotensin-(1-7).** *Arterioscler Thromb Vasc Biol* 2010, **30:**953-961.
226. Turlapaty PD, Lum G, Altura BM: **Vascular responsiveness and serum biochemical parameters in alloxan diabetes mellitus.** *Am J Physiol* 1980, **239:**E412-421.
227. Wang J, Wan R, Mo Y, Zhang Q, Sherwood LC, Chien S: **Creating a long-term diabetic rabbit model.** *Exp Diabetes Res* 2010, **2010:**289614.
228. Altura BM, Lum G, Turlapaty PD, Altura BT: **Sequential changes in serum glucose, triglycerides and cholesterol in aging of normal and alloxan-diabetic rats.** *Experientia* 1981, **37:**224-226.
229. Chera S, Baronnier D, Ghila L, Cigliola V, Jensen JN, Gu G, Furuyama K, Thorel F, Gribble FM, Reimann F, Herrera PL: **Diabetes recovery by age-dependent conversion of pancreatic delta-cells into insulin producers.** *Nature* 2014, **514:**503-507.
230. Chung CH, Levine F: **Adult pancreatic alpha-cells: a new source of cells for beta-cell regeneration.** *Rev Diabet Stud* 2010, **7:**124-131.
231. Bottino R, Balamurugan A, Smetanka C, Bertera S, He J, Rood PP, Cooper DK, Trucco M: **Isolation outcome and functional characteristics of young and adult pig pancreatic islets for transplantation studies.** *Xenotransplantation* 2007, **14:**74-82.
232. Gad SC, Dincer Z, Svendsen O, Skaanild MT: **The minipig.** In *Animal Models in Toxicology.* 2nd edition. Edited by Gad SC. Boca Raton: CRC/Taylor & Francis; 2007: 731-772
233. McAnulty PA, Barrow P, Marsden E: **Reproductive system including studies in juvenile minipigs.** In *The Minipig in Biomedical Research.* Edited by McAnulty PA, Dayan AD, Ganderup N-C, Hastings KL. Boca Raton: CRC Press/Taylor & Francis; 2012: 263-276
234. Christoffersen BO, Grand N, Golozoubova V, Svendsen O, Raun K: **Gender-associated Differences in Metabolic Syndrome-related Parameters in Gottingen Minipigs.** *Comp Med* 2007, **57:**493-504.
235. Davies A, Pearson G, Carr J: **The carcass composition of male, castrated male and female pigs resulting from two levels of feeding.** *J Agri Sci* 1980, **95:**251-259.
236. Berlin E, Khan MA, Henderson GR, Kliman PG: **Influence of age and sex on composition and lipid fluidity in miniature swine plasma lipoproteins.** *Atherosclerosis* 1985, **54:**187-203.
237. Bollen PJ, Madsen LW, Meyer O, Ritskes-Hoitinga J: **Growth differences of male and female Gottingen minipigs during ad libitum feeding: a pilot study.** *Lab Anim* 2005, **39:**80-93.
238. Kawaguchi H, Yamada T, Miura N, Noguchi M, Izumi H, Miyoshi N, Tanimoto A: **Sex differences of serum lipid profile in novel microminipigs.** *In Vivo* 2013, **27:**617-621.
239. Dubey RK, Jackson EK, Keller PJ, Imthurn B, Rosselli M: **Estradiol metabolites inhibit endothelin synthesis by an estrogen receptor-independent mechanism.** *Hypertension* 2001, **37:**640-644.

240. Han S-Z, Karaki H, Ouchi Y, Akishita M, Orimo H: **17b-estradiol inhibits Ca^{2+} influx and Ca^{2+} release induced by thromboxane A_2 in porcine coronary artery.** *Circulation* 1995, **91:**2619-2626.
241. Teoh H, Quan A, Leung SWS, Man RYK: **Differential effects of 17*b*-estradiol and testosterone on the contractile responses of porcine coronary arteries.** *Br J Pharmacol* 2000, **129:**1301-1308.
242. Farhat MY, Wolfe R, Vargas R, Foegh ML, Ramwell PW: **Effect of testosterone treatment on vasoconstrictor response of left anterior descending coronary artery in male and female pigs.** *J Cardiovasc Pharmacol* 1995, **25:**495-500.
243. Frank LA, Rohrbach BW, Bailey EM, West JR, Oliver JW: **Steroid hormone concentration profiles in healthy intact and neutered dogs before and after cosyntropin administration.** *Domest Anim Endocrinol* 2003, **24:**43-57.
244. Srinivasan K, Ramarao P: **Animal models in type 2 diabetes research: an overview.** *Indian J Med Res* 2007, **125:**451-472.
245. Marijic J, Li Q, Song M, Nishimaru K, Stefani E, Toro L: **Decreased expression of voltage- and Ca(2+)-activated K(+) channels in coronary smooth muscle during aging.** *Circ Res* 2001, **88:**210-216.
246. Aird WC: **Phenotypic heterogeneity of the endothelium: I. Structure, function, and mechanisms.** *Circ Res* 2007, **100:**158-173.
247. Berger JS, Hochman J, Lobach I, Adelman MA, Riles TS, Rockman CB: **Modifiable risk factor burden and the prevalence of peripheral artery disease in different vascular territories.** *J Vasc Surg* 2013, **58:**673-681 e671.
248. Forman DE, Alexander K, Brindis RG, Curtis AB, Maurer M, Rich MW, Sperling L, Wenger NK: **Improved Cardiovascular Disease Outcomes in Older Adults.** *F1000Res* 2016, **5**.
249. Kruse HJ, Bauriedel G, Heimerl J, Hofling B, Weber PC: **Role of L-type calcium channels on stimulated calcium influx and on proliferative activity of human coronary smooth muscle cells.** *J Cardiovasc Pharmacol* 1994, **24:**328-335.
250. Nilsson J, Sjolund M, Palmberg L, Von Euler AM, Jonzon B, Thyberg J: **The calcium antagonist nifedipine inhibits arterial smooth muscle cell proliferation.** *Atherosclerosis* 1985, **58:**109-122.
251. Decuypere JP, Monaco G, Missiaen L, De Smedt H, Parys JB, Bultynck G: **IP(3) Receptors, Mitochondria, and Ca Signaling: Implications for Aging.** *J Aging Res* 2011, **2011:**920178.
252. Hill BJF, Katwa LC, Wamhoff BR, Sturek M: **Enhanced endothelin(A) receptor-mediated calcium mobilization and contraction in organ cultured porcine coronary arteries.** *J Pharmacol Exp Ther* 2000, **295:**484-491.
253. Stehno-Bittel L, Laughlin MH, Sturek M: **Exercise training alters Ca release from coronary smooth muscle sarcoplasmic reticulum.** *Am J Physiol Heart Circ Physiol* 1990, **259:**H643-H647.
254. Tumbleson ME, Hicklin KW, Burks MF: **Serum cholesterol, triglyceride, glucose and total bilirubin concentrations, as functions of age and sex, in Sinclair(S-1) miniature swine.** *Growth* 1976, **40:**293-300.
255. Sawabe M: **Vascular aging: from molecular mechanism to clinical significance.** *Geriatr Gerontol Int* 2010, **10 Suppl 1:**S213-220.
256. Yildiz O: **Vascular smooth muscle and endothelial functions in aging.** *Ann N Y Acad Sci* 2007, **1100:**353-360.
257. Ghosh TK, Bian JH, Short AD, Rybak SL, Gill DL: **Persistent intracellular calcium pool depletion by thapsigargin and its influence on cell growth.** *J Biol Chem* 1991, **266:**24690-24697.

258. Lipskaia L, Hulot JS, Lompre AM: **Role of sarco/endoplasmic reticulum calcium content and calcium ATPase activity in the control of cell growth and proliferation.** *Pflugers Arch* 2009, **457:**673-685.
259. Moon SK, Thompson LJ, Madamanchi N, Ballinger S, Papaconstantinou J, Horaist C, Runge MS, Patterson C: **Aging, oxidative responses, and proliferative capacity in cultured mouse aortic smooth muscle cells.** *Am J Physiol Heart Circ Physiol* 2001, **280:**H2779-H2788.
260. Zhou RH, Vendrov AE, Tchivilev I, Niu XL, Molnar KC, Rojas M, Carter JD, Tong H, Stouffer GA, Madamanchi NR, Runge MS: **Mitochondrial oxidative stress in aortic stiffening with age: the role of smooth muscle cell function.** *Arterioscler Thromb Vasc Biol* 2012, **32:**745-755.
261. Libby P: **Murine "Model" Monotheism: An Iconoclast at the Altar of Mouse.** *Circ Res* 2015, **117:**921-925.
262. DG LEC, Cogger VC, McCuskey RS, R DEC, Smedsrod B, Sorensen KK, Warren A, Fraser R: **Age-related changes in the liver sinusoidal endothelium: a mechanism for dyslipidemia.** *Ann N Y Acad Sci* 2007, **1114:**79-87.
263. Ghebre YT, Yakubov E, Wong WT, Krishnamurthy P, Sayed N, Sikora AG, Bonnen MD: **Vascular Aging: Implications for Cardiovascular Disease and Therapy.** *Transl Med (Sunnyvale)* 2016, **6**.
264. Dubowitz N, Xue W, Long Q, Ownby JG, Olson DE, Barb D, Rhee MK, Mohan AV, Watson-Williams PI, Jackson SL, et al: **Aging is associated with increased HbA1c levels, independently of glucose levels and insulin resistance, and also with decreased HbA1c diagnostic specificity.** *Diabet Med* 2014, **31:**927-935.
265. Chung HY, Cesari M, Anton S, Marzetti E, Giovannini S, Seo AY, Carter C, Yu BP, Leeuwenburgh C: **Molecular inflammation: underpinnings of aging and age-related diseases.** *Ageing Res Rev* 2009, **8:**18-30.
266. Childs BG, Baker DJ, Wijshake T, Conover CA, Campisi J, van Deursen JM: **Senescent intimal foam cells are deleterious at all stages of atherosclerosis.** *Science* 2016, **354:**472-477.
267. Horton JD, Cohen JC, Hobbs HH: **PCSK9: a convertase that coordinates LDL catabolism.** *J Lipid Res* 2009, **50 Suppl:**S172-S177.
268. Teoh H, Man RYK: **Enhanced relaxation of porcine coronary arteries after acute exposure to a physiological level of 17b-estradiol involves non-genomic mechanisms and the cyclic AMP cascade.** *Br J Pharmacol* 2000, **129:**1739-1747.
269. Shanahan CM, Weissberg PL: **Smooth muscle cell heterogeneity - Patterns of gene expression in vascular smooth muscle cells in vitro and in vivo.** *Arterioscler Thromb Vasc Biol* 1998, **18:**333-338.
270. King KE, Iyemere VP, Weissberg PL, Shanahan CM: **Kruppel-like factor 4 (KLF4/GKLF) is a target of bone morphogenetic proteins and transforming growth factor beta 1 in the regulation of vascular smooth muscle cell phenotype.** *J Biol Chem* 2003, **278:**11661-11669.
271. Libby P: **Vascular biology of atherosclerosis: overview and state of the art.** *Am J Cardiol* 2003, **91:**3A-6A.
272. Puri R, Nicholls SJ, Shao M, Kataoka Y, Uno K, Kapadia SR, Tuzcu EM, Nissen SE: **Impact of statins on serial coronary calcification during atheroma progression and regression.** *J Am Coll Cardiol* 2015, **65:**1273-1282.
273. Kudryavtseva O, Aalkjaer C, Matchkov VV: **Vascular smooth muscle cell phenotype is defined by Ca2+-dependent transcription factors.** *FEBS J* 2013, **280:**5488-5499.

274. Heaps CL, Bowles DK, Sturek M, Laughlin MH, Parker JL: **Enhanced L-type Ca^{2+} channel current density in coronary smooth muscle of exercise trained swine is compensated to limit myoplasmic net Ca^{2+} accumulation.** *J Physiol* 2000, **528:**435-445.
275. Stegemann JP, Hong H, Nerem RM: **Mechanical, biochemical, and extracellular matrix effects on vascular smooth muscle cell phenotype.** *J Appl Physiol (1985)* 2005, **98:**2321-2327.
276. Iyemere VP, Proudfoot D, Weissberg PL, Shanahan CM: **Vascular smooth muscle cell phenotypic plasticity and the regulation of vascular calcification.** *J Intern Med* 2006, **260:**192-210.
277. Hao H, Gabbiani G, Bochaton-Piallat ML: **Arterial smooth muscle cell heterogeneity.** *Arterioscl Thromb Vasc Biol* 2003, **23:**1510-1520.
278. Rensen SS, Doevendans PA, van Eys GJ: **Regulation and characteristics of vascular smooth muscle cell phenotypic diversity.** *Neth Heart J* 2007, **15:**100-108.
279. Christen T, Bochaton-Piallat ML, Neuville P, Rensen S, Redard M, Van Eys G, Gabbiani G: **Cultured porcine coronary artery smooth muscle cells - A new model with advanced differentiation.** *Circulation Research* 1999, **85:**99-107.
280. Frid MG, Moiseeva EP, Stenmark KR: **Multiple phenotypically distinct smooth muscle cell populations exist in the adult and developing bovine pulmonary arterial media in vivo.** *Circ Res* 1994, **75:**669-681.
281. Christen T, Verin V, Bochaton-Piallat ML, Popowski Y, Ramaekers F, Debruyne P, Camenzind E, Van Eys G, Gabbiani G: **Mechanisms of neointima formation and remodeling in the porcine coronary artery.** *Circulation* 2001, **103:**882-888.
282. Wagner-Mann C, Hu Q, Sturek M: **Multiple effects of ryanodine on intracellular free Ca^{2+} in smooth muscle cells from bovine and porcine coronary artery: modulation of sarcoplasmic reticulum function.** *BrJPharmacol* 1992, **105:**903-911.
283. Badin JK, Bruning RS, Sturek M: **Effect of metabolic syndrome and aging on Ca2+ dysfunction in coronary smooth muscle and coronary artery disease severity in Ossabaw miniature swine.** *Exp Gerontol* 2018, **108:**247-255.
284. Satija R, Farrell JA, Gennert D, Schier AF, Regev A: **Spatial reconstruction of single-cell gene expression data.** *Nat Biotechnol* 2015, **33:**495-502.
285. Butler A, Hoffman P, Smibert P, Papalexi E, Satija R: **Integrating single-cell transcriptomic data across different conditions, technologies, and species.** *Nat Biotechnol* 2018, **36:**411-420.
286. Kapustin AN, Chatrou ML, Drozdov I, Zheng Y, Davidson SM, Soong D, Furmanik M, Sanchis P, De Rosales RT, Alvarez-Hernandez D, et al: **Vascular smooth muscle cell calcification is mediated by regulated exosome secretion.** *Circ Res* 2015, **116:**1312-1323.
287. Guerrero F, Herencia C, Almaden Y, Martinez-Moreno JM, Montes de Oca A, Rodriguez-Ortiz ME, Diaz-Tocados JM, Canalejo A, Florio M, Lopez I, et al: **TGF-beta prevents phosphate-induced osteogenesis through inhibition of BMP and Wnt/beta-catenin pathways.** *PLoS One* 2014, **9:**e89179.
288. Cai T, Sun D, Duan Y, Wen P, Dai C, Yang J, He W: **WNT/beta-catenin signaling promotes VSMCs to osteogenic transdifferentiation and calcification through directly modulating Runx2 gene expression.** *Exp Cell Res* 2016, **345:**206-217.
289. Herencia C, Rodriguez-Ortiz ME, Munoz-Castaneda JR, Martinez-Moreno JM, Canalejo R, Montes de Oca A, Diaz-Tocados JM, Peralbo-Santaella E, Marin C, Canalejo A, et al: **Angiotensin II prevents calcification in vascular smooth**

muscle cells by enhancing magnesium influx. *Eur J Clin Invest* 2015, **45:**1129-1144.
290. Cheng SL, Shao JS, Halstead LR, Distelhorst K, Sierra O, Towler DA: **Activation of vascular smooth muscle parathyroid hormone receptor inhibits Wnt/beta-catenin signaling and aortic fibrosis in diabetic arteriosclerosis.** *Circ Res* 2010, **107:**271-282.
291. Neven E, Persy V, Dauwe S, De Schutter T, De Broe ME, D'Haese PC: **Chondrocyte rather than osteoblast conversion of vascular cells underlies medial calcification in uremic rats.** *Arterioscler Thromb Vasc Biol* 2010, **30:**1741-1750.
292. Fernandes GS, Valdes AM: **Cardiovascular disease and osteoarthritis: common pathways and patient outcomes.** *Eur J Clin Invest* 2015, **45:**405-414.
293. Dremina ES, Sharov VS, Davies MJ, Schoneich C: **Oxidation and inactivation of SERCA by selective reaction of cysteine residues with amino acid peroxides.** *Chem Res Toxicol* 2007, **20:**1462-1469.
294. Balderas-Villalobos J, Molina-Munoz T, Mailloux-Salinas P, Bravo G, Carvajal K, Gomez-Viquez NL: **Oxidative stress in cardiomyocytes contributes to decreased SERCA2a activity in rats with metabolic syndrome.** *Am J Physiol Heart Circ Physiol* 2013, **305:**H1344-1353.
295. Du W, Frazier M, McMahon TJ, Eu JP: **Redox activation of intracellular calcium release channels (ryanodine receptors) in the sustained phase of hypoxia-induced pulmonary vasoconstriction.** *Chest* 2005, **128:**556S-558S.
296. Kiselyov K, Muallem S: **ROS and intracellular ion channels.** *Cell Calcium* 2016, **60:**108-114.
297. Gorlach A, Bertram K, Hudecova S, Krizanova O: **Calcium and ROS: A mutual interplay.** *Redox Biol* 2015, **6:**260-271.
298. Shanahan CM, Cary NR, Osbourn JK, Weissberg PL: **Identification of osteoglycin as a component of the vascular matrix. Differential expression by vascular smooth muscle cells during neointima formation and in atherosclerotic plaques.** *Arterioscler Thromb Vasc Biol* 1997, **17:**2437-2447.
299. Adam PJ, Weissberg PL, Cary NR, Shanahan CM: **Polyubiquitin is a new phenotypic marker of contractile vascular smooth muscle cells.** *Cardiovasc Res* 1997, **33:**416-421.
300. Shankman LS, Gomez D, Cherepanova OA, Salmon M, Alencar GF, Haskins RM, Swiatlowska P, Newman AA, Greene ES, Straub AC, et al: **KLF4-dependent phenotypic modulation of smooth muscle cells has a key role in atherosclerotic plaque pathogenesis.** *Nat Med* 2015, **21:**628-637.
301. Allahverdian S, Chehroudi AC, McManus BM, Abraham T, Francis GA: **Contribution of intimal smooth muscle cells to cholesterol accumulation and macrophage-like cells in human atherosclerosis.** *Circulation* 2014, **129:**1551-1559.
302. Bennett MR, Sinha S, Owens GK: **Vascular Smooth Muscle Cells in Atherosclerosis.** *Circ Res* 2016, **118:**692-702.
303. Nguyen AT, Gomez D, Bell RD, Campbell JH, Clowes AW, Gabbiani G, Giachelli CM, Parmacek MS, Raines EW, Rusch NJ, et al: **Smooth muscle cell plasticity: fact or fiction?** *Circ Res* 2013, **112:**17-22.
304. Chamley-Campbell J, Campbell GR, Ross R: **The smooth muscle cell in culture.** *Physiol Rev* 1979, **59:**1-61.
305. Orr AW, Hastings NE, Blackman BR, Wamhoff BR: **Complex regulation and function of the inflammatory smooth muscle cell phenotype in atherosclerosis.** *J Vasc Res* 2010, **47:**168-180.

306. Hayashi K, Saga H, Chimori Y, Kimura K, Yamanaka Y, Sobue K: **Differentiated phenotype of smooth muscle cells depends on signaling pathways through insulin-like growth factors and phosphatidylinositol 3-kinase.** *J Biol Chem* 1998, **273:**28860-28867.
307. Hayashi K, Takahashi M, Kimura K, Nishida W, Saga H, Sobue K: **Changes in the balance of phosphoinositide 3-kinase/protein kinase B (Akt) and the mitogen-activated protein kinases (ERK/p38MAPK) determine a phenotype of visceral and vascular smooth muscle cells.** *J Cell Biol* 1999, **145:**727-740.
308. Wang CC, Gurevich I, Draznin B: **Insulin affects vascular smooth muscle cell phenotype and migration via distinct signaling pathways.** *Diabetes* 2003, **52:**2562-2569.
309. Vallot O, Combettes L, Jourdon P, Inamo J, Marty I, Claret M, Lompré AM: **Intracellular Ca^{2+} handling in vascular smooth muscle cells is affected by proliferation.** *Arterioscler Thromb Vasc Biol* 2000, **20:**1225-1235.
310. Karagiannis GS, Weile J, Bader GD, Minta J: **Integrative pathway dissection of molecular mechanisms of moxLDL-induced vascular smooth muscle phenotype transformation.** *BMC Cardiovasc Disord* 2013, **13:**4.
311. Perisic Matic L, Rykaczewska U, Razuvaev A, Sabater-Lleal M, Lengquist M, Miller CL, Ericsson I, Rohl S, Kronqvist M, Aldi S, et al: **Phenotypic Modulation of Smooth Muscle Cells in Atherosclerosis Is Associated With Downregulation of LMOD1, SYNPO2, PDLIM7, PLN, and SYNM.** *Arterioscler Thromb Vasc Biol* 2016, **36:**1947-1961.
312. Zhu Q, Ni XQ, Lu WW, Zhang JS, Ren JL, Wu D, Chen Y, Zhang LS, Yu YR, Tang CS, Qi YF: **Intermedin reduces neointima formation by regulating vascular smooth muscle cell phenotype via cAMP/PKA pathway.** *Atherosclerosis* 2017, **266:**212-222.
313. King-Briggs KE, Shanahan CM: **TGF-beta superfamily members do not promote smooth muscle-specific alternative splicing, a late marker of vascular smooth muscle cell differentiation.** *Differentiation* 2000, **66:**43-48.
314. Toita R, Otani K, Kawano T, Fujita S, Murata M, Kang JH: **Protein kinase A (PKA) inhibition reduces human aortic smooth muscle cell calcification stimulated by inflammatory response and inorganic phosphate.** *Life Sci* 2018, **209:**466-471.
315. Yoshida T, Yamashita M, Horimai C, Hayashi M: **Smooth muscle-selective inhibition of nuclear factor-kappaB attenuates smooth muscle phenotypic switching and neointima formation following vascular injury.** *J Am Heart Assoc* 2013, **2:**e000230.
316. Yoshida T, Yamashita M, Horimai C, Hayashi M: **Smooth Muscle-Selective Nuclear Factor-kappaB Inhibition Reduces Phosphate-Induced Arterial Medial Calcification in Mice With Chronic Kidney Disease.** *J Am Heart Assoc* 2017, **6**.
317. Yang H, Curinga G, Giachelli CM: **Elevated extracellular calcium levels induce smooth muscle cell matrix mineralization in vitro.** *Kidney Int* 2004, **66:**2293-2299.
318. Jono S, McKee MD, Murry CE, Shioi A, Nishizawa Y, Mori K, Morii H, Giachelli CM: **Phosphate regulation of vascular smooth muscle cell calcification.** *Circ Res* 2000, **87:**E10-17.
319. Zhong W, Li B, Yang P, Chen R, Wang C, Wang Z, Shao C, Yuan W, Yan J: **CD137-CD137L interaction modulates neointima formation and the phenotype transformation of vascular smooth muscle cells via NFATc1 signaling.** *Mol Cell Biochem* 2018, **439:**65-74.

320. Chadjichristos CE, Morel S, Derouette JP, Sutter E, Roth I, Brisset AC, Bochaton-Piallat ML, Kwak BR: **Targeting connexin 43 prevents platelet-derived growth factor-BB-induced phenotypic change in porcine coronary artery smooth muscle cells.** *Circ Res* 2008, **102:**653-660.
321. Rolfe BE, Muddiman JD, Smith NJ, Campbell GR, Campbell JH: **ICAM-1 expression by vascular smooth muscle cells is phenotype-dependent.** *Atherosclerosis* 2000, **149:**99-110.
322. Sazonova OV, Lee KL, Isenberg BC, Rich CB, Nugent MA, Wong JY: **Cell-cell interactions mediate the response of vascular smooth muscle cells to substrate stiffness.** *Biophys J* 2011, **101:**622-630.
323. Kee HJ, Kim GR, Cho SN, Kwon JS, Ahn Y, Kook H, Jeong MH: **miR-18a-5p MicroRNA Increases Vascular Smooth Muscle Cell Differentiation by Downregulating Syndecan4.** *Korean Circ J* 2014, **44:**255-263.
324. Beamish JA, He P, Kottke-Marchant K, Marchant RE: **Molecular regulation of contractile smooth muscle cell phenotype: implications for vascular tissue engineering.** *Tissue Eng Part B Rev* 2010, **16:**467-491.
325. Sobue K, Hayashi K, Nishida W: **Expressional regulation of smooth muscle cell-specific genes in association with phenotypic modulation.** *Mol Cell Biochem* 1999, **190:**105-118.
326. Rattik S, Hultman K, Rauch U, Soderberg I, Sundius L, Ljungcrantz I, Hultgardh-Nilsson A, Wigren M, Bjorkbacka H, Fredrikson GN, Nilsson J: **IL-22 affects smooth muscle cell phenotype and plaque formation in apolipoprotein E knockout mice.** *Atherosclerosis* 2015, **242:**506-514.
327. Yoshiyama S, Chen Z, Okagaki T, Kohama K, Nasu-Kawaharada R, Izumi T, Ohshima N, Nagai T, Nakamura A: **Nicotine exposure alters human vascular smooth muscle cell phenotype from a contractile to a synthetic type.** *Atherosclerosis* 2014, **237:**464-470.
328. Worth NF, Rolfe BE, Song J, Campbell GR: **Vascular smooth muscle cell phenotypic modulation in culture is associated with reorganisation of contractile and cytoskeletal proteins.** *Cell Motil Cytoskeleton* 2001, **49:**130-145.
329. Zhang YN, Xie BD, Sun L, Chen W, Jiang SL, Liu W, Bian F, Tian H, Li RK: **Phenotypic switching of vascular smooth muscle cells in the 'normal region' of aorta from atherosclerosis patients is regulated by miR-145.** *J Cell Mol Med* 2016, **20:**1049-1061.
330. Tian L, Chen K, Cao J, Han Z, Wang Y, Gao L, Fan Y, Wang C: **Galectin3 induces the phenotype transformation of human vascular smooth muscle cells via the canonical Wnt signaling.** *Mol Med Rep* 2017, **15:**3840-3846.
331. Kwak BR, Mulhaupt F, Veillard N, Gros DB, Mach F: **Altered pattern of vascular connexin expression in atherosclerotic plaques.** *Arterioscler Thromb Vasc Biol* 2002, **22:**225-230.
332. Prakash SK, LeMaire SA, Guo DC, Russell L, Regalado ES, Golabbakhsh H, Johnson RJ, Safi HJ, Estrera AL, Coselli JS, et al: **Rare copy number variants disrupt genes regulating vascular smooth muscle cell adhesion and contractility in sporadic thoracic aortic aneurysms and dissections.** *Am J Hum Genet* 2010, **87:**743-756.
333. Wang L, Zhang J, Fu W, Guo D, Jiang J, Wang Y: **Association of smooth muscle cell phenotypes with extracellular matrix disorders in thoracic aortic dissection.** *J Vasc Surg* 2012, **56:**1698-1709, 1709 e1691.
334. Licht AH, Nubel T, Feldner A, Jurisch-Yaksi N, Marcello M, Demicheva E, Hu JH, Hartenstein B, Augustin HG, Hecker M, et al: **Junb regulates arterial contraction**

capacity, cellular contractility, and motility via its target Myl9 in mice. *J Clin Invest* 2010, **120:**2307-2318.
335. Korff T, Pfisterer L, Schorpp-Kistner M: **miR-663 and the miRaculous vascular smooth muscle phenotypic switch.** *Circ Res* 2013, **113:**1102-1105.
336. Moreno CA, Sobreira N, Pugh E, Zhang P, Steel G, Torres FR, Cavalcanti DP: **Homozygous deletion in MYL9 expands the molecular basis of megacystis-microcolon-intestinal hypoperistalsis syndrome.** *Eur J Hum Genet* 2018, **26:**669-675.
337. Pucovsky V, Harhun MI, Povstyan OV, Gordienko DV, Moss RF, Bolton TB: **Close relation of arterial ICC-like cells to the contractile phenotype of vascular smooth muscle cell.** *J Cell Mol Med* 2007, **11:**764-775.
338. Sazonova OV, Isenberg BC, Herrmann J, Lee KL, Purwada A, Valentine AD, Buczek-Thomas JA, Wong JY, Nugent MA: **Extracellular matrix presentation modulates vascular smooth muscle cell mechanotransduction.** *Matrix Biol* 2015, **41:**36-43.
339. Harhun MI, Huggins CL, Ratnasingham K, Raje D, Moss RF, Szewczyk K, Vasilikostas G, Greenwood IA, Khong TK, Wan A, Reddy M: **Resident phenotypically modulated vascular smooth muscle cells in healthy human arteries.** *J Cell Mol Med* 2012, **16:**2802-2812.
340. Yablonka-Reuveni Z, Christ B, Benson JM: **Transitions in cell organization and in expression of contractile and extracellular matrix proteins during development of chicken aortic smooth muscle: evidence for a complex spatial and temporal differentiation program.** *Anat Embryol (Berl)* 1998, **197:**421-437.
341. Yin H, Jiang Y, Li H, Li J, Gui Y, Zheng XL: **Proteasomal degradation of myocardin is required for its transcriptional activity in vascular smooth muscle cells.** *J Cell Physiol* 2011, **226:**1897-1906.
342. Orr AW, Lee MY, Lemmon JA, Yurdagul A, Jr., Gomez MF, Bortz PD, Wamhoff BR: **Molecular mechanisms of collagen isotype-specific modulation of smooth muscle cell phenotype.** *Arterioscler Thromb Vasc Biol* 2009, **29:**225-231.
343. Liao XH, Wang N, Zhao DW, Zheng DL, Zheng L, Xing WJ, Ma WJ, Bao LY, Dong J, Zhang TC: **STAT3 Protein Regulates Vascular Smooth Muscle Cell Phenotypic Switch by Interaction with Myocardin.** *J Biol Chem* 2015, **290:**19641-19652.
344. Ackers-Johnson M, Talasila A, Sage AP, Long X, Bot I, Morrell NW, Bennett MR, Miano JM, Sinha S: **Myocardin regulates vascular smooth muscle cell inflammatory activation and disease.** *Arterioscler Thromb Vasc Biol* 2015, **35:**817-828.
345. Herum KM, Lunde IG, Skrbic B, Florholmen G, Behmen D, Sjaastad I, Carlson CR, Gomez MF, Christensen G: **Syndecan-4 signaling via NFAT regulates extracellular matrix production and cardiac myofibroblast differentiation in response to mechanical stress.** *J Mol Cell Cardiol* 2013, **54:**73-81.
346. Kashiwada K, Nishida W, Hayashi K, Ozawa K, Yamanaka Y, Saga H, Yamashita T, Tohyama M, Shimada S, Sato K, Sobue K: **Coordinate expression of alpha-tropomyosin and caldesmon isoforms in association with phenotypic modulation of smooth muscle cells.** *J Biol Chem* 1997, **272:**15396-15404.
347. Rong JX, Shapiro M, Trogan E, Fisher EA: **Transdifferentiation of mouse aortic smooth muscle cells to a macrophage-like state after cholesterol loading.** *Proc Natl Acad Sci U S A* 2003, **100:**13531-13536.

348. Yamamoto M, Yamamoto K, Noumura T: **Type I collagen promotes modulation of cultured rabbit arterial smooth muscle cells from a contractile to a synthetic phenotype.** *Exp Cell Res* 1993, **204:**121-129.
349. McDaniel DP, Shaw GA, Elliott JT, Bhadriraju K, Meuse C, Chung KH, Plant AL: **The stiffness of collagen fibrils influences vascular smooth muscle cell phenotype.** *Biophys J* 2007, **92:**1759-1769.
350. Babaev VR, Antonov AS, Domogatsky SP, Kazantseva IA: **Phenotype related changes of intimal smooth muscle cells from human aorta in primary culture.** *Atherosclerosis* 1992, **96:**189-202.
351. Ang AH, Tachas G, Campbell JH, Bateman JF, Campbell GR: **Collagen synthesis by cultured rabbit aortic smooth-muscle cells. Alteration with phenotype.** *Biochem J* 1990, **265:**461-469.
352. Xiang D, Huang D, Gai L, Liu H: **Relationship between expression of type III collagen and phenotype of vascular smooth muscle cells in neointimal of stented coronary artery.** *Chin Med J (Engl)* 2000, **113:**324-327.
353. Johnstone SR, Ross J, Rizzo MJ, Straub AC, Lampe PD, Leitinger N, Isakson BE: **Oxidized phospholipid species promote in vivo differential cx43 phosphorylation and vascular smooth muscle cell proliferation.** *Am J Pathol* 2009, **175:**916-924.
354. Braun M, Pietsch P, Schror K, Baumann G, Felix SB: **Cellular adhesion molecules on vascular smooth muscle cells.** *Cardiovasc Res* 1999, **41:**395-401.
355. Gorgoulis VG, Zacharatos P, Kotsinas A, Kletsas D, Mariatos G, Zoumpourlis V, Ryan KM, Kittas C, Papavassiliou AG: **p53 activates ICAM-1 (CD54) expression in an NF-kappaB-independent manner.** *EMBO J* 2003, **22:**1567-1578.
356. Printseva O, Peclo MM, Gown AM: **Various cell types in human atherosclerotic lesions express ICAM-1. Further immunocytochemical and immunochemical studies employing monoclonal antibody 10F3.** *Am J Pathol* 1992, **140:**889-896.
357. Henderson N, Markwick LJ, Elshaw SR, Freyer AM, Knox AJ, Johnson SR: **Collagen I and thrombin activate MMP-2 by MMP-14-dependent and -independent pathways: implications for airway smooth muscle migration.** *Am J Physiol Lung Cell Mol Physiol* 2007, **292:**L1030-1038.
358. Blindt R, Zeiffer U, Krott N, Filzmaier K, Voss M, Hanrath P, vom Dahl J, Bosserhoff AK: **Upregulation of the cytoskeletal-associated protein Moesin in the neointima of coronary arteries after balloon angioplasty: a new marker of smooth muscle cell migration?** *Cardiovasc Res* 2002, **54:**630-639.
359. Torella D, Iaconetti C, Catalucci D, Ellison GM, Leone A, Waring CD, Bochicchio A, Vicinanza C, Aquila I, Curcio A, et al: **MicroRNA-133 controls vascular smooth muscle cell phenotypic switch in vitro and vascular remodeling in vivo.** *Circ Res* 2011, **109:**880-893.
360. Doevendans PA, van Eys G: **Smooth muscle cells on the move: the battle for actin.** *Cardiovasc Res* 2002, **54:**499-502.
361. Nilsson LM, Sun ZW, Nilsson J, Nordstrom I, Chen YW, Molkentin JD, Wide-Swensson D, Hellstrand P, Lydrup ML, Gomez MF: **Novel blocker of NFAT activation inhibits IL-6 production in human myometrial arteries and reduces vascular smooth muscle cell proliferation.** *Am J Physiol Cell Physiol* 2007, **292:**C1167-1178.
362. Bevilacqua A, Willis MS, Bultman SJ: **SWI/SNF chromatin-remodeling complexes in cardiovascular development and disease.** *Cardiovasc Pathol* 2014, **23:**85-91.

363. Marian AJ: **The enigma of genetics etiology of atherosclerosis in the post-GWAS era.** *Curr Atheroscler Rep* 2012, **14:**295-299.
364. Lino Cardenas CL, Kessinger CW, Cheng Y, MacDonald C, MacGillivray T, Ghoshhajra B, Huleihel L, Nuri S, Yeri AS, Jaffer FA, et al: **An HDAC9-MALAT1-BRG1 complex mediates smooth muscle dysfunction in thoracic aortic aneurysm.** *Nat Commun* 2018, **9:**1009.
365. Zhao N, Koenig SN, Trask AJ, Lin CH, Hans CP, Garg V, Lilly B: **MicroRNA miR145 regulates TGFBR2 expression and matrix synthesis in vascular smooth muscle cells.** *Circ Res* 2015, **116:**23-34.
366. Schmidt A, Gopfert C, Vlodavsky I, Volker W, Buddecke E: **Induction of a hypertrophic growth status of coronary smooth muscle cells is associated with an overexpression of TGF-beta.** *Eur J Cell Biol* 2002, **81:**138-144.
367. Abouhamed M, Reichenberg S, Robenek H, Plenz G: **Tropomyosin 4 expression is enhanced in dedifferentiating smooth muscle cells in vitro and during atherogenesis.** *Eur J Cell Biol* 2003, **82:**473-482.
368. Sung HJ, Eskin SG, Sakurai Y, Yee A, Kataoka N, McIntire LV: **Oxidative stress produced with cell migration increases synthetic phenotype of vascular smooth muscle cells.** *Ann Biomed Eng* 2005, **33:**1546-1554.
369. Moiseeva EP: **Adhesion receptors of vascular smooth muscle cells and their functions.** *Cardiovasc Res* 2001, **52:**372-386.
370. Tang L, Dai F, Liu Y, Yu X, Huang C, Wang Y, Yao W: **RhoA/ROCK signaling regulates smooth muscle phenotypic modulation and vascular remodeling via the JNK pathway and vimentin cytoskeleton.** *Pharmacol Res* 2018, **133:**201-212.
371. Wexler RK, Elton T, Pleister A, Feldman D: **Cardiomyopathy: an overview.** *Am Fam Physician* 2009, **79:**778-784.
372. Libby P, Ridker PM, Hansson GK: **Progress and challenges in translating the biology of atherosclerosis.** *Nature* 2011, **473:**317-325.
373. Rader DJ, Daugherty A: **Translating molecular discoveries into new therapies for atherosclerosis.** *Nature* 2008, **451:**904-913.
374. van der Schaaf RJ, Timmer JR, Ottervanger JP, Hoorntje JC, de Boer MJ, Suryapranata H, Zijlstra F, Dambrink JH: **Long-term impact of multivessel disease on cause-specific mortality after ST elevation myocardial infarction treated with reperfusion therapy.** *Heart* 2006, **92:**1760-1763.
375. Rodenbeck SD, Zarse CA, McKenney-Drake ML, Bruning RS, Sturek M, Chen NX, Moe SM: **Intracellular calcium increases in vascular smooth muscle cells with progression of chronic kidney disease in a rat model.** *Nephrol Dial Transplant* 2017, **32:**450-458.
376. Baro I, O'Neill SC, Eisner DA: **Changes of intracellular [Ca2+] during refilling of sarcoplasmic reticulum in rat ventricular and vascular smooth muscle.** *J Physiol* 1993, **465:**21-41.
377. Yoshikawa A, Van Breemen C, Isenberg G: **Buffering of plasmalemmal Ca^{2+} current by sarcoplasmic reticulum of guinea pig urinary bladder myocytes.** *Am J Physiol Cell Physiol* 1996, **271:**C833-C841.
378. Ganitkevich VY, Isenberg G: **Caffeine-induced release and reuptake of Ca^{2+} by Ca^{2+} stores in myocytes from guinea-pig urinary bladder.** *J Physiol (Lond)* 1992, **458:**99-117.
379. Bobe R, Hadri L, Lopez JJ, Sassi Y, Atassi F, Karakikes I, Liang L, Limon I, Lompre AM, Hatem SN, et al: **SERCA2a controls the mode of agonist-induced intracellular Ca2+ signal, transcription factor NFAT and proliferation in human vascular smooth muscle cells.** *J Mol Cell Cardiol* 2011, **50:**621-633.

380. Spillmann F, Miteva K, Pieske B, Tschope C, Van Linthout S: **High-density lipoproteins reduce endothelial-to-mesenchymal transition.** *Arterioscler Thromb Vasc Biol* 2015, **35:**1774-1777.
381. Wang Y, Ji L, Jiang R, Zheng L, Liu D: **Oxidized high-density lipoprotein induces the proliferation and migration of vascular smooth muscle cells by promoting the production of ROS.** *J Atheroscler Thromb* 2014, **21:**204-216.
382. Adachi T, Matsui R, Xu S, Kirber M, Lazar HL, Sharov VS, Schoneich C, Cohen RA: **Antioxidant improves smooth muscle sarco/endoplasmic reticulum Ca(2+)- ATPase function and lowers tyrosine nitration in hypercholesterolemia and improves nitric oxide-induced relaxation.** *Circ Res* 2002, **90:**1114-1121.
383. Dong Y, Zhang M, Wang S, Liang B, Zhao Z, Liu C, Wu M, Choi HC, Lyons TJ, Zou MH: **Activation of AMP-activated protein kinase inhibits oxidized LDL-triggered endoplasmic reticulum stress in vivo.** *Diabetes* 2010, **59:**1386-1396.
384. Adachi T, Matsui R, Weisbrod RM, Najibi S, Cohen RA: **Reduced sarco/endoplasmic reticulum Ca(2+) uptake activity can account for the reduced response to NO, but not sodium nitroprusside, in hypercholesterolemic rabbit aorta.** *Circulation* 2001, **104:**1040-1045.
385. Gheorghiade M, Bonow RO: **Chronic heart failure in the United States: a manifestation of coronary artery disease.** *Circulation* 1998, **97:**282-289.
386. Bart BA, Shaw LK, McCants CB, Jr., Fortin DF, Lee KL, Califf RM, O'Connor CM: **Clinical determinants of mortality in patients with angiographically diagnosed ischemic or nonischemic cardiomyopathy.** *J Am Coll Cardiol* 1997, **30:**1002-1008.
387. Gui MH, Ling Y, Liu L, Jiang JJ, Li XY, Gao X: **Effect of Metabolic Syndrome Score, Metabolic Syndrome, and Its Individual Components on the Prevalence and Severity of Angiographic Coronary Artery Disease.** *Chin Med J (Engl)* 2017, **130:**669-677.
388. Ahmadi A, Leipsic J, Feuchtner G, Gransar H, Kalra D, Heo R, Achenbach S, Andreini D, Al-Mallah M, Berman DS, et al: **Is metabolic syndrome predictive of prevalence, extent, and risk of coronary artery disease beyond its components? Results from the multinational coronary CT angiography evaluation for clinical outcome: an international multicenter registry (CONFIRM).** *PLoS One* 2015, **10:**e0118998.
389. Miura Y, Fukumoto Y, Shiba N, Miura T, Shimada K, Iwama Y, Takagi A, Matsusaka H, Tsutsumi T, Yamada A, et al: **Prevalence and clinical implication of metabolic syndrome in chronic heart failure.** *Circ J* 2010, **74:**2612-2621.
390. Lipskaia L, Limon I, Bobe R, Hajjar R: **Calcium Cycling in Synthetic and Contractile Phasic or Tonic Vascular Smooth Muscle Cells.** In *Current Basic and Pathological Approaches to the Function of Muscle Cells and Tissues - From Molecules to Humans.* Edited by Sugi H: IntechOpen; 2012
391. Beech DJ: **Ion channel switching and activation in smooth-muscle cells of occlusive vascular diseases.** *Biochem Soc Trans* 2007, **35:**890-894.
392. Masuo M, Toyo-oka T, Shin WS, Sugimoto T: **Growth-dependent alterations of intracellular Ca^{2+}-handling mechanisms of vascular smooth muscle cells: PDGF negatively regulates functional expression of voltage-dependent, IP_3-mediated, and Ca^{2+}-induced Ca^{2+} release channels.** *Circ Res* 1991, **69:**1327-1339.
393. Hou M, Moller S, Edvinsson L, Erlinge D: **Cytokines Induce Upregulation of Vascular P2Y2 Receptors and Increased Mitogenic Responses to UTP and ATP.** *Arteriosclerosis, Thrombosis, and Vascular Biology* 2000, **20:**2064-2069.

394. Wamhoff BR, Bowles DK, Dietz NJ, Hu Q, Sturek M: **Exercise training attenuates coronary smooth muscle phenotypic modulation and nuclear Ca^{2+} signaling.** *Am J Physiol Heart Circ Physiol* 2002, **283:**H2397-H2410.
395. Wamhoff BR, Dixon JL, Sturek M: **Atorvastatin treatment prevents alterations in coronary smooth muscle nuclear Ca^{2+} signaling associated with diabetic dyslipidemia.** *J Vasc Res* 2002, **39:**208-220.
396. Hill BJF, Wamhoff BR, Sturek M: **Functional nucleotide receptor expression and sarcoplasmic reticulum morphology in dedifferentiated porcine coronary smooth muscle cells.** *J Vasc Res* 2001, **38:**432-443.
397. Smith CD, Wang A, Vembaiyan K, Zhang J, Xie C, Zhou Q, Wu G, Chen SR, Back TG: **Novel carvedilol analogues that suppress store-overload-induced Ca2+ release.** *J Med Chem* 2013, **56:**8626-8655.
398. Yang B, Gwozdz T, Dutko-Gwozdz J, Bolotina VM: **Orai1 and Ca^{2+}-independent phospholipase A_2 are required for store-operated I_{catSOC} current, Ca^{2+} entry and proliferation of primary vascular smooth muscle cell.** *Am J Physiol Cell Physiol* 2011, **(In press)**.
399. Golovina VA: **Cell proliferation is associated with enhanced capacitative Ca^{2+} entry in human arterial myocytes.** *Am J Physiol Cell Physiol* 1999, **277:**C343-C349.
400. Kawanabe Y, Hashimoto N, Masaki T: **Ca2+ channels involved in endothelin-induced mitogenic response in carotid artery vascular smooth muscle cells.** *Am J Physiol Cell Physiol* 2002, **282:**C330-C337.
401. Kumar B, Dreja K, Shah SS, Cheong A, Xu SZ, Sukumar P, Naylor J, Forte A, Cipollaro M, McHugh D, et al: **Upregulated TRPC1 channel in vascular injury in vivo and its role in human neointimal hyperplasia.** *Circ Res* 2006, **98:**557-563.
402. Wray S, Burdyga T: **Sarcoplasmic reticulum function in smooth muscle.** *Physiol Rev* 2010, **90:**113-178.
403. Laughlin MH, Bowles DK, Duncker DJ: **The coronary circulation in exercise training.** *Am J Physiol Heart Circ Physiol* 2012, **302:**H10-H23.
404. Cheng H, Lederer WJ: **Calcium Sparks.** *Physiol Rev* 2008, **88:**1491-1545.
405. Ziomek G, van Breemen C, Esfandiarei M: **Drop in endo/sarcoplasmic calcium precedes the unfolded protein response in Brefeldin A-treated vascular smooth muscle cells.** *Eur J Pharmacol* 2015, **764:**328-339.
406. Thyberg J, Palmberg L, Nilsson J, Ksiazek T, Sjölund M: **Phenotype modulation in primary cultures of arterial smooth muscle cells: on the role of platelet-derived growth factor.** *Differentiation* 1983, **25:**156-167.
407. Gromada J, Dissing S, Bokvist K, Renstrom E, Frokjaer-Jensen J, Wulff BS, Rorsman P: **Glucagon-like peptide I increases cytoplasmic calcium in insulin-secreting beta TC3-cells by enhancement of intracellular calcium mobilization.** *Diabetes* 1995, **44:**767-774.
408. Gomez D, Swiatlowska P, Owens GK: **Epigenetic Control of Smooth Muscle Cell Identity and Lineage Memory.** *Arterioscler Thromb Vasc Biol* 2015, **35:**2508-2516.
409. Feil S, Fehrenbacher B, Lukowski R, Essmann F, Schulze-Osthoff K, Schaller M, Feil R: **Transdifferentiation of vascular smooth muscle cells to macrophage-like cells during atherogenesis.** *Circ Res* 2014, **115:**662-667.
410. Nemenoff RA, Horita H, Ostriker AC, Furgeson SB, Simpson PA, VanPutten V, Crossno J, Offermanns S, Weiser-Evans MC: **SDF-1alpha induction in mature smooth muscle cells by inactivation of PTEN is a critical mediator of**

exacerbated injury-induced neointima formation. *Arterioscler Thromb Vasc Biol* 2011, **31:**1300-1308.
411. Tang Z, Wang A, Yuan F, Yan Z, Liu B, Chu JS, Helms JA, Li S: **Differentiation of multipotent vascular stem cells contributes to vascular diseases.** *Nat Commun* 2012, **3:**875-887.
412. Bentzon JF, Weile C, Sondergaard CS, Hindkjaer J, Kassem M, Falk E: **Smooth Muscle Cells in Atherosclerosis Originate From the Local Vessel Wall and Not Circulating Progenitor Cells in ApoE Knockout Mice.** *Arterioscler Thromb Vasc Biol* 2006, **26:**2696-2702.
413. Bentzon JF, Sondergaard CS, Kassem M, Falk E: **Smooth Muscle Cells Healing Atherosclerotic Plaque Disruptions Are of Local, Not Blood, Origin in Apolipoprotein E Knockout Mice.** *Circulation* 2007, **116:**2053-2061.
414. Sata M, Saiura A, Kunisato A, Tojo A, Okada S, Tokuhisa T, Hirai H, Makuuchi M, Hirata Y, Nagai R: **Hematopoietic stem cells differentiate into vascular cells that participate in the pathogenesis of atherosclerosis.** *Nat Med* 2002, **8:**403-409.
415. Iwata H, Manabe I, Fujiu K, Yamamoto T, Takeda N, Eguchi K, Furuya A, Kuro-o M, Sata M, Nagai R: **Bone marrow-derived cells contribute to vascular inflammation but do not differentiate into smooth muscle cell lineages.** *Circulation* 2010, **122:**2048-2057.
416. Takeda Y, Nystoriak MA, Nieves-Cintron M, Santana LF, Navedo MF: **Relationship between Ca2+ sparklets and sarcoplasmic reticulum Ca2+ load and release in rat cerebral arterial smooth muscle.** *Am J Physiol Heart Circ Physiol* 2011, **301:**H2285-2294.
417. Sandberg WJ, Yndestad A, Oie E, Smith C, Ueland T, Ovchinnikova O, Robertson AK, Muller F, Semb AG, Scholz H, et al: **Enhanced T-cell expression of RANK ligand in acute coronary syndrome: possible role in plaque destabilization.** *Arterioscler Thromb Vasc Biol* 2006, **26:**857-863.
418. Kudryavtseva O, Herum KM, Dam VS, Straarup MS, Kamaev D, Briggs Boedtkjer DM, Matchkov VV, Aalkjaer C: **Downregulation of L-type Ca2+ channel in rat mesenteric arteries leads to loss of smooth muscle contractile phenotype and inward hypertrophic remodeling.** *Am J Physiol Heart Circ Physiol* 2014, **306:**H1287-1301.
419. Berra-Romani R, Mazzocco-Spezzia A, Pulina MV, Golovina VA: **Ca2+ handling is altered when arterial myocytes progress from a contractile to a proliferative phenotype in culture.** *Am J Physiol Cell Physiol* 2008, **295:**C779-790.
420. Potier M, Gonzalez JC, Motiani RK, Abdullaev IF, Bisaillon JM, Singer HA, Trebak M: **Evidence for STIM1- and Orai1-dependent store-operated calcium influx through ICRAC in vascular smooth muscle cells: role in proliferation and migration.** *FASEB J* 2009, **23:**2425-2437.
421. Barlow CA, Rose P, Pulver-Kaste RA, Lounsbury KM: **Excitation-transcription coupling in smooth muscle.** *J Physiol* 2006, **570:**59-64.
422. Trebak M, Ginnan R, Singer HA, Jourd'heuil D: **Interplay between calcium and reactive oxygen/nitrogen species: an essential paradigm for vascular smooth muscle signaling.** *Antioxid Redox Signal* 2010, **12:**657-674.
423. Tulenko TN, Sumner AE, Chen M, Huang Y, Laury-Kleintop L, Ferdinand FD: **The smooth muscle cell membrane during atherogenesis: A potential target for amlodipine in atheroprotection.** *Am Heart J* 2001, **141:**S1-S11.
424. Sathish V, Thompson MA, Bailey JP, Pabelick CM, Prakash YS, Sieck GC: **Effect of proinflammatory cytokines on regulation of sarcoplasmic reticulum Ca2+**

reuptake in human airway smooth muscle. *Am J Physiol Lung Cell Mol Physiol* 2009, **297:**L26-34.
425. Zhao MM, Xu MJ, Cai Y, Zhao G, Guan Y, Kong W, Tang C, Wang X: **Mitochondrial reactive oxygen species promote p65 nuclear translocation mediating high-phosphate-induced vascular calcification in vitro and in vivo.** *Kidney Int* 2011, **79:**1071-1079.
426. Tian L, Chen K, Cao J, Han Z, Gao L, Wang Y, Fan Y, Wang C: **Galectin-3-induced oxidized low-density lipoprotein promotes the phenotypic transformation of vascular smooth muscle cells.** *Mol Med Rep* 2015, **12:**4995-5002.
427. Saito E, Wachi H, Sato F, Seyama Y: **7-ketocholesterol, a major oxysterol, promotes pi-induced vascular calcification in cultured smooth muscle cells.** *J Atheroscler Thromb* 2008, **15:**130-137.
428. Goettsch C, Rauner M, Hamann C, Sinningen K, Hempel U, Bornstein SR, Hofbauer LC: **Nuclear factor of activated T cells mediates oxidised LDL-induced calcification of vascular smooth muscle cells.** *Diabetologia* 2011, **54:**2690-2701.
429. Nystoriak MA, Nieves-Cintron M, Navedo MF: **Capturing single L-type Ca(2+) channel function with optics.** *Biochim Biophys Acta* 2013, **1833:**1657-1664.
430. Mokelke EA, Dietz NJ, Eckman DM, Nelson MT, Sturek M: **Diabetic dyslipidemia and exercise affect coronary tone and differential regulation of conduit and microvessel K^+ current.** *Am J Physiol Heart Circ Physiol* 2005, **288:**H1233-H1241.
431. Fernandez-Velasco M, Ruiz-Hurtado G, Gomez AM, Rueda A: **Ca(2+) handling alterations and vascular dysfunction in diabetes.** *Cell Calcium* 2014, **56:**397-407.
432. Simard E, Sollradl T, Maltais JS, Boucher J, D'Orleans-Juste P, Grandbois M: **Receptor for Advanced Glycation End-Products Signaling Interferes with the Vascular Smooth Muscle Cell Contractile Phenotype and Function.** *PLoS One* 2015, **10:**e0128881.
433. Wang Z, Jiang Y, Liu N, Ren L, Zhu Y, An Y, Chen D: **Advanced glycation end-product Nepsilon-carboxymethyl-Lysine accelerates progression of atherosclerotic calcification in diabetes.** *Atherosclerosis* 2012, **221:**387-396.
434. Martin-Pardillos A, Sorribas V: **Effects of donor age and proliferative aging on the phenotype stability of rat aortic smooth muscle cells.** *Physiol Rep* 2015, **3**.
435. Lundberg MS, Crow MT: **Age-related changes in the signaling and function of vascular smooth muscle cells.** *Exp Gerontol* 1999, **34:**549-557.
436. Van Assche T, Fransen P, Guns PJ, Herman AG, Bult H: **Altered Ca2+ handling of smooth muscle cells in aorta of apolipoprotein E-deficient mice before development of atherosclerotic lesions.** *Cell Calcium* 2007, **41:**295-302.
437. Lehto S, Niskanen L, Suhonen M, Rönnemaa T, Laakso M: **Medial artery calcification - A neglected harbinger of cardiovascular complications in non-insulin-dependent diabetes mellitus.** *Arterioscler Thromb Vasc Biol* 1996, **16:**978-983.
438. Chen N, Moe S: **Vascular Calcification: Pathophysiology and Risk Factors.** *Curr Hypertens Rep* 2012, **14:**228-237.
439. Wu M, Rementer C, Giachelli CM: **Vascular Calcification: An Update on Mechanisms and Challenges in Treatment.** *Calcif Tissue Int* 2013.

440. Saleh Al-Shehabi T, Iratni R, Eid AH: **Anti-atherosclerotic plants which modulate the phenotype of vascular smooth muscle cells.** *Phytomedicine* 2016, **23:**1068-1081.

CURRICULUM VITAE

Jill Kimberly Badin

EDUCATION

2013 B.S. Molecular Biology, Biochemistry, and Bioinformatics
Towson University
Jess and Mildred Fisher College of Science and Mathematics
Towson, MD

2013 B.S. Chemistry
Towson University
Jess and Mildred Fisher College of Science and Mathematics
Towson, MD

2019 Ph.D. Physiology; Minor: Cardiovascular Science
Indiana University
Department of Cellular & Integrative Physiology
Indianapolis, IN
Mentor: Michael Sturek, Ph.D.

Doctoral Dissertation
Coronary Smooth Muscle Cell Cytodifferentiation and Intracellular Ca^{2+} Handling in Coronary Artery Disease

Research Committee

Michael Sturek, Ph.D. – Professor and Chair, Indiana University School of Medicine, Department of Cellular & Integrative Physiology

Carmella Evans-Molina, MD/Ph.D. – Assistant Professor of Medicine, Indiana University School of Medicine, Department of Medicine

Sharon M. Moe, MD – Professor of Medicine, Indiana University School of Medicine, Department of Medicine

Johnathan D. Tune, Ph.D. – Professor, Indiana University School of Medicine, Department of Cellular & Integrative Physiology

Awards/Fellowships

2009 Towson University Provost Scholarship

2009 Towson University Honors College Scholarship

2013 Towson Undergraduate Research Committee Travel Grant

2013 Fisher College of Science and Mathematics Travel Grant

2014 Indiana University School of Medicine Graduate Division University Fellowship

2018 Keystone Symposia Scholarship

TEACHING EXPERIENCE

Teaching Assistantships

Summer 2016

K531: Clinical Physiology/Pathophysiology I
Teaching Assistant, ECG Analysis
Indiana University School of Medicine
Indianapolis, IN

Fall 2016

GRAD G715 Biochemical Basis of Biological Processes
Teaching Assistant
Indiana University School of Medicine
Indianapolis, IN

Service/Outreach

May 2015: Science fair judge, Sherwood High School Science Fair, Sherwood High School, Sandy Spring, MD.

March 2017: Cardiac Anatomy Demonstration, Honors Anatomy and Physiology classes, Avon High School, Avon, IN.

PROFESSIONAL ORGANIZATIONS

Memberships

2014-present American Physiological Society

2014-present Indiana Physiological Society

2014-present Society for Experimental Biology and Medicine

PUBLICATIONS

Manuscripts

1) **Badin JK,** Bruning R, Sturek M. Effect of metabolic syndrome and aging on Ca^{2+} dysfunction in coronary smooth muscle and coronary artery disease severity in Ossabaw miniature swine. *Exp Gerontol* 108: 247-255. 2018. DOI: 10.1016/j.exger.2018.04.024.

2) **Badin JK,** Kole A, Stivers B, Progar V, Pareddy A, Alloosh M, Sturek M. Alloxan-induced diabetes exacerbates coronary atherosclerosis and calcification in Ossabaw miniature swine with metabolic syndrome. *J Transl Med* 16(1): 58. 2018. DOI: 10.1186/s12967-018-1431-9.

3) **Badin JK,** Progar V, Pareddy A, Cagle J, Alloosh M, Sturek M. Diabetogenic actions of alloxan are dependent on age. *Comp Med* 69(2):114-122. 2019. DOI: 10.30802/AALAS-CM-18-000037.

4) **Badin JK,** Eggenberger C, Rodenbeck SD, Alloosh M, Hashmi ZA, Wang IW, Sturek M. Intracellular Ca2+ dysregulation in coronary smooth muscle is similar in coronary disease of humans and Ossabaw miniature swine. (In Preparation).

Book Chapters

1) Resendiz M, Lo SCL, **Badin JK,** Chiu YJ and Zhou FC. Alcohol metabolism and epigenetic methylation and acetylation. *Molecular Aspects of Alcohol and Nutrition.* V.B. Patel (Ed). Oxford, UK: Elsevier, 2016.

Abstracts

1) **Badin JK** and Sturek M. Osteoprotegerin and receptor activator of nuclear factor-κB ligand alter intracellular Ca^{2+} handling in coronary smooth muscle cells in an *in vitro* model of coronary artery calcification. *FASEB J* 30:733.10, 2016.

2) **Badin JK**, Alloosh M, Chen RJ, Hashmi ZA, and Sturek M. The first evidence of decreased voltage-gated Ca^{2+} influx into coronary smooth muscle in ischemic versus non-ischemic cardiomyopathy in human transplant cardiectomy samples. *FASEB J* 31:1017.17, 2017.

3) Chen RJ, Alloosh M, **Badin JK**, Sturek M, Wang I, Wozniak T, and Hashmi ZA. Voltage-gated Ca^{2+} influx into coronary smooth muscle is decreased in ischemic versus non-ischemic cardiomyopathy – the first evidence from human transplant cardiectomy samples. *J Heart Lung Transplant* 36(4):S135, 2017.

4) Stivers B, **Badin JK**, Kole A, Progar V, Pareddy A, Alloosh M, and Sturek M. Diabetes exacerbates coronary artery atherosclerosis in Ossabaw miniature swine with metabolic syndrome. *FASEB J* 31:1014.16, 2017.

5) **Badin JK** and Sturek M. Coronary smooth muscle cytodifferentiation is associated with an increase in pro-inflammatory, pro-calcifying gene expression in an organ culture model of coronary artery disease. *FASEB J* 33:Ib511, 2019.

6) **Badin JK**, Eggenberger C, Rodenbeck SD, Alloosh M, Hashmi ZA, Wang IW, and Sturek M. Similar dysfunctional Ca2+ regulation in coronary smooth muscle from explanted human hearts and Ossabaw miniature swine strongly supports the translational relevance of this large animal model. *FASEB J* 33:689.5, 2019.

PRESENTATIONS

Oral Presentations

1) **Badin JK**. Diabetes exacerbates coronary atherosclerosis and calcification in Ossabaw miniature swine with metabolic syndrome. Eli Lilly Headquarters, June 2017, Indianapolis, IN.

2) **Badin, JK**. Diabetes exacerbates coronary atherosclerosis and calcification in Ossabaw miniature swine with metabolic syndrome. Keystone Symposia – Uncomplicating Diabetes: Reducing the Burden of Diabetes-Related End-Organ injury, March 2018, Santa Fe, NM.

Poster Presentations

1) **Badin JK** and Sturek M. Osteogenic factor regulation of calcium handling in coronary smooth muscle. Poster presentation, IUPUI Imaging Research Symposium, October 2015, Indianapolis, IN.

2) **Badin JK** and Sturek M. Receptor activator of nuclear factor-κB ligand induces arterial calcification in cultured porcine coronary arteries. Poster presentation, 6th Annual Conference of the Indiana Physiological Society, February 2016, Greencastle, IN.

3) **Badin JK** and Sturek M. Osteoprotegerin as a possible inhibitor of receptor activator of nuclear factor-κB ligand in arterial calcification and SERCA function in cultured porcine coronary arteries. Poster presentation, Experimental Biology, April 2016, San Diego, CA.

4) **Badin JK,** Bruning RS and Sturek M. Metabolic syndrome and advancing age alter coronary smooth muscle cell calcium handling similarly in an Ossabaw swine model. Poster presentation, 7th Annual Conference of the Indiana Physiological Society, February 2017, Indianapolis, IN.

5) **Badin JK,** Bruning RS, and Sturek M. Metabolic syndrome and advancing age alter coronary smooth muscle cell calcium handling similarly in an Ossabaw swine model. Poster presentation, Cardiovascular Aging: New Frontiers and Old Friends, August 2017, Westminster, CO.

6) **Badin JK**, Bruning RS, and Sturek M. Effect of metabolic syndrome and aging on Ca^{2+} dysfunction in coronary smooth muscle and coronary artery disease severity in Ossabaw miniature swine. Poster presentation, 8th Annual Conference of the Indiana Physiological Society, February 2018, Upland, IN.

7) **Badin JK,** Bruning R, and Sturek M. Effect of metabolic syndrome and aging on coronary artery disease severity and Ca^{2+} dysregulation in coronary smooth muscle in Ossabaw miniature swine. Poster presentation, Experimental Biology, April 2018, San Diego, CA.

8) **Badin JK** and Sturek M. Coronary smooth muscle cytodifferentiation is associated with an increase in pro-inflammatory, pro-calcifying gene expression in an organ culture model of coronary artery disease. Poster presentation, 9th Annual Conference of the Indiana Physiological Society, March 2019, Crawfordsville, IN.

9) **Badin JK,** Eggenberger C, Rodenbeck SD, Alloosh M, Hashmi ZA, Wang IW, and Sturek M. Ca^{2+} dysfunction in coronary smooth muscle from explanted human hearts strongly supports Ossabaw miniature swine as a large animal model for coronary artery disease. Poster presentation, Experimental Biology, April 2019, Orlando, FL.

10) **Badin JK** and Sturek M. Coronary smooth muscle cytodifferentiation is associated with an increase in pro-inflammatory, pro-calcifying gene expression in an organ culture model of coronary artery disease. Poster presentation, Experimental Biology, April 2019, Orlando, FL.